frontiers | Research Topics

# New insight into the roles of microorganisms in municipal and environmental engineering technologies/systems

**Edited by**
Xiaochen Chen, Hongbo Li, Ming Zeng,
Xianhua Liu and Ikuro Kasuga

**Coordinated by**
Xiaolin Ca

**Published in**
Frontiers in Microbiology

ISSN 1664-8714
ISBN 978-2-8325-4312-2
DOI 10.3389/978-2-8325-4312-2

## About Frontiers

Frontiers is more than just an open access publisher of scholarly articles: it is a pioneering approach to the world of academia, radically improving the way scholarly research is managed. The grand vision of Frontiers is a world where all people have an equal opportunity to seek, share and generate knowledge. Frontiers provides immediate and permanent online open access to all its publications, but this alone is not enough to realize our grand goals.

## Frontiers journal series

The Frontiers journal series is a multi-tier and interdisciplinary set of open-access, online journals, promising a paradigm shift from the current review, selection and dissemination processes in academic publishing. All Frontiers journals are driven by researchers for researchers; therefore, they constitute a service to the scholarly community. At the same time, the *Frontiers journal series* operates on a revolutionary invention, the tiered publishing system, initially addressing specific communities of scholars, and gradually climbing up to broader public understanding, thus serving the interests of the lay society, too.

## Dedication to quality

Each Frontiers article is a landmark of the highest quality, thanks to genuinely collaborative interactions between authors and review editors, who include some of the world's best academicians. Research must be certified by peers before entering a stream of knowledge that may eventually reach the public - and shape society; therefore, Frontiers only applies the most rigorous and unbiased reviews. Frontiers revolutionizes research publishing by freely delivering the most outstanding research, evaluated with no bias from both the academic and social point of view. By applying the most advanced information technologies, Frontiers is catapulting scholarly publishing into a new generation.

## What are Frontiers Research Topics?

Frontiers Research Topics are very popular trademarks of the *Frontiers journals series*: they are collections of at least ten articles, all centered on a particular subject. With their unique mix of varied contributions from Original Research to Review Articles, Frontiers Research Topics unify the most influential researchers, the latest key findings and historical advances in a hot research area.

Find out more on how to host your own Frontiers Research Topic or contribute to one as an author by contacting the Frontiers editorial office: frontiersin.org/about/contact

# New insight into the roles of microorganisms in municipal and environmental engineering technologies/systems

**Topic editors**
Xiaochen Chen – Fuzhou University, China
Hongbo Li – Nanjing University, China
Ming Zeng – Tianjin University of Science and Technology, China
Xianhua Liu – Tianjin University, China
Ikuro Kasuga – The University of Tokyo, Japan

**Topic Coordinator**
Xiaolin Cai – University of Chinese Academy of Sciences, China

**Citation**
Chen, X., Li, H., Zeng, M., Liu, X., Kasuga, I., Cai, X., eds. (2024). *New insight into the roles of microorganisms in municipal and environmental engineering technologies/systems*. Lausanne: Frontiers Media SA.
doi: 10.3389/978-2-8325-4312-2

# Table of contents

04 Editorial: New insight into the roles of microorganisms in municipal and environmental engineering technologies/systems
Xiaochen Chen, Ikuro Kasuga, Xianhua Liu, Hongbo Li, Ming Zeng and Xiaolin Cai

07 Rhizosphere and Straw Return Interactively Shape Rhizosphere Bacterial Community Composition and Nitrogen Cycling in Paddy Soil
Ya-Hui Zhao, Ning Wang, Meng-Kang Yu, Jian-Guang Yu and Li-Hong Xue

18 Efficacy of simultaneous hexavalent chromium biosorption and nitrogen removal by the aerobic denitrifying bacterium *Pseudomonas stutzeri* YC-34 from chromium-rich wastewater
Keyin Yang, Huijun Bu, Ying Zhang, Hongxia Yu, Sining Huang, Lixia Ke and Pei Hong

31 Differences, links, and roles of microbial and stoichiometric factors in microplastic distribution: A case study of five typical rice cropping regions in China
Yao Yao, Lili Wang, Lingxuan Gong, Gang Li, Weiming Xiu, Xiaomei Yang, Bingchang Tan, Jianning Zhao and Guilong Zhang

46 Environmental drivers and interaction mechanisms of heavy metal and antibiotic resistome exposed to amoxicillin during aerobic composting
Ning Liu, Gang Li, Ya Su, Yi Zhao, Jun Ma and Guangqun Huang

58 Research progress of electrochemical oxidation and self-action of electric field for medical wastewater treatment
Jun Tang, Heng Zheng, Jinzhong Cai, Jiang Liu, Yangyang Wang and Jun Deng

64 A novel algicidal properties of fermentation products from *Pseudomonas* sp. Ps3 strain on the toxic red tide dinoflagellate species
Luwei Zheng, Hong Lin, Barathan Balaji-Prasath, Yuping Su, Ying Wang, Yi Zheng and Guanglang Yu

77 Effect of the bacterial community assembly process on the microbial remediation of petroleum hydrocarbon-contaminated soil
Xuehao Zheng, Belay Tafa Oba, Chenbo Shen, Luge Rong, Bin Zhang, Ling Huang, Lujie Feng, Jiani Liu, Tiantian Du and Yujie Deng

85 Dispersive biofilm from membrane bioreactor strains: effects of diffusible signal factor addition and characterization by dispersion index
Wonjung Song, Junhee Ryu, Jaehyun Jung, Youngjae Yu, Suyoung Choi and Jihyang Kweon

97 Pb(II)-inducible proviolacein biosynthesis enables a dual-color biosensor toward environmental lead
De-long Zhu, Yan Guo, Bing-chan Ma, Yong-qin Lin, Hai-jun Wang, Chao-xian Gao, Ming-qi Liu, Nai-xing Zhang, Hao Luo and Chang-ye Hui

frontiers | Frontiers in Microbiology

TYPE Editorial
PUBLISHED 05 January 2024
DOI 10.3389/fmicb.2023.1349701



OPEN ACCESS

EDITED AND REVIEWED BY
William James Hickey,
University of Wisconsin-Madison,
United States

*CORRESPONDENCE
Xiaochen Chen
✉ chenxiaochen@fzu.edu.cn

RECEIVED 05 December 2023
ACCEPTED 18 December 2023
PUBLISHED 05 January 2024

CITATION
Chen X, Kasuga I, Liu X, Li H, Zeng M and Cai X (2024) Editorial: New insight into the roles of microorganisms in municipal and environmental engineering technologies/systems.
*Front. Microbiol.* 14:1349701.
doi: 10.3389/fmicb.2023.1349701



# Editorial: New insight into the roles of microorganisms in municipal and environmental engineering technologies/systems

Xiaochen Chen[1]*, Ikuro Kasuga[2], Xianhua Liu[3], Hongbo Li[4], Ming Zeng[5] and Xiaolin Cai[6]

[1]Innovation Center for Soil Remediation and Restoration Technologies, College of Environment and Safety Engineering, Fuzhou University, Fuzhou, Fujian, China, [2]Department of Urban Engineering, Graduate School of Engineering, The University of Tokyo, Tokyo, Japan, [3]School of Environmental Science and Engineering, Tianjin University, Tianjin, China, [4]School of Environment, Nanjing University, Nanjing, China, [5]College of Marine and Environmental Sciences, Tianjin University of Science and Technology, Tianjin, China, [6]College of Resources and Environment, University of Chinese Academy of Sciences, Beijing, China

KEYWORDS

**municipal engineering, environmental engineering, microorganisms, conventional contaminants, emerging contaminants, advanced technologies/systems**

Editorial on the Research Topic
New insight into the roles of microorganisms in municipal and environmental engineering technologies/systems

Aiming at promoting human wellbeing, the municipal and environmental scientists and engineers have developed many technologies and systems to deal with a variety of contaminants (e.g., nutrients, heavy metals, organic contaminants, and pathogens) existing in our ambient environment, in which microorganisms play important roles. On the one hand, microorganisms act a leading role, contributing to the degradation and transformation of the contaminants via metabolism. On the other hand, as a part of the targeted environments or even targeted pollutants, the passive microbial communities can actively sense and respond to the environmental changes, which reflects the performance of the applied technologies/systems or their influences on the health of ecosystems and living organisms.

As modernization, urbanization and industrialization prevail, the environmental quality of the earth keeps on deteriorating. Moreover, some new contaminants come into people's sight, and seem to shift from "unprecedented" to "ubiquitous" overnight, including the latest research hotspots like microplastics (MPs) and antibiotic resistance genes (ARGs). These emerging contaminants and the conventional contaminants could independently or interactively challenge the existing engineering technologies and systems by increasing the level of uncertainty and the risks of malfunction and failure (Bayabil et al., 2022; Puri et al., 2023). Hence, it is very crucial to keep our knowledge about the roles of related microorganisms up to date, so that guidance on the upgrade, optimization and innovation of the technologies/systems could be timely and efficiently offered. Fortunately, a dozen of high-quality papers answered our call-for-papers, and nine are eventually collected in our Research Topic, which cover the Research Topic mainly from three aspects.

The first aspect is the interactions between microbes and contaminants, focusing on mechanistical elucidation. There are three papers involved. Firstly, microbiological nitrogen removal from wastewater is a key issue in municipal and environmental engineering, which in common sense is very susceptible to high concentrations of co-existing heavy metals (HMs). Yang et al. made a breakthrough in advanced wastewater treatment, as a unique aerobic denitrifier was successfully isolated. In addition to efficient auto-aggregating capacity, it showed the potential in simultaneously achieving the nitrogen removal and the biosorption and reduction of highly toxic Cr(VI). Secondly, soil contamination by petroleum hydrocarbons (PHs) is another chronic problem worldwide. Although the PH-degrading bacteria for remediation purpose are available, Zheng X. et al. noticed that the role of microbial ecological processes, including microbial interactions, had been neglected. One of their key findings was that the deterministic assembly of microbial communities mediated the efficient PHs removal. Accordingly, it is recommended to avoid significant soil disturbance during remediation, as directional regulation of microbial ecological functions plays a key role. Thirdly, aerobic composting is a common practice in centralized treatment and resourcilization of manure, while the combined pollution of HMs and ARGs has drawn broad attention. Liu et al. comprehensively studied the interactive mechanisms and environmental drivers of HMs resistome, antibiotic resistance and microbiome. Key findings related to amoxicillin exposure, such as the elevation of HMs and antibiotic resistome, and the discovery of two biomarkers and an important driver, potentially contribute to the synergistic treatment of these pollutants.

The second aspect is microbial sensing and responses to environmental changes, and four papers are involved. Firstly, biofilm universally exists in municipal/environmental water and wastewater treatment processes, and its excessive formation inevitably deteriorates system performance. With a signal compound *cis*-2-Decenoic acid, Song et al. succeeded in controlling the quorum sensing systems and the consequent functions of biofilm microbial communities, including motility, enzyme production, and extracellular polymeric substance. The results contribute to the evaluation on dispersive intensity of biofilm and the relevant biofouling control practices. Secondly, since severe air pollution is caused by straw combustion, straw return on land is highly recommended in the field of agro-environmental engineering. It is worth noting that the interactions between rice roots (rhizosphere) and straw return is likely to significantly influence the establishment of soil microbial community structure and nitrogen cycle, determining soil fertility. Zhao et al.'s study provides a deep insight into the pronounced impacts of straw amendments, and reference for straw return practice. Thirdly, new contaminant MPs widely exist in agroecosystems, but the influencing factors on its geographic distribution, both the biological and the abiotic, remains poorly understood. Yao et al. carried out a case study of five typical rice cropping regions in China, focusing on differences, links and roles of stoichiometric and microbial influences. The findings enrich our knowledge about the toxicology and health risk related to MPs. Lastly, based on synthetic biology (gene transcription), an invention about detecting lead in environmental water was made by Zhu et al. Their dual-color biosensor with direct reading by naked eyes and colorimetric quantification has many advantages in toxic heavy metal monitoring and commercialization potential, such as wide detection (concentration) range, few interfering factors (co-existing metals), user friendliness, and low cost.

The third aspect including two papers is monitoring and control of microbial stability, as well as the relevant environmental and health risks. Red tide caused by dinoflagellates, a form of eutrophication, is threatening water quality and human health of almost all the densely-populated coastal regions. Zheng L. et al. came up with a novel controlling approach, i.e., using the fermentation products from *Pseudomonas* sp. Ps3 strain, which turned out to be very effective in algae-lysis and inhibition in bench scale. In addition, in post-COVID-19 era, public health and safety is still of great concern. Medical wastewater contains a large number of pathogens, and requires careful and effective treatment. Tang et al. composed a comprehensive review on electrochemical disinfection technology for medical wastewater. By reviewing its development status, proposing three-stage system, and discussing its prospects, this paper provide guidance on the research and employment of this promising technology.

As abovementioned, these papers greatly enrich our knowledge about the roles of microorganisms in municipal and environmental engineering. However, as guest editors, we realize that there are still important topics or fields missing, especially for novel approaches for the enhancement of microbial performance, e.g., coupling with functional materials (Echeverria et al., 2020) and rhizoremediation (Kotoky et al., 2018); and bioenvironmental and energy engineering processes for organic waste recycling and agricultural/aquaculture system (Wang et al., 2017). Therefore, Volume II of this Research Topic is recently released, aiming at further assisting the scientists and engineers rise up to the complicated environmental challenges.

## Author contributions

XCh: Writing – original draft, Writing – review & editing. IK: Writing – review & editing. XL: Writing – review & editing. HL: Writing – review & editing. MZ: Writing – review & editing. XCa: Writing – original draft.

## Funding

The author(s) declare that no financial support was received for the research, authorship, and/or publication of this article.

## Acknowledgments

The editors would like to express sincere gratitude to all the authors and reviewers for your valuable contributions to this Research Topic.

## Conflict of interest

The authors declare that the research was conducted in the absence of any commercial or financial relationships that could be construed as a potential conflict of interest.

## Publisher's note



## References

Bayabil, H., Teshome, F., and Li, Y. (2022). Emerging contaminants in soil and water. *Front. Environ. Sci.* 10, 873499. doi: 10.3389/fenvs.2022.873499

Echeverria, C., Ozkan, J., Pahlevani, F., Willcox, M., and Sahajwalla, V. (2020). Multifunctional marine bio-additive with synergistic effect for non-toxic flame-retardancy and anti-microbial performance. *Sustain. Mater. Technol.* 25, e00199. doi: 10.1016/j.susmat.2020.e00199

Kotoky, R., Rajkumari, J., and Pandey, P. (2018). The rhizosphere microbiome: significance in rhizoremediation of polyaromatic hydrocarbon contaminated soil. *J. Environ. Manage.* 217, 858–870. doi: 10.1016/j.jenvman.2018.04.022

Puri, M., Gandhi, K., and Kumar, M. (2023). Emerging environmental contaminants: A global perspective on policies and regulations. *J. Environ. Manage.* 332, 117344. doi: 10.1016/j.jenvman.2023.117344

Wang, X., Li,. Z., Long, P., Yan, L., Gao, W., Chen, Y., et al. (2017). Sustainability evaluation of recycling in agricultural systems by emergy accounting. *Resour. Conserv. Recycl.* 117, 114–124. doi: 10.1016/j.resconrec.2016.11.009

frontiers | Frontiers in Microbiology

ORIGINAL RESEARCH
published: 07 July 2022
doi: 10.3389/fmicb.2022.945927

# Rhizosphere and Straw Return Interactively Shape Rhizosphere Bacterial Community Composition and Nitrogen Cycling in Paddy Soil

*Ya-Hui Zhao[1†], Ning Wang[1,2,3*†], Meng-Kang Yu[1,4], Jian-Guang Yu[1,2,3] and Li-Hong Xue[1,2,3]*

*[1] Key Laboratory of Agro-Environment in Downstream of Yangtze Plain, Ministry of Agriculture, P.R. China, Jiangsu Academy of Agricultural Sciences, Nanjing, China, [2] School of the Environment and Safety Engineering, Jiangsu University, Zhenjiang, China, [3] Jiangsu Key Laboratory for Food Quality and Safety, State Key Laboratory Cultivation Base of Ministry of Science and Technology, Nanjing, China, [4] Henan Institute of Science and Technology, Xinxiang, China*

Currently, how rice roots interact with straw return in structuring rhizosphere communities and nitrogen (N) cycling functions is relatively unexplored. In this study, paddy soil was amended with wheat straw at 1 and 2% w/w and used for rice growth. The effects of the rhizosphere, straw, and their interaction on soil bacterial community composition and N-cycling gene abundances were assessed at the rice maturity stage. For the soil without straw addition, rice growth, i.e., the rhizosphere effect, significantly altered the bacterial community composition and abundances of N-cycling genes, such as archaeal and bacterial *amoA* (*AOA* and *AOB*), *nirK*, and *nosZ*. The comparison of bulk soils between control and straw treatments showed a shift in bacterial community composition and decreased abundance of *AOA*, *AOB*, *nirS*, and *nosZ*, which were attributed to sole straw effects. The comparison of rhizosphere soils between control and straw treatments showed an increase in the *nifH* gene and a decrease in the *nirK* gene, which were attributed to the interaction of straw and the rhizosphere. The number of differentially abundant genera in bulk soils between control and straw treatments was 13–23, similar to the number of 16–22 genera in rhizosphere soil between control and straw treatment. However, the number of genera affected by the rhizosphere effect was much lower in soil amended with straw (3–4) than in soil without straw addition (9). Results suggest possibly more pronounced impacts of straw amendments in shaping soil bacterial community composition.

**Keywords: rhizosphere, straw return, bacterial communities, nitrogen cycling, interactively**

OPEN ACCESS

***Edited by:***
*Hongbo Li,*
*Nanjing University, China*

***Reviewed by:***
*Jun Zhao,*
*Nanjing Normal University, China*
*Jing Ding,*
*Yantai University, China*

***Correspondence:**
*Ning Wang*
*wang.ning4113@163.com*

*[†] These authors have contributed equally to this work*

***Specialty section:***
*This article was submitted to Microbiotechnology, a section of the journal Frontiers in Microbiology*

***Received:*** *17 May 2022*
***Accepted:*** *13 June 2022*
***Published:*** *07 July 2022*

***Citation:***
*Zhao Y-H, Wang N, Yu M-K, Yu J-G and Xue L-H (2022) Rhizosphere and Straw Return Interactively Shape Rhizosphere Bacterial Community Composition and Nitrogen Cycling in Paddy Soil. Front. Microbiol. 13:945927. doi: 10.3389/fmicb.2022.945927*

## HIGHLIGHTS

- Bulk and rhizosphere differed in bacterial communities and N-cycling genes.
- Straw amendment altered bacterial community composition and N-cycling.
- High numbers of genera were affected by straw in the rhizosphere than in the bulk.
- Fewer genera were affected by the rhizosphere when straw was returned to the soil.
- Straw amendments affected bacterial communities more pronouncedly than the rhizosphere.

## INTRODUCTION

The rhizosphere is a hotspot of root–microbe interaction that critically links with soil functions and plant nutrient acquisition (Moreau et al., 2019). *Via* root exudation, rhizodeposition, and nutrient uptake, plant roots are powerful drivers of microbial community assembly (Hu et al., 2018). Previous studies have shown that rhizosphere microbial communities are distinct from bulk soil (Li et al., 2018). Rhizosphere effects on microbial communities could be a result of taxonomic shifts, which in turn shape patterns of ecological interactions regulating the structure, function, and potential resilience of soil microbial communities (Wu et al., 2017; Langarica-Fuentes et al., 2018; Yuan et al., 2018). In particular, the potential for adaptive plant–microbe feedback is relevant for plant nitrogen (N) acquisition, which is a limiting nutrient in most agricultural ecosystems (Pérez-Izquierdo et al., 2019). Rhizosphere microbes can increase soil N supply to the plant and have substantial feedback on plant productivity *via* regulating N-cycling processes (Emmett et al., 2019; Pérez-Izquierdo et al., 2019). Recent studies have shown that the rhizosphere is enriched in functional genes related to N fixation (*nifH*), nitrification (*amoA*, *hao*), and denitrification (*narG*, *nirS*/*nirK*, *norB*, and *nosZ*) compared to bulk soils (Ai et al., 2013; Li et al., 2014; Wang et al., 2017). In agricultural systems, in-depth knowledge on factors controlling rhizosphere microbial communities and N-cycling may help inform agricultural management systems that harness rhizosphere processes to recouple plant–microbial N supply and demand to limit N losses (Ollivier et al., 2011; Bowles et al., 2015; Yu et al., 2015) while guaranteeing the health and productivity of plants (Manoeli et al., 2017; Zhalnina et al., 2018; Ding et al., 2019; Emmett et al., 2019; Maarastawi et al., 2019).

In agricultural systems, soil microbial communities and nutrient cycling are usually affected by the interactions of agricultural managements (e.g., straw return) and the rhizosphere environment (Schmidt et al., 2019). Among various agricultural managements, straw return is widely applied to increase soil organic carbon and soil fertility (Meng et al., 2017; Wang et al., 2018, 2020). Many studies have monitored changes in the soil microbial community following straw application (Zhao et al., 2016; Chen et al., 2017; Yang et al., 2019). In the early stage after straw return, bacteria dominate the crop residue decomposition, while fungi dominate at the later stage (Paterson et al., 2008; Marschner et al., 2011). In particular, crop residue return in flooded paddy soil significantly increases the relative abundance of Firmicute and decreases the abundance of Proteobacteria, thereby altering microbial community compositions (Wang et al., 2018). In addition, *via* altering the microorganism, straw return increases N fixation and reduces N losses, thereby increasing plant-N supply (Choudhury and Kennedy, 2004; Maeda et al., 2010; Chen et al., 2017). The responses of the microbial communities in bulk soils to agricultural management could help predict biogeochemical processes at the field or ecosystem scale (McGuire and Treseder, 2010; Graham et al., 2016). However, rhizosphere microbial communities, which are of critical importance for agricultural productivity, are shaped by interactions between agricultural management and plant selection processes (Schmidt et al., 2019). So far, how rice roots interact with straw return in structuring rhizosphere communities and N-cycling functions is relatively unexplored. The difference in microbial communities and N-cycling between bulk and rhizosphere soils without straw return can be contributed to rhizosphere effects, while the shifts of bulk soil induced by straw addition can be regarded as straw effects. In comparison, the interaction effects of rhizosphere and straw can be reflected by the variation in microbial communities and N-cycling in the rhizosphere with the straw return.

To explore the rhizosphere, straw, and their interaction effects on paddy soil microbial communities and N-cycling, a representative paddy soil was collected, added with wheat straw at two application rates (1 and 2%), and then used for rice growth under greenhouse conditions. Soil microbial communities and N-cycling-related gene abundances were measured for both bulk and rhizosphere soils at the rice maturity stage. The specific objectives were to (1) determine bacterial community diversity, composition, and N-cycling genes in bulk and rhizosphere with and without straw addition and (2) assess the relative roles of the rhizosphere, straw, and their interaction in influencing paddy soil bacterial diversity, composition, and N-cycling genes. This knowledge can contribute to better managing rhizosphere interactions and promoting both plant productivity and agroecosystem sustainability.

## MATERIALS AND METHODS

### Soil and Straw

Rice soil was collected from paddy fields of Taizhou, Jiangsu, China. The soil was derived from the fluvial deposit (Wang et al., 2021). After collection, the soil was air-dried, sieved (2 mm mesh), and homogenized for soil property analyses and rice growth. Soil properties were determined, including pH (6.79, 1:5 of soil-to-water ratio), total organic carbon (TOC, 23.7 g $kg^{-1}$), total nitrogen (TN, 1.15 g $kg^{-1}$), alkali-hydro nitrogen (AN, 36.7 mg $kg^{-1}$), available phosphorus (AP, 27.4 mg $kg^{-1}$), and available potassium (AK, 260 mg $kg^{-1}$) (Wang et al., 2021). Wheat straw was collected from a wheat production field during the harvest season. After air-drying, the straw was crushed to powder form and analyzed for contents of carbon (C, 46.5%) and N (0.48%). The ratio of C/N in the straw was 96.9.

### Experiment Setup

To assess the influences of straw return on soil microbial community, three soil treatments were performed in triplicates, namely, (1) control treatment without straw amendment, (2) straw treatment by adding 1% w/w wheat straw (dry weight basis, dw), and (3) straw treatment by adding 2% w/w wheat straw (dw). Straw was added at 1 and 2% to represent the straw return of ∼12 and 24 t $ha^{-1}$ under field conditions.

To allow for rice cultivation in a greenhouse, soils without or with straw addition were filled into pots using rhizo-bags separating bulk and rhizosphere. Initially, soils without or with

**TABLE 1** | Chemical characteristics of the rhizosphere and bulk soils without and with straw addition at the rice maturity stage ($n = 3$).

| Treatment | pH | EC μm cm$^{-1}$ | TOC (g kg$^{-1}$) | TN (g kg$^{-1}$) | AN (mg kg$^{-1}$) | $NH_4^+$-N (mg kg$^{-1}$) | $NO_3^-$ N (mg kg$^{-1}$) | AP (mg kg$^{-1}$) | AK (mg kg$^{-1}$) |
|---|---|---|---|---|---|---|---|---|---|
| BS0 | 6.97 ± 0.05$^{c}$ | 435 ± 3.30$^{a}$ | 8.85 ± 0.56$^{d}$ | 0.98 ± 0.02$^{e}$ | 88.6 ± 9.77$^{a}$ | 7.91 ± 0.26$^{b}$ | 9.65 ± 0.33$^{e}$ | 27.9 ± 3.45$^{a}$ | 70.0 ± 2.65$^{cd}$ |
| BS1 | 7.10 ± 0.07$^{ab}$ | 353 ± 51.4$^{a}$ | 9.93 ± 0.11$^{c}$ | 1.01 ± 0.03$^{de}$ | 108 ± 5.27$^{a}$ | 7.63 ± 0.40$^{b}$ | 11.8 ± 0.43$^{d}$ | 31.3 ± 2.62$^{a}$ | 115 ± 11.5$^{b}$ |
| BS2 | 7.11 ± 0.06$^{ab}$ | 398 ± 78.1$^{a}$ | 10.5 ± 0.05$^{b}$ | 1.14 ± 0.01$^{b}$ | 114 ± 5.01$^{a}$ | 10.0 ± 0.85$^{a}$ | 14.5 ± 0.24$^{c}$ | 29.5 ± 0.74$^{a}$ | 146 ± 21.7$^{a}$ |
| RS0 | 7.09 ± 0.05$^{b}$ | 390 ± 9.59$^{a}$ | 8.43 ± 0.32$^{d}$ | 1.04 ± 0.02$^{cd}$ | 104 ± 10.6$^{a}$ | 6.18 ± 0.05$^{c}$ | 21.6 ± 1.22$^{b}$ | 28.4 ± 1.09$^{a}$ | 47.3 ± 20.6$^{d}$ |
| RS1 | 7.18 ± 0.07$^{ab}$ | 372 ± 55.3$^{a}$ | 10.0 ± 0.18b$^{c}$ | 1.05 ± 0.01$^{c}$ | 98.8 ± 2.78$^{a}$ | 6.22 ± 0.45$^{c}$ | 23.1 ± 1.69$^{b}$ | 30.1 ± 4.40$^{a}$ | 79.0 ± 16.0$^{c}$ |
| RS2 | 7.22 ± 0.08$^{a}$ | 412 ± 20.9$^{a}$ | 11.1 ± 0.12$^{a}$ | 1.23 ± 0.01$^{a}$ | 95.5 ± 27.4$^{a}$ | 6.31 ± 0.63$^{c}$ | 34.4 ± 0.33$^{a}$ | 27.1 ± 2.39$^{a}$ | 140 ± 12.1$^{ab}$ |

*BS0, bulk soil without straw addition; BS1, bulk soil with addition of 1% straw addition; BS2, bulk soil with addition of 2% straw addition; RC, rhizosphere soil without straw addition; RS1, rhizosphere soil with addition of 1% straw addition; RS2, rhizosphere soil with addition of 2% straw addition; EC, electrical conductivity; TOC, total organic carbon; TN, total nitrogen; AN, available nitrogen; $NH_4^+$, ammonium; $NO_3^-$, nitrate; AP, available phosphorus; AK, available potassium. Different superscript letters indicate significant ($p < 0.05$) differences in various treatments.*

straw amendment were added with fertilizers, including urea (250 mg N kg$^{-1}$ dry soil), calcium superphosphate (60 mg P kg$^{-1}$ dry soil), and potassium chloride (100 mg K kg$^{-1}$ dry soil). Then, 1.5 kg dry weight (dw) of soil was transferred into rhizo-bags (30 μm nylon mesh, diameter 7.5 cm × height 23 cm), which were then placed in the center of polyvinyl chloride pots (diameter 15 cm × height 23 cm). Then, another 4.5 kg dw of soil was weighed into the pot to fill the space outside of the rhizo-bags. The rhizo-bags allow small molecular substrates to penetrate but prohibit roots to penetrate, thereby being a good way to divide rhizosphere from bulk soils (Nie et al., 2015). Soils were flooded for 3 days prior to the transplantation of rice seedlings (cv. Nanjing 9108). Uniform seedlings 3 days after germination were transplanted, with one seedling in each pot. Following transplantation, rice was daily flooded to maintain ∼2 cm overlying water during the period from seedling to flowering, while at the filling stage, rice was under the alternation of wetting and drying conditions to improve rice yield. At the maturity stage, i.e., 122 days after transplantation, rice was moved out from the rhizo-bags. The rhizosphere soils inside the rhizo-bags were collected and sieved (2 mm) to remove roots. The bulk soils outside the rhizo-bags were also collected and sieved. The rhizosphere and bulk soils were used for the analyses of soil properties, soil bacterial community structure, and N-related functional genes.

## Soil Property Analyses

The dried soils were mixed with $CO_2$-removed water at a soil:water ratio of 1:5 (w/v) prior to measurements of pH and electrical conductivity (EC) using corresponding electrodes. The soil was oxidized with potassium dichromate and measured for TOC using titration with ferrous ammonium sulfate. Soil TN was measured by an elemental analyzer (Vario MAX CNS, Elementar, Germany). AN was measured using the alkali solution diffusion method (Lu, 2000). Concentrations of soil ammonium ($NH_4^+$) and nitrate ($NO_3^-$) were analyzed using ion chromatography (ICS-3000, Dionex, United States) following extraction with 2 M KCl. AK and AP were measured using an inductively coupled plasma optical emission spectrometer (Optima 5300DV, PerkinElmer, United States).

## Bacterial Community Analyses

A total of 18 soil samples, collected from bulk and rhizosphere of control and straw treatments, were subjected to soil bacterial community diversity and composition analysis using Illumina sequencing. Genomic DNA in the soil samples was extracted using a FastDNA SPIN Kit. The bacterial 16S rRNA gene was amplified using primers [515F (5′–GTGCCAGCMGCCGCGG–3′), 907R (5′–CCGTCAATTCMTTTRAGTTT–3′)] that target V4–V5 region. The thermal profile of PCR included an initial denaturation at 95°C for 3 min, 30-cycle denaturing at 95°C for 30 , annealing at 58°C for 1 min, extension at 72°C for 45 s, and a final extension step at 72°C for 10 min. Equal amounts of PCR products from different samples (barcoded) were mixed, purified, and quantified prior to Illumina sequencing at Shanghai Lingen Genomics Institute, China (Wang et al., 2015).

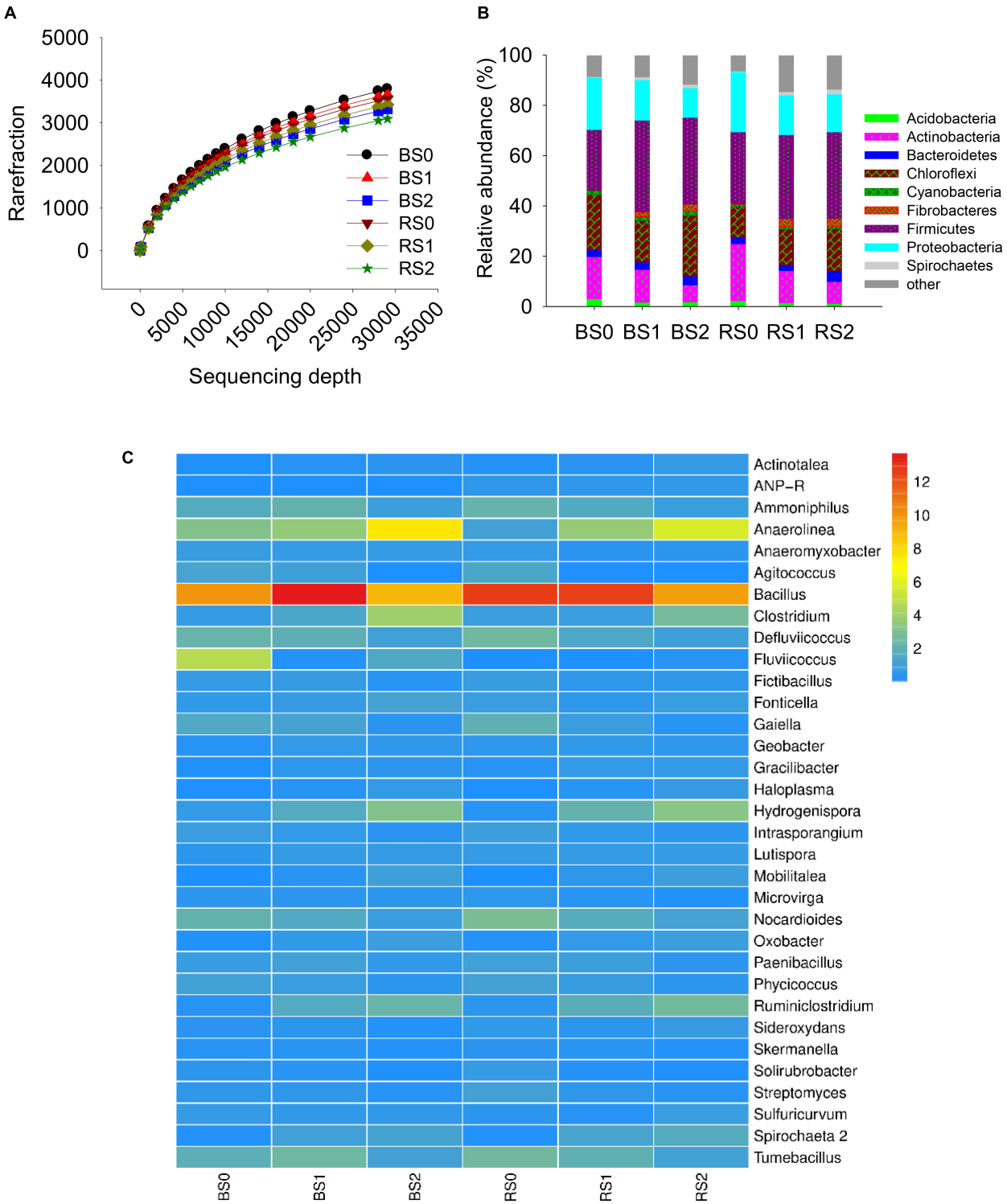


**FIGURE 1 |** Rarefaction distribution **(A)**, and the relative abundances in class **(B)** and genera **(C)** level of bacterial community composition in bulk and rhizosphere of paddy soils with and without straw amendment. Each column represents the mean value of triplicate analyses. BS0, bulk soil without straw addition; BS1, bulk soil with addition of 1% straw addition; BS2, bulk soil with addition of 2% straw addition; RS0, rhizosphere soil without straw addition; RS1, rhizosphere soil with addition of 1% straw addition; RS2, rhizosphere soil with addition of 2% straw addition.

**TABLE 2 |** Diversity and abundance indices of bacterial community with and without straw addition.

| Treatments | Richness index | Diversity index | | Coverage index |
|---|---|---|---|---|
| | Chao | Shannon | Simpson | Coverage |
| BS0 | 5458 ± 219$^{a}$ | 6.893 ± 0.162$^{a}$ | 0.00458 ± 0.00222$^{a}$ | 0.9584 ± 0.0047$^{a}$ |
| BS1 | 5427 ± 285$^{a}$ | 6.879 ± 0.063$^{a}$ | 0.00392 ± 0.00040$^{a}$ | 0.9634 ± 0.0093$^{a}$ |
| BS2 | 5165 ± 323$^{ab}$ | 6.696 ± 0.124$^{ab}$ | 0.00478 ± 0.00056$^{a}$ | 0.9699 ± 0.0047$^{a}$ |
| RS0 | 5110 ± 217$^{ab}$ | 6.827 ± 0.143$^{ab}$ | 0.00409 ± 0.00121$^{a}$ | 0.9620 ± 0.0060$^{a}$ |
| RS1 | 5446 ± 338$^{a}$ | 6.696 ± 0.047$^{ab}$ | 0.00469 ± 0.00040$^{a}$ | 0.9702 ± 0.0051$^{a}$ |
| RS2 | 4740 ± 236$^{b}$ | 6.613 ± 0.091$^{b}$ | 0.00477 ± 0.00141$^{a}$ | 0.9692 ± 0.0065$^{a}$ |

*BS0, bulk soil without straw addition; BS1, bulk soil with addition of 1% straw addition; BS2, bulk soil with addition of 2% straw addition; RS0, rhizosphere soil without straw addition; RS1, rhizosphere soil with addition of 1% straw addition; RS2, rhizosphere soil with addition of 2% straw addition. Different superscript letters indicated significant ($p < 0.05$) differences in various treatments.*

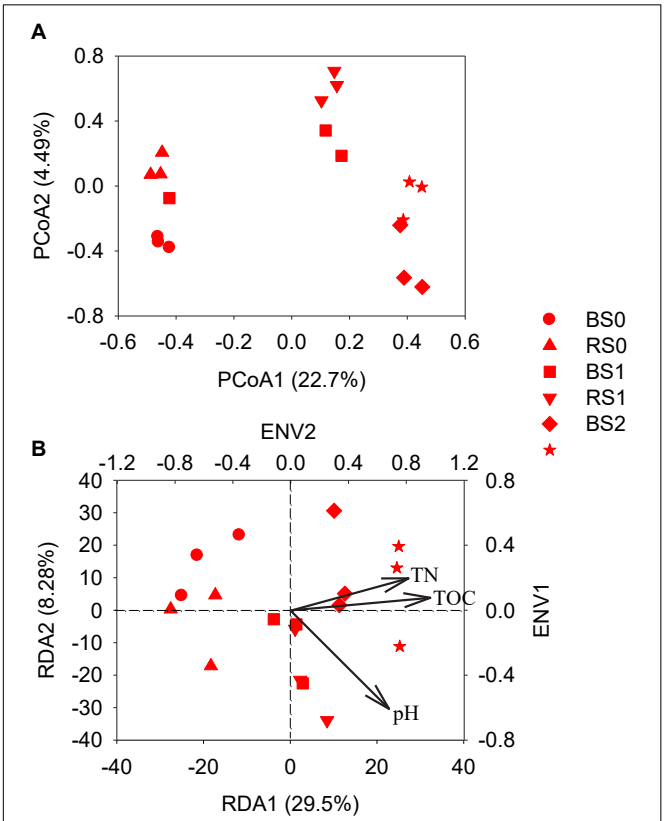


**FIGURE 2 |** Principal coordinate analysis (PCoA) and redundancy analysis (RDA) of bacterial community composition **(A,B)** in rhizosphere and bulk from paddy soils with and without straw amendment. BS0, bulk soil without straw addition; BS1, bulk soil with addition of 1% straw addition; BS2, bulk soil with addition of 2% straw addition; RS0, rhizosphere soil without straw addition; RS1, rhizosphere soil with addition of 1% straw addition; RS2, rhizosphere soil with addition of 2% straw addition.

The sequence data were processed using the Quantitative Insights into Microbial Ecology toolkit (QIIME, version 1.7.0) the data presented in the study are deposited in the GenBank Data repository, accession number PRJNA847362. After removing the low quality or ambiguous reads, the identified sequences were then clustered into operational taxonomic units (OTUs) at a 97% similarity level, and the representative sequence (i.e., the most abundant sequence) was assigned to taxonomy by an RDP classifier (version 2.2; Wang et al., 2007). Based on the OTU matrix, principal coordinate analysis (PCoA) was performed to assess the differences in overall community composition between bulk and rhizosphere with different amounts of the straw amendment (Lozupone et al., 2005). Moreover, heatmaps based on genus level and redundancy analysis (RDA) were conducted using R software (version 2.14.0) and the community ecology package vegan (2.0–4) to identify soil properties (including pH, EC, TOC, TN, AN, $NH_4^+$–N, $NO_3^-$–N, AP, and AK) contributing to the altered bacterial community (Oksanen et al., 2013). Envfit function (999 permutations) analyses were used to remove environmental variables that insignificantly contributed to the total soil bacterial community variance. Significant differences in the major genus of bacterial community composition between rhizosphere and bulk soils or between control and straw treatments were assessed by Student's *t*-test ($p < 0.05$).

## N-Cycling Functional Genes

Primer pairs of *nifHF/nifHR* (Rosch et al., 2002), Arch-*amoA*-F/Arch-*amoA*-R (Francis et al., 2005), *amoA-1F/amoA-1R* (Rotthauwe et al., 1997), *nirK-F1aCu/nirK-R3Cu* (Throbäck et al., 2004), *nirS-cd3aF/nirS-R3cd* (Hallin and Lindgren, 1999), and *nosZ*-F/*nosZ-1622*R (Throbäck et al., 2004) were used to quantify *nifH*, archaeal and bacterial *amoA* (*AOA* and *AOB*), *nirK*, *nirS*, and *nosZ* genes in soil samples using real-time PCR system (ABI 7500, American), respectively (**Supplementary Table 2**). Following DNA extraction, each gene was amplified using a 20 μl system, i.e., 10 μl SYBR® Premix Ex Taq™ II (2×), 0.4 μl ROX reference Dye II (50×), 0.8 μl forward primer (10 μM), 0.8 μl reverse primer (10 μM), 6 μl $ddH_2O$, and 2 μl template DNA (20 ng). Real-time PCR conditions for target genes are listed in **Supplementary Table 2**. Gene standard curves were constructed based on gradient dilutions of standard plasmids containing each gene with known copy numbers. To ensure correct amplification, DNA extracts were highly diluted to eliminate the inhibition. To ensure no contamination during qPCR, negative controls without DNA templates were included in each patch of gene amplification. In addition, gene quantification of each sample was performed in three parallel

real-time PCR reactions, with reactions of efficiencies > 90% and correlation coefficients $r^2 > 0.99$ being accepted. Target gene copy numbers of each sample were calculated from the standard curves and expressed on a basis of soil dw (copies $g^{-1}$ dw soil).

# RESULTS

## Soil Properties

For control treatment without straw return, there were significant differences in soil properties between rhizosphere and bulk (**Table 1**), indicating the sole rhizosphere effects. Soil TN (1.04 g $kg^{-1}$) and $NO_3^-$–N (21.6 mg $kg^{-1}$) concentrations were significantly higher in the rhizosphere than in bulk soil (0.98 g $kg^{-1}$ and 9.65 mg $kg^{-1}$). In contrast, the rhizosphere showed significantly lower $NH_4^+$–N concentration (6.18 mg $kg^{-1}$) than bulk soil (7.91 mg $kg^{-1}$). The pH of the rhizosphere was 7.09, significantly higher than that of bulk soil (6.97). There were insignificant differences in other soil properties.

For bulk soil, changes in soil properties with straw addition were observed (**Table 1**), indicating the sole straw effects. Excluding EC, AN, and AP, significant increases were observed in bulk soil pH (from 6.97 to 7.11), TOC (from 8.85 to 10.5 g $kg^{-1}$), TN (from 0.98 to 1.14 g $kg^{-1}$), $NH_4^+$–N (from 7.91 to 10.0 mg $kg^{-1}$), $NO_3^-$–N (from 9.65 to 14.5 mg $kg^{-1}$), and AK (from 70.0 to 146 mg $kg^{-1}$) with straw addition.

Changes in rhizosphere soil properties were also observed following straw addition (**Table 1**), indicating the interactions of rhizosphere and straw. Like bulk soil, EC, AN, and AP insignificantly changed with straw addition. In addition, $NH_4^+$–N concentrations (6.22–6.31 mg $kg^{-1}$) of straw-treaded rhizosphere soils were also not significantly different from that of control rhizosphere soil (6.18 mg $kg^{-1}$). In comparison, straw addition significantly increased rhizosphere soil pH (from 7.09 to 7.22), TOC (from 8.43 to 11.1 g $kg^{-1}$), TN (from 1.04 to 1.23 g $kg^{-1}$), $NO_3^-$–N (from 21.6 to 34.4 mg $kg^{-1}$), and AK (from 47.3 to 140 mg $kg^{-1}$).

Nitrogen content in the root, shoot, and rice from paddy soils with different amounts of straw addition are listed in **Supplementary Table 1**, showing that straw addition significantly increased the N content in the root, shoot, and rice from paddy soils.

## Bacterial Community Diversity and Composition

Rarefaction of observed species showed that even at a sequencing depth of 290,704, the diversity of soil bacteria continued increasing rapidly with increasing sequencing depth (**Figure 1A**), suggesting the high diversity of soil bacteria. Insignificant differences in Chao, Shannon, Simpson, and Coverage index at the sequencing depth were observed between bulk and rhizosphere soils or between control and straw treatments (**Table 2**), suggesting that rhizosphere, straw, and their interactions had no effects on internal bacterial community diversity.

The major bacterial community compositions at class level were Actinobacteria (3.53–11.1%), Alphaproteobacteria (3.84–11.1%), Anaerolineae (6.22–22.0%), Bacilli (13.4–22.7%), Clostridia (6.99–20.4%), Deltaproteobacteria (3.21–5.19%), and Gammaproteobacteria (4.19–10.7%) (**Figure 1B**). The major bacterial community compositions at genus level were *Anaerolinea* (1.12–7.57%), *Bacillus* (9.67–13.7%), *Clostridium* (0.71–3.97%), *Defluviicoccus* (1.04–2.54%), *Fonticella* (0.58–1.20%), *Nocardioides* (0.87–2.84%), *Tumebacillus* (1.16–2.60%), with *Bacillus* being the dominant genera (**Figure 1C**).

The PCoA showed that the bacterial community compositions of the rhizosphere soils were significantly different from that of the bulk soils for control treatment or straw treatment at 1% (**Figure 2A**). However, for straw addition at 2%, the bacterial community compositions of bulk soils were overlapped with those of rhizosphere according to Adonis analysis ($p > 0.05$).

Regardless of bulk and rhizosphere soils, the bacterial community compositions of soils with straw addition were significantly separated from those of soils without straw addition ($p < 0.05$). This indicated that straw addition significantly changed the bacterial community composition of both bulk and rhizosphere soils, while root growth significantly altered the bacterial community composition for soils without and with a lower rate of straw addition. At higher straw application, the relatively stronger influence of straw might have obscured the effect of the rhizosphere on bacterial community compositions.

By envfit function (999 permutations), soil pH, TN, and TOC were found to be significantly correlated with the bacterial community composition at the OTU level (**Figure 2B**). RDA showed that variation in these three factors together explained 41.5% of soil bacterial community composition variation in bulk and rhizosphere soils with or without straw addition.

## Number of Differentially Abundant Genera

The genera whose relative abundance significantly varied with straw, rhizosphere, or their interaction effects were identified (**Figure 3**). By comparing bulk and rhizosphere soils without straw addition, a total of nine genera showed significant ($p < 0.05$) differences in relative abundances. However, by comparing bulk and rhizosphere soils treated with 1 or 2% straw, three or four genera were identified (**Figures 3A–C**), suggesting that the rhizosphere effect might be weakened when straw was returned to the soil.

For the straw effect, the number of differentially abundant taxa between bulk soils without and with the addition of straw at 1% was 13, while the number was 23 when straw was added at 2% (**Figures 3D,E**). These results suggested that compared to the rhizosphere effect, the straw effect affected more genera, highlighting the possible stronger impacts of straw amendments on soil bacterial community composition.

For the interaction effect of rhizosphere and straw, we observed 16 and 22 differentially abundant genera in rhizosphere

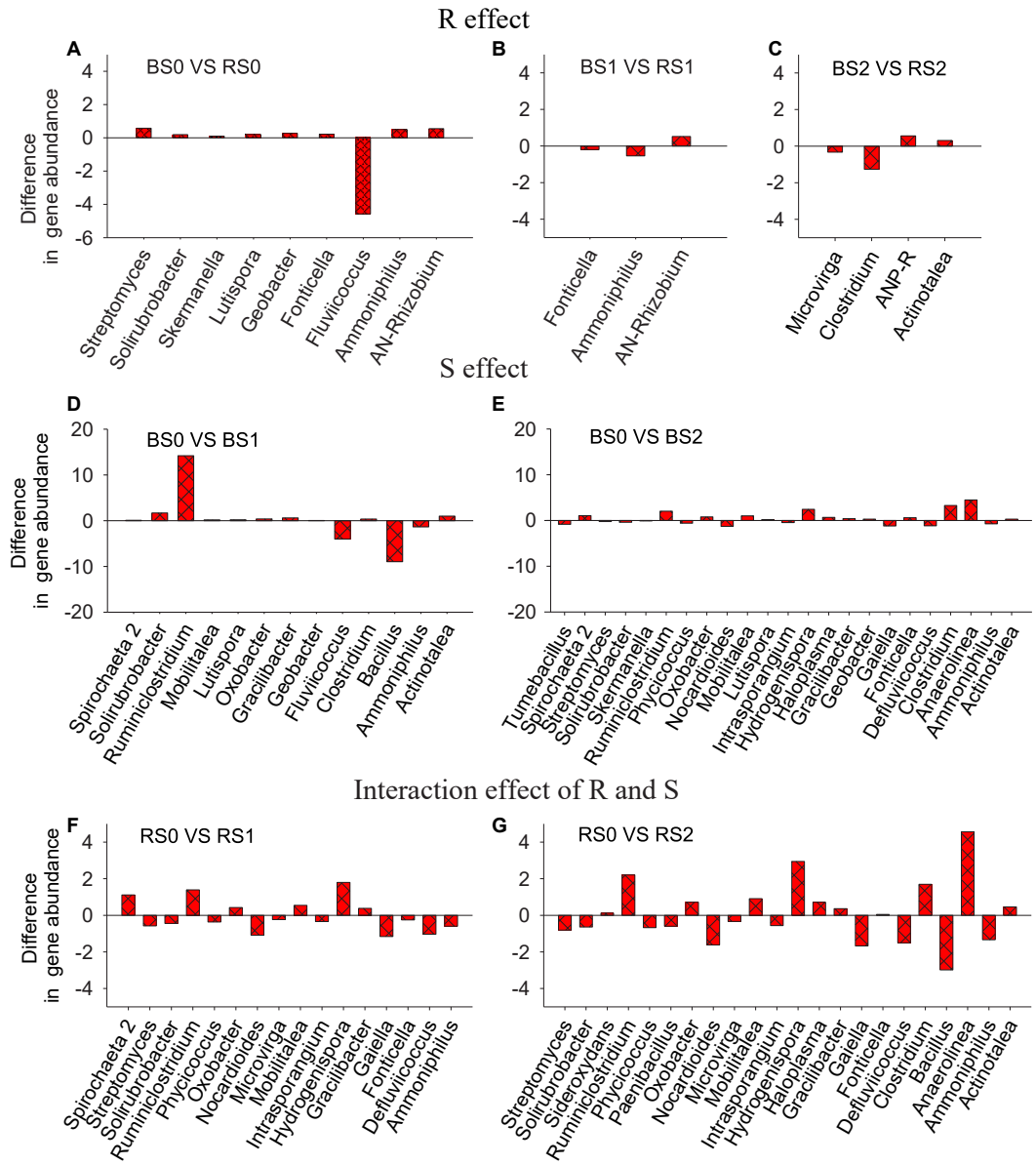


**FIGURE 3 |** Responses of genera abundances in bacterial community composition to rhizosphere (R, **A–C**), straw (S, **D,E**) effects, or their interaction (R × S, **F,G**). R effect can be reflected by the difference in microbial communities between bulk and rhizosphere soils without straw return; S effect can be reflected by the variation in microbial communities in bulk soil with and without straw return; the interaction effect of R and S can be reflected by the variation in microbial communities in rhizosphere with straw return.

soils when comparing control and 1% straw treatments and comparing control and 2% straw treatments (**Figures 3F,G**).

## N-Cycling Functional Genes

Bulk and rhizosphere soils without or with straw amendment varied in N-cycling functional genes (**Figure 4**). For control soils without straw addition, the abundances of archaeal *amoA*, *nirK*, and *nosZ* genes were significantly higher in the rhizosphere, but the abundance of bacterial *amoA* gene was lower compared to bulk soils. There were insignificant differences in the abundances of *nifH* and *nirS* genes between bulk and rhizosphere soils without straw addition. In comparison, for soils with 1% straw application, the gene abundances of archaeal *amoA* and bacterial *amoA* were lower in the rhizosphere than in bulk, while other genes were similar between rhizosphere and bulk. For soils with 2% straw application, *nifH* gene abundance was significantly higher in the rhizosphere compared to bulk soils.

For bulk soils, straw amendment significantly decreased the gene abundances of archaeal *amoA* and bacterial *amoA*, which decreased at higher extents at a higher straw application rate (**Figure 4**). The gene abundances of *nirS* and *nosZ* were also significantly decreased in bulk soils with straw addition, but

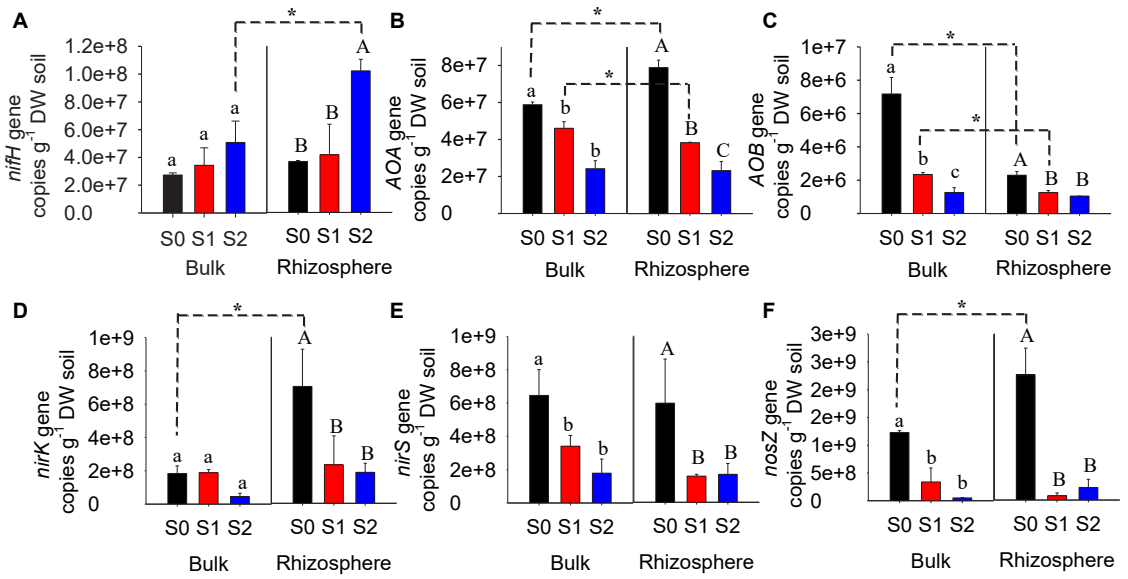


**FIGURE 4 |** Genes copy number of N-cycling genes (*nifH*, *AOA*, *AOB*, *nirK*, *nirS*, and *nosZ*) in bulk and rhizosphere of paddy soils with and without straw amendment **(A–F)**. Different upper letters indicated significant ($p < 0.05$) differences in various treatments; *Indicates significant ($p < 0.05$) differences between bulk and rhizosphere. S0, soil without straw addition; S1, soil with 1% straw addition; S2, soil with 2% straw addition.

unaffected by the straw application rate. No obvious difference in *nifH* and *nirK* gene abundances was observed in bulk soils with the straw amendment.

Like bulk soils, the straw amendment also significantly decreased the gene abundance of archaeal *amoA*, bacterial *amoA*, *nirK*, *nirS,* and *nosZ* in rhizosphere soils (**Figure 4**). At a higher rate of straw addition, the gene abundance of archaeal *amoA* was decreased to a higher extent, while the gene abundance of bacterial *amoA*, *nirK*, *nirS,* and *nosZ* was decreased at similar extents when 1 and 2% straw were amended. In comparison, the gene abundance of *nifH* was increased by 2% straw addition, while it was not affected by 1% straw addition.

## DISCUSSION

In this study, we assessed how root and straw return acted individually or in combination in shaping bacterial community composition and N-cycling functions. Rhizosphere is a unique zone and plays a vital role in N fixation, nitrification, and denitrification (Arth et al., 1998; Nie et al., 2014; Moreau et al., 2019). We observed that the rhizosphere significantly altered soil bacterial community composition (**Figure 2A**), and the changes in soil pH, TOC, and TN concentrations were critical factors in shifting the soil microbial community, explaining 41.5% of the total variation of soil bacterial community composition in paddy soil (**Table 1** and **Figure 2B**). Soil characteristics were reported to be important factors in shaping microbial community composition (GraAff et al., 2010; Zhalnina et al., 2015; Ji et al., 2021). The rhizosphere effect could result in the change of soil characteristics (**Table 1**), thereby obviously altering the microbial community.

With regard to N-cycling functions, the release of oxygen from rice root is favorable for soil nitrification (Armstrong, 1971). Previous studies showed that ammonia-oxidizing archaea were more abundant in the rhizosphere than in bulk soil (Chen et al., 2008), suggesting that *AOA* is more dominant in the rhizosphere paddy soil and more influenced by root exudation (e.g., oxygen, carbon dioxide) than *AOB*. We observed similarly that the rhizosphere was enriched in the *AOA* gene in this study (**Figures 4B,C**). In addition, root exudates could be used as C sources for denitrifying bacteria growth, thereby increasing the denitrification activity (Baudoin et al., 2003). In this study, we observed that function genes (*nirK* and *nosZ*) related to denitrification were enriched in the rhizosphere (**Figures 4D–F**), which might depend on the nutrient concentration and habitat selection.

Compared to the rhizosphere effect, the straw return may play a more pronounced role in shaping the bacterial community composition (**Figure 3**). During the whole stage of rice growth, the degradation of straw could supply C for bacterial growth (Murase et al., 2006). However, at the mature stage, root exudation was relatively low, decreasing the contribution of C from the rhizosphere. Thus, higher numbers of genera were affected by straw return than the rhizosphere effect (**Figure 3**). Moreover, the shift of bacterial community composition in bulk soils was observed to be stronger at 2% straw than 1% application (**Figure 2A**), suggesting that the straw effect on the bacterial community composition was more remarkable at a higher amendment rate. This might be related to greater changes in soil pH, TOC, and TN concentration at a higher rate of straw application (**Table 1** and **Figure 2B**). For N-cycling functions, different from the rhizosphere effect, the straw effect decreased the abundance of *AOA*, *AOB*, *nirS*, and *nosZ* (**Figure 4**) since straw addition decreased the available N (Wang et al., 2018).

Under straw amendment, the rhizosphere also significantly altered soil bacterial community composition (**Figure 2A**). However, higher numbers of genera were affected by the effect of the rhizosphere when the soil was not amended with straw return compared to that with the straw return, suggesting that the rhizosphere effect might be weakened when straw was returned to the soil, possibly due to the more pronounced impacts of straw amendments. In addition, there was no obvious difference in *nifH* between bulk and rhizosphere soils for control treatment, but rhizosphere soil displayed significantly higher *nifH* abundance than bulk when the soil was amended with straw addition (**Figure 4A**). Straw addition into soils increased soil C/N ratio but decreased soil-available N (**Table 1**), which might stimulate the N-fixing microorganism to transfer more N into the soil. However, the limit-available N could also decrease the activity of nitrification and denitrification microbes (Xiao and Tang, 2014), thus *AOA* and *AOB* abundance were decreased and no obvious increase in denitrification gene was observed for rhizosphere with straw addition in this study.

A higher rate of straw application shaped the bacterial communities of rhizosphere soils more remarkably. The shift of bacterial community composition and the changed genera in rhizosphere soils were observed to be higher at 2% straw than 1% application (**Figures 1B,C**, 2A). This might be related to greater changes in pH, TOC, and TN concentration of rhizosphere soils at a higher rate of straw application (**Table 1** and **Figure 2B**). For N-cycling genes, straw addition in the rhizosphere soils decreased the abundance of *AOA*, *AOB*, *nirS*, and *nosZ* (**Figure 4**). However, the response of *nifH* and *nirK* genes to the effect of straw addition in rhizosphere soil was different from their response to straw effect in bulk soil (**Figure 4**). Compared to bulk soil, the rhizosphere supplies more N to plants, which might stimulate the N-fixing microorganism and further decrease *nirK* gene abundance (Hou et al., 2018; Wen et al., 2019). Thus, the interaction effect of rhizosphere and straw increased the *nifH* gene but decreased the *nirK* gene.

## CONCLUSION

The rhizosphere interacts with the straw return to shape rhizosphere microbial community composition and N-cycling processes. Compared to the rhizosphere effect, the straw return may play a more pronounced role in shaping the bacterial community composition of rice paddy soil at the mature stage. Reframing research priorities to better understand the rhizosphere and agricultural management interactions has important implications for assessing the ecology and functions of rhizosphere microbial communities, which could help guide plant-oriented strategies to improve productivity and agroecosystem sustainability.

## DATA AVAILABILITY STATEMENT

The data presented in the study are deposited in the GenBank Data repository, accession number PRJNA847362.

## AUTHOR CONTRIBUTIONS

Y-HZ conducted the incubation experiments, measured soil property and N-cycling functional genes, data analysis, and wrote the manuscript. NW managed the whole project, designed all the experiments, and jointly wrote the manuscript. M-KY measured soil property. J-GY and L-HX helped with manuscript revision. All authors contributed to the article and approved the submitted version.

## FUNDING

This study was supported by the National Natural Science Foundation of China (41601261) and the Natural Science Foundation of Jiangsu Province (SBK2020022180).

## SUPPLEMENTARY MATERIAL

The Supplementary Material for this article can be found online at: https://www.frontiersin.org/articles/10.3389/fmicb.2022.945927/full#supplementary-material

## REFERENCES

Ai, C., Liang, G., Sun, J., Wang, X., He, P., and Zhou, W. (2013). Different roles of rhizosphere effect and long-term fertilization in the activity and community structure of ammonia oxidizers in a calcareous fluvo-aquic soil. *Soil Biol. Biochem.* 57, 30–42.doi: 10.1016/j.soilbio.2012.08.003

Armstrong, W. (1971). Radial oxygen losses from intact rice roots as affected by distance from the apex, respiration and waterlogging. *Physiol. Plantarum.* 25, 192–197.doi: 10.1111/j.1399-3054.1971.tb01427.x

Arth, I., Frenzel, P., and Conrad, R. (1998). Denitrification coupled to nitrification in the rhizosphere of rice. *Soil Biol. Biochem.* 30, 509–515. doi: 10.1016/j.femsec.2004.04.015

Baudoin, E., Benizri, E., and Guckert, A. (2003). Impact of artificial root exudates on the bacterial community structure in bulk soil and maize rhizosphere. *Soil Biol. Biochem.* 35, 1183–1192.doi: 10.1016/S0038-0717(03)00179-2

Bowles, T. M., Hollander, A. D., Steenwerth, K., and Jackson, L. E. (2015). Tightly-coupled plantsoil nitrogen cycling: comparison of organic farms across an agricultural landscape. *Plos One.* 10:e0131888. doi: 10.1371/journal.pone.0131888

Chen, X. P., Zhu, Y. G., Xia, Y., Shen, J. P., and He, J. Z. (2008). Ammonia-oxidizing archaea: important players in paddy rhizosphere soil? *Environ. Microbiol.* 10, 1978–1987. doi: 10.1111/j.1462-2920.2008.01613.x

Chen, Z., Wang, H., Liu, X., Zhao, X., Lu, D., Zhou, J., et al. (2017). Changes in soil microbial community and organic carbon fractions under short-term straw return in a rice–wheat cropping system. *Soil Till. Res.* 165, 121–127.doi: 10.1016/j.still.2016.07.018

Choudhury, E., and Kennedy, I. R. (2004). Prospects and potentials for systems of biological nitrogen fixation in sustainable rice production. *Biol. Fert. Soils* 39, 219–227.doi:10.1007/s00374-003-0706-2

Ding, L. J., Cui, H. L., Nie, S. A., Long, X. E., Duan, G. L., and Zhu, Y. G. (2019). Microbiomes inhabiting rice roots and rhizosphere. *FEMS Microbial. Ecol.* 95:fiz040.

Emmett, B. D., Buckley, D. H., and Drinkwater, L. E. (2019). Plant growth rate and nitrogen uptake shape rhizosphere bacterial community composition and activity in an agricultural field. *N. Phytol.* 225, 960–973. doi: 10.1111/nph.16171

Francis, C. A., Roberts, K. J., Beman, J. M., Santoro, A. E., and Oakley, B. B. (2005). Ubiquity and diversity of ammonia-oxidizing Archaea in water columns and sediments of the ocean. *PNAS* 102, 14683–14688. doi: 10.1073/pnas.0506625102

GraAff, M., Classen, A. T., and Schadt, C. (2010). Labile soil carbon inputs mediate the soil microbial community composition and plant residue decomposition rates. *N. Phytol.* 188, 1055–1064. doi: 10.1111/j.1469-8137.2010.03427.x

Graham, E. B., Knelman, J. E., Schindlbacher, A., Siciliano, S., Breulmann, M., Yannarell, A., et al. (2016). Microbes as engines of ecosystem function: when does community structure enhance predictions of ecosystem processes? *Front. Microbial.* 7:214. doi: 10.3389/fmicb.2016.00214

Hallin, S., and Lindgren, P. E. (1999). PCR detection of genes encoding nitrite reductase in denitrifying bacteria. *Appl. Environ. Microbiol.* 65, 1652–1657.doi: 10.1128/AEM.65.4.1652-1657.1999

Hou, S. P., Ai, C., Zhou, W., Liang, G. Q., and He, P. (2018). Structure and assembly cues for rhizospheric nirK- and nirS-type denitrifier communities in long-term fertilized soils. *Soil Biol. Biochem.* 119, 32–40.doi: 10.1016/j.soilbio.2018.01.007

Hu, L. F., Robert, C. A. M., Selma, C., Zhang, X., Meng, Y., Li, B. B., et al. (2018). Root exudate metabolites drive plant-soil feedbacks on growth and defense by shaping the rhizosphere microbiota. *Nat. Commun.* 9:2738. doi: 10.1038/s41467-018-05122-7

Ji, L. D., Si, H. L., He, J. Q., Fan, L. Q., and Li, L. Q. (2021). The shifts of maize soil microbial community and networks are related to soil properties under different organic fertilizers. *Rhizosphere* 19:100388.doi: 10.1016/j.rhisph.2021.100388

Langarica-Fuentes, A., Manrubia, M., Giles, M. E., Mitchell, S. S., and Daniell, T. J. (2018). Effect of model root exudate on denitrifier community dynamics and activity at different water-filled pore space levels in a fertilised soil. *Soil Biol. Biochem.* 120, 70–79.doi: 10.1016/j.soilbio.2018.01.034

Li, H., Su, J. Q., Yang, X. R., and Zhu, Y. G. (2018). Distinct rhizosphere effect on active and total bacterial communities in paddy soils. *Sci. Total Environ.* 649, 422–430.doi: 10.1016/j.scitotenv.2018.08.373

Li, X., Rui, J., Xiong, J., Li, J., He, Z., Zhou, J., et al. (2014). Functional potential of soil microbial communities in the maize rhizosphere. *PLoS One.* 9:e112609. doi: 10.1371/journal.pone.0112609

Lozupone, C., Hamady, M., and Knight, R. (2005). UniFrac–An online tool for comparing microbial community diversity in a phylogenetic context. *Nat. N. Biol.* 241, 184–186. doi: 10.1186/1471-2105-7-371

Lu, R. (2000). *Analysis Methods of Soil Agricultural Chemistry*. China: Agricultural Science and Technology Publishing House.

Maarastawi, S. A., Frindte, K., Bodelier, P., and Knief, C. (2019). Rice straw serves as additional carbon source for rhizosphere microorganisms and reduces root exudate consumption. *Soil Biol. Biochem.* 135, 235–238.doi: 10.1016/j.soilbio.2019.05.007

Maeda, K., Morioka, R., Hanajima, D., and Osada, T. (2010). The impact of using mature compost on nitrous oxide emission and the denitrifier community in the cattle manure composting process. *Microb. Ecol.* 59, 25–36. doi: 10.1007/s00248-009-9547-3

Manoeli, L., Korthals, G. W., Mattias, D. H., Janssens, T. K. S., and Kuramae, E. E. (2017). Soil microbiome is more heterogeneous in organic than in conventional farming system. *Front. Microbiol.* 7:2064. doi: 10.3389/fmicb.2016.02064

Marschner, P., Umar, S., and Baumann, K. (2011). The microbial community composition changes rapidly in the early stages of decomposition of wheat residue. *Soil Biol. Biochem.* 43, 445–451.doi: 10.1016/j.soilbio.2010.11.015

McGuire, K. L., and Treseder, K. K. (2010). Microbial communities and their relevance for ecosystem models: decomposition as a case study. *Soil Biol Biochem.* 42, 529–535.doi: 10.1016/j.soilbio.2009.11.016

Meng, F. Q., Dungait, J. A. J., Xu, X. L. R., Bol, Z. X., and Wu, W. L. (2017). Coupled incorporation of maize (zea mays l.) straw with nitrogen fertilizer increased soil organic carbon in fluvic cambisol. *Geoderma* 304, 19–27.doi: 10.1016/j.geoderma.2016.09.010

Moreau, D., Bardgett, R. D., Finlay, R. D., Jones, D. L., and Philippot, L. A. (2019). A plant perspective on nitrogen cycling in the rhizosphere. *Funct. Ecol.* 33, 540–552.doi: 10.1111/1365-2435.13303

Murase, J., Matsui, Y., Katoh, M., Ugimoto, A., and Kimura, M. (2006). Incorporation of 13C-labeled rice-straw-derived carbon into microbial communities in submerged rice field soil and percolating water. *Soil Biol. Biochem.* 38, 3483–3491.doi: 10.1016/j.soilbio.2006.06.005

Nie, S. A., Xu, H. J., Li, S., Li, H., and Su, J. Q. (2014). Relationships between abundance of microbial functional genes and the status and fluxes of carbon and nitrogen in rice rhizosphere and bulk soils. *Pedosphere* 24, 645–651.

Nie, S. A., Li, H., Yang, X. R., Zhang, Z. J., Weng, B. S., Huang, F. Y., et al. (2015). Nitrogen loss by anaerobic oxidation of ammonium in rice rhizosphere. *ISME J.* 9, 2059–2067.

Oksanen, J., Blanchet, F. G., Kindt, R., Legendre, P., O'Hara, R. G., and Simpson, G. L. (2013). *Multivariate Analysis of Ecological Communities in R: Vegan Tutorial. R package version 1.7*.

Ollivier, J., Töwe, S., Bannert, A., Hai, B., Kastl, E. M., Meyer, A., et al. (2011). Nitrogen turnover in soil and global change. *FEMS Microbiol. Ecol.* 78, 3–16.

Paterson, E., Osler, G., Dawson, L. A., Gebbing, T., Sim, A., and Ord, B. (2008). Labile and recalcitrant plant fractions are utilised by distinct microbial communities in soil: independent of the presence of roots and mycorrhizal fungi. *Soil Biol. Biochem.* 40, 1103–1113.doi: 10.1016/j.soilbio.2007.12.003

Pérez-Izquierdo, M., Zabal-Aguirre, M., González-Martínez, S. C., Buée, M., Verdú, M., and Rincón, A. (2019). Plant intraspecific variation modulates nutrient cycling through its below ground rhizospheric microbiome. *J. Ecol.* 107, 1594–1605.doi: 10.1111/1365-2745.13202

Rosch, C., Mergel, A., and Bothe, H. (2002). Biodiversity of denitrifying and dinitrogen-fixing bacteria in an acid forest soil. *Appl. Environ. Microbiol.* 68, 3818–3829. doi: 10.1128/AEM.68.8.3818-3829.2002

Rotthauwe, J. H., Witzel, K. P., and Liesack, W. (1997). The ammonia monooxygenase structural gene amoA as a functional marker: molecular fine-scale analysis of natural ammonia-oxidizing populations. *Appl. Environ. Microb.* 63, 4704–4712. doi: 10.1128/aem.63.12.4704-4712.1997

Schmidt, J. E., Kent, A. D., Brisson, V. L., and Gaudin, A. (2019). Agricultural management and plant selection interactively affect rhizosphere microbial community structure and nitrogen cycling. *Microbiome* 7:146. doi: 10.1186/s40168-019-0756-9

Throbäck, I. N., Enwall, K., Jarvis, A., and Hallin, S. (2004). Reassessing PCR primers targeting nirS, nirK and nosZ genes for community surveys of denitrifying bacteria with DGGE. *FEMS Microbiol. Ecol.* 49, 401–417. doi: 10.1016/j.femsec.2004.04.011

Wang, C., Zheng, M., Song, W., Wen, S., Wang, B., Zhu, C., et al. (2017). Impact of 25 years of inorganic fertilization on diazotrophic abundance and community structure in an acidic soil in southern China. *Soil Biol. Biochem.* 113, 240–249.

Wang, N., Chen, Z., Li, H. B., Su, J. Q., Zhao, F., and Zhu, Y. G. (2015). Bacterial community composition at anodes of microbial fuel cells for paddy soils: the effects of soil properties. *J. Soil. Sediment.* 15, 926–936.doi: 10.1007/s11368-014-1056-4

Wang, N., Luo, J. L., Juhasz, A., Li, H. B., and Yu, J. G. (2020). Straw decreased N2O emissions from flooded paddy soils via altering denitrifying bacterial community compositions and soil organic carbon fractions. *FEMS Microbiol. Ecol.* 96:fiaa046. doi: 10.1093/femsec/fiaa046

Wang, N., Yu, J. G., Zhao, Y. H., Chang, Z. Z., Shi, X. X., Ma, L. Q., et al. (2018). Straw enhanced CO2 and CH4 but decreased N2O emissions from flooded paddy soils: changes in microbial community compositions. *Atmos. Environ.* 174, 171–179.doi: 10.1016/j.atmosenv.2017.11.054

Wang, N., Zhao, Y. H., Yu, J. G., Xue, X. M., and Yang, L. Z. (2021). Roles of bulk and rhizosphere denitrifying bacteria in denitrification from paddy soils under straw return condition. *J. Soil. Sediment.* 21, 2179–2191.doi: 10.1007/s11368-021-02942-x

Wang, Q., Garrity, G. M., Tiedje, J. M., et al. (2007). Naive Bayesian classifier for rapid assignment of rRNA sequences into the new bacterial taxonomy. *Appl. Environ. Microb.* 73, 5261–5267. doi: 10.1128/AEM.00062-07

Wen, Z. L., Yang, M. K., Du, M. H., Zhong, Z. Z., Lu, Y. T., Wang, G. H., et al. (2019). Enrichments/derichments of root-associated bacteria related to plant growth and nutrition caused by the growth of an epsps-transgenic maize line in the field. *Front. Microbial.* 10:1335–1335. doi: 10.3389/fmicb.2019.01335

Wu, H., Wang, X., He, X., Zhang, S., Liang, R., and Jian, S. (2017). Effects of root exudates on denitrifier gene abundance, community structure and activity in a micro-polluted constructed wetland. *Sci. Total Environ.* 598, 697–703. doi: 10.1016/j.scitotenv.2017.04.150

Xiao, J., and Tang, J. H. (2014). Nitrogen removal with nitrification and denitrification via nitrite. *Adv. Mater. Res.* 908, 175–178.doi: 10.4028/www.scientific.net/AMR.908.175

Yang, L., Bai, J., Zeng, N., Zhou, X., Liao, Y. L., Lu, Y. H., et al. (2019). Diazotroph abundance and community structure are reshaped by straw return and mineral fertilizer in rice-rice-green manure rotation. *Appl. Soil Ecol* 136, 11–20.doi: 10.1016/j.apsoil.2018.12.015

Yu, C., Hu, X. M., Deng, W., Li, Y., Xiong, C., Ye, C. H., et al. (2015). Changes in soil microbial community structure and functional diversity in the rhizosphere surrounding mulberry subjected to long-term fertilization. *Appl. Soil Ecol.* 86, 30–40.doi: 10.1016/j.apsoil.2014.09.013

Yuan, J., Zhao, J., Tao, W., Zhao, M., Li, R., Pim, G., et al. (2018). Root exudates drive the soil-borne legacy of aboveground pathogen infection. *Microbiome.* 6:156. doi: 10.1186/s40168-018-0537-x

Zhalnina, K., Dias, R., Quadros, P. D. D., Davis-Richardson, A., and Triplett, E. W. (2015). Soil pH determines microbial diversity and composition in the park grass experiment. *Microb. Ecol.* 69, 395–406.doi: 10.1007/s00248-014-0530-2

Zhalnina, K., Louie, K. B., Hao, Z., Mansoori, N., Rocha, U. N. D., Shi, S. J., et al. (2018). Dynamic root exudate chemistry and microbial substrate preferences drive patterns in rhizosphere microbial community assembly. *Nat. Microbiol.* 3, 470–480. doi: 10.1038/s41564-018-0129-3

Zhao, S., Li, K., Zhou, W., Qiu, S., Huang, S., and He, P. (2016). Changes in soil microbial community, enzyme activities and organic matter fractions under long-term straw return in north-central China. *Agr. Ecosyst. Environ.* 216, 82–88.doi: 10.1016/j.agee.2015.09.028

**Conflict of Interest:** The authors declare that the research was conducted in the absence of any commercial or financial relationships that could be construed as a potential conflict of interest.

**Publisher's Note:** All claims expressed in this article are solely those of the authors and do not necessarily represent those of their affiliated organizations, or those of the publisher, the editors and the reviewers. Any product that may be evaluated in this article, or claim that may be made by its manufacturer, is not guaranteed or endorsed by the publisher.

frontiers | Frontiers in Microbiology

TYPE Original Research
PUBLISHED 05 August 2022
DOI 10.3389/fmicb.2022.961815



OPEN ACCESS

EDITED BY
Xiaochen Chen,
Fuzhou University, China

REVIEWED BY
Nan Wu,
Tianjin Agricultural University, China
Chunyong Wang,
Liaoning University of Technology, China
Tomohiro Tobino,
The University of Tokyo, Japan

*CORRESPONDENCE
Lixia Ke
klixia@ahnu.edu.cn
Pei Hong
peihong@ahnu.edu.cn

SPECIALTY SECTION
This article was submitted to Microbiotechnology, a section of the journal Frontiers in Microbiology

RECEIVED 05 June 2022
ACCEPTED 11 July 2022
PUBLISHED 05 August 2022

CITATION
Yang K, Bu H, Zhang Y, Yu H, Huang S, Ke L and Hong P (2022) Efficacy of simultaneous hexavalent chromium biosorption and nitrogen removal by the aerobic denitrifying bacterium *Pseudomonas stutzeri* YC-34 from chromium-rich wastewater. *Front. Microbiol.* 13:961815. doi: 10.3389/fmicb.2022.961815



# Efficacy of simultaneous hexavalent chromium biosorption and nitrogen removal by the aerobic denitrifying bacterium *Pseudomonas stutzeri* YC-34 from chromium-rich wastewater

Keyin Yang, Huijun Bu, Ying Zhang, Hongxia Yu, Sining Huang, Lixia Ke* and Pei Hong*

College of Life Sciences, School of Ecology and Environment, Collaborative Innovation Center of Recovery and Reconstruction of Degraded Ecosystem in Wanjiang Basin Co-founded by Anhui Province and Ministry of Education, Anhui Normal University, Wuhu, China

The impact of high concentrations of heavy metals and the loss of functional microorganisms usually affect the nitrogen removal process in wastewater treatment systems. In the study, a unique auto-aggregating aerobic denitrifier (*Pseudomonas stutzeri* strain YC-34) was isolated with potential applications for Cr(VI) biosorption and reduction. The nitrogen removal efficiency and denitrification pathway of the strain were determined by measuring the concentration changes of inorganic nitrogen during the culture of the strain and amplifying key denitrification functional genes. The changes in auto-aggregation index, hydrophobicity index, and extracellular polymeric substances (EPS) characteristic index were used to evaluate the auto-aggregation capacity of the strain. Further studies on the biosorption ability and mechanism of cadmium in the process of denitrification were carried out. The changes in tolerance and adsorption index of cadmium were measured and the micro-characteristic changes on the cell surface were analyzed. The strain exhibited excellent denitrification ability, achieving 90.58% nitrogen removal efficiency with 54 mg/L nitrate-nitrogen as the initial nitrogen source and no accumulation of ammonia and nitrite-nitrogen. Thirty percentage of the initial nitrate-nitrogen was converted to $N_2$, and only a small amount of $N_2O$ was produced. The successful amplification of the denitrification functional genes, *norS*, *norB*, *norR*, and *nosZ*, further suggested a complete denitrification pathway from nitrate to nitrogen. Furthermore, the strain showed efficient aggregation capacity, with the auto-aggregation and hydrophobicity indices reaching 78.4 and 75.5%, respectively. A large amount of protein-containing EPS was produced. In addition, the strain effectively removed 48.75, 46.67, 44.53, and 39.84% of Cr(VI) with the initial concentrations of 3, 5, 7, and 10 mg/L, respectively, from the nitrogen-containing synthetic wastewater. It also could reduce Cr(VI) to the less toxic Cr(III). FTIR measurements and

characteristic peak deconvolution analysis demonstrated that the strain had a robust hydrogen-bonded structure with strong intermolecular forces under the stress of high Cr(VI) concentrations. The current results confirm that the novel denitrifier can simultaneously remove nitrogen and chromium and has potential applications in advanced wastewater treatment for the removal of multiple pollutants from sewage.

KEYWORDS

**strain YC-34, auto-aggregation, extracellular polymeric substances (EPS), nitrogen removal, Cr(VI) stress**

## Introduction

Biological wastewater treatment processes are the most widely used methods for the removal of organic and inorganic pollutants from wastewater treatment technologies (Cai et al., 2020; Nguyen et al., 2021; Uluseker et al., 2021). The advanced nitrate removal is performed by denitrifying functional microbiota, which is the critical process to achieve the standard discharge of nitrogen. The direct addition of functional bacteria to the biological treatment system remains one of the most common methods (Laothamteep et al., 2022; Ma et al., 2022). However, this method yields slow results due to the low initial concentration of functional bacteria compared to native microorganisms, which may result in the loss of functional bacteria (Chen et al., 2015). Auto-aggregation refers to the inter-cellular interaction of bacteria spontaneously gathering to facilitate the attachment of functional microorganisms to the biofilm (Adav et al., 2008; Hong et al., 2020). For biofilm formation, a better option may be to immobilize EPS-producing bacteria on a carrier and then add the bioimmobilized carrier to the reactor (Zhao et al., 2018; Hong et al., 2021). This approach may reduce the loss of functional bacteria and increase the initial concentration of EPS-producing bacteria, thus facilitating biofilm development. Till now, a few aerobic denitrifiers with auto-aggregation ability have been reported, such as, *Klebsiella* sp. TN-10, *Enterobacter* sp. strain FL, and *Methylobacterium gregans* DC-1 (Wei et al., 2016; Fan et al., 2019; Hong et al., 2019). Therefore, the acquisition and application of auto-aggregating strains could have a major impact on accelerating biofilm formation and shortening the start-up time of biofilm reactors.

On the other hand, many municipal wastewater treatment plants are responsible for treating some industrial wastewater and domestic wastewater (Luhar et al., 2021). However, the rapid industrial development has increased the risk of excessive heavy metals discharge from wastewater treatment plants (Wang et al., 2018). The excessive concentration of heavy metal ions may lead to the unstable performance of the wastewater treatment system, lowering the efficiency of the denitrification process (Ochoa-Herrera et al., 2009; Zhou et al., 2021). Among the heavy metals, chromium is one of the most common ones, which is found in wastewater from industries such as steel manufacturing, electroplating, leather tanning, pulp production, landfills, etc. (Truskewycz et al., 2018; Tsybulskaya et al., 2019). Hexavalent chromium easily enters the cytoplasmic matrix through the cell membrane of denitrifying bacteria, which changes the conformation of enzymes and blocks the necessary functional groups of microorganisms, leading to a decrease in the denitrification capacity of bacteria (Colussi et al., 2009; Konovalova et al., 2009). Currently, the inhibitory effect of metal cadmium on denitrification has been alleviated by supplementing bio-promoters such as biotin, cytokinin, and L-cysteine (Wang et al., 2015, 2021; Zhou et al., 2021). However, the addition of exogenous substances may require the creation of new compounds containing the relevant structural units and increase the cost of the denitrification process (Palanivel et al., 2020; Wen et al., 2022). In comparison, heavy metal removal by denitrifying bacteria themselves is a clean, environmentally friendly, and efficient removal strategy (Peng et al., 2019; Hong et al., 2022).

The denitrification process is catalyzed by four enzymes: nitrate reductase (Nar/Nap), nitrite reductase (Nir), nitric oxide reductase (Nor), and nitrous oxide reductase (Nos), encoded by the genes *nar*/*nap*, *nir*, *nor* and *nos*, respectively. $N_2O$, as an intermediate metabolite, is the third most powerful greenhouse gas after $CO_2$ and $CH_4$ (Uraguchi et al., 2009). The application of denitrifying bacteria with complete denitrification pathways to reduce $N_2O$ has become a hot research topic for controlling greenhouse gas emissions from agricultural soils and water bodies (Perez-Garcia et al., 2017; Harris et al., 2021). The release of large amounts of nitrous oxide from denitrifying bacteria would hinder their denitrification applications (Tallec et al., 2008; Miyahara et al., 2010; Shoun et al., 2012). Therefore, such denitrifying bacteria are explored to develop environmentally friendly nitrogen transformation methods.

To reduce functional microbial loss and unstable nitrogen removal under high concentration chromium stress, a novel strain of auto-aggregating denitrifying bacteria, *Pseudomonas*

*stutzeri* YC-34, was screened and obtained in this study. Firstly, the nitrate reduction capability, nitrogen balance, and nitrogen-removal genes of strain YC-34 were analyzed. Secondly, the aggregation property and mechanisms of this strain were revealed by EPS content and spectroscopic measurements, aggregation and hydrophobicity index tests. Thirdly, the tolerance of the strain to Cr(VI) was analyzed, and its potential application was evaluated by experimentally investigating the influence of Cr(VI) on nitrogen removal and EPS production. The research might provide useful information for the development of biotechnological relevant microorganisms to control integrated contamination.

# Materials and methods

## Culture mediums

Enrichment medium (EM, g/L): $KNO_3$ 5.0, sodium succinate dibasic hexahydrate11.1, $KH_2PO_4$ 1.0, $Na_2HPO_4{\cdot}12H_2O$ 7.03, $MgSO_4{\cdot}7H_2O$ 0.13, $NH_4Cl$ 0.2, trace element solution 2 mL, pH 7.0.

Bromothymol Aroma Blue solid medium (BTB, g/L): $KNO_3$ 1.0, trisodium citrate dehydrate 5.3, $KH_2PO_4$ 0.6, $FeSO_4{\cdot}7H_2O$ 0.03, $CaCl_2$ 0.1, $MgSO_4{\cdot}7H_2O$ 0.6, 1% bromothymol aroma blue 1 mL, agar 20, pH 7.0.

Nitrogen removal medium (NR, g/L): sodium succinate dibasic hexahydrate11.1, $KH_2PO_4$ 0.1, $MgSO_4{\cdot}7H_2O$ 0.1, $KNO_3$ 0.36, trace element solution 2 mL, pH 7.0 (simulation of synthetic wastewater).

Contents of trace element solution (g/L): $FeCl_2{\cdot}4H_2O$ 1.8, $CoCl_2{\cdot}6H_2O$ 0.25, $NiCl_2{\cdot}6H_2O$ 0.01, $CuCl_2{\cdot}2H_2O$ 0.01, $MnCl_2{\cdot}4H_2O$ 0.70, $ZnCl_2$ 0.1, $H_3BO_3$ 0.5, $Na_2MoO_4{\cdot}2H_2O$, $NaSeO_3{\cdot}5H_2O$ 0.01 (Qing et al., 2018).

## Enrichment cultures and isolation of aerobic denitrifiers

Seed sludge was collected from the Huwanwei wastewater treatment system, located in Hefei, China (117°15′79.81″E, 31°70′68.10″N). Five milliliter of the seed sludge was added to a 250 mL triangular flask containing 100 mL of EM and incubated in a shaker at 30°C and 120 r/min for 24 h. Then, 5 mL of culture medium was transferred to a fresh sterile EM medium and the enrichment was repeated for three rounds. The last obtained culture medium was sequentially diluted in a gradient from $10^{-1}$ to $10^{-7}$. 0.2 mL of the diluted samples were added to BTB and incubated at 30°C in an incubator until the appearance of single colonies. Single blue colonies were selected, purified by multiple scribing, and stored at 4°C in the refrigerator. Each single purified colony was examined separately using NR, which used nitrate as the only nitrogen source. After comparing the $NO_3^-$-N removal rates, the most efficient colony was labeled YC-34 and cultured in NR for further studies. All media were disinfected at 121°C for 20 m and all tests were performed in three repetitions.

## Determination of denitrification-related indices of the strain

### Gene amplification

Two milliliter suspension of YC-34 was transferred to 100-mL NR in a 250-mL triangular flask and incubated at 30°C and 120 rpm. After a 24 h culture in NR, a bacterial genomic DNA extraction kit (BK2021081230, DiscoverBeads company, China) was used following the manufacturer's instructions to extract DNA from the strain suspension. The primers and amplification steps for 16S rRNA and denitrification genes are shown in Table 1. PCR products were sequenced by the I-congene Biotechnology company (Wuhan, China) and then analyzed using the BLAST tool of the NCBI database. A phylogenetic tree of the 16S rRNA was constructed by MEGA software (version 6.0). Strain YC-34 has been submitted to the China Center for Type Culture Collection (CCTCC) (Wuhan, China) with the accession number of CCTCC M 20211100).

### Nitrogen removal test

Two milliliter culture suspension of strain YC-37 was added to a 250-mL triangular flask containing 100 mL NR and incubated in an incubator shaker (120 rpm) at 30°C. Samples were collected every 6 h to measure the $OD_{600}$ value and the concentrations of TN, $NH_4^+$, $NO_2^-$ and $NO_3^-$. Under sterile conditions, 2 mL of the pre-incubated strain suspension was inoculated into a 250 mL serum bottle containing 100 mL NR. A blank control without inoculation of the bacterial solution was also set up. The serum bottles were aerated with 99.99% pure oxygen, tightly plugged with rubber sealing plugs, and placed in an incubator for 48 h at 30°C. The nitrogen balance was calculated by measuring the starting and final nitrogen content. The starting $NO_3^-$-N content was the initial TN concentration. The final nitrogen measurement indices included TN, $NH_4^+$N, $NO_2^-$N, $NO_3^-$N, organic nitrogen (Org-N), intracellular nitrogen, and gaseous nitrogen concentration. The Org-N concentration was determined by subtracting the $NO_3^-$-N, $NH_4^+$-N, and $NO_2^-$-N concentrations from the final TN concentration. In addition, the headspace gas sample in the serum bottle was withdrawn and assayed for $N_2O$ and $N_2$ content using GC-MS (Agilent, USA). The bacteria were freeze-dried. The intracellular nitrogen percentage was determined by an elemental analyzer (FLASH 2000, Thermo Fisher Scientific) and the intracellular nitrogen content was calculated by combining the weight of the bacteria.

TABLE 1 The primers and conditions of PCR.

| Genes | Primers | Conditions of PCR | | | | | | |
|---|---|---|---|---|---|---|---|---|
| 16s rRNA | 5'-AGAGTTTGATCCTGGCTCAG-3'/5'-GGTTACCTTGTTACGACTT-3' | 95°C, 5 min | 94°C, 30 s | 69°C, 1 min | 72°C, 1 min | 35 cycles | 72°C, 10 min | Qing et al., 2018 |
| *napA* | 5'-TCTGGACCATGGGCTTCAACCA-3'/5'-ACGACGACCGGCCAGCGCAG-3' | 95°C, 5 min | 94°C, 30 s | 69°C, 1 min | 72°C, 1 min | 35 cycles | 72°C, 10 min | Qing et al., 2018 |
| *nirS* | 5'-GAACCTCAAGACCACTACCATC-3'/5'-CCTTCCAGTTGTGCTCCTT-3' | 95°C, 5 min | 94°C, 30 s | 57°C, 1 min | 72°C, 1 min | 35 cycles | 72°C, 10 min | Hong et al., 2022 |
| *norR* | 5'-GGAAATGACCAAGAACGAGC-3'/5'-AGGTAGCAGACCAGACCGAT-3' | 95°C, 5 min | 94°C, 30 s | 59°C, 1 min | 72°C, 1 min | 35 cycles | 72°C, 10 min | Hong et al., 2022 |
| *nosZ* | 5'-GGTAACCTTGACAACACCGA-3'/5'-ATGACGAAGCCGTGAGACA-3' | 95°C, 5 min | 94°C, 30 s | 58°C, 1 min | 72°C, 1 min | 35 cycles | 72°C, 10 min | Hong et al., 2022 |

## Factors affecting nitrogen removal

NR was used as the tested medium, and the culture conditions were consistent with those described above. The medium composition and condition were adjusted accordingly to the tested variables. Influencing variables included the carbon source, carbon: nitrogen (C/N) ratio (changing the quantity of nitrogen content while maintaining a fixed quantity of carbon content), pH, temperature, and dissolved oxygen (DO, controlled by changing rotation speed). The carbon-based resources (sodium succinate, trisodium citrate, sucrose, sodium acetate, and seignette salt), C/N proportions (5, 10, 15, 30, and 60), pH (5, 7, and 9), temperature (25, 30, and 35°C) and rotational speed (90, 120, and 150 rpm) were chosen as the dependent variables. All testing media were cultured for 30 h, and $OD_{600}$ and $NO_3^-$ were measured.

## Determination of indicators related to strain aggregation

Samples were taken periodically during the culture process of strain YC-34 in NR to determine indicators related to aggregation. Auto-aggregation and hydrophobicity indices were determined, and EPS extraction was performed with reference to Hong et al. (2019). Briefly, the auto-aggregation index was determined by spectrophotometry after static precipitation, while the hydrophobicity index was measured by spectrophotometry after hexadecane adsorption. Furthermore, EPS was extracted by the cation exchange resin method. The sum of polysaccharides and proteins represented EPS content, which was measured by anthrone colorimetry and the Lowry method separately (Eboigbodin and Biggs, 2008). EPS was treated with freezing intervention and then ground with infrared grade KBr powder, made into disks. Subsequently, Fourier transform infrared spectroscopy (FTIR) was used for measurement (Nicolet Nexus, Thermo, USA).

## Determination of cadmium biosorption-related indicators

Bulk tests were conducted in an aseptic NR medium to investigate the ability of strain YC-34 to remove $NO_3^-$ in the presence of Cr(VI). According to reports, wastewater with Cr(VI) usually contained <10 mg/L (Das et al., 2016; Sharma and Malaviya, 2016). Therefore, the initial cadmium concentration in the culture medium was adjusted to 0, 3, 5, 7, and 10 mg/L by adding the corresponding concentrations of potassium dichromate to the NR medium. Pre-cultured YC-34 was incubated (1%, v/v) in an NR medium containing different concentrations of Cr(VI) at

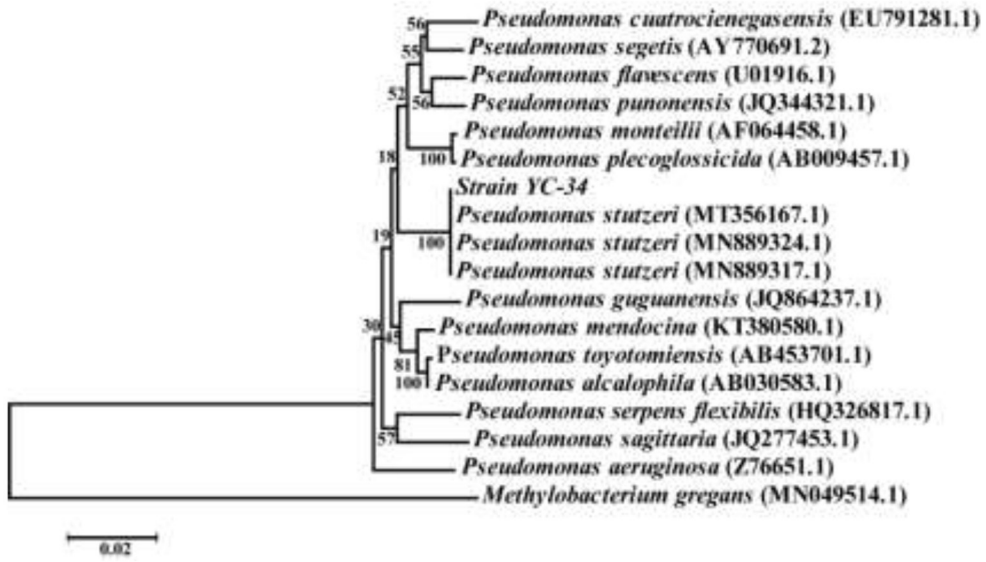


FIGURE 1
The phylogenetic tree of *Pseudomonas stutzeri* strain YC-34 and related strains.

30°C and 120 rpm. After 48 h of culture, the content and composition of EPS, $OD_{600}$, and TN were measured, and the nitrate and Cr(VI) content were determined. The 1,5-Diphenylcarbazide spectrophotometric method was used to mearsure the concentration of Cr(VI) (He et al., 2015) while the total Cr concentration was determined by atomic absorption spectrometry (AA-7003, EWAI, Beijing, China). The Cr(III) was evaluated by subtracting Cr(VI) from the total Cr (An et al., 2020). After fixing in aqueous 2.5% glutaraldehyde for 12 h and gradient dehydration with different concentrations of ethanol, the cells were observed under a scanning electron microscope (SEM, Hitachi, Japan) (Hong et al., 2019).

## Analytical methods

The concentrations of TN, $NH_4^+$-N, $NO_3^+$-N, and $NO_2^-$-N were measured with reference methods described in the Chinese national standards (NY525-2012). The amide I region (1,700–1,600 $cm^{-1}$) of the FTIR data was analyzed to extract information regarding protein secondary structures (Jia et al., 2017). In addition, secondary derivative spectroscopy and deconvolution spectroscopy of the amide I region and type of hydrogen bonding in the region of 3,000–3,800 $cm^{-1}$ were performed using Peakfit software (version 4.12). SPSS 19.0 software (IBM SPSS, Armonk, NY, USA) was used for all data processing and statistical analyses. Line and bar charts were drawn using Origin 2021 (Origin Lab, Northampton, MA, USA).

# Results and discussion

## Identification and characterization of YC-34

After multiple cycles of enrichment in EM and plate scribing on BTB solid medium, the auto-aggregation denitrifier YC-34 was obtained. The strain was off-white, convex, and opaque, with a smooth, moist, and thick surface on BTB. PCR amplification results revealed that the whole length of the 16S rRNA sequence of YC-34 was ~1,375 bp (GenBank number: MZ855228). YC-34 was found to be highly associated with *Pseudomonas sp*. strain SM12 (GenBank number: MT356167), with 99% similarity. Phylogenetic analysis based on 16S rRNA gene sequencing indicated that YC-34 had a close relationship with *Pseudomonas stutzeri* (Figure 1). Therefore, strain YC-34 was identified as a *Pseudomonas stutzeri* strain.

## Analysis of nitrogen-removal characteristics

The nitrogen removal characteristics of strain YC-34 were analyzed by using nitrate as the single nitrogen source (Figure 2). From 0 to 60 h, $NO_3^-$-N was reduced from the original 54.12–5.10 mg/L with an elimination efficiency of 90.58%. Moreover, the accruals of nitrite and ammonia were almost zero during the whole incubation period. *Pseudomonas stutzeri* strains were previously reported as aerobic denitrifying bacteria with the ability to accumulate nitrite (Zhu et al., 2012; Hong

et al., 2021). However, nitrite enrichment inhibits the functions of microorganisms in the nitrogen, phosphorus, and sulfate removal process, such as anaerobic ammonium oxidation bacteria, methanogenic archaea, and sulfate-reducing bacteria (Auguet et al., 2016; Wang et al., 2019). Therefore, due to its efficient nitrate-nitrogen removal and minimal accumulation of ammonia-nitrogen and nitrite, strain YC-34 showed excellent denitrification performance.

The N conversion pathway for strain YC-34 was explored by N balance. The N balance data are shown in Table 2. Comparing the initial and final nitrogen concentrations, 31.1% of the original nitrate was transformed into intracellular nitrogen, 17.8% was converted into organic nitrogen, 8.5% was turned into $N_2O$, and 30.0% was transformed into $N_2$. As described by Huang et al. (2015), the denitrification procedure requires the participation of multiple enzymes. The related genes n*apA*, *nirS*, *norR* and *nosZ* were amplified and were found to be 877, 310, 1,001, and 1,051 bp, respectively (Figure 3). The genes corresponded to four enzymes (NAP, NIR, NOR, and NOS). NAP played an essential role in the conversion of $NO_3^-$ to $NO_2^-$ (Zhu et al., 2012). The *napA* gene is often used as a functional marker to identify aerobic denitrifying bacteria (Feng et al., 2018; Lang et al., 2019; Zhang et al., 2019). The amplification of the *nirS* gene indicates that heme c in strain YC-34 is responsible for electron transport from the electron donor cytochrome c551, while heme d1 is responsible for nitrite binding and reduction to nitric oxide (Baker et al., 1997). The enzymes NOR and NOS are encoded by the *norR* and *nosZ* genes, respectively, which promote the production of $N_2O$ and $N_2$, respectively (Zhang et al., 2012). The nitrate-nitrogen removal pathway of strain YC-34 was like the reported strains, *Pseudomonas stutzeri* strain XL-2; *Pseudomonas stutzeri* KY-37; *Pseudomonas oligotrophica* JM10B5a$^T$ (Zhao et al., 2018; Hong et al., 2022; Zhang et al., 2022). Combined with the nitrogen balance and denitrification gene amplification, strain YC-34 exhibited a complete N pathway: Nitrate → Nitrite → Nitric coxide → Nitrous oxide → Nitrogen.

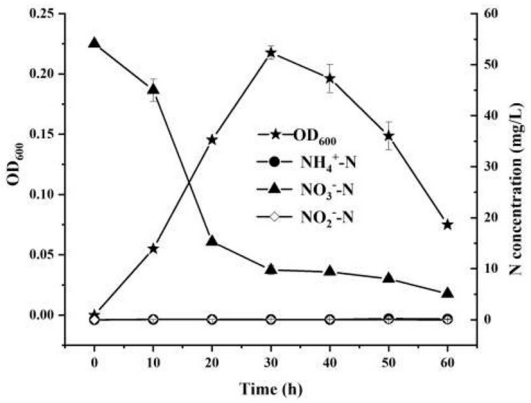


FIGURE 2
The nitrate removal and cell growth performance of YC-34 strain.

## Effects of different influencing factors on the denitrification performance of YC-34

### Carbon source

As shown in Figure 4A, sodium succinate, trisodium citrate, and sucrose were tested for strain YC-34 growth with a $NO_3^-$ elimination efficiency of 93.08, 58.72, and 42.51%, respectively. Sodium succinate might be the optimal carbon source, which consisted of the carbon using of *Bacillus methylotrophicus* strain L7 (Zhang et al., 2012).

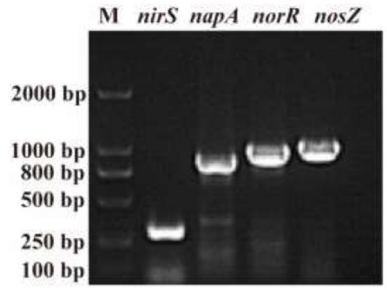


FIGURE 3
The amplification results of *nirS*, *norR*, *nosZ*, and *napA* genes (M: DL 2000 DNA marker).

TABLE 2 The N balance of strain YC-34 after 48 h cultivation.

| Initial N (mg) | Final N (mg) | | | | | | | Error |
|---|---|---|---|---|---|---|---|---|
| | $NO_3^-$-N | $NO_2^-$-N | $NH_4^+$-N | Org-N | Intracellular N | $N_2O$ | $N_2$ | |
| 2.17 ± 0.008 | 0.07 ± 0.005 | UN | 0.003 | 0.48 ± 0.009 | 0.84 ± 0.011 | 0.28 ± 0.015 | 0.81 ± 0.005 | 7.8% |

UD, Undetectable.
Error% = 100× (Initial N-Final N)/Initial N.

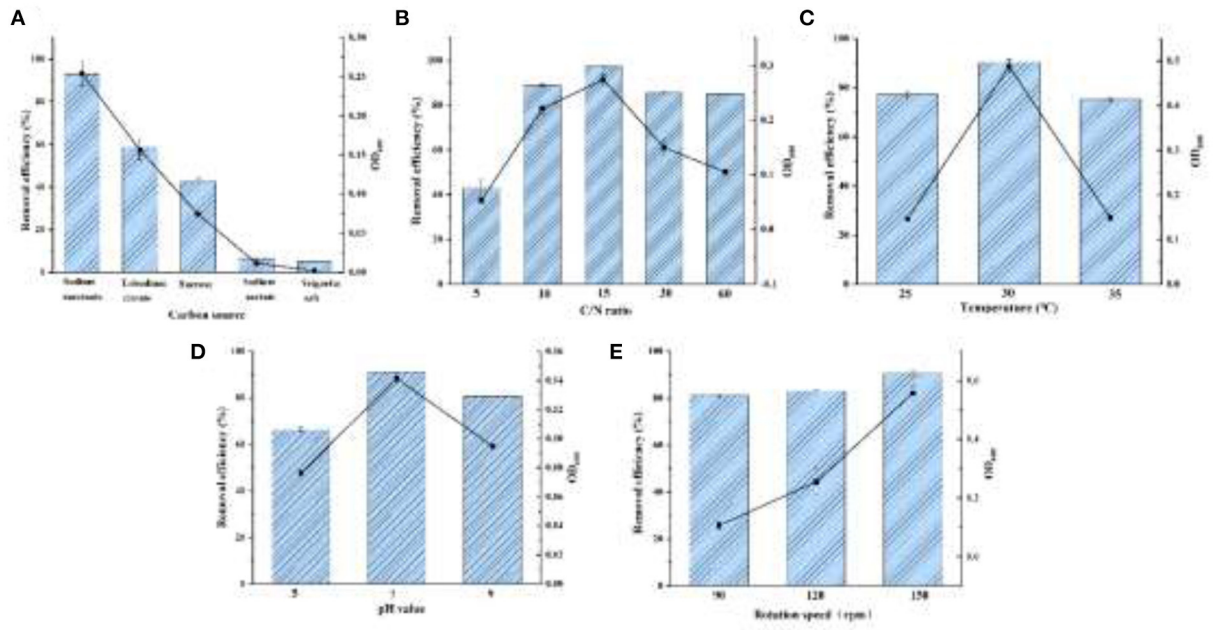


FIGURE 4
The effects for denitrification capacity by the conditions of carbon source **(A)**, C/N ratio **(B)**, temperature **(C)**, pH **(D)**, and DO **(E)**.

## C/N ratio

Aerobic denitrifiers usually require a C/N ratio of about 9–10 (Ren et al., 2021). The removal of nitrate by *Halomonas Alkaliphile* HRL-9 with a C/N ratio of 20 was significantly higher than that of 10 (Ren et al., 2019). As displayed in Figure 4B, YC-34 could adapt to C/N ratios ranging from 5 to 60. As the ratio gradually increased from 5 to 60, the utilization of $NO_3^-$ initially presented an increasing trend followed by a decreasing trend. YC-34 reached its peak efficiency (97.37% $NO_3^-$ removal) at a C/N ratio of 15.

## Temperature

YC-34 could maintain efficient nitrogen removal from 25 to 35°C (Figure 4C). The maximum removal capacity of $NO_3^-$ reached 90.43% at 30°C, which was similar to the *Marinobacter* strain NNA5 (Liu et al., 2016). Moreover, the $OD_{600}$ of the strain is higher than that of other temperatures under the condition of 30°C. This indicated that YC-34 might be a mesophilic strain.

## pH

Figure 4D presented the $NO_3^-$ removal properties of YC-34 under the initial pH of 5, 7, and 9 with a maximum removal value of 66.30, 91.10, and 80.82%, respectively. The optimal pH condition of YC-34 was similar to that of *Acinetobacter* sp. YT03, which maintained a high nitrogen removal capacity at a pH of 7 (Li et al., 2019). This indicated that the optimum pH for YC-34 growth was neutral.

## Shaking speed

An increase in shaking speed represents an increase in DO. The denitrification rate of strain *Acinetobacter* sp. YT03 was reported to increase as the rotation speed increased. As the rotation speed was increased from 50 rpm to 250 rpm, the nitrogen removal rate reached the maximum value of 93.9% at 250 rpm (Li et al., 2019). The strain YC-34 showed a similar performance to *Acinetobacter* sp. YT03, which showed a maximum nitrogen removal efficiency of 90.4% at 150 rpm (Figure 4E). According to the experimental results, sodium succinate was the most suitable carbon source for YC-34. The optimum C/N ratio was 15, the suitable temperature was 30°C, and the optimum pH was 7. YC-34 also showed outstanding denitrification performance in suboptimal factors, which confirmed the strong environmental adaptability of YC-34.

# Analysis of prominent auto-aggregation features and mechanisms

## Auto-aggregation ability and hydrophobicity of YC-34

As shown in Figure 5A, YC-34 presented a significant auto-aggregation ability as the auto-aggregation index progressively rose to 78.4% at 42h. The value was higher than that of the *Enterobacter* sp. strain FL and *Escherichia coli* MG1655 (Eboigbodin and Biggs, 2008; Wang et al., 2018). The surface

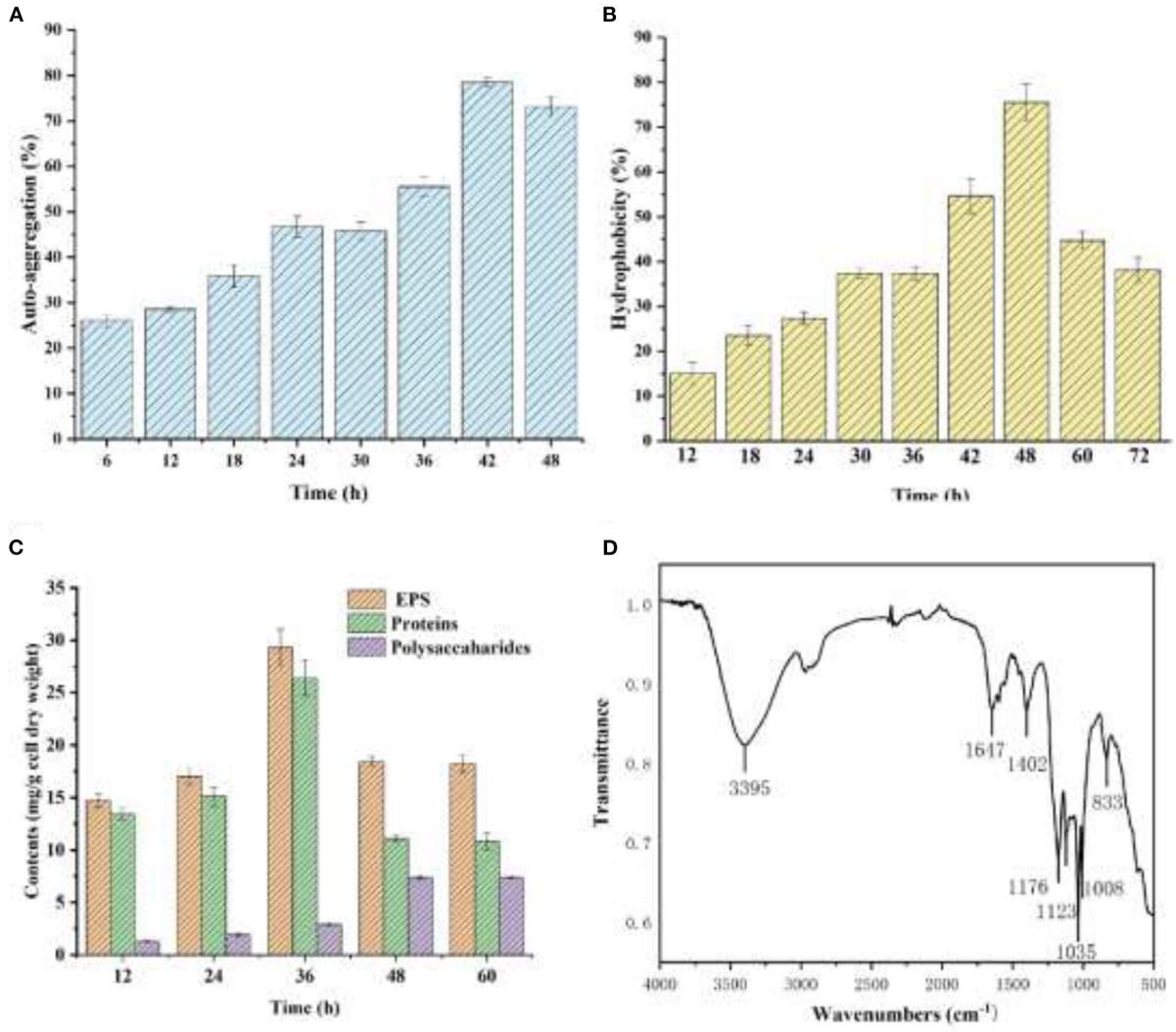


FIGURE 5
Auto-aggregation index **(A)** and hydrophobicity index **(B)** of the strain YC-34, Fourier transform infrared spectra **(C)** and composition **(D)** of EPS.

TABLE 3 The content of protein secondary structure of strain YC-34.

| | β-Sheets (%) | Random coil (%) | α-Helices (%) | β-turn (%) |
|---|---|---|---|---|
| EPS | 37.07% | — | — | 62.93% |

hydrophobicity of YC-34 gradually increased from 15.0% at 6 h to 75.5% at 48 h (Figure 5B), which was significantly higher than that of *Sphingomonas* sp. YY2 (Lang et al., 2019). These results were consistent with *Bifidobacteria* with its hydrophobicity presenting a positive correlation with aggregation ability (Collado et al., 2007).

## EPS characteristics

As presented in Figure 5C, the protein and polysaccharide concentrations rose progressively from 12 to 36 h. YCh.... t-Yc-34 was rich in proteins. Figure 5D displays the infrared wavebands of EPS. The 3,395 $cm^{-1}$ peaks represented the tensile oscillation of O-H. The peak of 1,647 $cm^{-1}$ corresponded to the C=O stretching oscillation of amide-I, which was identified as the random coil of protein secondary structure. The peak at 1,402 $cm^{-1}$ was attributed to the COO-deformation vibration due to the presence of uronic acid. The wavebands at 800 and 1,200 $cm^{-1}$ were attributed to the C-H deformation vibration. The results confirmed that the main components of EPS produced by YC-34 were proteins and polysaccharides. To investigated the effect of proteins in the auto-aggregation of YC-34, the primary structure of proteins was further studied. As shown in Table 3,

the secondary structures were composed of 37.07% β-sheets and 62.93% β-turns, whereas the α-helix structures and random coil were not found. There was a higher content of β-turn than β-sheet. Fewer α-helices in the protein resulted in a "loose" protein structure, exposing more hydrophobic amino acids, leading to stronger hydrophobicity. The auto-aggregation ability and surface hydrophobicity of bacteria were closely related to biofilm formation (Wang and Li, 2022). Proteins and polysaccharides in EPS were essential in promoting initial bacterial adhesion and biofilm development (Zhu et al., 2018). Replenishment of EPS-producing bacteria in wastewater biofilm treatment systems may facilitate EPS production, and enhance initial adhesion and biofilm development, and eventually leading to accelerated biofilm formation. This would reduce the loss of nitrogen removal functional bacteria, and serve to achieve enhanced deep nitrogen removal from wastewater.

## Analysis of the effect and mechanism of Cr (VI)-removal by YC-34

Some previous studies have shown that EPS has various binding and biosorption capacities for different kinds of heavy metals (Yue et al., 2015). In view of a large amount of EPS secretion by YC-34, the nitrogen removal characteristics of YC-34 in response to heavy metal Cr(VI) stress were further investigated. As presented in Figure 6A, the $NO_3^-$-N removal efficiency of YC-34 was 82.6, 81.5, 83.6, 83.0, and 81.8% at initial Cr(VI) concentrations of 0, 3, 5, 7, and 10 mg/L, respectively. After 48 h of incubation, the total Cr concentrations decreased to 1.54, 2.62, 3.88, and 6.02 mg/L, respectively (Figure 6B). Chromium loss might result from the biosorption of YC-34, with the adsorption efficiency reaching 48.75, 46.67, 44.53, and 39.84% at 3, 5, 7, and 10 mg/L initial Cr(VI) contents, respectively. By comparing the reduction traits of Cr(VI) and total Cr, strain YC-34 showed similar chromium removal characteristics to strain AL-6, converting hexavalent chromium to the less toxic Cr(III) (An et al., 2020).

The mechanism of chromium adsorption by strain YC-34 was further explored from the micro-characteristics of the cell surface. The accumulation of EPS increased with increasing Cr(VI) concentration, reaching a maximum of 26.32 mg/g cell dry weight under the initial 10 mg/L Cr(VI) condition (Figure 6C). The EPS encapsulation of Cr(VI) by strain YC-34 was observed under SEM (Figure 6D), which was similar to the results of Zhou et al. (2021). The adsorptive removal of chromium by strain YC-34 may be achieved through adsorption sites on EPS (Jin et al., 2014; Pi et al., 2020), while the large

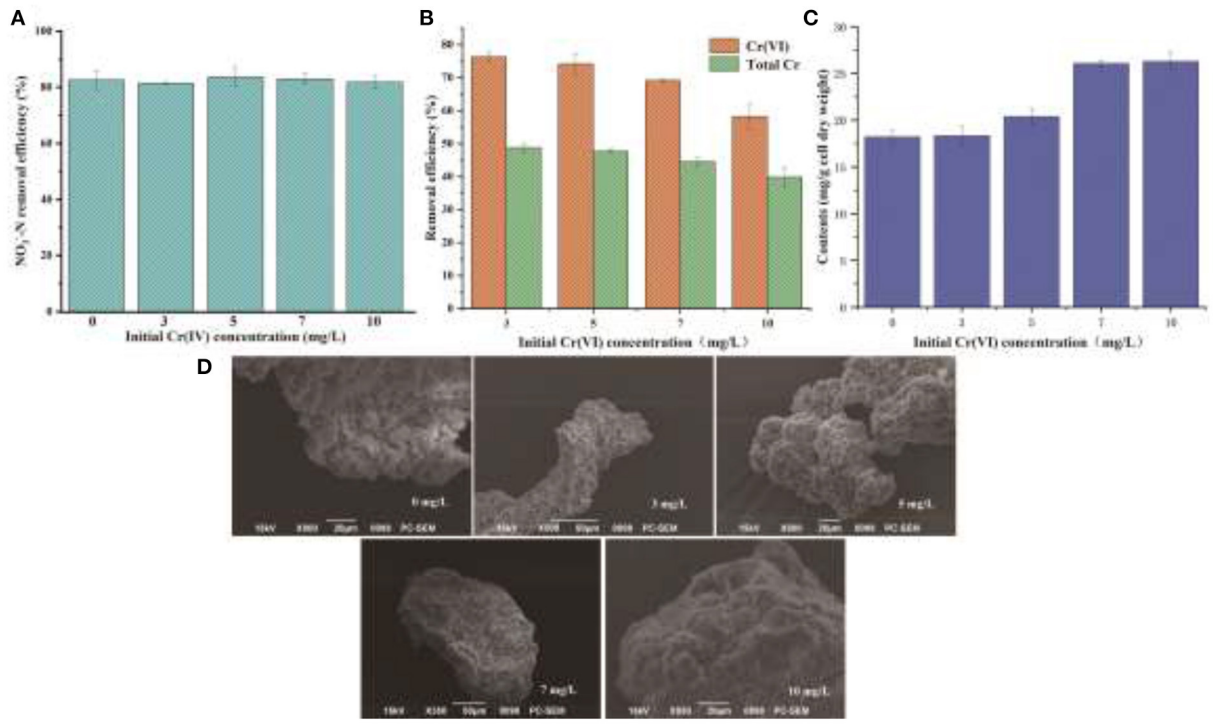


FIGURE 6
Denitrification capacity **(A)**, Cr removal **(B)**, EPS generation **(C)** under the different concentrations of Cr(VI); morphology of EPS at different Cr(VI) concentrations of 0, 3, 5, 7, and 10 mg/L under SEM observation **(D)**.

amount of EPS production helps strains to establish a stable structure that protects them from hazardous environments (Miao et al., 2018). Moreover, FTIR measurements and analysis showed almost no change in the transmittance of the measured bands of strianYC-34 in the groups with initial Cr(IV) of 0, 3 and 5 mg/L (Figure 7). Cell surface polymers are generally supported by a hydrogen bonding system, and the higher the proportion of hydrogen bonds, the stronger the intermolecular interactions (Cai et al., 2021). Further deconvolution analysis of FT-IR results in the 3,800–3,000 $cm^{-1}$ band showed that the hydrogen bonding types were significantly higher in the 0, 3, and 5 mg/L groups than in the 7 and 10 mg/L groups,

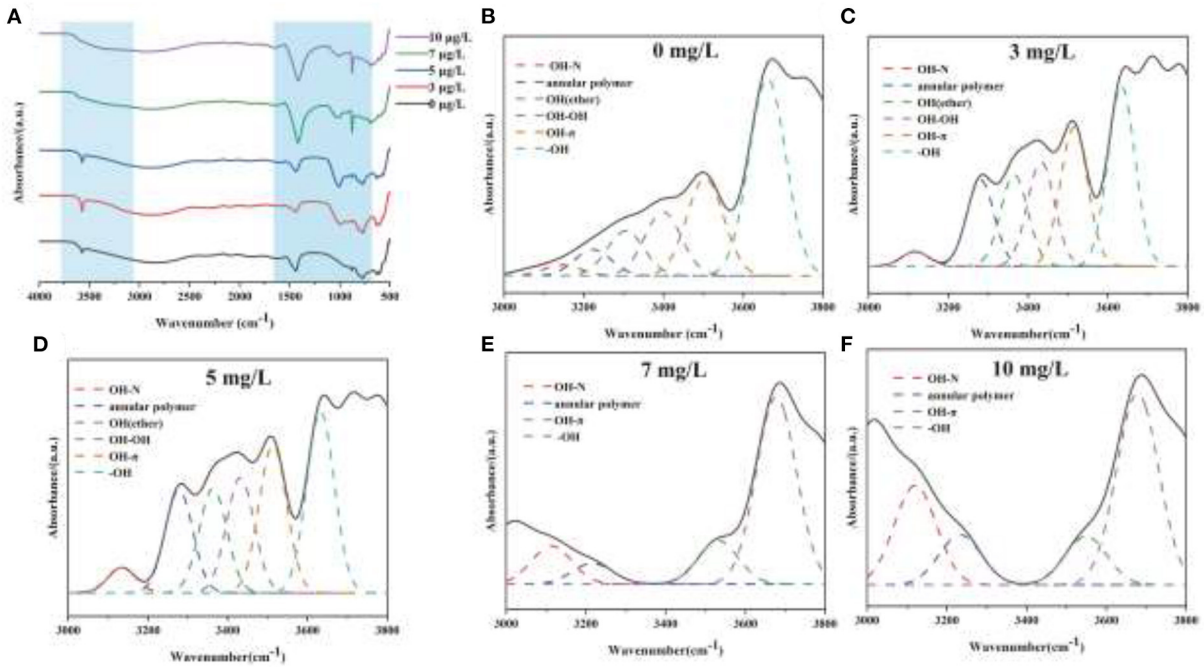


FIGURE 7
FT-IR spectra of strain YC-34 under different Cr(VI) stress **(A)** and their deconvoluted results for 0 **(B)**, 3 **(C)**, 5 **(D)**, 7 **(E)**, and 10 mg/L **(F)** at the region (3,000–4,000 $cm^{-1}$).

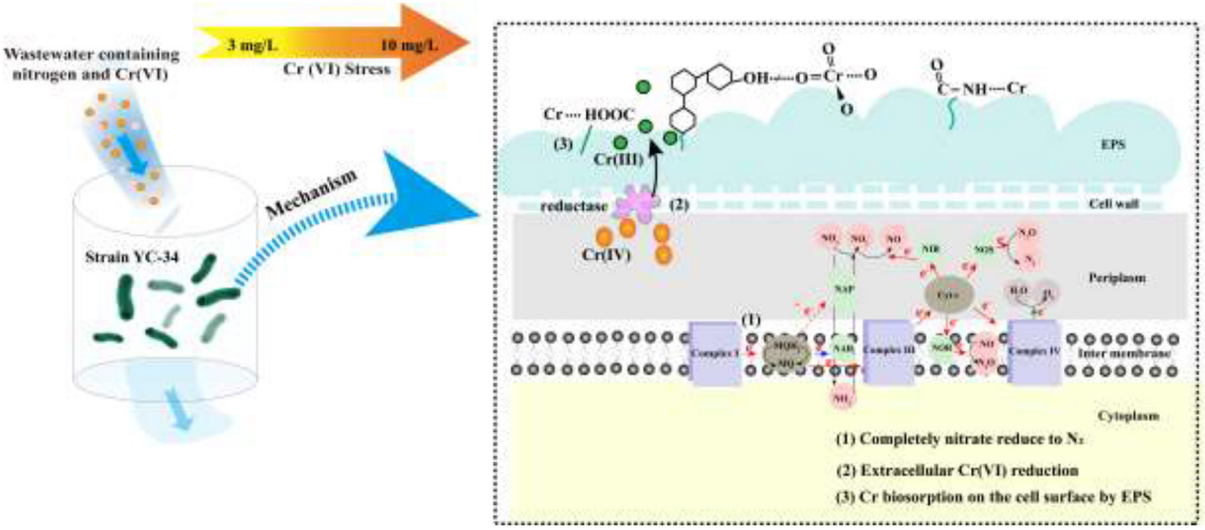


FIGURE 8
The speculative nitrate conversion and Cr(VI) removal mechanism of strain YC-34.

implying that the intermolecular forces on the bacterial surface weakened at Cr(IV) concentrations above 5 mg/L. In summary, considering the nitrogen removal pathway and the extracellular Cr(IV) adsorption characteristics analysis (Figure 8), the main removal mechanisms of strain YC-34 facing cadmium stress may be due to the adsorption of functional groups on the surface.

## Conclusion

A novel auto-aggregation aerobic denitrifier (*Pseudomonas stutzeri* strain YC-34) was isolated, demonstrating superior environmental adaptability and the ability to remove Cr(VI) in synthetic wastewater. YC-34 attained a high $NO_3^-$-N removal efficiency of 90.58% and showed fine adaptability to different culture conditions. Based on nitrogen balance and denitrification gene amplification analysis, the strain YC-34 presented a complete nitrogen pathway for Nitrate → Nitrite → Nitric oxide → Nitrous oxide → Nitrogen. Strain YC-34 produced a large amount of EPS, especially when exposed to Cr(VI), which in turn provided more abundant functional groups and strong hydrogen bonds to adsorb cadmium. These studies indicated that YC-34 has a superior potential for simultaneously treating synthetic wastewater contaminated with nitrogen and Cr(VI).

## Data availability statement

The datasets presented in this study can be found in online repositories. The names of the repository/repositories and accession number(s) can be found in the article/supplementary material.

## Author contributions

PH: conceptualization, methodology, software, data curation, writing-original draft, and writing-review and editing. KY: writing-original draft, methodology, and data curation. HB, YZ, HY, and SH: data curation and investigation. LK: conceptualization, methodology, supervision, and writing-review and editing. All authors contributed to the article and approved the submitted version.

## Funding

This research was supported by Key Research and Development Projects in Anhui Province (202104i07020001), National Natural Science Foundation of China (42107079), Anhui Natural Science Foundation (2108085QD159), the University Synergy Innovation Program of Anhui Province (GXXT-2020-075), Natural Science Foundation of Universities of Anhui Province (KJ2020A0076), and Anhui Normal University Student Innovation and Entrepreneurship Training Program.

## Conflict of interest

The authors declare that the research was conducted in the absence of any commercial or financial relationships that could be construed as a potential conflict of interest.

## Publisher's note

All claims expressed in this article are solely those of the authors and do not necessarily represent those of their affiliated organizations, or those of the publisher, the editors and the reviewers. Any product that may be evaluated in this article, or claim that may be made by its manufacturer, is not guaranteed or endorsed by the publisher.

## References

Adav, S. S., Lee, D. J., and Tay, J. H. (2008). Extracellular polymeric substances and structural stability of aerobic granule. *Water Res.* 42, 1644–1650. doi: 10.1016/j.watres.2007.10.013

An, Q., Zhou, Y., Zhao, B., and Huang, X. L. (2020). Efficient ammonium removal through heterotrophic nitrification-aerobic denitrification by *Acinetobacter baumannii* strain AL-6 in the presence of Cr(VI). *J. Biosci. Bioeng.* 130, 622–629. doi: 10.1016/j.jbiosc.2020.07.010

Auguet, O., Pijuan, M., Borrego, C. M., and Gutierrez, O. (2016). Control of sulfide and methane production in anaerobic sewer systems by means of downstream nitrite dosage. *Sci. Total Environ.* 550, 1116–1125. doi: 10.1016/j.scitotenv.2016.01.130

Baker, S. C., Saunders, N. F., Willis, A. C., Ferguson, S. J., Hajdu, J., and Fülöp, V. (1997). Cytochrome cd1 structure: unusual haem environments in a nitrite reductase and analysis of factors contributing to beta-propeller folds. *J. Mol. Biol.* 269, 440–455. doi: 10.1006/jmbi.1997.1070

Cai, H., Wang, Y., Wu, K., and Guo, W. (2020). Enhanced hydrophilic and electrophilic properties of polyvinyl Chloride (PVC) biofilm carrier. *Polymers* 12, 1240. doi: 10.3390/polym12061240

Cai, S., Wu, H., Hong, P., Donde, O. O., Wang, C., Fang, T., et al. (2021). Bioflocculation effect of *Glyptotendipes tokunagai* on different Microcystis species: interactions between secreted silk and extracellular polymeric substances. *Chemosphere* 277, 130321. doi: 10.1016/j.chemosphere.2021.130321

Chen, Q., Ni, J., Ma, T., Liu, T., and Zheng, M. (2015). Bioaugmentation treatment of municipal wastewater with heterotrophic-aerobic nitrogen removal bacteria in a pilot-scale SBR. *Bioresour. Technol.* 183, 25–32. doi: 10.1016/j.biortech.2015.02.022

Collado, M. C., Meriluoto, J., and Salminen, S. (2007). Measurement of aggregation properties between probiotics and pathogens: *in vitro* evaluation of different methods. *J. Microbiol. Methods* 71, 71–74. doi: 10.1016/j.mimet.2007.07.005

Colussi, I., Cortesi, A., Vedova, L. D., Gallo, V., and Robles, F. K. C. (2009). Start-up procedures and analysis of heavy metals inhibition on methanogenic activity in EGSB reactor. *Bioresour. Technol.* 100, 6290–6294. doi: 10.1016/j.biortech.2009.07.041

Das, C., Naseera, K., Ram, A., Meena, R. M., and Ramaiah, N. (2016). Bioremediation of tannery wastewater by a salt-tolerant strain of *Chlorella vulgaris*. *J. Appl. Phycol.* 29, 235–243. doi: 10.1007/s10811-016-0910-8

Eboigbodin, K. E., and Biggs, C. A. (2008). Characterization of the extracellular polymeric substances produced by *Escherichia coli* using infrared spectroscopic, proteomic, and aggregation studies. *Biomacromolecules* 9, 686–695. doi: 10.1021/bm701043c

Fan, H. C., Yu, J., Chen, R. P., and Yu, L. (2019). Preparation of a bioflocculant by using acetonitrile as sole nitrogen source and its application in heavy metals removal. *J. Hazard. Mater.* 363, 242–247. doi: 10.1016/j.jhazmat.2018.09.063

Feng, Y., Feng, J., and Shu, Q. L. (2018). Isolation and characterization of heterotrophic nitrifying and aerobic denitrifying *Klebsiella pneumoniae* and *Klebsiella variicola* strains from various environments. *J. Appl. Microbiol.* 124, 1195–1211. doi: 10.1111/jam.13703

Harris, E., Diaz-Pines, E., Stoll, E., Schloter, M., Schulz, S., Duffner, C., et al. (2021). Denitrifying pathways dominate nitrous oxide emissions from managed grassland during drought and rewetting. *Sci. Adv.* 7, eabb7118. doi: 10.1126/sciadv.abb7118

He, D., Zheng, M., Ma, T., Li, C., and Ni, J. (2015). Interaction of Cr(VI) reduction and denitrification by strain Pseudomonas aeruginosa PCN-2 under aerobic conditions. *Bioresour. Technol.* 185, 346–352. doi: 10.1016/j.biortech.2015.02.10910.1016/j.biortech.2015.02.109

Hong, P., Shu, Y. L., Wu, X. Q., Wang, C. B., Tian, C. C., Wu, H. L., et al. (2019). Efficacy of zero nitrous oxide emitting aerobic denitrifying bacterium, *Methylobacterium gregans* DC-1 in nitrate removal with strong auto-aggregation property. *Bioresour. Technol.* 293, 122083. doi: 10.1016/j.biortech.2019.122083

Hong, P., Wu, X., Shu, Y., Wang, C., Tian, C., Wu, H., et al. (2020). Bioaugmentation treatment of nitrogen-rich wastewater with a denitrifier with biofilm-formation and nitrogen-removal capacities in a sequencing batch biofilm reactor. *Bioresour. Technol.* 303, 122905. doi: 10.1016/j.biortech.2020.122905

Hong, P., Yang, K., Shu, Y., Xiao, B., Wu, H., Xie, Y., et al. (2021). Efficacy of auto-aggregating aerobic denitrifiers with coaggregation traits for bioaugmentation performance in biofilm-formation and nitrogen-removal. *Bioresour. Technol.* 337, 125391. doi: 10.1016/j.biortech.2021.125391

Hong, P., Zhang, K., Dai, Y., Yuen, C. N. T., Gao, Y., Gu, Y., et al. (2022). Application of aerobic denitrifier for simultaneous removal of nitrogen, zinc, and bisphenol A from wastewater. *Bioresour. Technol.* 354, 127192. doi: 10.1016/j.biortech.2022.127192

Huang, T. L., Guo, L., Zhang, H. H., Su, J. F., Wen, G., and Zhang, K. (2015). Nitrogen-removal efficiency of a novel aerobic denitrifying bacterium, *Pseudomonas stutzeri* strain ZF31, isolated from a drinking-water reservoir. *Bioresour. Technol.* 196, 209–216. doi: 10.1016/j.biortech.2015.07.059

Jia, F., Yang, Q., Liu, X., Li, X., Li, B., Zhang, L., et al. (2017). Stratification of extracellular polymeric substances (EPS) for aggregated anammox microorganisms. *Environ. Sci. Technol.* 51, 3260–3268. doi: 10.1021/acs.est.6b05761

Jin, J. T., Wu, G. X., Zhang, Z. H., and Guan, Y. T. (2014). Effect of extracellular polymeric substances on corrosion of cast iron in the reclaimed wastewater. *Bioresour. Technol.* 165, 162–165. doi: 10.1016/j.biortech.2014.01.117

Konovalova,V. V., Dmytrenko, G. M., Nigmatullin, R. R., Bryk, M. T., and Gvozdyak, P. I. (2009). Chromium(VI) reduction in a membrane bioreactor with immobilized Pseudomonas cells. *Enzym. Microb. Technol.* 33, 899–907. doi: 10.1016/S0141-0229(03)00204-7

Lang, X. D., Li, Q. W., Xu, Y. C., Ji, M. M., Yan, G. X., and Guo, S. H. (2019). Aerobic denitrifiers with petroleum metabolizing ability isolated from caprolactam sewage treatment pool. *Bioresour. Technol.* 290, 121719. doi: 10.1016/j.biortech.2019.121719

Laothamteep, N., Naloka, K., and Pinyakong, O. (2022). Bioaugmentation with zeolite-immobilized bacterial consortium OPK results in a bacterial community shift and enhances the bioremediation of crude oil-polluted marine sandy soil microcosms. *Environ. Pollut.* 292(Pt A), 118309. doi: 10.1016/j.envpol.2021.118309

Li, B., Lv, R., Xiao, Y., Hu, W., Mai, Y. L., Zhang, J. W., et al. (2019). A novel nitrite-base aerobic denitrifying bacterium *Acinetobacter* sp. YT03 and its transcriptome analysis. *Front. Microbiol.* 10, 2580. doi: 10.3389/fmicb.2019.02580

Liu, Y., Ai, G. M., Miao, L. L., and Liu, Z. P. (2016). *Marinobacter* strain NNA5, a newly isolated and highly efficient aerobic denitrifier with zero $N_2O$ emission. *Bioresour. Technol.* 206, 9–15. doi: 10.1016/j.biortech.2016.01.066

Luhar, I., Luhar, S., Abdullah, M. M. A. B., Razak, R. A., Vizureanu, P., Sandu, A. V., et al. (2021). A state-of-the-art review on innovative geopolymer composites designed for water and wastewater treatment. *Materials* 14, 7456. doi: 10.3390/ma14237456

Ma, H., Zhao, Y., Yang, K., Wang, Y., Zhang, C., and Ji, M. (2022). Application oriented bioaugmentation processes: Mechanism, performance improvement and scale-up. *Bioresour. Technol.* 344(Pt B), 126192. doi: 10.1016/j.biortech.2021.126192

Miao, L., Zhang, Q., Wang, S. Y., Li, B. K., Wang, Z., Zhang, S. J., et al. (2018). Characterization of EPS compositions and microbial community in an Anammox SBBR system treating landfill leachate. *Bioresour. Technol.* 249, 108–116. doi: 10.1016/j.biortech.2017.09.151

Miyahara, M., Kim, S. W., Fushinobu, S., Takaki, K., Yamada, T., Watanabe, A., et al. (2010). Aerobic denitrification by Pseudomonas stutzeri TR2 has the potential to reduce nitrous oxide emission from wastewater treatment plants. *Appl. Environ. Microbiol.* 76, 4619–4625. doi: 10.1128/AEM.01983-09

Nguyen, P. Y., Carvalho, G., Reis, M. A. M., and Oehmen, A. (2021). A review of the biotransformations of priority pharmaceuticals in biological wastewater treatment processes. *Water Res.* 188, 116446. doi: 10.1016/j.watres.2020.116446

Ochoa-Herrera, V., Banihani, Q., León, G., Khatri, C., Field, J. A., and Sierra-Alvarez, R. (2009). Toxicity of fluoride to microorganisms in biological wastewater treatment systems. *Water Res.* 43, 3177–3186. doi: 10.1016/j.watres.2009.04.032

Palanivel, T. M., Sivakumar, N., Al-Ansari, A., and Victor, R. (2020). Bioremediation of copper by active cells of *Pseudomonas stutzeri* LA3 isolated from an abandoned copper mine soil. *J. Environ. Manag.* 253, 109706. doi: 10.1016/j.jenvman.2019.109706

Peng, H., Li, D., Ye, J., Xu, H., Xie, W., Zhang, Y., et al. (2019). Biosorption behavior of the *Ochrobactrum* MT180101 on ionic copper and chelate copper. *J. Environ. Manag.* 235, 224–230. doi: 10.1016/j.jenvman.2019.01.060

Perez-Garcia, O., Mankelow, C., Chandran, K., Villas-Boas, S. G., and Singhal, N. (2017). Modulation of nitrous oxide ($N_2O$) accumulation by primary metabolites in denitrifying cultures adapting to changes in environmental C and N. *Environ. Sci. Technol.* 51, 13678–13688. doi: 10.1021/acs.est.7b03345

Pi, S. S., Li, A., Cui, D., Su, Z., Zhou, L., and Ma, F. (2020). Enhanced adsorption performance and regeneration of magnetic Fe3O4 nanoparticles assisted extracellular polymeric substances in sulfonamide-contaminated water. *Environ. Sci. Pollut. Res. Int.* 227, 4866–4875. doi: 10.1007/s11356-019-06956-4

Qing, H., Donde, O. O., Tian, C. C., Wang, C. B., Wu, X. Q., Feng, S. S., et al. (2018). Novel heterotrophic nitrogen removal and assimilation characteristic of the newly isolated bacterium *Pseudomonas stutzeri* AD-1. *J. Biosci. Bioeng.* 126, 339–345. doi: 10.1016/j.jbiosc.2018.03.010

Ren, J. L., Ma, H. J., Liu, Y., Ruan, Y. J., Wei, C. Z., Song, J., et al. (2021). Characterization of a novel marine aerobic denitrifier *Vibrio* spp. AD2 for efficient nitrate reduction without nitrite accumulation. *Environ. Sci. Pollut. Res. Int.* 28, 30807–30820. doi: 10.1007/s11356-021-12673-8

Ren, J. L., Wei, C. Z., Ma, H. J., Dai, M. Y., Fan, J. Z., Liu, Y., et al. (2019). The Nitrogen-removal efficiency of a novel high-efficiency salt-tolerant aerobic denitrifier, *Halomonas Alkaliphile* HRL-9, isolated from a seawater biofilter. *Int. J. Environ. Res. Public Health.* 16, 4451. doi: 10.3390/ijerph16224451

Sharma, S., and Malaviya, P. (2016). Bioremediation of tannery wastewater by chromium resistant novel fungal consortium. *Eco. Eng.* 91, 419–425. doi: 10.1016/j.ecoleng.2016.03.005

Shoun, H., Fushinobu, S., Jiang, L., Kim, S. W., and Wakagi, T. (2012). Fungal denitrification and nitric oxide reductase cytochrome P450nor. *Phil. Trans. R. Soc. Lond. B. Biol. Sci.* 367, 1186–1194. doi: 10.1098/rstb.2011.0335

Tallec, G., Garnier, J., Billen, G., and Gousailles, M. (2008). Nitrous oxide emissions from denitrifying activated sludge of urban wastewater treatment plants, under anoxia and low oxygenation. *Bioresour. Technol.* 99, 2200–2209. doi: 10.1016/j.biortech.2007.05.025

Truskewycz, A., Shukla, R., and Ball, A. S. (2018). Phytofabrication of iron nanoparticles for hexavalent chromium remediation. *ACS Omega* 3, 10781–10790. doi: 10.1021/acsomega.8b00410

Tsybulskaya, O. N., Ksenik, T. V., Yudakov, A. A., and Slesarenko, V. V. (2019). Reagent decontamination of liquid chrome-containing industrial wastes. *Environ. Technol. Innov.* 13, 1–10. doi: 10.1016/j.eti.2018.10.003

Uluseker, C., Kaster, K. M., Thorsen, K., Basiry, D., Shobana, S., Jain, M., et al. (2021). A review on occurrence and spread of antibiotic resistance in

wastewaters and in wastewater treatment plants: mechanisms and perspectives. *Front. Microbiol.* 12, 717809. doi: 10.3389/fmicb.2021.717809

Uraguchi, D., Ueki,Y., and Ooi, T. (2009). Chiral organic ion pair catalysts assembled through a hydrogen-bonding network. *Science* 326, 120–123. doi: 10.1126/science.1176758

Wang, H., and Li, L. (2022). Comprehensive evaluation of probiotic property, hypoglycemic ability and antioxidant activity of lactic acid bacteria. *Foods* 11, 1363. doi: 10.3390/foods11091363

Wang, Q., Chen, Q., Yan, D., and Xin, S. (2018). Distribution, ecological risk, and source analysis of heavy metals in sediments of Taizihe River, China. *Environ. Earth Sci*. 77, 569. doi: 10.1007/s12665-018-7750-6

Wang, Q., Zhao, Y., Zhai, S., Liu, D., Zhou, X., Wang, Y., et al. (2021). Application of different redox mediators induced bio-promoters to accelerate the recovery of denitrification and denitrifying functional microorganisms inhibited by transient Cr(VI) shock. *J. Hazard. Mater*. 420, 126664. doi: 10.1016/j.jhazmat.2021.126664

Wang, X., Wang, W., Zhang, J., Wang, S., and Li, J. (2019). Dominance of *Candidatus saccharibacteria* in SBRs achieving partial denitrification: effects of sludge acclimating methods on microbial communities and nitrite accumulation. *RSC Adv*. 9, 11263–11271. doi: 10.1039/C8RA09518C

Wang, Y., Zhao, Y., Ji, M., and Zhai, H. (2015). Nitrification recovery behavior by bio-accelerators in copper-inhibited activated sludge system. *Bioresour. Technol.* 192, 748–755. doi: 10.1016/j.biortech.2015.06.015

Wei, W., Wang, Q. L., Li, A., Yang, J. X., Ma, F., Pi, S. S., et al. (2016). Biosorption of Pb (II) from aqueous solution by extracellular polymeric substances extracted from *Klebsiella* sp. J1: adsorption behavior and mechanism assessment. *Sci. Rep*. 6, 31575. doi: 10.1038/srep31575

Wen, J., Okyere, S. K., Wang, S., Wang, J., Xie, L., Ran, Y., et al. (2022). Endophytic fungi: an effective alternative source of plant-derived bioactive compounds for pharmacological studies. *J. Fungi* 8, 205. doi: 10.3390/jof8020205

Yue, Z. B., Li, Q., Li, C. C., Chen, T. H., and Wang, J. (2015). Component analysis and heavy metal adsorption ability of extracellular polymeric substances (EPS) from sulfate reducing bacteria. *Bioresour. Technol.* 194, 399–402. doi: 10.1016/j.biortech.2015.07.042

Zhang, M., Li, A., Yao, Q., Xiao, B., and Zhu, H. (2022). *Pseudomonas oligotrophica* sp. nov., a novel denitrifying bacterium possessing nitrogen removal capability under low carbon-nitrogen ratio condition. *Front. Microbiol.* 13, 882890. doi: 10.3389/fmicb.2022.882890

Zhang, Q. L., Liu, Y., Ai, G. M., Miao, L. L., Zheng, H. Y., and Liu, Z. P. (2012). The characteristics of a novel heterotrophic nitrification-aerobic denitrification bacterium, *Bacillus methylotrophicus* strain L7. *Bioresour. Technol.* 108, 35–44. doi: 10.1016/j.biortech.2011.12.139

Zhang, W., Yan, C., Shen, J. N., Wei, R. P., Gao, Y., Miao, A., et al. (2019). Characterization of aerobic denitrifying bacterium *Pseudomonas mendocina* strain GL6 and its potential application in wastewater treatment plant effluent. *Int. J. Environ. Res. Public Health*. 16, 364. doi: 10.3390/ijerph16030364

Zhao, B., Cheng, D. Y., Tan, P., An, Q., and Guo, J. S. (2018). Characterization of an aerobic denitrifier *Pseudomonas stutzeri* strain XL-2 to achieve efficient nitrate removal. *Bioresour. Technol.* 250, 564–573. doi: 10.1016/j.biortech.2017.11.038

Zhou, X., Zhai, S., Zhao, Y., Liu, D., Wang, Q., and Ji, M. (2021). Rapid recovery of inhibited denitrification with cascade Cr(VI) exposure by bio-accelerant: characterization of chromium distributions, EPS compositions and denitrifying communities. *J. Hazard. Mater.* 411, 125087. doi: 10.1016/j.jhazmat.2021.125087

Zhu, B., Song, L., Kong, X., Macleod, L. C., and Xu, P. (2018). A novel regulator modulates glucan production, cell aggregation and biofilm formation in *Streptococcus sanguinis* SK36. *Front. Microbiol.* 9, 1154. doi: 10.3389/fmicb.2018.01154

Zhu, L., Ding, W., Feng, L. J., Kong, Y., Xu, J., and Xu, X. Y. (2012). Isolation of aerobic denitrifiers and characterization for their potential application in the bioremediation of oligotrophic ecosystem. *Bioresour. Technol.* 108, 1–7. doi: 10.1016/j.biortech.2011.12.033

frontiers | Frontiers in Microbiology

TYPE Original Research
PUBLISHED 02 September 2022
DOI 10.3389/fmicb.2022.985239



OPEN ACCESS

EDITED BY
Xianhua Liu,
Tianjin University, China

REVIEWED BY
Xinhou Zhang,
Nanjing Normal University, China
Jiaoyue Wang,
Institute of Applied Ecology (CAS), China
Chen Tu,
Institute of Soil Science (CAS), China

*CORRESPONDENCE
Lili Wang
lili0229ok@126.com

SPECIALTY SECTION
This article was submitted to Terrestrial Microbiology, a section of the journal Frontiers in Microbiology

RECEIVED 03 July 2022
ACCEPTED 08 August 2022
PUBLISHED 02 September 2022

CITATION
Yao Y, Wang L, Gong L, Li G, Xiu W, Yang X, Tan B, Zhao J and Zhang G (2022) Differences, links, and roles of microbial and stoichiometric factors in microplastic distribution: A case study of five typical rice cropping regions in China.
*Front. Microbiol.* 13:985239.
doi: 10.3389/fmicb.2022.985239



# Differences, links, and roles of microbial and stoichiometric factors in microplastic distribution: A case study of five typical rice cropping regions in China

Yao Yao[1], Lili Wang[1]*, Lingxuan Gong[1], Gang Li[1], Weiming Xiu[1], Xiaomei Yang[2,3], Bingchang Tan[1], Jianning Zhao[1] and Guilong Zhang[1]

[1]Agro-Environmental Protection Institute, Ministry of Agriculture and Rural Affairs, Tianjin, China, [2]College of Natural Resources and Environment, Northwest A&F University, Yangling, China, [3]Soil Physics and Land Management Group, Wageningen University & Research, Wageningen, Netherlands

Microplastics (MPs), as new pollutants in agroecosystems, have already attracted widespread attention from scientists. However, our understanding of MP geographic distribution and its influencing factors across spatial scales remains poor. Here, a regional-scale field investigation was conducted to assess the distribution characteristic of MPs in five major rice-growing regions of China, and we explored the roles of biological and abiotic factors, especially stoichiometry and microbial influences on MP distribution. MPs were observed in all sampling sites, averaging 6,390 ± 2,031 items·kg$^{-1}$. Sizes less than 0.5 mm and black and transparent MPs dominated. Fiber, classified as one of the MP shapes, occurred most frequently. MP community analysis, firstly used in paddy soil, revealed more black MPs abundance in Henan (HE), more rayon, blue, and other colors MPs in Hunan (HN), more transparent MPs in Tianjing (TJ), and more PE MPs in Heilongjiang (DB). Higher MP community diversity was found in most south paddy soils of this study, due to a broader range of sources. C/N showed a positive relationship with pellet-shaped MP abundance and MPs of size between 2 and 5 mm ($P < 0.05$). Chao1 index of soil microbial communities was positively correlated with the MP abundance, MPs of size less than 0.5 mm, and fiber abundance. The minimum temperature was positively correlated with MP abundance ($P < 0.05$), implying the potential effects of the freeze-thaw process might exist. The regression analysis highlighted the important role of population quantity in determining MP abundance ($R = 0.421$, $P = 0.02$). This study confirmed the wide distribution

of MPs in different soil depths of paddy lands in China and demonstrated that its distribution was influenced by population quantity and environmental variables, such as microbiology. These findings could provide a basis for the toxicological behavior of MPs and the potential risk to human health.

KEYWORDS

microplastics, microbiology, stoichiometric ratio, paddy soils, bacterial diversity

## Introduction

Due to the extensive use and inappropriate disposal of plastic products, microplastic (MP) pollution has been recognized as a new threat to our earth systems and have become a research hotspot for scholars (Hu et al., 2019; Leifheit et al., 2021). Much evidence has verified the existence of MPs in oceans (Jiang Y. et al., 2020), fresh water (Miao et al., 2020), atmospheres (Dong et al., 2021), soils and other mediums (Abayomi et al., 2017; Bergmann et al., 2019; Wang et al., 2021). Polymer types, abundance, and distribution characteristics varied among different environments. Until now, most current studies focused on aquatic ecosystems. However, agroecosystems are a massive sink for MPs, with long-lasting presence and harmful effects. MPs could affect soil physicochemical properties, including soil bulk density, pH, and soil aggregates (Machado et al., 2018, 2019; Wang F. et al., 2020), and could even be toxic to microorganisms and soil animals (Jiang X. et al., 2020; Li et al., 2020). It has also been shown that MPs can accumulate in plants (Zhang H. et al., 2022), and are transferred through the food chain and food web, ultimately endangering human health (Huerta Lwanga et al., 2017; Wong et al., 2020). In addition, the release of additives in MPs (Li et al., 2020) and the adsorption of MPs to other agricultural soil pollutants such as heavy metals, antibiotics, and pesticides increase the risk of MPs (Dong et al., 2020b; Wang T. et al., 2020). Therefore, exploring the MP distribution in agricultural ecosystems is crucial to assess their ecological effects on farmland and human health.

To date, MP pollution has been serious in agricultural fields and many factors lead to its accumulation. For example, wind speed, precipitation, freeze-thaw cycling, and alternating wet and dry processes among different geographical locations can affect the migration, accumulation, and degradation of MPs (Wang et al., 2021; Yu et al., 2022; Zhang H. et al., 2022). Similarly, MP distribution could be influenced by soil properties. One study in Shouguang, Shandong Province, showed the correlation between soil texture and MP distribution, with sandy soils having more aeration pores, which facilitated MP transport, and loamy soils having tiny pores that facilitated long-term MP accumulations (Yu et al., 2021). Also, pH could affect MP distribution due to high pH inhibiting the adsorption between negatively charged MPs and soil, thus increasing their transport (Luo et al., 2020). Soil organic carbon (SOC) acted as a substrate to promote microbial degradation of MPs, the improvement of soil pore space caused by SOC could promote MP migration (Zhang S. et al., 2020; Guo et al., 2021). Furthermore, different regional land use patterns and crop types vary the use of mulch, tillage practices, and fertilizer application (Wang et al., 2021; Zhang H. et al., 2022), thus influencing the MP abundance. For instance, the pores produced by corn roots accelerated the MP movement (Guo et al., 2020; Li H. et al., 2021). Thus, exploring MPs among different agricultural soils is vitally essential for evaluating the risk of MPs to cropping systems. However, the role of activated carbon components [i.e., dissolved organic carbon (DOC)], microbial communities, and stoichiometric ratios (e.g., C/N, N/P) on MP distribution and their coupling relationship, remain largely unstudied.

Rice is an essential food crop with a large planting area, previous studies have revealed the adverse effects of MPs on rice germination, growth, and yield through metabolomics and transcriptomics (Zhang et al., 2021; Chen et al., 2022; Wu et al., 2022). Hence, investigating and studying the distribution characteristics of MPs in paddy soils is crucial for food security, plant and animal growth, and human health (Wang et al., 2021). Kim et al. (2021) found that MPs in Korean paddy soil of 0–5 cm depth were about 160 $\pm$ 92 items·kg$^{-1}$. An investigation showed 16.1 $\pm$ 3.5 items·kg$^{-1}$ MPs in paddy and duck rice fields (Lv et al., 2019). Existing studies also explored the effects of MPs on microorganisms, functional genes, greenhouse gas emissions, and migration and transformation of other heavy metals in rice paddy land (Dong et al., 2020a; Xiao et al., 2021; Han et al., 2022; Sun X. et al., 2022; Yang X. et al., 2022). However, the related previous researches are rather fragmented, and have a considerable discrepancy, while regional studies on the spatial partitioning characteristics of soil MPs and the influencing mechanisms in paddy soils are critically limited.

The properties of MPs are complex, including diverse shapes, colors, sizes, polymer types, and additives types (Rochman et al., 2019). Consequently, we should consider MPs as a collection of different pollutants rather than one pollutant when researching the source, fate, and impact of MPs on organisms and ecosystems (Rochman et al., 2019; Zhou et al., 2020). Recently, the new "MP communities" was proposed

to solve this problem. MPs combined with various colors, shapes, and polymer types were regarded as MP communities, similar to microbial communities (Zhou et al., 2020, 2022; Li C. et al., 2021). MP communities could comprehensively describe MP characteristics and pollution and analyze the associations and differences in MPs in different environmental units or compartments, which is more conducive to the effective control of MP (Wang et al., 2019; Li C. et al., 2021; Zhou et al., 2022). Through integrated analysis, there is a particular link between MP communities in five environments (freshwater, seawater, freshwater sediment, sea sediment, and soil), which decreases with the increase in geographical location (Li C. et al., 2021). A study in the world's third-largest river found MPs in different compartments were significantly district and highly correlated with geographical distance through MP community analysis (Yuan et al., 2022). Zhou et al. (2022) found that complex point and non-point sources in urban soils could cause the inhomogeneity and heterogeneity of MP communities.

China's rice cropping areas span several climatic zones, resulting in multiple environmental factors and differences in the distribution of MPs. There is still a lack of knowledge on the distribution characteristics of MPs in different paddy soils, especially for the coupling relationship between MP distribution and soil properties, and meteorological conditions. Therefore, this study selected five major rice cropping areas in China. The objectives were to (1) determine and compare the abundance, distribution, and characteristics of MPs in different paddy soils and depths, and identify their potential sources; (2) apply the MP communities concept in paddy soils for the first time, and evaluate the differences and association of MP distribution, and provide a basis for MP risk assessment; (3) elucidate the coupling relationship among soil microbial communities, C/N, climatic conditions, and MP distribution and characteristics.

# Materials and methods

## Study site and sample collection

Five major rice cropping regions in China were selected for this study. Specific locations are shown in **Figure 1**. The details of sampling sites were shown in **Supplementary materials**.

Soil samples were collected before the rice harvest in October 2021, and three plots (10 m × 10 m) were selected as three replicates for each sampling site. Using the S-shaped sampling method, 15 sampling points were selected for each plot. And 0–20 cm and 20–40 cm soil samples were taken, respectively with a 5 cm diameter soil auger. The soil samples from the same plot were mixed evenly to represent the entire sampling point. Stones and visible stubbles were removed and packed into aluminum boxes, and quickly brought back to the laboratory in ice boxes. Soil samples were divided into three parts, one part was stored at −80°C for microbial identification, one part was freeze-dried (Eyela freeze dryer, FDU-1200) for MP identification, and the remaining part was used for the determination of the soil physical and chemical properties.

## Microplastic extraction and identification

Microplastics were extracted from soil samples by density separation method, based on EPA and technical regulation for monitoring marine MP (Trial) (Masura et al., 2015) with modifications (Li et al., 2020; Wang et al., 2021; Zhang H. et al., 2022).

A 10 g lyophilized soil sample and 500 ml Zinc chloride solution ($ZnCl_2$) were added to a 2 L beaker, stirred continuously for 48 h, then left to stand, transferred in batches to a partition funnel, then left to stand for 24 h. The upper liquid lay was collected and filtered through a 0.45 μm filter membrane and set aside. The flotation process was repeated three times as described above to ensure that all MPs were extracted. The material on the filter membrane was ultrasonically backwashed into a beaker, and the filter membrane was processed for microscopic examination to confirm that no MPs remained, then was placed in a heated temperature-controlled and speed-controlled shaker after adding Fenton reagent and hydrogen peroxide, and was then digested for 72 h. Then the solution was passed through a 0.45 μm filter membrane again.

Dried sample membranes were observed under a stereoscopic (Leica LAS X) microscope with a high-resolution digital camera and the number, size, shape, and color of MPs were all recorded. The polymer types of all MPs were identified using μ-FT-IR (is10, America). The spectra were measured in the range of 700–4,000 $cm^{-1}$, with a resolution of 8 $cm^{-1}$ and a scan count of 32. The test results were compared with a library of synthetic polymer spectra, and the sample composition was judged based on a match of more than 70%.

## Microplastic communities

This study applies the MP community concept in paddy soils and evaluates the differences and association of MP distribution.

Analysis of similarities (ANOSIM) and linear discriminant analysis (LDA) were used to compare differences between soil MP communities in the different geographic position; LDA effect size (LEfSe) was used to analyze the soil characteristic MP types in each sampling sites; LEfSe analysis is available on http://huttenhower.sph.harvard.edu/galaxy. The similarity of MP communities among different environments was tested by mantel based on Bray-Curtis distance. Previous studies have described the characteristics of MP pollution and speculated the source only through the single MP feature index, such as shape diversity index (Wang et al., 2019) and polymer type

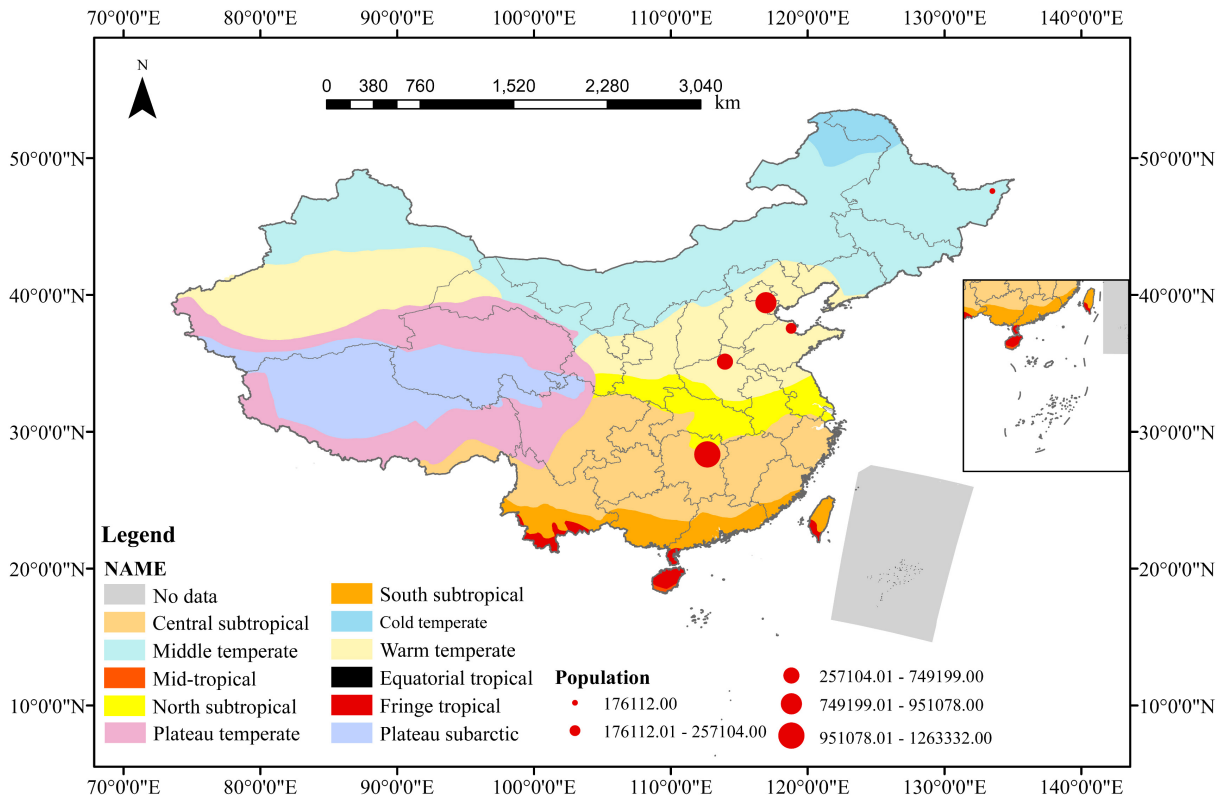


FIGURE 1
Soil sampling sites in this study.

diversity index (Zhou et al., 2019). However, MPs are a group of contaminants aggregated with multiple properties, and it is not sufficient to describe them with a single diversity indicator (Zhou et al., 2022). Fully and comprehensively considering three diversity indices of color, size, and polymer type, a multiple composite index (MDII index) proposed by Li C. et al. (2021) was used to compare the diversity of MP communities and help in pollution source analysis.

$$\mathrm{MDII} = (Simpson\_shape \times Simpson\_color \times Simpson\_polymer)^{1/3}$$

## Determination of soil physical and chemical properties

In this study, we tested four activated carbon components: microbial biomass carbon (MBC), DOC, particulate organic carbon (POC), and permanganate oxidizable carbon (POXC) and the methods followed by Shen et al. (2021). MBC was fumigated with chloroform, extracted with potassium sulfate, and determined by a total organic carbon analyzer (Multi N/C3100, Hamburg, Germany). DOC was extracted using a water-soil ratio of 5:1, shaken at 25°C for 30 min, and centrifuged at 4,500 rpm for 20 min; the supernatant was passed through a 0.45 μm filter membrane and then analyzed by Multi N/C 3000 total organic carbon/total carbon analyzer (Multi N/C 3000, Hamburg, Germany). POC was extracted by $(NaPO_3)_6$ and then determined by SOC that failed to pass the 0.053 mm sieve. POXC was obtained by $KMnO_4$ (333 mM) oxidation and calculated by its loss. C/N, C/P, and N/P were the ratio of total carbon to total nitrogen, total carbon to total phosphorus, and total nitrogen to total phosphorus, respectively.

## DNA extraction, amplification and sequencing of soil microorganisms

Soil microbiome DNA was extracted based on the instructions of the Power Soil DNA Isolation Kit (MO BIO Laboratories, Carlsbad, CA, United States). DNA mass and concentration was determined using a 1% agarose gel electrophoresis and spectrometer. The V3–V4 region of the bacterial 16srRNA gene was amplified using primers 338 F (5′-ACTCCTACGGGAGGCAGCAG-3′) and 806 R (5′-GGACTACNNGGGTATCTAAT-3′), and 8 bp of barcode sequence was added to each of the upstream and downstream 5′ primer ends to distinguish between the different samples. The PCR product was detected by a 1% agarose gel

electrophoresis and purified with Agencourt AMPure XP nucleic acid purification kit. Then, the microbial diversity sequencing library was constructed and paired-end sequencing was performed using Illumina MiSeq PE300 high-throughput sequencing platform.

## Quality control

To avoid atmospheric and potential human contamination and ensure the accuracy of this experiment, we conducted strict quality control during the experiment by wearing masks, cotton lab coats, and gloves. All vessels were cleaned with ultrapure water and the cleanliness of each experimental apparatus was ensured. Two control experiments were set up to eliminate the influence of the control and the reagent, and a control spiking experiment with a recovery rate of 98–100% was also set up.

## Data analysis

All data were processed and analyzed using Excel 2013, SPSS 24, and R studio. Origin and R studio were used for graphical plotting. Duncan method in One-way ANOVA was used to compare the differences between distinct paddy soils, and an independent sample *T*-test was used to analyze the differences between different depths of soil in the same geographic position. The correlation between different MP indicators and environmental factors was tested using Spearman non-parametric method. The relative abundance of bacterial taxa (phylum) of different paddy soils was performed on Tutools platform https://www.cloudtutu.com. And the analysis of soil species in different soils was performed on Stamp software. The meteorological data were obtained from National Renewable Energy Laboratory. And the population quantity was obtained from http://www.citypopulation.de/.

# Results

## Soil chemical and microbial properties in different paddy soils

Soil properties varied among geographical locations and depths (**Table 1**). A higher C/N was found in the two soil layers of Shandong (SD), with 13.49 ± 1.06 in the topsoil layer (0–20 cm) and 14.52 ± 0.56 in subsoil (20–40 cm). The C/P and N/P of Hunan (HN) in the topsoil layer were the highest, with the value of 58.23 ± 1.70, and 4.86 ± 0.09, respectively.

The microbial diversity index Chao1 in the topsoil of the Tianjing (TJ) site showed lower values than that of other types at the topsoil. At the subsoil layer, HN had higher Chao1 than that in TJ and Heilongjiang (DB) soils. Additionally, we further analyzed the core microbes at two soil layers of the five sites (**Figure 2**). At the phylum level, the bacterial compositions of five soils were dominated by *Acidobacteriota*, *Chloroflexi*, *Proteobacteria*, *Bacteroidota*, and *Nitrospirota*. The abundance of *Nitrospirota* was significantly higher in HN, whereas the abundance of *Proteobacteria* in HN was significantly lower than that in SD (**Supplementary Figure 1**). Also, the highest abundance of *Bacteroidota* was found in SD (**Supplementary Figure 1**). Moreover, DB in subsoil had a higher abundance of *Myxococcota* than SD and HN, while SD had a lower abundance of *Myxococcota* than TJ (**Supplementary Figure 1**). The highest abundance of *Nitrospirota* and *Verrucomicro* in subsoil layers were found in HN and DB, respectively (**Supplementary Figure 1**).

## Microplastic properties in different paddy soils

Microplastics were found in all sampling sites, with an average of 6,390 ± 2,031 items·kg$^{-1}$. Geographical position, soil layers, and interaction significantly affected MP abundance (**Supplementary Table 1**; $P < 0.05$). The highest and lowest MP abundance in all samples were measured in topsoil layers of HN and SD, with the value of 10,300 items·kg$^{-1}$ and 4,000 items·kg$^{-1}$, respectively. In subsoil layers, SD, Henan (HE), and HN had higher MP abundance than TJ and DB (**Figure 3A**; $P < 0.05$). In topsoil layers, HN had higher MP abundance than others, while SD had lower MP abundance than others. MP abundance in the topsoil layers of HN was significantly higher than that of subsoil layers, while MP abundance in topsoil layers of SD and HE was significantly lower than that of subsoil layers (**Figure 3A**; $P < 0.05$).

The size distribution of MPs is shown in **Supplementary Figures 2A,B**, and was divided into <0.5 mm, 0.5–1 mm, 1–2 mm, and 2–5 mm. Overall, the proportion of MPs less than 0.5 mm at all the sampling sites was the largest, followed by 0.5–1 mm. In regards to different sampling sites, the abundance of particle size less than 0.5 mm showed the highest concentration (60.89%) in the topsoil of HN. The subsoil layer of TJ had significantly higher particles (30.67%) ranging from 0.5 to 1 mm than those of others. The MPs sized between 2 and 5 mm showed the highest concentration in the topsoil layer of SD (33.95%) (**Supplementary Figures 2C–F**; $P < 0.05$).

Microplastics were categorized by color as white, black, transparent, blue, and other colors. Transparent and black were the most common colors in all samples, accounting for 2.6–67.86%, and 7.1–71.79%, respectively (**Figures 4A,B**). The abundance of black MPs in the subsoil layer of SD and DB was higher than those in other soils, and the abundance of transparent MPs was the lowest in the subsoil layer of DB (**Figures 4C–F**; $P < 0.05$).

10.3389/fmicb.2022.985239

TABLE 1 Soil properties of different paddy soils.

| Type | Depth | pH | SOC | POXC | POC | C/N | C/P | N/P |
|---|---|---|---|---|---|---|---|---|
| SD | 0–20 cm | 7.92 ± 2.61Bb | 9.40 ± 2.61Ca | 3.45 ± 0.05Ca | 3.97 ± 0.01Ca | 13.49 ± 1.06Aa | 13.52 ± 1.50Da | 1.04 ± 0.02Ea |
| | 20–40 cm | 8.44 ± 0.03Aa | 7.03 ± 0.47Eb | 2.59 ± 0.37Eb | 4.35 ± 0.66Ca | 14.52 ± 0.56Aa | 11.97 ± 0.82Da | 0.82 ± 0.02Eb |
| HE | 0–20 cm | 7.83 ± 0.03Cb | 9.82 ± 1.05Ca | 2.76 ± 0.14Db | 1.68 ± 0.20Ea | 10.32 ± 0.99Ca | 15.18 ± 1.47CDa | 1.47 ± 0.02Da |
| | 20–40 cm | 7.88 ± 0.02Ca | 8.50 ± 0.22Da | 3.99 ± 0.46Da | 1.95 ± 0.29Ea | 10.54 ± 0.11Ca | 13.17 ± 0.48Da | 1.25 ± 0.04Db |
| TJ | 0–20 cm | 8.12 ± 0.02Ab | 8.50 ± 0.52Ca | 3.23 ± 0.19Cb | 3.21 ± 0.33Da | 9.31 ± 0.35Ca | 16.87 ± 0.83Ca | 1.81 ± 0.03Ca |
| | 20–40 cm | 8.37 ± 0.03Ba | 10.46 ± 0.24Ca | 4.61 ± 0.18Ca | 3.41 ± 0.26Da | 9.70 ± 0.14Da | 16.76 ± 0.18Ca | 1.73 ± 0.04Cb |
| HN | 0–20 cm | 6.91 ± 0.10Da | 16.51 ± 0.55Ba | 6.24 ± 0.05Aa | 10.28 ± 0.40Ba | 11.99 ± 0.19Ba | 58.23 ± 1.70Aa | 4.86 ± 0.09Aa |
| | 20–40 cm | 6.55 ± 0.06Db | 15.54 ± 0.47Bb | 6.13 ± 0.32Ba | 11.52 ± 1.00Aa | 11.90 ± 0.28Ba | 51.51 ± 2.36Ab | 4.33 ± 0.11Ab |
| DB | 0–20 cm | 5.49 ± 0.06Ea | 18.81 ± 0.84Ab | 4.58 ± 0.61Bb | 15.41 ± 0.01Aa | 9.82 ± 0.25Ca | 34.09 ± 1.34Ba | 3.47 ± 0.05Bb |
| | 20–40 cm | 5.46 ± 0.02Ea | 19.20 ± 0.65Aa | 7.61 ± 0.15Aa | 7.01 ± 0.40Bb | 9.33 ± 0.28Db | 33.95 ± 1.20Bb | 3.64 ± 0.03Bb |

SOC, soil organic carbon, g•kg$^{-1}$; DOC, dissolved organic carbon, mg•kg$^{-1}$; MBC, microbial biomass carbon, mg•kg$^{-1}$; POXC, permanganate oxidizable carbon, g•kg$^{-1}$; POC, particulate organic carbon, g•kg$^{-1}$; C/N, ratio of total carbon to total nitrogen; C/P, ratio of total carbon to total phosphorus; N/P, ratio of total nitrogen to total phosphorus.
Different capital letters indicate the significant difference among sampling sites, and different lowercase letters indicate the significant differences between soil depths ($P < 0.05$) ($n = 3$).

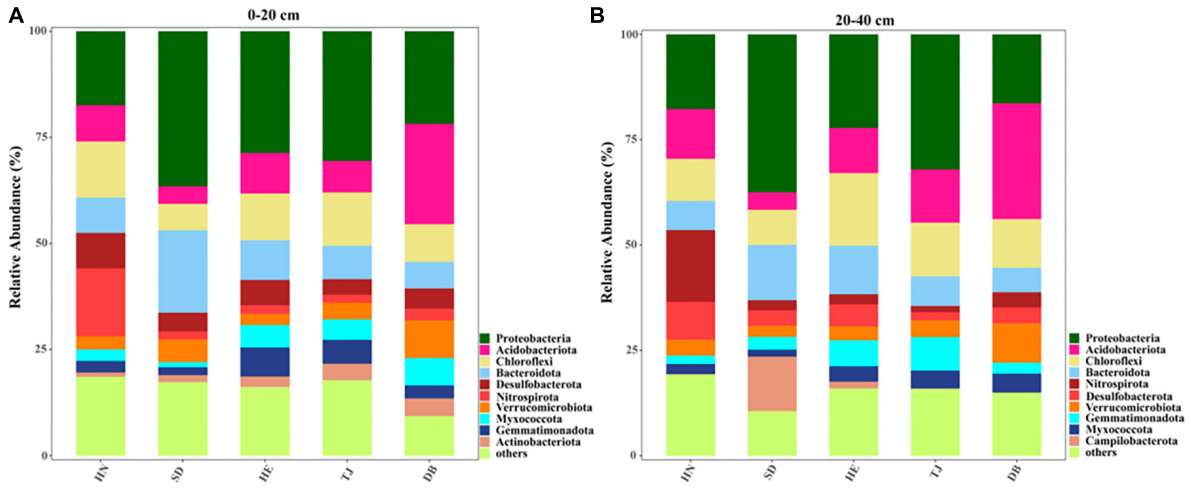


FIGURE 2
The relative abundance of bacterial taxa (phylum) in different paddy soils; **(A)** 0–20 cm; **(B)** 20–40 cm.

Particle shapes were categorized as fiber, pellet, fragment, foam, and film in all samples, with the shape and composition of MP in different soil types and layers varying greatly. As shown in Figure 3B, fiber was the most common shape in paddy soils, accounting for 91.8–100%. There was only fiber in the subsoil layers of HE and DB. Overall, the topsoil layer had more abundant MP shapes than those of the subsoil layers in this study. MPs shaped like foam and film were only found in the topsoil layer of TJ and subsoil in HN, respectively.

Nine types of polymers were identified from all sampling sites, which were Rayon, polyethylene (PE), polypropylene (PP), PP + PE, polyethylene terephthalate (PET), and Polyester, Acrylic, polystyrene (PS), and PA (nylon) (Figure 3C). Among them, rayon was dominant, accounting for 26.58–82.05%. Polyester was the second most abundant type of MPs, accounting for 3.49–64.57%, of which the topsoil layer of HE had the highest polyester concentration. Additionally, DB had higher PE than other sites.

## Microplastic community characteristics in different paddy soils

Analysis of similarities showed that the effect of geographical position on the composition of the MP communities was significantly greater than that of soil layers (Figure 5A; $R = 0.418$, $P = 0.001$). LDA axes1 and LDA axes2 explained the differences of 66.96 and 23.81% for MP communities among different locations, respectively (Figure 5B). HE and HN were significantly different

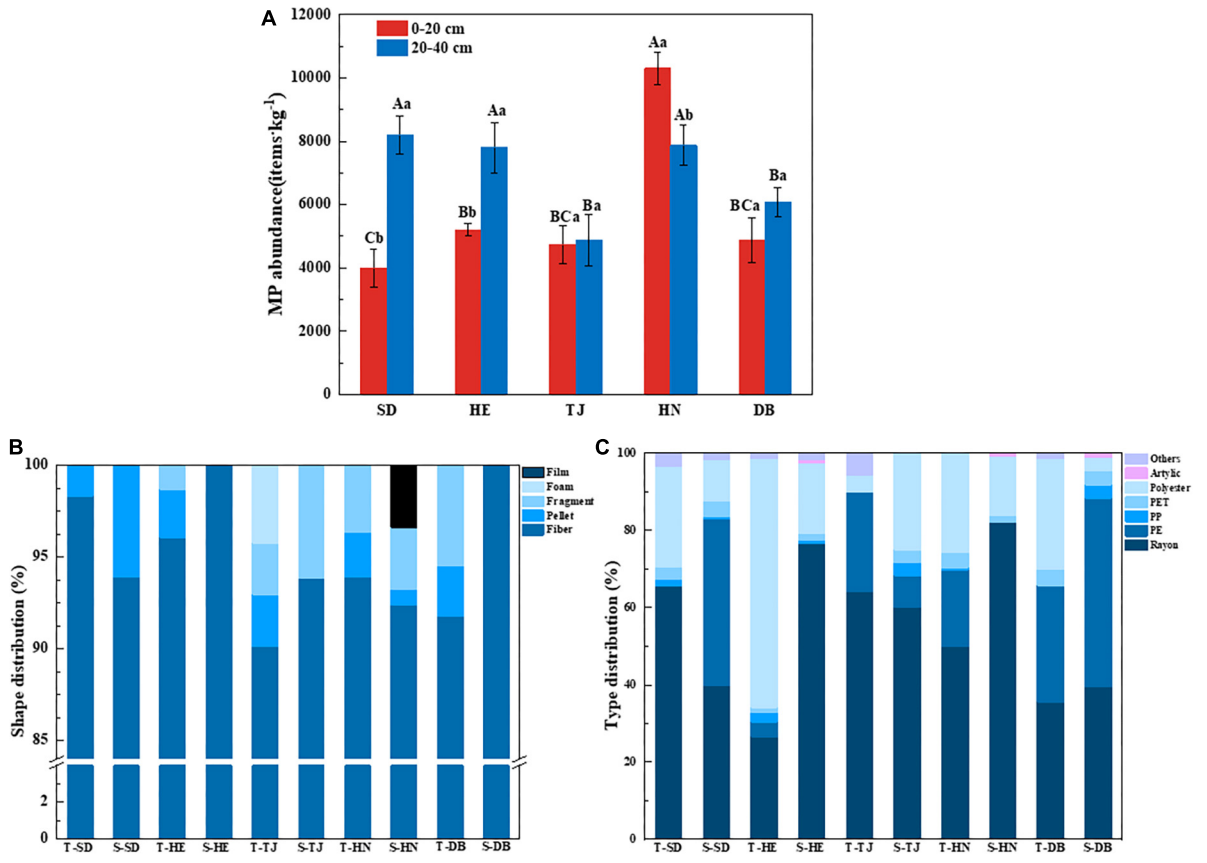


FIGURE 3
Microplastic (MP) abundance in different paddy soils **(A)**; percentage of MP shape distribution **(B)** and compositions **(C)** of paddy soils among different geographic positions. T-: 0–20 cm layer; S-: 20–40 cm layer. Different capital letters indicate the significant difference among different geographic positions, and different lowercase letters indicate the significant differences between soil depths ($P < 0.05$) ($n = 3$).

from the other communities, but the MP communities of SD, DB, and TJ were not clearly distinguished on the LD1 and LD2 axes. LEfSe analysis was used to find the significantly discriminant MP types in each soil (Figure 5C). We found that there were more black MP abundances in HE, more rayon, blue, and other colors' MPs in HN, more transparent MPs in TJ, and more PE MPs in DB. Each respective soil type has a characteristic MP type, except for SD.

In addition, we analyzed the similarity of MP communities by Mantel test based on Bray-Curtis distance (Supplementary Figure 4A). There was a certain positive correlation between MP communities of different locations, with the coefficient R between 0.38 and 0.86. The correlation coefficient between TJ and HE, as well as between DB, SD, and HE, as well as between TJ and SD were significant. MDII index was used to reflect the composition of MP communities, indicating the number of pollution sources. In this study, we found that HN and DB had higher MP community diversity, implying that these two soils had a wider range of MP sources (Supplementary Figure 4B).

## Correlation analysis among soil properties, meteorological conditions and microplastic characteristics

Microplastic abundance of both pellet shape and size between 2 and 5 mm, positively correlated with C/N (Figure 6A). The abundance of fragment-shaped MPs, positively correlated with C/P as well as N/P (Figure 6A). There was an extremely significantly positive correlation between the Chao1 index and MP abundance, fiber, and size less than 0.5 mm (Figure 6A). Furthermore, we also analyzed the relationship between meteorological conditions and MP distribution characteristics (Figure 6B). The abundance of dominant MP shapes and sizes was proportional to average temperature, minimum temperature, and precipitation. There was a significantly positive correlation between MP abundance and average temperature, minimum temperature, and precipitation. Interestingly, we found solar radiation was inversely proportionated to MP abundance, fiber, fragment, pellet, and size less than 0.5 mm in top soil layers

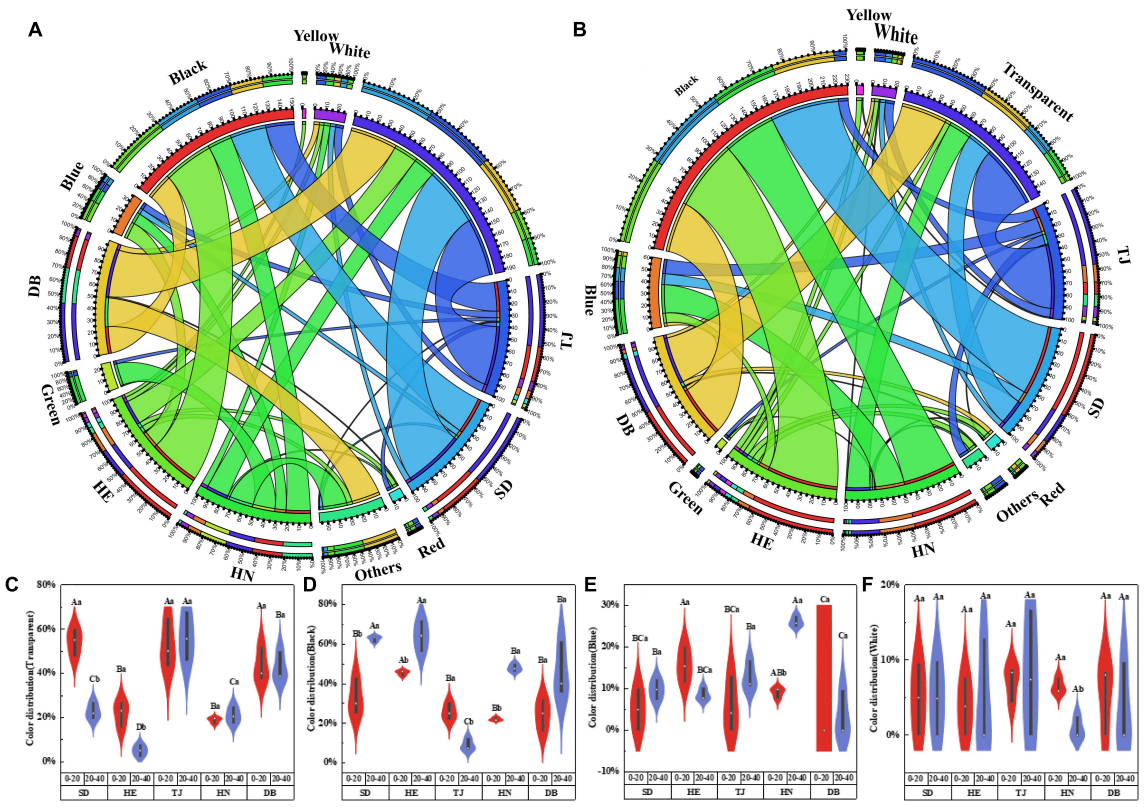


FIGURE 4
Color **(A)** in 0–20 cm, color **(B)** in 20–40 cm distribution of MPs in different paddy soils; violin plots showing the variance analysis of four colors: transparent **(C)**; black **(D)**; blue **(E)**; white **(F)**. Different capital letters indicate the significant difference among different geographic positions, and different lowercase letters indicate the significant differences between soil depths ($P < 0.05$) ($n = 3$).

(**Supplementary Figure 5**). Additionally, positive relationships between population quantities and MP abundance were observed (**Figure 7**).

# Discussion

## The occurrence of microplastics in paddy soils as affected by human activities

Firsthand evidence of the MP pollution characteristics in the soils along different geographical locations and soil layers is thoroughly explored in this study. MPs were detected in all the paddy land sites from the north to the south of China (**Figure 3A**), indicating the severity and prevalence of MP pollution. The concentration of MPs ranges from 4,000 to 10,300 items·kg$^{-1}$ (**Figure 3A**), which is comparable to those in previous studies, such as 320–12,560 items·kg$^{-1}$ in vegetable farmland of Wuhan (Chen et al., 2020), and 900–40,800 items·kg$^{-1}$ in cultivated soil of Yunnan in China (Huang B. et al., 2021). Zhou et al. (2019) reported the MP abundance ranged from 43,000 to 6,20,000 items·kg$^{-1}$ in Wuhan vegetable patches, which was much higher than our results. This may be because the Wuhan vegetable patches were located near an industrial area with various pollution sources (Zhou et al., 2019). In addition, the MP abundance in our study was much higher than other results, such as a concentration of 0–260 items·kg$^{-1}$ in the greenhouse soil of Qinghai Tibet (Feng et al., 2021) and 240–3,660 items·kg$^{-1}$ in the farmland of Qinghai (Lang et al., 2022). This is because Qinghai is far from industrial and commercial areas, the high population density, complex pollution sources, and frequent human activities (Lang et al., 2022; Yang L. et al., 2022) leading to a higher MP abundance in our study area.

Overall, these studies showed that MPs were widespread in various agricultural soils and their abundance fluctuated widely. The variation of MP abundance in different agricultural areas may depend on numerous factors, such as sewage irrigation, pollution source, crop type, tillage practices, fertilizer application, mulch use, and so on (Ding et al., 2020; Lang et al., 2022). Also, in our study, divergent differences were found in MP abundance among different paddy lands, and MP abundance in the topsoil layer of HN was significantly

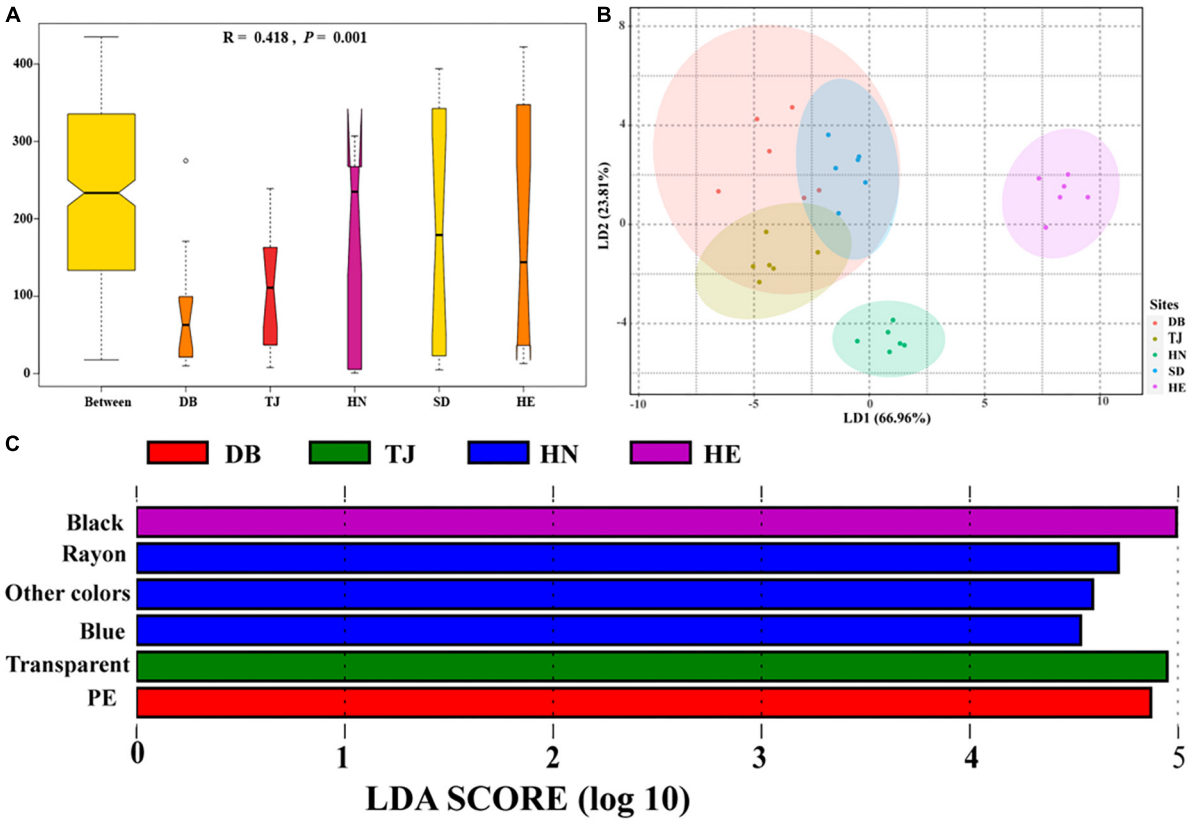


FIGURE 5
Differences of microplastic communities based on shape, color, and polymer types in different environments. Analysis of similarities (ANOSIM) was used for variance testing, and *y*-axis represents the dissimilarity ranks between and within environments, **(A)**; Linear discriminant analysis (LDA) was used to maximize the differences of paddy soils among geographic positions, **(B)**; LDA Effect Size (LEfSe) was used to identify characteristic microplastic types of paddy soils among geographic positions, **(C)**.

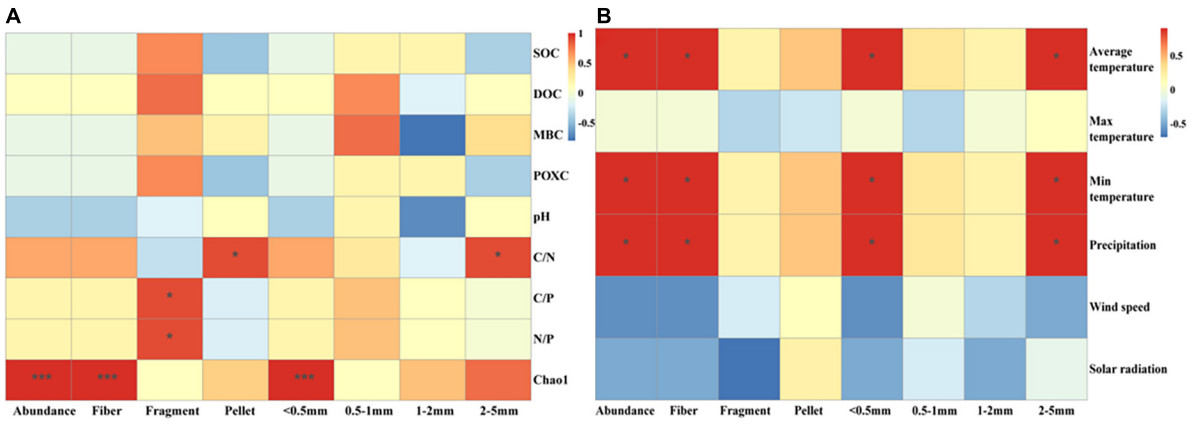


FIGURE 6
Linkage of main shape and size MP abundance with soil properties **(A)** and meteorological factors **(B)**. Significant differences of paddy soils among geographic positions were indicated by $*P < 0.05$, $**P < 0.01$, $***P < 0.001$.

higher than that in other soils (Figure 3A). This might be due to: (1) The HN sampling sites were surrounded by a higher population quantity (Figure 1) which may have frequent human activities; (2) The source of irrigation water in the HN rice-growing area is from a tributary of the Xiangjiang River, which has been reported to be rich in MPs in its water and sediment

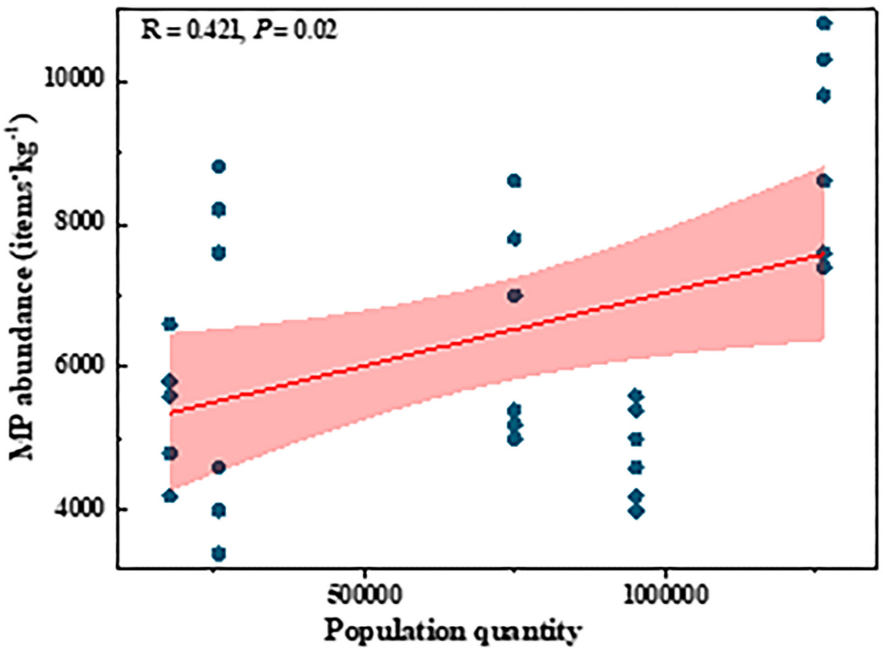


FIGURE 7
Linear correlations between MP abundance and population quantity.

(Wen et al., 2018; Yin et al., 2019); (3) HN rice is grown over two seasons per years, and the amount and frequency of irrigation were higher than those in the other regions of this study. Previous studies found that irrigation source, frequency, and volume may contribute to the differences in MP abundance of various agricultural sources (Wang et al., 2021).

Microplastics in the soil come from a wide variety of sources, including agricultural activities, atmospheric deposition, irrigation water, sludge application, and roads (Sommer et al., 2018; Bergmann et al., 2019; Ding et al., 2020; Corradini et al., 2021). The color, shape, and polymer type of MPs may be indicative of the potential sources to some extent. Fibers were the dominant shape in paddy soils of our study (**Figure 3B**). Fibers may come from fishing nets, fishing line, rope breakage, and synthetic laundry (Abayomi et al., 2017; Mahon et al., 2017; Zhang X. et al., 2020), and were widely found in the Yongjiang River (Zhang X. et al., 2020), Xiangjiang River (Yin et al., 2019), Pearl River (Lin et al., 2018), as well as Yangtze River (Wang et al., 2017). A large number of fibers in paddy soils may have originated from irrigation water, synthetic fibers have also been used as indicators of wastewater sludge (Corradini et al., 2021). Although the irrigation water of DB and HE was groundwater with lower MP abundance, it may become contaminated with MPs while flowing from the irrigation source to the farm (Bläsing and Amelung, 2018), resulting in fiber MP pollution. Pellets were found in all topsoil layers among the different geographic positions. Pellets mainly originated from personal care products such as toothpaste and face wash in domestic wastewaters (Isobe, 2016), implying the source of MPs in paddy soil potentially originated from these irrigated waters. The foam was only found in the topsoil of TJ (**Figure 3B**), which may be due to TJ's proximity to the Bohai Sea, frequent fishing activities generated foam (Xu et al., 2021), and the small density of foam made it difficult to migrate downward and it stayed in the surface layer. Fragment and film were found in paddy soils, mostly from agricultural tools, plastic packaging material, and woven bags (Antunes et al., 2013; Cao et al., 2021). Moreover, transparent and black MPs accounted for the majority of MPs in our study (**Figures 4C,D**). Transparent MPs usually come from plastic bags and plastic film (Chen et al., 2020; Wang et al., 2021), and they could also be caused by long-term weathering and discoloration of colored MPs (Zhu, 2015). Other colors of MPs may come from colored bags and colored laundry (Browne et al., 2011; Wen et al., 2018), and are easily predated by other organisms (Hoarau et al., 2014), resulting in lower abundance. MPs less than 0.5 mm accounted for the largest proportion in our study (**Supplementary Figures 2A,B**), indicating tillage and agricultural machinery accelerated the degradation of MPs (Yu et al., 2021).

In addition, MDII index was proposed to reflect MP community diversity and indicate pollution complexity (Li C. et al., 2021). Richer colors, shapes, and polymer types may have more uniform contamination sources (Wang et al., 2019; Li C. et al., 2021; Zhu et al., 2021). The MDII

index of HN was significantly larger than that of SD and TJ, indicating the sources of pollution in HN with higher population quantities were more extensive and each source contributed equally.

## Effect of soil microbial communities and soil stoichiometry on microplastic distribution in paddy soils

It is well known that soil properties can affect the migration and transformation of MPs, while MPs can also affect soil properties (Qian et al., 2021; Sajjad et al., 2022; Zhang H. et al., 2022; Zhang J. et al., 2022). There are strong interactions between soil microorganisms and MPs. MPs could provide habitats for microorganisms (Miao et al., 2020), but MPs are selective and only promote the growth of specific microorganisms (Li et al., 2020). In addition, some microorganisms can use MPs as a carbon source (Seeley et al., 2020), both to provide energy for their growth and to promote the degradation of MPs through secreted oxidoreductases and hydrolases (Sudhakar et al., 2008). Furthermore, the degradation process of MPs may produce toxic substances such as DPB, affecting the growth of microorganisms (Wang et al., 2018). However, the coupling relationship between MPs and microorganisms is still limited, especially in the paddy soils of China. The Chao1 index is commonly used as a diversity index to indicate the abundance of microbial species. Our study found a significantly positive correlation between Chao1 and MP abundance (**Figure 6A**). On the one hand, MPs could provide habitats and a carbon source to microorganisms and promote their growth. On the other hand, microorganisms increased MP abundance and the percentage of less than 0.5 mm MPs by aging large pieces of plastics and MPs. Moreover, we revealed a significantly positive correlation between Chao1 and fiber abundance. This is because the large surface area and rich adsorption sites of fiber could facilitate microorganism attachment and growth (Rillig et al., 2017a; Dong et al., 2021), and the shape of fiber could increase the porosity and aeration of soil to promote growth (Wan et al., 2019). Analysis of soil microbial community composition revealed the dominant species in paddy soils including *Acidobacteriota*, *Chloroflexi*, *Proteobacteria*, *Bacteroidota*, and *Nitrospirota* (**Figures 2A,B**). Previous studies also confirmed the ability of MPs to promote the growth of *Proteobacteria*, *Bacteroidota*, *Actinobacteria*, *Acidobacteriota*, etc. (Qian et al., 2018; Huang et al., 2019; Qi et al., 2020). *Proteobacteria* was reported to be related to the aging of refractory polymers such as MPs (Yan et al., 2021).

Interestingly, we found soil MP abundance varied inconsistently with the two soil layers of the sampling sites (**Figure 3A**). MP abundance in SD and HE increased with soil depth, while MP abundance in HN decreased with soil depth, and the MP abundance in DB did not show significant variance between different depths. Some previous studies reported tilling may result in a uniform distribution of MPs under a vertical gradient (Harms et al., 2021), while others detected MP abundance decreased with the increase of depths due to the activity of earthworms (Harms et al., 2021). The variation of MPs at different soil depths may be influenced by various factors such as microorganisms, soil porosity, agricultural practices, protozoa, plant roots, fungi, etc. (Rillig et al., 2017b; Bläsing and Amelung, 2018; Cao et al., 2021; Zhang H. et al., 2022), contributing to the vertical variation of MPs in different paddy soils of this study. Additionally, the clayey texture and tiny porosity of the soil in HN (Liu et al., 2018) prevented MPs from moving down from the surface layer, resulting in a higher abundance of soil MP in topsoil than in subsoil.

The concentration and ratio of C, N, and P could be considered the main drivers of microbial diversity and organic carbon decomposition (Bradshaw et al., 2012; Guo and Jiang, 2019). Previous studies also revealed N and P could promote microbial growth and release oxidoreductase and hydrolase increasing soil fertility, thus effectively degrading MPs (Zhang H. et al., 2022). We found that C/N was positively associated with size 2–5 mm MPs and pellets. The high C/N suppressed the decomposition of organic matter and the abundance of microbes (Cleveland and Liptzin, 2007), leading to the accumulation of 2–5 mm MPs. Unlike other MP shapes, pellets can bind with soil particles and did not reduce soil capacity (Sun Y. et al., 2022). *Proteobacteria* which could age MPs preferred to settlement in low capacitance soils (Sun Y. et al., 2022). Likewise, N/P and C/P positively related with fragments. Another study found *Gemmatimonadota* and *Proteobacteria* with degradable MPs (Zhang S. et al., 2020; Yan et al., 2021; Yi et al., 2021) were strongly inversely associated with N/P (Delgado-Baquerizo et al., 2017), which also explains our result. Furthermore, the C, N, and P contained in MPs and their additives (De Souza Machado et al., 2019) also affected the stoichiometric ratio of the soil, enhancing the correlation between them. Overall, there is still a large gap in the study of the effect of soil stoichiometric ratio on MP characteristics and their mechanism, with more in-depth research needed in the future.

## Effect of meteorological conditions on the microplastic distribution in paddy soils

This study monitored MP communities in paddy soils from the North to the South of China, with average temperatures ranging from 2.9 to 16.8°C. The abundance, shape, size, and polymer type of soil MP differed significantly along geographical position. This may be caused by pollution sources, population scale, human activity intensity, soil properties, and

meteorological conditions (Li C. et al., 2021; Yang L. et al., 2022; Zhang H. et al., 2022). The characteristic MPs of HN were rayon and blue (**Figure 5C**), which mainly come from the wastewater from synthetic clothing washing (Xu et al., 2021), as well as higher temperatures and more frequent irrigation activities. The characteristic MPs in TJ were transparent (**Figure 5C**), indicating a high degree of MP weathering in the TJ area (Zhu, 2015). Furthermore, large quantities of PE were found in DB (**Figure 5C**), which may be due to the use of plastic film made of PE (Kim et al., 2021) due to lower temperature conditions in the northeast parts of China.

Furthermore, MP communities in different paddy soils were found to be correlated through the Mantel test based on Bray-Curtis distance in this study (**Figure 4A**). The possible reasons are: (1) They may have similar contamination sources (Li C. et al., 2021); (2) MP could be transported by the atmosphere as well as surface runoff (Dong et al., 2021; Zhang H. et al., 2022). MP communities in SD, TJ, and HE were significantly correlated because soil properties and meteorological conditions were similar in the same climatic zones. These correlations suggested that MPs may move between different geographic positions, providing direct evidence of MP cycling (Bank and Hansson, 2019; Rochman and Hoellein, 2020).

In our study, the monthly mean temperature was positively related to MP abundance, fiber, MPs with size less than 0.5 mm, as well as MPs with size between 2 and 5 mm (**Figure 6B**). The highest average temperature was found in HN, and the highest MP abundance was also found in HN. Elevated temperatures promoted the aging of large plastic and low molecules through physical and chemical effects (Qian et al., 2021). Our results are supported by Zhang's findings, which reported a positive 0 cm ground temperature dependence of MP abundance in the Qinghai-Tibet Plateau (Zhang H. et al., 2022). The suitable temperature could promote the growth of microorganisms, thus accelerating the aging of large pieces of plastic and MPs, increasing the abundance of MPs and MPs with sizes less than 0.5 mm and 2–5 mm. Moreover, there was a significantly positive correlation between MP abundance and precipitation. The presence of MPs in the atmosphere has been widely demonstrated and they could enter terrestrial ecosystems through rainfall (Dong et al., 2021; Huang Y. et al., 2021). Research showed that precipitation was a positive driver of atmospheric MP deposition and contributed to MP accumulation on Qinghai-Tibet Plateau (Yang L. et al., 2022; Zhang H. et al., 2022). Another study also found that up to 21.9 g/L of MPs in atmospheric sediment, contributed to most of the MP entering Nam Co Lake (Dong et al., 2021). Hence, MPs may be present in the atmosphere and accumulate in the soil during precipitation.

Moreover, we also found MP abundance in 0–20 cm layer was inversely correlated with solar radiation (**Supplementary Figure 5**). Previous studies concluded that stronger solar radiation and ultraviolet light can promote decomposition and increase MP abundance (Liu et al., 2014; Singh, 2015; Feng et al., 2021), which is inconsistent with our results. This indicated that the effect of solar radiation on MPs was limited in this study. It might be due to that the refraction and reflection of UV light by water in paddy soil weaken the effect of solar radiation on MPs. HN is in a subtropical monsoon climate, which is wet and rainy, and has many clouds causing solar radiation intensity to break. The high density of rice cultivation also hinders the aging effect of UV radiation from the sun. Additionally, we found wind speed was inversely correlated with MP abundance, which is inconsistent with another study in which a positive correlation between MPs and wind speed was found. This may be due to high-density rice cultivation (Wang et al., 2021) and the long-term flooding state of paddy soil weakening the effect of wind speed on MP transport.

Another amazing finding was that the minimum temperature in our study showed a positive correlation between MPs and MPs with sizes less than 0.5 mm and 2–5 mm, which is most likely due to the alteration of the freeze-thaw process. Previous studies found that freeze-thaw accelerated the aging and degradation of MPs, reduced their particle size, increased their adsorption capacity, and changed their molecular chemical structure through variations in moisture and surface heat balance (Chen et al., 2021). During the freezing period, the soil was cold, shaded, and anoxic, decreasing the rate of MP aging, while during the thawing period, the soil acted as an MP sink releasing MPs and accelerating their aging process (Chen et al., 2021; Dong et al., 2021). Thus, when the minimum temperature rose, it could expedite the melting of the permafrost later and the release of MPs, and also promote the large pieces of plastic and MP degradation. This verifies the results of our study that DB with the lowest minimum temperature had lower MP abundance.

## Conclusion

In this study, we conducted a comprehensive study to investigate the geographical distribution patterns and impact factors of MPs in the paddy field at regional scales. Overall, MPs were widely distributed in the soils, fiber-shaped and size less than 0.5 mm MPs dominated, implying that paddy soils are heavily polluted with MPs. We proposed that irrigation might be the main potential MP source. Furthermore, planting patterns, soil physicochemical properties, meteorological conditions, and population quantity were verified to affect the transport, accumulation, and fragmentation of MPs in paddy soils. Our findings fill the gap in our understanding of the distribution characteristics and influencing factors of MPs in paddy soils from the North to the South of China In the future, more attention was highly expected to be exerted into the toxicological behavior of MPs in rice paddy field and the potential transport of MPs to the human food chain.

## Data availability statement

The datasets presented in this study can be found in online repositories. The names of the repository/repositories and accession number(s) can be found below: NCBI SRA, PRJNA858258.

## Author contributions

YY: investigation, data curation, visualization, and writing – original draft preparation. LW: conceptualization, supervision, writing – review and editing, and funding acquisition. LG and WX: visualization. GL: methodology and data curation. XY, BT, and JZ: review and editing. GZ: project administration. All authors contributed to the article and approved the submitted version.

## Funding

This work was supported by National Key R&D Program of China (2021YFD1700900), Central Public-interest Scientific Institution Basal Research Fund (2022-jbkyywf-wll), and Cooperative Innovation Project of International Cooperation Program of CAAS (2022-wll).

## Conflict of interest

The authors declare that the research was conducted in the absence of any commercial or financial relationships that could be construed as a potential conflict of interest.

## Publisher's note



## Supplementary material

The Supplementary Material for this article can be found online at: https://www.frontiersin.org/articles/10.3389/fmicb.2022.985239/full#supplementary-material

## References

Abayomi, O. A., Range, P., Al-Ghouti, M. A., Obbard, J. P., Almeer, S. H., and Ben-Hamadou, R. (2017). Microplastics in coastal environments of the Arabian Gulf. *Mar. Pollut. Bull.* 124, 181–188.

Antunes, J., Frias, J., Micaelo, A., and Sobral, P. (2013). Resin pellets from beaches of the Portuguese coast and adsorbed persistent organic pollutants. *Estuar. Coast. Shelf Sci.* 130, 62–69.

Bank, M. S., and Hansson, S. V. (2019). The plastic cycle: A novel and holistic paradigm for the Anthropocene. *Environ. Sci. Technol.* 53, 7177–7179. doi: 10.1021/acs.est.9b02942

Bergmann, M., Mützel, S., Primpke, S., Tekman, M. B., Trachsel, J., and Gerdts, G. (2019). White and wonderful? Microplastics prevail in snow from the Alps to the Arctic. *Sci. Adv.* 5:eaax1157. doi: 10.1126/sciadv.aax1157

Bläsing, M., and Amelung, W. (2018). Plastics in soil: Analytical methods and possible sources. *Sci. Total Environ.* 612, 422–435.

Bradshaw, C., Kautsky, U., and Kumblad, L. (2012). Ecological stoichiometry and multi-element transfer in a coastal ecosystem. *Ecosystems* 15, 591–603.

Browne, M. A., Crump, P., Niven, S. J., Teuten, E., Tonkin, A., Galloway, T., et al. (2011). Accumulation of microplastic on shorelines woldwide: Sources and sinks. *Environ. Sci. Technol.* 45, 9175–9179. doi: 10.1021/es201811s

Cao, L., Wu, D., Liu, P., Hu, W., Xu, L., Sun, Y., et al. (2021). Occurrence, distribution and affecting factors of microplastics in agricultural soils along the lower reaches of Yangtze River. China. *Sci. Total Environ.* 794:148694. doi: 10.1016/j.scitotenv.2021.148694

Chen, S., Feng, Y., Han, L., Li, D., Feng, Y., Jeyakumar, P., et al. (2022). Responses of rice (Oryza sativa L.) plant growth, grain yield and quality, and soil properties to the microplastic occurrence in paddy soil. *J. Soils Sediments* 22, 2174–2183.

Chen, X., Huang, G., Gao, S., and Wu, Y. (2021). Effects of permafrost degradation on global microplastic cycling under climate change. *J. Environ. Chem. Eng.* 9:106000.

Chen, Y., Leng, Y., Liu, X., and Wang, J. (2020). Microplastic pollution in vegetable farmlands of suburb Wuhan, central China. *Environ. Pollut.* 257:113449. doi: 10.1016/j.envpol.2019.113449

Cleveland, C. C., and Liptzin, D. (2007). C: N: P stoichiometry in soil: Is there a "Redfield ratio" for the microbial biomass? *Biogeochemistry* 85, 235–252.

Corradini, F., Casado, F., Leiva, V., Huerta-Lwanga, E., and Geissen, V. (2021). Microplastics occurrence and frequency in soils under different land uses on a regional scale. *Sci. Total Environ.* 752:141917. doi: 10.1016/j.scitotenv.2020.141917

De Souza Machado, A. A., Lau, C. W., Kloas, W., Bergmann, J., Bachelier, J. B., Faltin, E., et al. (2019). Microplastics can change soil properties and affect plant performance. *Environ. Sci. Technol.* 53, 6044–6052.

Delgado-Baquerizo, M., Reich, P. B., Khachane, A. N., Campbell, C. D., Thomas, N., Freitag, T. E., et al. (2017). It is elemental: Soil nutrient stoichiometry drives bacterial diversity. *Environ. Microbiol.* 19, 1176–1188.

Ding, L., Zhang, S., Wang, X., Yang, X., Zhang, C., Qi, Y., et al. (2020). The occurrence and distribution characteristics of microplastics in the agricultural soils of Shaanxi Province, in north-western China. *Sci. Total Environ.* 720:137525. doi: 10.1016/j.scitotenv.2020.137525

Dong, H., Wang, L., Wang, X., Xu, L., Chen, M., Gong, P., et al. (2021). Microplastics in a Remote Lake Basin of the Tibetan Plateau: Impacts of Atmospheric Transport and Glacial Melting. *Environ. Sci. Technol.* 55, 12951–12960. doi: 10.1021/acs.est.1c03227

Dong, Y., Gao, M., Qiu, W., and Song, Z. (2020b). Adsorption of arsenite to polystyrene microplastics in the presence of humus. *Environ. Sci. Process. Impacts* 22, 2388–2397. doi: 10.1039/d0em00324g

Dong, Y., Gao, M., Liu, X., Qiu, W., and Song, Z. (2020a). The mechanism of polystyrene microplastics to affect arsenic volatilization in arsenic-contaminated paddy soils. *J. Hazard. Mater.* 398:122896. doi: 10.1016/j.jhazmat.2020.122896

Feng, S., Lu, H., and Liu, Y. (2021). The occurrence of microplastics in farmland and grassland soils in the Qinghai-Tibet plateau: Different land use and mulching time in facility agriculture. *Environ. Pollut.* 279:116939. doi: 10.1016/j.envpol.2021.116939

Guo, J., Huang, X., Xiang, L., Wang, Y., Li, Y., Li, H., et al. (2020). Source, migration and toxicology of microplastics in soil. *Environ. Int.* 137:105263.

Guo, X., and Jiang, Y. (2019). Spatial characteristics of ecological stoichiometry and their driving factors in farmland soils in Poyang Lake Plain, Southeast China. *J. Soils Sediments* 19, 263–274.

Guo, Z., Zhang, X., Dungait, J. A., Green, S. M., Wen, X., and Quine, T. A. (2021). Contribution of soil microbial necromass to SOC stocks during vegetation recovery in a subtropical karst ecosystem. *Sci. Total Environ.* 761:143945. doi: 10.1016/j.scitotenv.2020.143945

Han, L., Chen, L., Li, D., Ji, Y., Feng, Y., Feng, Y., et al. (2022). Influence of polyethylene terephthalate microplastic and biochar co-existence on paddy soil bacterial community structure and greenhouse gas emission. *Environ. Pollut.* 292:118386. doi: 10.1016/j.envpol.2021.118386

Harms, I. K., Diekötter, T., Troegel, S., and Lenz, M. (2021). Amount, distribution and composition of large microplastics in typical agricultural soils in Northern Germany. *Sci. Total Environ.* 758:143615. doi: 10.1016/j.scitotenv.2020.143615

Hoarau, L., Ainley, L., Jean, C., and Ciccione, S. (2014). Ingestion and defecation of marine debris by loggerhead sea turtles, Caretta caretta, from by-catches in the South-West Indian Ocean. *Mar. Pollut. Bull.* 84, 90–96. doi: 10.1016/j.marpolbul.2014.05.031

Hu, D., Shen, M., Zhang, Y., Li, H., and Zeng, G. (2019). Microplastics and nanoplastics: Would they affect global biodiversity change? *Environ. Sci. Pollut.* 26, 19997–20002. doi: 10.1007/s11356-019-05414-5

Huang, B., Sun, L., Liu, M., Huang, H., He, H., Han, F., et al. (2021). Abundance and distribution characteristics of microplastic in plateau cultivated land of Yunnan Province, China. *Environ. Sci. Pollut. Res.* 28, 1675–1688. doi: 10.1007/s11356-020-10527-3

Huang, Y., He, T., Yan, M., Yang, L., Gong, H., Wang, W., et al. (2021). Atmospheric transport and deposition of microplastics in a subtropical urban environment. *J. Hazard. Mater.* 416:126168. doi: 10.1016/j.jhazmat.2021.126168

Huang, Y., Zhao, Y., Wang, J., Zhang, M., Jia, W., and Qin, X. (2019). LDPE microplastic films alter microbial community composition and enzymatic activities in soil. *Environ. Pollut.* 254:112983. doi: 10.1016/j.envpol.2019.112983

Huerta Lwanga, E., Mendoza Vega, J., Ku Quej, V., de los Chi, A., Sanchez del Cid, L., Chi, C., et al. (2017). Field evidence for transfer of plastic debris along a terrestrial food chain. *Sci. Rep.* 7:14071. doi: 10.1038/s41598-017-14588-2

Isobe, A. (2016). Percentage of microbeads in pelagic microplastics within Japanese coastal waters. *Mar. Pollut. Bull.* 110, 432–437. doi: 10.1016/j.marpolbul.2016.06.030

Jiang, X., Chang, Y., Zhang, T., Qiao, Y., Klobučar, G., and Li, M. (2020). Toxicological effects of polystyrene microplastics on earthworm (*Eisenia fetida*). *Environ. Pollut.* 259:113896. doi: 10.1016/j.envpol.2019.113896

Jiang, Y., Yang, F., Zhao, Y., and Wang, J. (2020). Greenland Sea Gyre increases microplastic pollution in the surface waters of the Nordic Seas. *Sci. Total Environ.* 712:136484. doi: 10.1016/j.scitotenv.2019.136484

Kim, S.-K., Kim, J.-S., Lee, H., and Lee, H.-J. (2021). Abundance and characteristics of microplastics in soils with different agricultural practices: Importance of sources with internal origin and environmental fate. *J. Hazard. Mater.* 403:123997. doi: 10.1016/j.jhazmat.2020.123997

Lang, M., Wang, G., Yang, Y., Zhu, W., Zhang, Y., Ouyang, Z., et al. (2022). The occurrence and effect of altitude on microplastics distribution in agricultural soils of Qinghai Province, northwest China. *Sci. Total Environ.* 810:152174. doi: 10.1016/j.scitotenv.2021.152174

Leifheit, E. F., Lehmann, A., and Rillig, M. C. (2021). Potential effects of microplastic on arbuscular mycorrhizal fungi. *Front. Plant Sci.* 12:626709. doi: 10.3389/fpls.2021.626709

Li, C., Gan, Y., Dong, J., Fang, J., Chen, H., Quan, Q., et al. (2020). Impact of microplastics on microbial community in sediments of the Huangjinxia Reservoir—water source of a water diversion project in western China. *Chemosphere* 253:126740. doi: 10.1016/j.chemosphere.2020.126740

Li, C., Gan, Y., Zhang, C., He, H., Fang, J., Wang, L., et al. (2021). "Microplastic communities" in different environments: Differences, links, and role of diversity index in source analysis. *Water Res.* 188:116574. doi: 10.1016/j.watres.2020.116574

Li, H., Lu, X., Wang, S., Zheng, B., and Xu, Y. (2021). Vertical migration of microplastics along soil profile under different crop root systems. *Environ. Pollut.* 278:116833. doi: 10.1016/j.envpol.2021.116833

Lin, L., Zuo, L.-Z., Peng, J.-P., Cai, L.-Q., Fok, L., Yan, Y., et al. (2018). Occurrence and distribution of microplastics in an urban river: A case study in the Pearl River along Guangzhou City, China. *Sci. Total Environ.* 644, 375–381. doi: 10.1016/j.scitotenv.2018.06.327

Liu, E., He, W., and Yan, C. (2014). 'White revolution'to 'white pollution'—agricultural plastic film mulch in China. *Environ. Res. Lett.* 9:091001.

Liu, Z., Xu, J., Li, X., and Wang, J. (2018). Mechanisms of biochar effects on thermal properties of red soil in south China. *Geoderma* 323, 41–51.

Luo, Y., Zhang, Y., Xu, Y., Guo, X., and Zhu, L. (2020). Distribution characteristics and mechanism of microplastics mediated by soil physicochemical properties. *Sci. Total Environ.* 726:138389. doi: 10.1016/j.scitotenv.2020.138389

Lv, W., Zhou, W., Lu, S., Huang, W., Yuan, Q., Tian, M., et al. (2019). Microplastic pollution in rice-fish co-culture system: A report of three farmland stations in Shanghai, China. *Sci. Total Environ.* 652, 1209–1218. doi: 10.1016/j.scitotenv.2018.10.321

Machado, A. A. D., Lau, C. W., Kloas, W., Bergmann, J., Bacheher, J. B., Faltin, E., et al. (2019). Microplastics Can Change Soil Properties and Affect Plant Performance. *Environ. Sci. Technol.* 53, 6044–6052.

Machado, A. A. D., Lau, C. W., Till, J., Kloas, W., Lehmann, A., Becker, R., et al. (2018). Impacts of Microplastics on the Soil Biophysical Environment. *Environ. Sci. Technol.* 52, 9656–9665.

Mahon, A. M., O'Connell, B., Healy, M. G., O'Connor, I., Officer, R., Nash, R., et al. (2017). Microplastics in sewage sludge: Effects of treatment. *Environ. Sci. Technol.* 51, 810–818.

Masura, J., Baker, J., Foster, G., and Arthur, C. (2015). *Laboratory Methods for the Analysis of Microplastics in the Marine Environment: Recommendations for Quantifying Synthetic Particles in Waters and Sediments*. Washington, DC: NOAA.

Miao, L., Wang, C., Adyel, T. M., Wu, J., Liu, Z., You, G., et al. (2020). Microbial carbon metabolic functions of biofilms on plastic debris influenced by the substrate types and environmental factors. *Environ. Int.* 143:106007. doi: 10.1016/j.envint.2020.106007

Qi, Y. L., Ossowicki, A., Yang, X. M., Lwanga, E. H., Dini-Andreote, F., Geissen, V., et al. (2020). Effects of plastic mulch film residues on wheat rhizosphere and soil properties. *J. Hazard. Mater.* 387:121711. doi: 10.1016/j.jhazmat.2019.121711

Qian, H., Zhang, M., Liu, G., Lu, T., Qu, Q., Du, B., et al. (2018). Effects of Soil Residual Plastic Film on Soil Microbial Community Structure and Fertility. *Water Air Soil Pollut.* 229:261.

Qian, J., Tang, S., Wang, P., Lu, B., Li, K., Jin, W., et al. (2021). From source to sink: Review and prospects of microplastics in wetland ecosystems. *Sci. Total Environ.* 758:143633. doi: 10.1016/j.scitotenv.2020.143633

Rillig, M. C., Ingraffia, R., and Machado, A. A. D. S. (2017). Microplastic Incorporation into Soil in Agroecosystems. *Front. Plant Sci.* 8:1805. doi: 10.3389/fpls.2017.01805

Rillig, M. C., Ziersch, L., and Hempel, S. (2017). Microplastic transport in soil by earthworms. *Sci. Rep.* 7:1362.

Rochman, C. M., Brookson, C., Bikker, J., Djuric, N., Earn, A., Bucci, K., et al. (2019). Rethinking microplastics as a diverse contaminant suite. *Environ. Toxicol. Chem.* 38, 703–711. doi: 10.1002/etc.4371

Rochman, C. M., and Hoellein, T. (2020). The global odyssey of plastic pollution. *Science* 368, 1184–1185. doi: 10.1126/science.abc4428

Sajjad, M., Huang, Q., Khan, S., Khan, M. A., Yin, L., Wang, J., et al. (2022). Microplastics in the soil environment: A critical review. *Environ. Technol. Innov.* 27:102408.

Seeley, M. E., Song, B., Passie, R., and Hale, R. C. (2020). Microplastics affect sedimentary microbial communities and nitrogen cycling. *Nat. Commun.* 11:2372.

Shen, X., Wang, L., Yang, Q., Xiu, W., Li, G., Zhao, J., et al. (2021). Dynamics of soil organic carbon and labile carbon fractions in soil aggregates affected by different tillage managements. *Sustainability* 13:1541.

Singh, A. K. (2015). *Engineered Nanoparticles: Structure, Properties And Mechanisms Of Toxicity*. Cambridge: Academic Press.

Sommer, F., Dietze, V., Baum, A., Sauer, J., Gilge, S., Maschowski, C., et al. (2018). Tire abrasion as a major source of microplastics in the environment. *Aerosol Air Qual. Res.* 18, 2014–2028.

Sudhakar, M., Doble, M., Murthy, P. S., and Venkatesan, R. (2008). Marine microbe-mediated biodegradation of low-and high-density polyethylenes. *Int. Biodeterior. Biodegr.* 61, 203–213.

Sun, X., Zhang, X., Xia, Y., Tao, R., Zhang, M., Mei, Y., et al. (2022). Simulation of the effects of microplastics on the microbial community structure and nitrogen cycle of paddy soil. *Sci. Total Environ.* 818:151768. doi: 10.1016/j.scitotenv.2021.151768

Sun, Y., Duan, C., Cao, N., Li, X., Li, X., Chen, Y., et al. (2022). Effects of microplastics on soil microbiome: The impacts of polymer type, shape, and concentration. *Sci. Total Environ.* 806:150516. doi: 10.1016/j.scitotenv.2021.150516

Wan, Y., Wu, C. X., Xue, Q., and Hui, X. M. N. (2019). Effects of plastic contamination on water evaporation and desiccation cracking in soil. *Sci. Total Environ.* 654, 576–582. doi: 10.1016/j.scitotenv.2018.11.123

Wang, F., Zhang, X., Zhang, S., Zhang, S., and Sun, Y. (2020). Interactions of microplastics and cadmium on plant growth and arbuscular mycorrhizal fungal communities in an agricultural soil. *Chemosphere* 254:126791. doi: 10.1016/j.chemosphere.2020.126791

Wang, T., Yu, C., Chu, Q., Wang, F., Lan, T., and Wang, J. (2020). Adsorption behavior and mechanism of five pesticides on microplastics from agricultural polyethylene films. *Chemosphere* 244:125491. doi: 10.1016/j.chemosphere.2019.125491

Wang, J., Li, J., Liu, S., Li, H., Chen, X., Peng, C., et al. (2021). Distinct microplastic distributions in soils of different land-use types: A case study of Chinese farmlands. *Environ. Pollut.* 269:116199. doi: 10.1016/j.envpol.2020.116199

Wang, T., Zou, X., Li, B., Yao, Y., Zang, Z., Li, Y., et al. (2019). Preliminary study of the source apportionment and diversity of microplastics: Taking floating microplastics in the South China Sea as an example. *Environ. Pollut.* 245, 965–974. doi: 10.1016/j.envpol.2018.10.110

Wang, W., Ndungu, A. W., Li, Z., and Wang, J. (2017). Microplastics pollution in inland freshwaters of China: A case study in urban surface waters of Wuhan, China. *Sci. Total Environ.* 575, 1369–1374. doi: 10.1016/j.scitotenv.2016.09.213

Wang, Z., You, Y., Xu, W., Chen, W., Zeng, J., Zhao, X., et al. (2018). Dimethyl phthalate altered the microbial metabolic pathways in a Mollisol. *Eur. J. Soil Sci.* 69, 439–449.

Wen, X., Du, C., Xu, P., Zeng, G., Huang, D., Yin, L., et al. (2018). Microplastic pollution in surface sediments of urban water areas in Changsha, China: Abundance, composition, surface textures. *Mar. Pollut. Bull.* 136, 414–423. doi: 10.1016/j.marpolbul.2018.09.043

Wong, J. K. H., Lee, K. K., Tang, K. H. D., and Yap, P.-S. (2020). Microplastics in the freshwater and terrestrial environments: Prevalence, fates, impacts and sustainable solutions. *Sci. Total Environ.* 719:137512. doi: 10.1016/j.scitotenv.2020.137512

Wu, X., Hou, H., Liu, Y., Yin, S., Bian, S., Liang, S., et al. (2022). Microplastics affect rice (*Oryza sativa L.*) quality by interfering metabolite accumulation and energy expenditure pathways: A field study. *J. Hazard. Mater.* 422:126834.

Xiao, M., Shahbaz, M., Liang, Y., Yang, J., Wang, S., Chadwicka, D. R., et al. (2021). Effect of microplastics on organic matter decomposition in paddy soil amended with crop residues and labile C: A three-source-partitioning study. *J. Hazard. Mater.* 416:126221. doi: 10.1016/j.jhazmat.2021.126221

Xu, L., Cao, L., Huang, W., Liu, J., and Dou, S. (2021). Assessment of plastic pollution in the Bohai Sea: Abundance, distribution, morphological characteristics and chemical components. *Environ. Pollut.* 278:116874. doi: 10.1016/j.envpol.2021.116874

Yan, Y., Chen, Z., Zhu, F., Zhu, C., Wang, C., and Gu, C. (2021). Effect of polyvinyl chloride microplastics on bacterial community and nutrient status in two agricultural soils. *Bull. Environ. Contam. Toxicol.* 107, 602–609.

Yang, L., Kang, S., Wang, Z., Luo, X., Guo, J., Gao, T., et al. (2022). Microplastic characteristic in the soil across the Tibetan Plateau. *Sci. Total Environ.* 828:154518. doi: 10.1016/j.scitotenv.2022.154518

Yang, X., Li, Z., Ma, C., Yang, Z., Wei, J., Wang, T., et al. (2022). Microplastics influence on Hg methylation in diverse paddy soils. *J. Hazard. Mater.* 423:126895. doi: 10.1016/j.jhazmat.2021.126895

Yi, M., Zhou, S., Zhang, L., and Ding, S. (2021). The effects of three different microplastics on enzyme activities and microbial communities in soil. *Water Environ. Res.* 93, 24–32.

Yin, L., Jiang, C., Wen, X., Du, C., Zhong, W., Feng, Z., et al. (2019). Microplastic pollution in surface water of urban lakes in Changsha, China. *Int. J. Environ. Res. Public Health* 16:1650.

Yu, H., Zhang, Y., Tan, W., and Zhang, Z. (2022). Microplastics as an Emerging Environmental Pollutant in Agricultural Soils: Effects on Ecosystems and Human Health. *Front. Environ. Sci.* 10:855292. doi: 10.3389/fenvs.2022.855292

Yu, L., Zhang, J., Liu, Y., Chen, L., Tao, S., and Liu, W. (2021). Distribution characteristics of microplastics in agricultural soils from the largest vegetable production base in China. *Sci. Total Environ.* 756:143860. doi: 10.1016/j.scitotenv.2020.143860

Yuan, W., Christie-Oleza, J. A., Xu, E. G., Li, J., Zhang, H., Wang, W., et al. (2022). Environmental fate of microplastics in the world's third-largest river: Basin-wide investigation and microplastic community analysis. *Water Res.* 210:118002. doi: 10.1016/j.watres.2021.118002

Zhang, H., Huang, Y., An, S., Li, H., Deng, X., Wang, P., et al. (2022). Land-use patterns determine the distribution of soil microplastics in typical agricultural areas on the eastern Qinghai-Tibetan Plateau. *J. Hazard. Mater.* 426:127806. doi: 10.1016/j.jhazmat.2021.127806

Zhang, J., Ren, S., Xu, W., Liang, C., Li, J., Zhang, H., et al. (2022). Effects of plastic residues and microplastics on soil ecosystems: A global meta-analysis. *J. Hazard. Mater.* 435:129065. doi: 10.1016/j.jhazmat.2022.129065

Zhang, Q., Zhao, M., Meng, F., Xiao, Y., Dai, W., and Luan, Y. (2021). Effect of Polystyrene Microplastics on Rice Seed Germination and Antioxidant Enzyme Activity. *Toxics* 9:179. doi: 10.3390/toxics9080179

Zhang, S., Wang, J., and Hao, X. (2020). Fertilization accelerates the decomposition of microplastics in mollisols. *Sci. Total Environ.* 722:137950. doi: 10.1016/j.scitotenv.2020.137950

Zhang, X., Leng, Y., Liu, X., Huang, K., and Wang, J. (2020). Microplastics' pollution and risk assessment in an urban river: A case study in the Yongjiang River, Nanning City, South China. *Expos. Health* 12, 141–151.

Zhou, Y., Liu, X., and Wang, J. (2019). Characterization of microplastics and the association of heavy metals with microplastics in suburban soil of central China. *Sci. Total Environ.* 694:133798. doi: 10.1016/j.scitotenv.2019.133798

Zhou, Y., Wang, J., Zou, M., Jia, Z., Zhou, S., and Li, Y. (2020). Microplastics in soils: A review of methods, occurrence, fate, transport, ecological and environmental risks. *Sci. Total Environ.* 748:141368.

Zhou, Y., Wang, J., Zou, M., Yin, Q., Qiu, Y., Li, C., et al. (2022). Microplastics in urban soils of Nanjing in eastern China: Occurrence, relationships, and sources. *Chemosphere* 303:134999. doi: 10.1016/j.chemosphere.2022.134999

Zhu, X. (2015). Optimization of elutriation device for filtration of microplastic particles from sediment. *Mar. Pollut. Bull.* 92, 69–72. doi: 10.1016/j.marpolbul.2014.12.054

Zhu, X., Ran, W., Teng, J., Zhang, C., Zhang, W., Hou, C., et al. (2021). Microplastic pollution in nearshore sediment from the Bohai Sea coastline. *Bull. Environ. Contam. Toxicol.* 107, 665–670. doi: 10.1007/s00128-020-02866-1

frontiers | Frontiers in Microbiology

TYPE Original Research
PUBLISHED 04 January 2023
DOI 10.3389/fmicb.2022.1079114



OPEN ACCESS

EDITED BY
Hongbo Li,
Nanjing University, China

REVIEWED BY
Jing Ding,
Yantai University, China
Jonathan Chen,
Quanzhou Normal University, China

*CORRESPONDENCE
Jun Ma
jma@iue.ac.cn
Guangqun Huang
huanggq@cau.edu.cn

SPECIALTY SECTION
This article was submitted to Microbiotechnology, a section of the journal Frontiers in Microbiology

RECEIVED 25 October 2022
ACCEPTED 28 November 2022
PUBLISHED 04 January 2023

CITATION
Liu N, Li G, Su Y, Zhao Y, Ma J and Huang G (2023) Environmental drivers and interaction mechanisms of heavy metal and antibiotic resistome exposed to amoxicillin during aerobic composting. *Front. Microbiol.* 13:1079114. doi: 10.3389/fmicb.2022.1079114



# Environmental drivers and interaction mechanisms of heavy metal and antibiotic resistome exposed to amoxicillin during aerobic composting

Ning Liu[1,2], Gang Li[1,2], Ya Su[3], Yi Zhao[4], Jun Ma[1,2]* and Guangqun Huang[3]*

[1]Key Laboratory of Urban Environment and Health, Ningbo Urban Environment Observation and Research Station, Institute of Urban Environment, Chinese Academy of Sciences, Xiamen, China, [2]Zhejiang Key Laboratory of Urban Environmental Processes and Pollution Control, CAS Haixi Industrial Technology Innovation Center in Beilun, Ningbo, China, [3]Engineering Laboratory for AgroBiomass Recycling and Valorizing, College of Engineering, China Agricultural University, Beijing, China, [4]School of Water Resources and Environment, China University of Geosciences (Beijing), Beijing, China

The environmental accumulation and spread of antibiotic resistance pose a major threat to global health. Aerobic composting has become an important hotspot of combined pollution [e.g., antibiotic resistance genes (ARGs) and heavy metals (HMs)] in the process of centralized treatment and resource utilization of manure. However, the interaction mechanisms and environmental drivers of HMs resistome (MRGs), antibiotic resistance (genotype and phenotype), and microbiome during aerobic composting under the widely used amoxicillin (AMX) selection pressure are still poorly understood. Here, we investigated the dynamics of HMs bioavailability and their MRGs, AMX-resistant bacteria (ARB) and antibiotic resistome (ARGs and *intI1*), and bacterial community to decipher the impact mechanism of AMX by conducting aerobic composting experiments. We detected higher exchangeable HMs and MRGs in the AMX group than the control group, especially for the *czrC* gene, indicating that AMX exposure may inhibit HMs passivation and promote some MRGs. The presence of AMX significantly altered bacterial community composition and AMX-resistant and -sensitive bacterial structures, elevating antibiotic resistome and its potential transmission risks, in which the proportions of ARB and *intI1* were greatly increased to 148- and 11.6-fold compared to the control group. Proteobacteria and Actinobacteria were significant biomarkers of AMX exposure and may be critical in promoting bacterial resistance development. *S0134_terrestrial_group* was significantly negatively correlated with $bla_{TEM}$ and *czrC* genes, which might play a role in the elimination of some ARGs and MRGs. Except for the basic physicochemical (MC, C/N, and pH) and nutritional indicators ($NO_3^-$-N, $NH_4^+$-N), Bio-Cu may be an important environmental driver regulating bacterial resistance during composting. These findings suggested the importance of the interaction mechanism of combined pollution and its synergistic treatment during aerobic composting need to be emphasized.

KEYWORDS

beta-lactam resistance genes, antibiotic resistant bacteria, exchangeable heavy metals, heavy metal resistome, waste utilization

## Introduction

With the overuse, misuse, and abuse of antibiotics in modern medicine and the livestock industry in the last decades (Yao L. et al., 2020; Zhang et al., 2020; Zou et al., 2020; Wang et al., 2021), antimicrobial resistance has developed into one of the most urgent public health crises in recent years (Zhu et al., 2017a; Vos et al., 2019; Joshi and Kim, 2020; Dai et al., 2022). According to statistics, the global defined daily doses of antibiotics reached 34.8 billion in 2015 and have increased by 65% since 2000 (Zhao R. et al., 2019). Amoxicillin (AMX) is currently the most important and frequently used broad-spectrum β-lactam antibiotic, accounting for 50–70% of total antibiotic consumption globally (Chen et al., 2017; Liu et al., 2018). Specifically, AMX is the most commonly used human and animal antibiotic among 36 different drug types in China (Liu et al., 2019), with doses up to 500 mg/kg used in pig feed (Liu et al., 2018). However, antibiotics usage in animal husbandry (Zhang et al., 2017a) can shift animal microbiome, enrich antibiotic resistance genes (ARGs), and subsequently transfer to livestock manure and its products (Qiu et al., 2022). Hence, livestock production is considered an important hotspot and key point-source of antibiotic resistant bacteria (ARB) and ARGs dissemination (Youngquist et al., 2016; Awasthi et al., 2019; Deng et al., 2020; Lu et al., 2020; Tang et al., 2020). Previous studies have shown that β-lactam resistance genes are the top three types of ARGs in manure samples from 17 dairy farms in Shanxi Province, China (Zhou et al., 2016; Liu et al., 2018). The Class I integrase gene (*intI1*), which gene cassette usually contains ARGs (Zhang et al., 2017a; Zhang R. et al., 2019), can mediate horizontal gene transfer (HGT) thereby facilitating ARGs spread among microorganisms (Yin et al., 2017; Zhang J. et al., 2019; Wang et al., 2023). Due to persistent environmental selection of antibiotic residue and fecal contamination containing antimicrobial resistant determinants, it is anticipated that about 300 million people will die prematurely by 2055 worldwide (Joshi and Kim, 2020).

It is noteworthy that heavy metals (HMs), such as copper (Cu) and zinc (Zn), were often used as important feed additives to promote the growth of livestock (Zhang J. et al., 2019; Zhang et al., 2020). However, due to the poor absorption and difficult degradation of HMs (Yin et al., 2017; Zhang et al., 2017b), they usually coexist with antibiotics and other harmful substances (Imran et al., 2019; Wang R.Z. et al., 2020; Yao N. et al., 2020) in breeding wastes (Awasthi et al., 2019; Zhang R. et al., 2019; Chen et al., 2020) and compost products (Guo et al., 2019; Deng et al., 2020; Zhang et al., 2020). These environmental pollutants (HMs, antibiotics, etc.) can release (co-)selection pressure, induce HMs resistome (MRGs) development and mobile genetic elements (including *intI1*) mediated HGT (Imran et al., 2019; Zhao Y. et al., 2019; Lu et al., 2020) and accelerate the spread of bacterial resistance (Zhao et al., 2017; Vos et al., 2019), thereby seriously threatening the environmental health (Guo et al., 2019; Imran et al., 2019; Yang et al., 2019). Worse still, even HMs of low concentration has high persistence (Yin et al., 2017; Vos et al., 2019) and strong selective pressure of antibiotic resistance in certain cases (Imran et al., 2019; Zhang J. et al., 2019), among which Cu was shown to be the strongest ability to promote ARGs conjugate transfer (Ji et al., 2012; Guo et al., 2019; Zhang R. et al., 2019).

Pig manure is a typical microenvironment contaminated with antibiotics and HMs (Zhang et al., 2017b; Zhang J. et al., 2019; Zhang R. et al., 2019), where the concentration of HMs is several times that of antibiotics (Awasthi et al., 2019; Imran et al., 2019). It has been reported that aerobic composting has the potential to reduce the bioavailability of HMs (Yin et al., 2017; Deng et al., 2020), antibiotic concentrations, and their drug resistance (Youngquist et al., 2016; Zhou et al., 2016; Awasthi et al., 2019), while utilizing livestock manure as resources (Liu et al., 2017a,b, 2018; Guo et al., 2019; Kumar Awasthi et al., 2019; Qiu et al., 2019; Tang et al., 2020). However, the removal effect of composting will largely vary depending on the composting environment, process conditions, and various pollutants (Zhang J. et al., 2019; Zhang et al., 2020). Up to date, many studies on the removal (Youngquist et al., 2016; Liu et al., 2018; Awasthi et al., 2019; Tang et al., 2020; Zhang et al., 2020) and effects (Meng et al., 2015; Qian et al., 2016; Yin et al., 2017; Liu et al., 2019; Deng et al., 2020) of various antibiotics or HMs during aerobic composting have been made. However, there is still a lack of research on the dynamics and interaction mechanisms of HMs resistome, AMX bacterial resistance (genotype and phenotype), and microbiome during aerobic composting under the widely used AMX selection pressure. Therefore, more studies are needed to decipher the impact mechanism of AMX on various complex pollutants in the process of fecal aerobic composting and the risk of bacterial resistance.

Thus, the objectives of our study were (1) to characterize the dynamics of HMs bioavailability and their resistome (MRGs) with or without AMX exposure, (2) to explore the effects of AMX selection pressure on AMX bacterial resistance (ARB) and antibiotic resistome (ARGs and *intI1*), and (3) to decipher the environmental drivers and interaction mechanisms of bacterial taxonomic and functional (ARGs, MRGs, *intI1*, etc.) community composition during composting. Our findings will provide insights into organic waste resource utilization and pollutant risk

control mechanisms underpinning the cleaner production of intensive animal husbandry and better development of organic circular agriculture.

# Materials and methods

## Materials and chemicals

Pig manure was obtained from a large-scale pig farm in Shunyi District (Beijing, China), with prior assurance that no antibiotics were applied to the sampled pigs during the breeding process. Wheat straw was collected from Shangzhuang Experimental Station of China Agricultural University and cut into 3–5 cm segments (Liu et al., 2017a,b, 2019). AMX (98%) was gained from Huamaike Biological Technology Company, Ltd. (Beijing, China). The chemicals used in HM extraction were of analytical grade.

## Experimental design

In this study, two groups of fresh pig manure (about 5.2 kg) were fully mixed with 100 mg/kg (dry weight) AMX aqueous solution or an equivalent amount of ultrapure water (control), and then a certain amount of wheat straw and ultrapure water were mixed uniformly, according to the ratio of total carbon and total nitrogen (C/N) of 20:1 and moisture content (MC) of 65% (Liu et al., 2019). After being completely mixed and equilibrated for about 6 h (Qian et al., 2016; Liu et al., 2019), the two groups of initial compost mixture were placed in two parallel sets of in-laboratory aerobic composting reactor systems (Supplementary Figure S1), as the experimental group (AMX group) and the control group without AMX (CK group). Both groups of reactors were continuously ventilated by 0.2 L/(kg-*VS*-min). The basic physicochemical properties of initial composting materials have been determined and listed in Supplementary Table S1. The above settings of composting conditions and AMX concentration were based on the existing reports and our previous studies (Kotzerke et al., 2011; Liu et al., 2018, 2019).

According to the aerobic composting periods (Liu et al., 2018), about 120 g of the compost mixture was sampled on days 0, 2, 4, 6, 9, 15, and 21, and the basic physicochemical, biological, and heavy metal-related indicators were determined. Furthermore, the viable counts of AMX-resistant bacteria and total culturable bacteria (TCB) were performed immediately on the day of sampling. The presence of AMX resistance genes ($bla_{TEM}$, $bla_{VIM}$), Cu resistance gene (*copA*), Zn resistance gene (*czrC*), and *intI1* were determined by real-time fluorescence quantitative PCR (qPCR) for day 0, 2, 6, 15, and 21 samples. Combined with the existing reports and our previous studies, *TEM*- and *VIM*-type β-lactam resistance genes, as the most common and highly abundant ARGs in animal breeding and clinical environments, can significantly enhance the zoonotic potential (Pomba et al., 2004). Together with *copA*- and *czrC*-type MRGs, they are often used as indicator genes of bacterial resistance contamination (Narciso-da-Rocha et al., 2014). Moreover, *intI1* is widely used as an important universal marker for human pollutants (Gillings et al., 2015; Yin et al., 2017). The bacterial community of compost on days 2, 6, and 15 were analyzed according to different representative composting stages based on 16S rRNA gene sequencing. Samples used for molecular biological determinations were first lyophilized with a vacuum freeze dryer (Martin Christ Alpha 1–2 LD plus, Germany) for the same low MC, then ground with a 1-mm sieve and frozen at −80°C for DNA extraction. Other samples were kept at −20°C for physicochemical parameters analysis. The compost piles were fully mixed manually before and after each sampling.

## Measurement and analysis methods

### Basic physicochemical and biological indicators

Temperature sensor systems were used to monitor the temperature of the piles and ambient temperature in real-time during composting. Organic matter (OM), MC, C/N, pH, $NH_4^+$-N, and $NO_3^-$-N were determined concerning the existing methods (Liu et al., 2017a,b, 2019). Since the level of mobility is an important indicator to measure the potential risk of HMs in the environment (Nemati et al., 2011), exchangeable HMs have also attracted attention as the most active and bioavailable high-risk metal forms. Therefore, the most bioavailable and risky exchangeable copper (bio-Cu) and exchangeable zinc (bio-Zn) were detected according to the improved BCR sequential extraction method (Nemati et al., 2011).

### Viable counts of ARB and TCB

According to the maximum value of the bacterial Minimum Inhibition Concentration, AMX-resistant bacteria and TCB were counted on R2A medium with and without 32 mg/L AMX by referring to previous experience (Liu et al., 2020). The colony formation unit (CFU) per gram was calculated by the formula (1). All measurements in this study were performed in duplicate.

$$\mathrm{CFU}\left(\frac{1}{\mathrm{ml}}\right)=\frac{\text{colony count}}{\text{sample volume}(\mathrm{ml})\times\text{dilutionrate}} \quad (1)$$

### DNA extraction and qPCR

According to the manufacturer's instructions, a Soil Genomic DNA Extraction Kit (Kangwei Century, China) was used to extract DNA from composting samples. After the design of related primers (Supplementary Table S2), the presence of two β-lactam resistance genes ($bla_{TEM}$, $bla_{VIM}$), two MRGs (*copA*, *czrC*), and *intI1* were determined by standard

PCR (Liu et al., 2019). The PCR products were examined by 1% (w/v) agarose gel electrophoresis after the reaction, and the detected genes were quantified using the ABI 7500 Real-Time PCR System (Applied Biosystems, United States). Absolute abundances of genes were expressed as copy number per gram of dry compost.

### Bacterial 16S rRNA gene high-throughput sequencing

16S rRNA gene sequencing was conducted with the Illumina MiSeq platform, and the 16S V3-V4 region was amplified using primers U341F (ACTCCTACGGGAGGCAGCAG) and U806R (GGACTACHVGGGTWTCTAAT). USEARCH was used for quality control of raw data, and UPARSE was used for clustering of qualified sequences with 97% similarity to form operational classification unit (OTU).

## Statistical analysis

Repeated measurements were expressed as mean ± standard deviation (SD, indicated by the error bar in the figures). Excel 2016 (Microsoft, United States), SPSS 25 (IBM, United States), and OriginProV.8.5 SR1 (OriginLab Corp., United States) were used for basic statistical analysis. Shannon-Wiener curves, principal coordinates analysis (PCoA), heatmap, correlation analysis, and genus-level phylogenetic tree were performed by R3.4.1 software. Redundancy analysis (RDA) was carried out based on CANOCO 5.0. Correlation network analysis (Spearman, $r > 0.6$, $p < 0.05$) was conducted by R3.4.1 software and Gephi0.9.3 software.

# Results and discussion

## Changes of exchangeable HMs and their resistome (MRGs) during composting

As important indicators of environmental HMs potential risks, exchangeable HMs (bio-Cu and bio-Zn) can sensitively reflect the dynamic changes of HM morphology and toxicity during composting. The concentrations of bio-Cu and bio-Zn in the two groups leveled off after first decreasing during composting, presenting a relatively consistent change trend (Figures 1A,B). The results reflected that aerobic composting treatment will reduce the migration rate and bioavailability of Cu and Zn to a certain extent, thereby effectively reducing the toxicity and potential risks of HMs in the products. Comparatively, the concentrations of bio-Cu and bio-Zn in the AMX group were slightly higher than those in the CK group during the early stage of composting. This difference indicated that the addition of AMX likely hindered the passivation process of HMs and, thus, increased the risks of HMs contamination and the co-selection pressure of inducing bacterial resistance, which was also confirmed by previous reports (Song et al., 2017; Vos et al., 2019).

We found that the abundance of *copA* and *czrC* in the AMX group was higher at the initial stage of composting (Figures 1C,D), especially the difference between the two groups of *czrC* was the most significant ($p < 0.05$, *t*-test), further illustrating the vital role of AMX selective pressure on the promotion of HM resistance and adaptation cost of MRGs-carrying bacteria (Imran et al., 2019; Zhang et al., 2020). Notably, AMX may have a stronger promotion effect on some Zn resistome. In the late stage of composting, the abundance of *copA* in the two groups increased rapidly then fell, while *czrC* of the two groups was very low and stable, probably because *copA*-carrying bacteria mainly dominated the composting maturity stage and were strongly affected by microbial succession at this stage. According to Figure 1, AMX selective pressure may significantly inhibit the passivation of HMs while promoting the development of some MRGs, thereby raising the potential risk of HM toxicity and bacterial resistance in the environment.

## Changes of AMX bacterial resistance (phenotype and genotype) during composting

### AMX-resistant bacteria and their proportion of resistance

As shown in Figure 2A, the number of AMX-resistant bacteria in the two groups fell sharply with the rapid increase in compost temperature (Supplementary Figure S2A) on days 0–2, which also restricted TCB (Supplementary Figure S2B). The temperature of compost piles on days 3–9 decreased slowly, with a significant recovery in the middle period, which resulted in a slight increase in the number of AMX-resistant bacteria and TCB in the two groups. As the compost temperature gradually decreased toward ambient temperature (days 10–21), the composting microenvironment became more suitable for the growth and reproduction of microorganisms. Therefore, a sharp increase in the number of AMX-resistant bacteria and TCB was observed, followed by a decrease due to nutrient deficiency.

The proportion of AMX-resistant bacteria in the AMX group in the early stage of composting were significantly higher than those in the CK group (days 0–4; Figure 2B), implying the influence of AMX selective pressure on the enhancement of AMX bacterial resistance (Vos et al., 2019; Zou et al., 2020). However, in the later stage of composting, the number of AMX-resistant bacteria and TCB in the AMX group was significantly lower ($p < 0.01$, *t*-test) than that in the CK group (Figure 2A; Supplementary Figure S2B), while the proportion of AMX resistance (Figure 2B) was similar between the two groups, suggesting the inhibitory effect of AMX addition on microbial growth and reproduction (Liu et al., 2019).

### ARGs and intI1 of the compost piles

According to Figures 3A,B, the $bla_{TEM}$ and $bla_{VIM}$ gene abundances in the AMX treatment were initially higher than those of the CK treatment. Both genes in the AMX group experienced

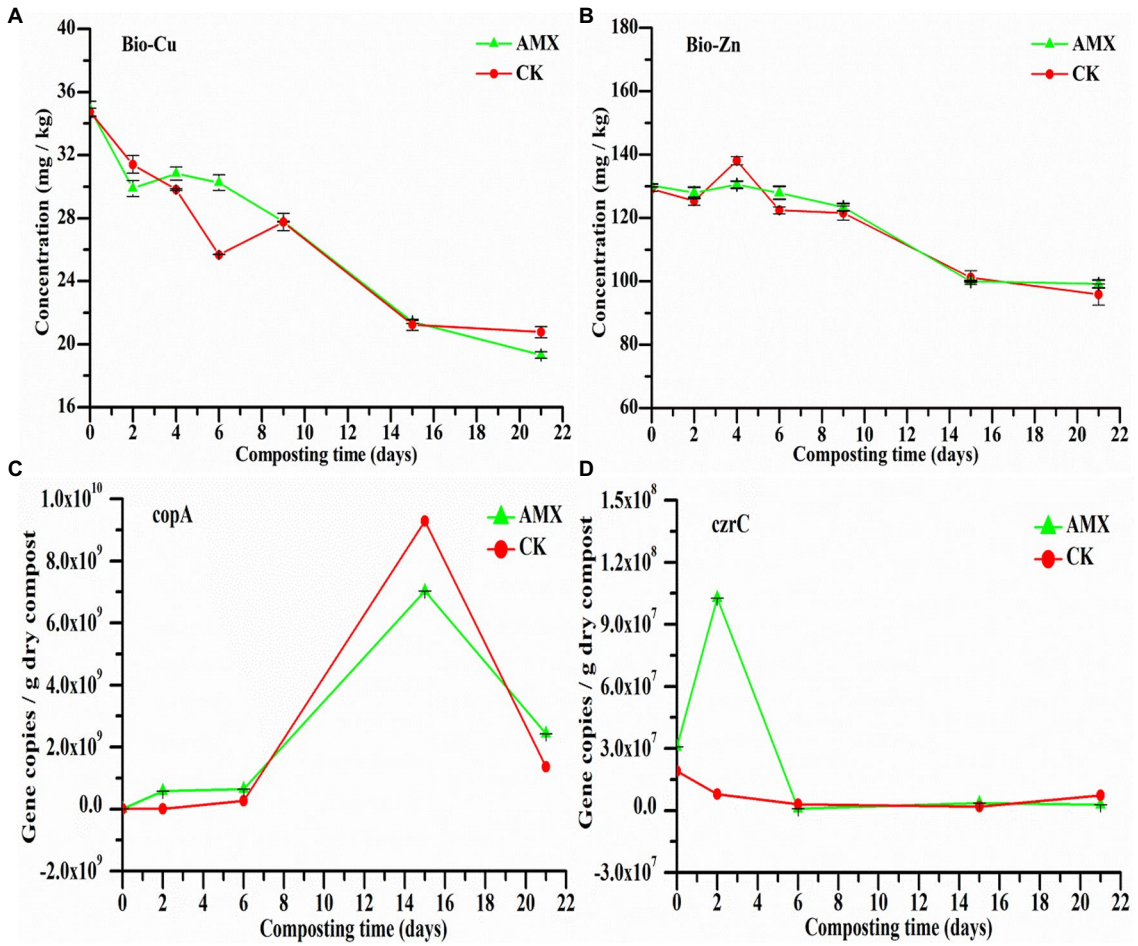


FIGURE 1
Dynamic changes of **(A)** exchangeable Cu (bio-Cu), **(B)** exchangeable Zn (bio-Zn), **(C)** Cu resistance gene (*copA*), and **(D)** Zn resistance gene (*czrC*) during composting.

a tendency to decline first, followed by an increase, and then a gradual decrease, which may be due to the dual effect of the high-temperature environment (Supplementary Figure S2A) and antibiotic selective pressure in the early stage of composting. With the piles' temperature decrease in the late stage of composting and the long-term co-selection of AMX-HM pollution (Imran et al., 2019; Wang R.Z. et al., 2020; Yao N. et al., 2020), the abundance of the two β-lactam resistance genes in the AMX group obviously increased compared with the CK group.

As shown in Figure 3C, the absolute abundance of *intI1* gene in the two groups changed similarly during composting, both demonstrating an initially decreasing trend followed by an increase. Comparatively, the abundance of *intI1* in the AMX group was always 1.3–11.6 times greater than that in the CK group, even at the day 0, and maintained a rapid growth trend in the late stage of composting. Compared with $bla_{TEM}$ and $bla_{VIM}$, *intI1* was significantly increased during the equilibration phase before the start of composting (day 0), indicating that it would be greatly increased in a very short period of time and persistently affected by AMX exposure, which may be a non-negligible problem in the spread of bacterial resistance. Furthermore, while the high temperature of the thermophilic phase greatly reduced the number of bacteria (Supplementary Figure S2) and *intI1* gene in both groups, the co-selection pressure of AMX and HMs still provided a strong selective advantage for their resistant bacteria (Figure 2) and resistome (Figures 1C,D, 3) in the AMX group. This further confirmed the crucial role of antibiotics in promoting the development of bacterial resistance (antibiotics, HMs, etc.) and its transmission risk (Imran et al., 2019).

## Changes of bacterial communities during composting

A total of 397 operational taxonomic units (OTUs) were detected in compost samples. According to the Shannon-Wiener curves of the compost samples (Supplementary Figure S3), the sequencing data were sufficient to reflect the vast majority of microbial information in all samples. After leveling the minimum sequence number of the samples, alpha diversity analysis was

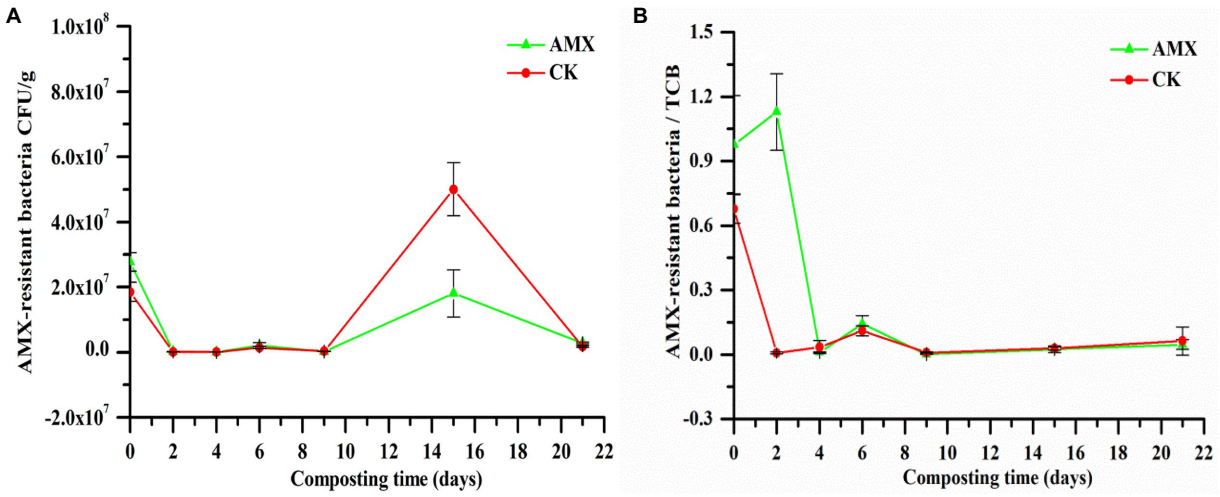


FIGURE 2
Dynamic changes of **(A)** AMX-resistant bacteria and **(B)** AMX-resistant bacteria / total culturable bacteria (TCB) during composting.

performed on the two groups of compost samples (Supplementary Figure S4). The three diversity indices of the AMX group were higher than those of the CK group as a whole, confirming that the bacterial community of the AMX group was relatively rich and uniform with higher community diversity (Supplementary Figures S4A–C). Moreover, there was a greater difference in species lineage among samples in the CK group when considering species abundance and evolutionary distance (Supplementary Figure S4D). In summary, although AMX selective pressure reduced the absolute abundances of culturable bacteria (Supplementary Figure S2B), the richness and evenness of the bacterial community were relatively high (Supplementary Figure S4), which may indicate the effect of AMX on the alteration of microbial community structure during composting and the selective pressure on AMX-sensitive and -resistant bacteria. According to the PCoA, PC1 and PC2 accounted for 85.6% of the total variation of the bacterial community (Figure 4A). Principal coordinates analysis of the bacterial community revealed that the samples of different composting periods were clearly separated along the PCo1 axis, and some clustering of composting samples from the same period was also observed. The difference in bacterial community composition between the two groups decreased gradually as the number of composting days increased, illustrating that the impact of the composting periods and habitat on the bacterial community structure was particularly significant (Yin et al., 2017). Furthermore, AMX addition significantly affected the bacterial community structure in the early stage of composting, which is consistent with the above results (Supplementary Figure S4).

It can be seen from Figures 4B,C that the bacterial community of the two groups continued to change during composting, while the differences in community composition gradually decreased. Among the communities, Firmicutes, Proteobacteria, Actinobacteria, and Bacteroidetes were the dominant phylum bacteria during the whole composting process (Figure 4B), accounting for 95.2–99.9% of the bacterial 16S rRNA gene sequences (Supplementary Figure S5). As shown in Figure 4B, the relative abundance (RA) of Firmicutes was the highest in the early stage of composting and the RA in the AMX group was lower than that in the CK group, but decreased rapidly as the compost matured. This may be since Firmicutes, beneficial bacteria for promoting cellulose degradation, widely exist in animal intestines, compost, and soil environment, and dominate the heating and thermophilic phases of composting (Yin et al., 2017; Liu et al., 2019). Moreover, high concentrations of antibiotics will significantly inhibit their growth and reproduction (Qian et al., 2016; Guo et al., 2017; Liu et al., 2019), resulting in a significant reduction of Firmicutes RA in the AMX group. According to Figure 4B, RA of Bacteroides increased significantly in the mature composting stage of the two groups and was relatively higher in the CK group. In Figure 4C, it can be seen that Sphingobacteriia, Flavobacteriia, and Bacteroidia (which belong to Bacteroides) also displayed the same regularities and cluster. Bacteroides are a kind of bacteria attributed to the degradation of high-molecular-weight compounds and the growth of supporting materials, which mainly grow in the middle and late stages of composting (Zhu et al., 2017b; Liu et al., 2019). The RA of Proteobacteria and Actinobacteria (most notably in Proteobacteria) in the AMX group increased with composting maturity and was significantly higher than that in the CK group during the early stage of composting (Figure 4B). This large difference may be attributed to the dominance of both bacteria in the cooling and mature stages of composting, where the abundance of Actinobacteria is mostly used to mark the degree of maturity (Liu et al., 2019; Zhang et al., 2020). Previous studies have shown that both bacteria have a significant positive correlation with ARGs (Yin et al., 2017), and their RA will also

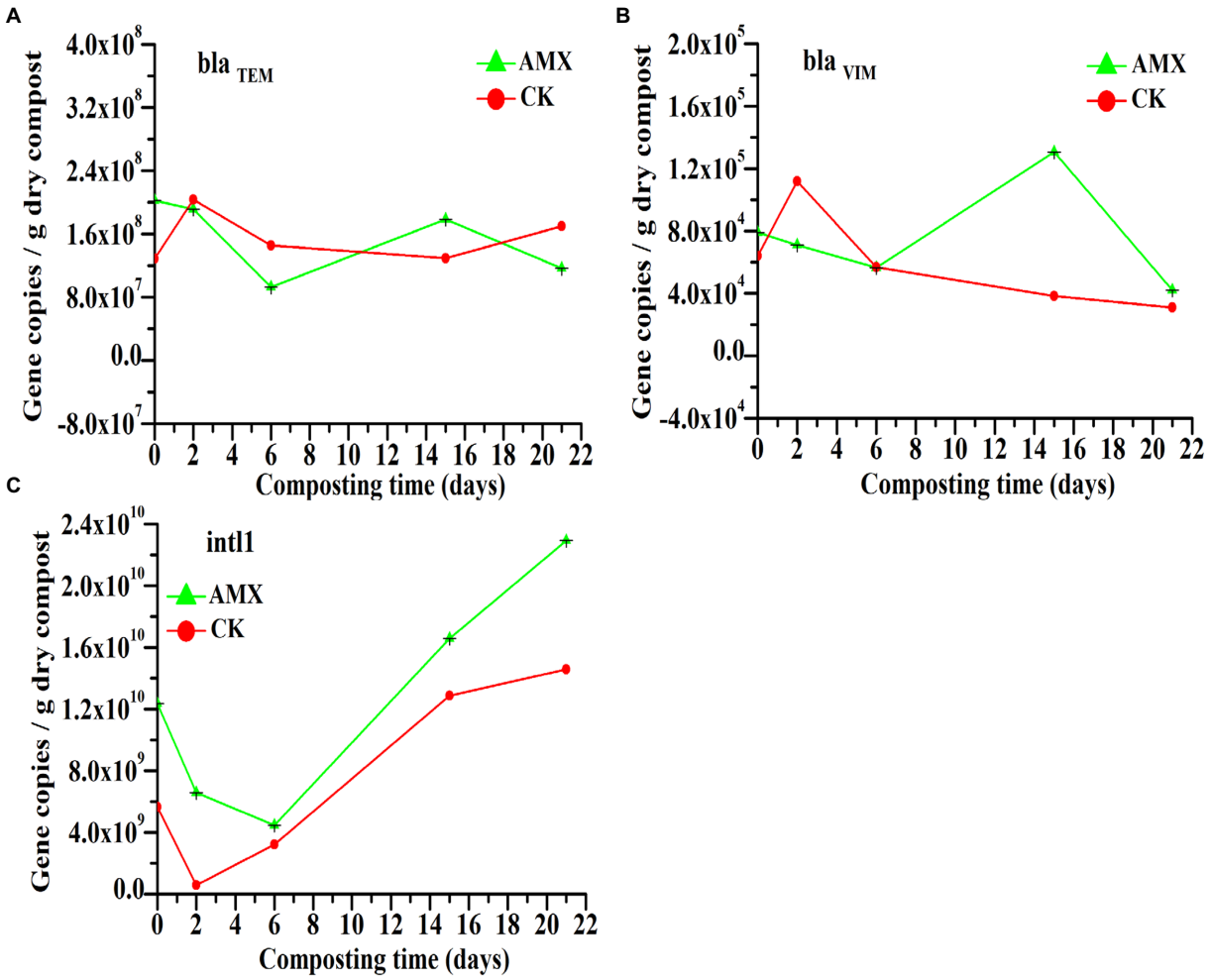


FIGURE 3
Dynamic changes in the copy number of **(A)** $bla_{TEM}$, **(B)** $bla_{VIM}$, and **(C)** *intI1* during composting.

be significantly increased in the presence of high concentrations of antibiotics (Guo et al., 2017). Besides, the driving force of the increased resistance in the compost was mainly attributed to Proteobacteria (Meng et al., 2015), in which γ-Proteobacteria has a strong resistance potential to high-concentration antibiotics (Zhu et al., 2017b). Moreover, β-Proteobacteria is considered to be the original source of *intI1*, which has become the core of antibiotic resistance due to its ability to capture and express multiple ARGs (Guo et al., 2017; Zhu et al., 2017b). The above conclusions were also further confirmed in Figure 4C, where the variation rules of α, β, γ-Proteobacteria, and Actinobacteria were similar and clustered with each other. Therefore, the high concentration of AMX added to the experimental group can selectively inhibit the growth and reproduction of sensitive bacteria, such as Firmicutes. This provided a more favorable living environment for drug-resistant Proteobacteria and Actinobacteria, thus affecting and changing the bacterial community structure and drug resistance level during composting.

LEfSe analysis (threshold set to 2) was used to further reveal the differences between the two groups of bacterial community during composting (Figure 4D). Compared with the CK group, the species with significantly different abundance in the AMX group were Hahellaceae, Hahella, Enteractinococcus, and Marmoricola (Supplementary Figure S6), where the former two species belong to γ-Proteobacteria and the latter two to Actinobacteria. Proteobacteria is the main host of ARGs and has a high tolerance to antibiotics, while Actinobacteria is the main producer of antibiotics and usually carries a variety of ARGs (Qian et al., 2016; Zhang et al., 2020). Therefore, this finding was consistent with the relevant conclusions in Figures 4B,C and previous literature reports, further confirming the significant role of AMX in reshaping the structure of environmental microbial communities and promoting bacterial resistance. Studies have shown that Enteractinococcus is a type of Micrococcaceae commonly found in animal feces (Cao et al., 2012), while Marmoricola is the gram-positive aerobic bacteria

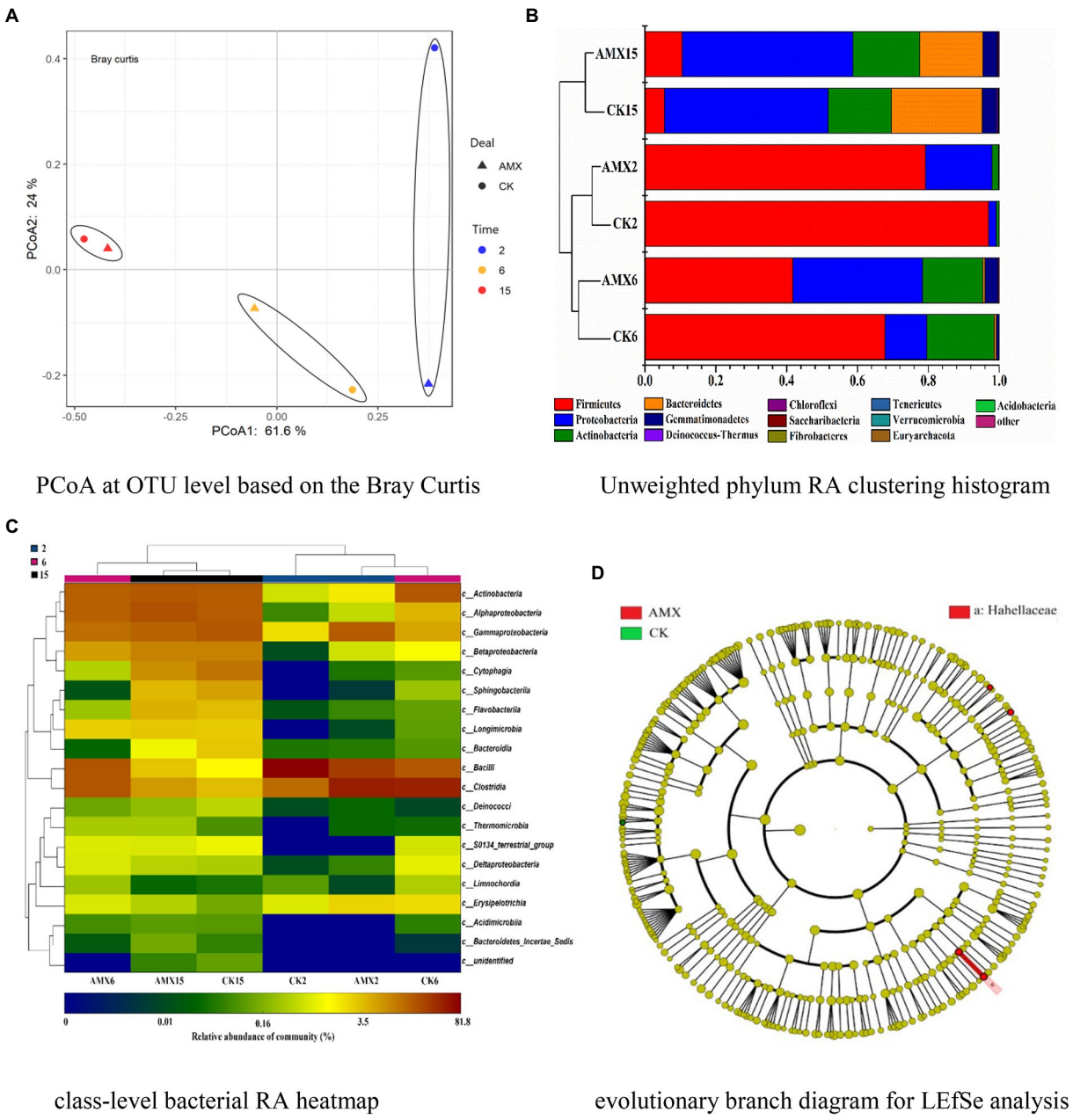


PCoA at OTU level based on the Bray Curtis

Unweighted phylum RA clustering histogram

class-level bacterial RA heatmap

evolutionary branch diagram for LEfSe analysis

FIGURE 4
Features of bacterial community during composting. **(A)** PCoA at OTU level based on the Bray Curtis. **(B)** Unweighted phylum RA clustering histogram. **(C)** Class-level bacterial RA heatmap. **(D)** Evolutionary branch diagram for LEfSe analysis.

belonging to the Nocardiaceae (Habib et al., 2020). Both of them have been reported to exist in the aerobic composting environment of livestock feces as the main Actinobacteria (Chen et al., 2015).

## Correlation analysis of the compost piles

Redundancy analysis was carried out to further reveal the correlation between the bacterial community structure and its function and environmental factors during composting, which can explain 86.8% of the total species variation (Figure 5A). Differences in the bacterial community structure gradually reduced with the extension of composting time, which intuitively reflected the severe succession and stable formation of the bacterial community structure during composting. A noteworthy correlation was observed between the thermophilic period of composting and the dynamic changes in the basic physiochemical indicators, exchangeable HMs, β-lactam resistance genes, *czrC* gene, and Firmicutes.

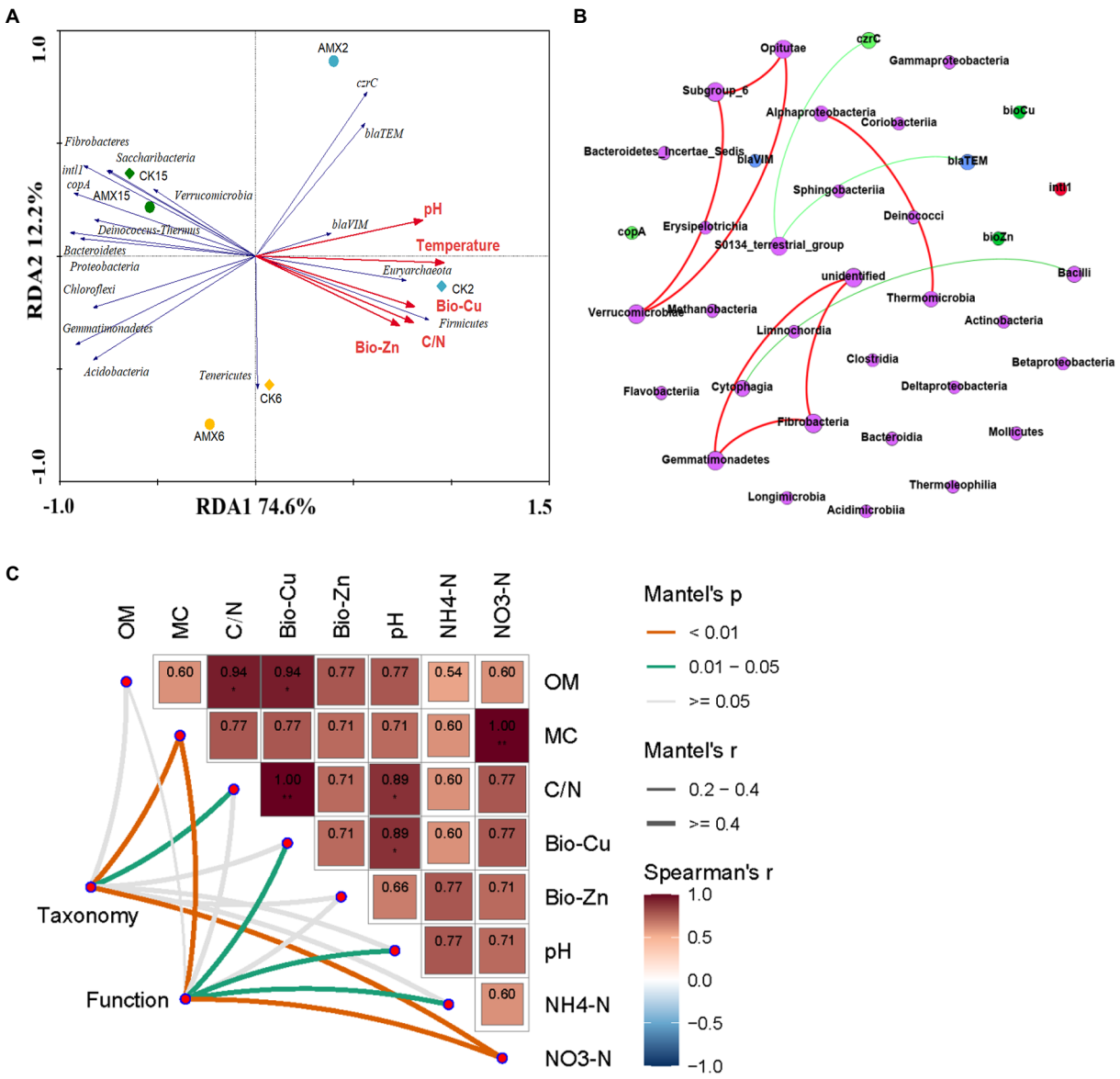


FIGURE 5
Environmental drivers of compost microbial community composition: **(A)** RDA of the relationships between the main bacterial phylum (more than 1% of the total bacterial abundance, blue arrows) and environmental factors (red arrows), **(B)** network analysis of the relationships among class-level bacteria (purple nodes), ARGs (blue nodes), MRGs (light green nodes), HMs (green nodes), and *intI1* (red nodes), and **(C)** pairwise comparisons of environmental factors were shown, with color gradients representing Spearman's correlation coefficients. Taxonomic (based on family-level bacteria) and functional (based on ARGs, MRGs, *intI1*, ARB, TCB, and ARB/TCB) community composition was related to each environmental factor by Mantel tests. Edge width denotes the Mantel's *r* statistic for the corresponding distance correlations, and edge color represents the statistical significance.

Proteobacteria, Actinobacteria, and Bacteroidetes were mainly distributed in the composting maturation stage and were directly related to the dynamic changes of *copA* gene and *intI1* gene. This correlation demonstrated the significant impact of the composting stages (especially the thermophilic period) and bacterial community structure on the composting microenvironment, HM forms, and resistance genes. Furthermore, it can also be suggested that Proteobacteria, Actinobacteria, and Bacteroidetes were likely the main factors directly affecting the development and spread of HM resistance and antibiotic resistance during composting.

To further verify the interaction pattern between the microbial communities in the two groups of different composting environments, the relationships among class-level bacteria, ARGs, MRGs, Bio-HMs, and *intI1* were revealed by network analysis (Figure 5B). More positive edges (red, 7) than negative edges (green, 3) were detected in a network of the compost. Seven different class-level bacteria (except for unidentified) had a significant positive

correlation with each other ($p < 0.05$), which was consistent with the results of the RDA analysis. *Bacilli* (belonging to Firmicutes) and *Cytophagia* (belonging to Bacteroidetes) were significantly negatively correlated ($p < 0.05$), which were the dominant bacterial communities in the early composting period and the late composting periods, respectively, (Figure 4B). *S0134_terrestrial_group*, which belongs to the Gemmatimonadetes, was significantly negatively correlated with $bla_{TEM}$ gene and *czrC* gene ($p < 0.05$). Combined with Figure 4B, Gemmatimonadetes were mainly detected in the middle and late stages of compost samples (AMX6, AMX15, and CK15), and probably play an important role in the reduction of $bla_{TEM}$ gene and *czrC* gene. Therefore, it is recommended in future studies to further explore the role of Gemmatimonadetes in removing other ARGs and MRGs during aerobic composting, especially β-lactams and zinc.

Moreover, to identify environmental drivers in our study (Sunagawa et al., 2015), we correlated distance-corrected dissimilarities of taxonomic and functional community composition with those of compost environmental factors (Figure 5C). Overall, MC and $NO_3^-$-N were the strongest correlates of both taxonomic and functional composition during composting, while no significant correlations were found for OM and Bio-Zn. Bio-Cu, pH, and $NH_4^+$-N were only weakly correlated with functional community, as well as C/N with taxonomic composition, and the other correlations were not statistically significant (Figure 5C). It can be seen that, except for the basic physicochemical (MC, C/N, and pH) and nutritional indicators ($NO_3^-$-N, $NH_4^+$-N), Bio-Cu may be an important environmental driver affecting taxonomic and functional community composition in composting environments, as well as an important potential factor regulating bacterial resistance.

## Conclusion

Our study found that aerobic composting could effectively decrease HMs bioavailability, which may alleviate the combined pollutions and (co-)selection pressure of AMX and HMs. AMX selective pressure played an important role in inhibiting HMs passivation and bacterial growth, shifting bacterial community composition and AMX-sensitive and -resistant bacteria structures, and increasing some MRGs, AMX bacterial resistance, and their potential risks, especially for *czrC* and *intI1*. Proteobacteria and Actinobacteria, as significant biomarkers of AMX exposure, may be critical in promoting the development and spread of bacterial resistance. *S0134_terrestrial_group* was significantly negatively correlated with $bla_{TEM}$ and *czrC* gene, which may be critical in reducing some ARGs and MRGs. Except for the basic physicochemical (MC, C/N, and pH) and nutritional indicators ($NO_3^-$-N, $NH_4^+$-N) during composting, Bio-Cu may be an important environmental driver affecting taxonomic and functional community composition and regulating bacterial resistance. Therefore, it is necessary to further explore the efficient removal technology of combined pollutants and the interaction mechanisms between important microorganisms and contaminants in the process of composting, to promote the harmless treatment, resource recovery, and agricultural utilization of organic waste.

## Data availability statement

The data presented in the study are deposited in the Genome Sequence Archive (Genomics, Proteomics & Bioinformatics 2021) repository, accession number CRA009005 that are publicly accessible at: https://ngdc.cncb.ac.cn/gsa.

## Author contributions

NL: conceptualization, methodology, investigation, software, formal analysis, writing—original draft, visualization, and writing—review and editing. GL: investigation, methodology, and review and editing. YS: investigation and visualization. YZ: article revision and grammar correction. JM: methodology, review and editing, and supervision. GH: resources, writing—review and editing, supervision, and funding acquisition. All authors contributed to the article and approved the submitted version.

## Funding

This work was financially supported by the National Natural Science Foundation of China (31771684, 42090063, and 42107407), Ningbo Science and Technology Plan Project (2021S030) and the Project funded by China Postdoctoral Science Foundation (2022M713076).

## Conflict of interest

The authors declare that the research was conducted in the absence of any commercial or financial relationships that could be construed as a potential conflict of interest.

## Publisher's note

All claims expressed in this article are solely those of the authors and do not necessarily represent those of their affiliated organizations, or those of the publisher, the editors and the reviewers. Any product that may be evaluated in this article, or claim that may be made by its manufacturer, is not guaranteed or endorsed by the publisher.

## Supplementary material

The Supplementary material for this article can be found online at: https://www.frontiersin.org/articles/10.3389/fmicb.2022.1079114/full#supplementary-material

# References


Awasthi, M. K., Chen, H., Awasthi, S. K., Duan, Y., Liu, T., Pandey, A., et al. (2019). Application of metagenomic analysis for detection of the reduction in the antibiotic resistance genes (ARGs) by the addition of clay during poultry manure composting. *Chemosphere* 220, 137–145. doi: 10.1016/j.chemosphere.2018.12.103

Cao, Y. R., Jiang, Y., Jin, R. X., Han, L., He, W. X., Li, Y. L., et al. (2012). Enteractinococcus coprophilus gen. Nov., sp. nov., of the family Micrococcaceae, isolated from Panthera tigris amoyensis faeces, and transfer of Yaniella fodinae Dhanjal et al. 2011 to the genus Enteractinococcus as Enteractinococcus fodinae comb. nov. *Int. J. Syst. Evol. Microbiol.* 62, 2710–2716. doi: 10.1099/ijs.0.034249-0

Chen, X., Li, G. D., Li, Q. Y., Hu, C. J., Qiu, S. M., Jiang, Y., et al. (2015). Enteractinococcus lamae sp. nov. and Enteractinococcus viverrae sp. nov., isolated from animal faeces. *Antonie Van Leeuwenhoek* 108, 1477–1483. doi: 10.1007/s10482-015-0603-3

Chen, J., Liu, Y. S., Zhang, J. N., Yang, Y. Q., Hu, L. X., Yang, Y. Y., et al. (2017). Removal of antibiotics from piggery wastewater by biological aerated filter system: treatment efficiency and biodegradation kinetics. *Bioresour. Technol.* 238, 70–77. doi: 10.1016/j.biortech.2017.04.023

Chen, J., Yu, X., Li, C., Tang, X., and Sun, Y. (2020). Removal of tetracycline via the synergistic effect of biochar adsorption and enhanced activation of persulfate. *Chem. Eng. J.* 382:122916. doi: 10.1016/j.cej.2019.122916

Dai, D., Brown, C., Burgmann, H., Larsson, D. G. J., Nambi, I., Zhang, T., et al. (2022). Long-read metagenomic sequencing reveals shifts in associations of antibiotic resistance genes with mobile genetic elements from sewage to activated sludge. *Microbiome* 10:20. doi: 10.1186/s40168-021-01216-5

Deng, W., Zhang, A., Chen, S., He, X., Jin, L., Yu, X., et al. (2020). Heavy metals, antibiotics and nutrients affect the bacterial community and resistance genes in chicken manure composting and fertilized soil. *J. Environ. Manag.* 257:109980. doi: 10.1016/j.jenvman.2019.109980

Gillings, M. R., Gaze, W. H., Pruden, A., Smalla, K., Tiedje, J. M., and Zhu, Y. G. (2015). Using the class 1 integron-integrase gene as a proxy for anthropogenic pollution. *ISME J.* 9, 1269–1279. doi: 10.1038/ismej.2014.226

Guo, H., Gu, J., Wang, X., Tuo, X., Yu, J., and Zhang, R. (2019). Key role of cyromazine in the distribution of antibiotic resistance genes and bacterial community variation in aerobic composting. *Bioresour. Technol.* 274, 418–424. doi: 10.1016/j.biortech.2018.12.005

Guo, A., Gu, J., Wang, X., Zhang, R., Yin, Y., Sun, W., et al. (2017). Effects of superabsorbent polymers on the abundances of antibiotic resistance genes, mobile genetic elements, and the bacterial community during swine manure composting. *Bioresour. Technol.* 244, 658–663. doi: 10.1016/j.biortech.2017.08.016

Habib, N., Khan, I. U., Xiao, M., Li, S., Saqib, M., Xian, W.-D., et al. (2020). Marmoricola caldifontis sp. nov., a novel actinobacterium isolated from a hot spring. *Int. J. Syst. Evol. Microbiol.* 70, 2053–2058. doi: 10.1099/ijsem.0.004016

Imran, M., Das, K. R., and Naik, M. M. (2019). Co-selection of multi-antibiotic resistance in bacterial pathogens in metal and microplastic contaminated environments: an emerging health threat. *Chemosphere* 215, 846–857. doi: 10.1016/j.chemosphere.2018.10.114

Ji, X., Shen, Q., Liu, F., Ma, J., Xu, G., Wang, Y., et al. (2012). Antibiotic resistance gene abundances associated with antibiotics and heavy metals in animal manures and agricultural soils adjacent to feedlots in Shanghai; China. *J. Hazard. Mater.* 235-236, 178–185. doi: 10.1016/j.jhazmat.2012.07.040

Joshi, A., and Kim, K. H. (2020). Recent advances in nanomaterial-based electrochemical detection of antibiotics: challenges and future perspectives. *Biosens. Bioelectron.* 153:112046. doi: 10.1016/j.bios.2020.112046

Kotzerke, A., Fulle, M., Sharma, S., Kleineidam, K., Welzl, G., Lamshöft, M., et al. (2011). Alterations in total microbial activity and nitrification rates in soil due to amoxicillin-spiked pig manure. *J. Plant Nutr. Soil Sci.* 174, 56–64. doi: 10.1002/jpln.200900210

Kumar Awasthi, M., Chen, H., Duan, Y., Liu, T., Kumar Awasthi, S., Wang, Q., et al. (2019). An assessment of the persistence of pathogenic bacteria removal in chicken manure compost employing clay as additive via meta-genomic analysis. *J. Hazard. Mater.* 366, 184–191. doi: 10.1016/j.jhazmat.2018.11.108

Liu, N., Han, H., Yin, H., Han, L., and Huang, G. (2018). Variations in the fate and risk analysis of amoxicillin and its degradation products during pig manure aerobic composting. *J. Hazard. Mater.* 346, 234–241. doi: 10.1016/j.jhazmat.2017.11.050

Liu, N., Hou, T., Yin, H., Han, L., and Huang, G. (2019). Effects of amoxicillin on nitrogen transformation and bacterial community succession during aerobic composting. *J. Hazard. Mater.* 362, 258–265. doi: 10.1016/j.jhazmat.2018.09.028

Liu, N., Xu, L., Han, L., Huang, G., and Ciric, L. (2020). Microbiological safety and antibiotic resistance risks at a sustainable farm under large-scale open-air composting and composting toilet systems. *J. Hazard. Mater.* 401:123391. doi: 10.1016/j.jhazmat.2020.123391

Liu, N., Zhou, J., Han, L., and Huang, G. (2017a). Characterization of lignocellulosic compositions' degradation during chicken manure composting with added biochar by phospholipid fatty acid (PLFA) and correlation analysis. *Sci. Total Environ.* 586, 1003–1011. doi: 10.1016/j.scitotenv.2017.02.081

Liu, N., Zhou, J., Han, L., Ma, S., Sun, X., and Huang, G. (2017b). Role and multi-scale characterization of bamboo biochar during poultry manure aerobic composting. *Bioresour. Technol.* 241, 190–199. doi: 10.1016/j.biortech.2017.03.144

Lu, X. M., Lu, P. Z., and Liu, X. P. (2020). Fate and abundance of antibiotic resistance genes on microplastics in facility vegetable soil. *Sci. Total Environ.* 709:136276. doi: 10.1016/j.scitotenv.2019.136276

Meng, F., Gao, G., Yang, T.-T., Chen, X., Chao, Y., Na, G., et al. (2015). Effects of fluoroquinolone antibiotics on reactor performance and microbial community structure of a membrane bioreactor. *Chem. Eng. J.* 280, 448–458. doi: 10.1016/j.cej.2015.06.025

Narciso-da-Rocha, C., Varela, A. R., Schwartz, T., Nunes, O. C., and Manaia, C. M. (2014). blaTEM and vanA as indicator genes of antibiotic resistance contamination in a hospital-urban wastewater treatment plant system. *J. Glob. Antimicrob. Resist.* 2, 309–315. doi: 10.1016/j.jgar.2014.10.001

Nemati, K., Abu Bakar, N. K., Abas, M. R., and Sobhanzadeh, E. (2011). Speciation of heavy metals by modified BCR sequential extraction procedure in different depths of sediments from Sungai Buloh, Selangor, Malaysia. *J. Hazard. Mater.* 192, 402–410. doi: 10.1016/j.jhazmat.2011.05.039

Pomba, C. F., Correia, J. D., and Canica, M. M. (2004). Genetic relatedness between human and animal polymorphic blaTEM genes strengthen zoonotic potential. *Infect. Genet. Evol.* 4:285. doi: 10.1093/jac/dkh307

Qian, X., Sun, W., Gu, J., Wang, X. J., Sun, J. J., Yin, Y. N., et al. (2016). Variable effects of oxytetracycline on antibiotic resistance gene abundance and the bacterial community during aerobic composting of cow manure. *J. Hazard. Mater.* 315, 61–69. doi: 10.1016/j.jhazmat.2016.05.002

Qiu, T., Huo, L., Guo, Y., Gao, M., Wang, G., Hu, D., et al. (2022). Metagenomic assembly reveals hosts and mobility of common antibiotic resistome in animal manure and commercial compost. *Environ. Microbiome* 17:42. doi: 10.1186/s40793-022-00437-x

Qiu, X., Zhou, G., Zhang, J., and Wang, W. (2019). Microbial community responses to biochar addition when a green waste and manure mix are composted: a molecular ecological network analysis. *Bioresour. Technol.* 273, 666–671. doi: 10.1016/j.biortech.2018.12.001

Song, J., Rensing, C., Holm, P. E., Virta, M., and Brandt, K. K. (2017). Comparison of metals and tetracycline as selective agents for development of tetracycline resistant bacterial communities in agricultural soil. *Environ. Sci. Technol.* 51, 3040–3047. doi: 10.1021/acs.est.6b05342

Sunagawa, S., Coelho, L. P., Chaffron, S., Kultima, J. R., Labadie, K., Salazar, G., et al. (2015). Structure and function of the global ocean microbiome. *Science* 348:1261359. doi: 10.1126/science.1261359

Tang, Z., Xi, B., Huang, C., Tan, W., Li, W., Zhao, X., et al. (2020). Mobile genetic elements in potential host microorganisms are the key hindrance for the removal of antibiotic resistance genes in industrial-scale composting with municipal solid waste. *Bioresour. Technol.* 301:122723. doi: 10.1016/j.biortech.2019.122723

Vos, M., Sibleyras, L., Lo, L. K., Hesse, E., Gaze, W. H., and Klümper, U. (2019). Zinc can counteract selection for ciprofloxacin resistance. *FEMS Microbiol. Lett.* 367:fnaa038. doi: 10.1093/femsle/fnaa038

Wang, R. Z., Huang, D. L., Liu, Y. G., Zhang, C., Lai, C., Wang, X., et al. (2020). Synergistic removal of copper and tetracycline from aqueous solution by steam-activated bamboo-derived biochar. *J. Hazard. Mater.* 384:121470. doi: 10.1016/j.jhazmat.2019.121470

Wang, S., Zeng, D., Jin, B., Su, Y., and Zhang, Y. (2023). Deciphering the role of polyethylene microplastics on antibiotic resistance genes and mobile genetic elements fate in sludge thermophilic anaerobic digestion process. *Chem. Eng. J.* 452. doi: 10.1016/j.cej.2022.139520

Wang, L., Zheng, J., and Huang, X. (2021). Co-composting materials can further affect the attenuation of antibiotic resistome in soil application. *Waste Manag.* 135, 329–337. doi: 10.1016/j.wasman.2021.09.016

Yang, Y., Liu, G., Ye, C., and Liu, W. (2019). Bacterial community and climate change implication affected the diversity and abundance of antibiotic resistance genes in wetlands on the Qinghai-Tibetan plateau. *J. Hazard. Mater.* 361, 283–293. doi: 10.1016/j.jhazmat.2018.09.002

Yao, L., Li, Y., Li, Z., Shen, D., Feng, H., Zhou, H., et al. (2020). Prevalence of fluoroquinolone, macrolide and sulfonamide-related resistance genes in landfills from East China, mainly driven by MGEs. *Ecotoxicol. Environ. Saf.* 190:110131. doi: 10.1016/j.ecoenv.2019.110131

Yao, N., Li, C., Yu, J., Xu, Q., Wei, S., Tian, Z., et al. (2020). Insight into adsorption of combined antibiotic-heavy metal contaminants on graphene oxide in water. *Sep. Purif. Technol.* 236:116278. doi: 10.1016/j.seppur.2019.116278

Yin, Y., Gu, J., Wang, X., Song, W., Zhang, K., Sun, W., et al. (2017). Effects of copper addition on copper resistance, antibiotic resistance genes, and intl1 during swine manure composting. *Front. Microbiol.* 8:344. doi: 10.3389/fmicb.2017.00344

Youngquist, C. P., Mitchell, S. M., and Cogger, C. G. (2016). Fate of antibiotics and antibiotic resistance during digestion and composting: a review. *J. Environ. Qual.* 45, 537–545. doi: 10.2134/jeq2015.05.0256

Zhang, R., Gu, J., Wang, X., Li, Y., Liu, J., Lu, C., et al. (2019). Response of antibiotic resistance genes abundance by graphene oxide during the anaerobic digestion of swine manure with copper pollution. *Sci. Total Environ.* 654, 292–299. doi: 10.1016/j.scitotenv.2018.11.094

Zhang, R., Gu, J., Wang, X., Qian, X., Duan, M., Sun, W., et al. (2017a). Relationships between sulfachloropyridazine sodium, zinc, and sulfonamide resistance genes during the anaerobic digestion of swine manure. *Bioresour. Technol.* 225, 343–348. doi: 10.1016/j.biortech.2016.10.057

Zhang, M., He, L. Y., Liu, Y. S., Zhao, J. L., Zhang, J. N., Chen, J., et al. (2020). Variation of antibiotic resistome during commercial livestock manure composting. *Environ. Int.* 136:105458. doi: 10.1016/j.envint.2020.105458

Zhang, J., Lu, T., Chai, Y., Sui, Q., Shen, P., and Wei, Y. (2019). Which animal type contributes the most to the emission of antibiotic resistance genes in large-scale swine farms in China? *Sci. Total Environ.* 658, 152–159. doi: 10.1016/j.scitotenv.2018.12.175

Zhang, R., Wang, X., Gu, J., and Zhang, Y. (2017b). Influence of zinc on biogas production and antibiotic resistance gene profiles during anaerobic digestion of swine manure. *Bioresour. Technol.* 244, 63–70. doi: 10.1016/j.biortech.2017.07.032

Zhao, Y., Cocerva, T., Cox, S., Tardif, S., Su, J., Zhu, Y., et al. (2019). Evidence for co-selection of antibiotic resistance genes and mobile genetic elements in metal polluted urban soils. *Sci. Total Environ.* 656, 512–520. doi: 10.1016/j.scitotenv.2018.11.372

Zhao, R., Feng, J., Liu, J., Fu, W., Li, X., and Li, B. (2019). Deciphering of microbial community and antibiotic resistance genes in activated sludge reactors under high selective pressure of different antibiotics. *Water Res.* 151, 388–402. doi: 10.1016/j.watres.2018.12.034

Zhao, Z., Wang, J., Han, Y., Chen, J., Liu, G., Lu, H., et al. (2017). Nutrients, heavy metals and microbial communities co-driven distribution of antibiotic resistance genes in adjacent environment of mariculture. *Environ. Pollut.* 220, 909–918. doi: 10.1016/j.envpol.2016.10.075

Zhou, B., Wang, C., Zhao, Q., Wang, Y., Huo, M., Wang, J., et al. (2016). Prevalence and dissemination of antibiotic resistance genes and coselection of heavy metals in Chinese dairy farms. *J. Hazard. Mater.* 320, 10–17. doi: 10.1016/j.jhazmat.2016.08.007

Zhu, Y., Wang, Y., Jiang, X., Zhou, S., Wu, M., Pan, M., et al. (2017b). Microbial community compositional analysis for membrane bioreactor treating antibiotics containing wastewater. *Chem. Eng. J.* 325, 300–309. doi: 10.1016/j.cej.2017.05.073

Zhu, Y., Zhao, Y., Li, B., Huang, C., Zhang, S., Yu, S., et al. (2017a). Continental-scale pollution of estuaries with antibiotic resistance genes. *Nat. Microbiol.* 2:16270. doi: 10.1038/nmicrobiol.2016.270

Zou, Y., Xiao, Y., Wang, H., Fang, T., and Dong, P. (2020). New insight into fates of sulfonamide and tetracycline resistance genes and resistant bacteria during anaerobic digestion of manure at thermophilic and mesophilic temperatures. *J. Hazard. Mater.* 384:121433. doi: 10.1016/j.jhazmat.2019.121433

frontiers | Frontiers in Microbiology

TYPE Mini Review
PUBLISHED 06 January 2023
DOI 10.3389/fmicb.2022.1083974



OPEN ACCESS

EDITED BY
Ikuro Kasuga,
The University of Tokyo, Japan

REVIEWED BY
Veerachandra Kranti Yemmireddy,
The University of Texas Rio Grande Valley,
United States

*CORRESPONDENCE
Heng Zheng
✉ 635881104@qq.com
Yangyang Wang
✉ wangyangyang0317@163.com
Jun Deng
✉ 46569624@qq.com

SPECIALTY SECTION
This article was submitted to Microbiotechnology, a section of the journal Frontiers in Microbiology

RECEIVED 29 October 2022
ACCEPTED 14 December 2022
PUBLISHED 06 January 2023

CITATION
Tang J, Zheng H, Cai J, Liu J, Wang Y and Deng J (2023) Research progress of electrochemical oxidation and self-action of electric field for medical wastewater treatment.
*Front. Microbiol.* 13:1083974.
doi: 10.3389/fmicb.2022.1083974



# Research progress of electrochemical oxidation and self-action of electric field for medical wastewater treatment

Jun Tang[1], Heng Zheng[1,2]*, Jinzhong Cai[3], Jiang Liu[2], Yangyang Wang[1,2]* and Jun Deng[4,5]*

[1]Department of Neurothoracic Surgery, The Third People's Hospital of Hubei Province Yangluo Campus, Jianghan University, Wuhan, China, [2]College of Resources and Environmental Engineering, Wuhan University of Technology, Wuhan, China, [3]Department of Interventional Radiology, Shenzhen People's Hospital (The First Affiliated Hospital, Southern University of Science and Technology), Shenzhen, China, [4]College of Chemistry, Chemical Engineering and Life Sciences, Wuhan University of Technology, Wuhan, China, [5]Department of Emergency, The Third People's Hospital of Hubei Province, Jianghan University, Wuhan, China

A large number of pathogenic microorganisms exist in medical wastewater, which could invade the human body through the water and cause harm to human health. With the global pandemic coronavirus (COVID-19), public health safety become particularly important, and medical wastewater treatment is an important part of it. In particular, electrochemical disinfection technology has been widely studied in medical wastewater treatment due to its greenness, high efficiency, convenient operation, and other advantages. In this paper, the development status of electrochemical disinfection technology in the treatment of medical wastewater is reviewed, and an electrochemical three-stage disinfection system is proposed for the treatment of medical wastewater. Moreover, prospects for the electrochemical treatment of medical wastewater will be presented. It is hoped that this review could provide insight and guidance for the research and application of electrochemical disinfection technology to treat medical wastewater.

KEYWORDS

**medical wastewater, disinfection, electrochemical oxidation, electrolytic chlorination, self-action of electric field**

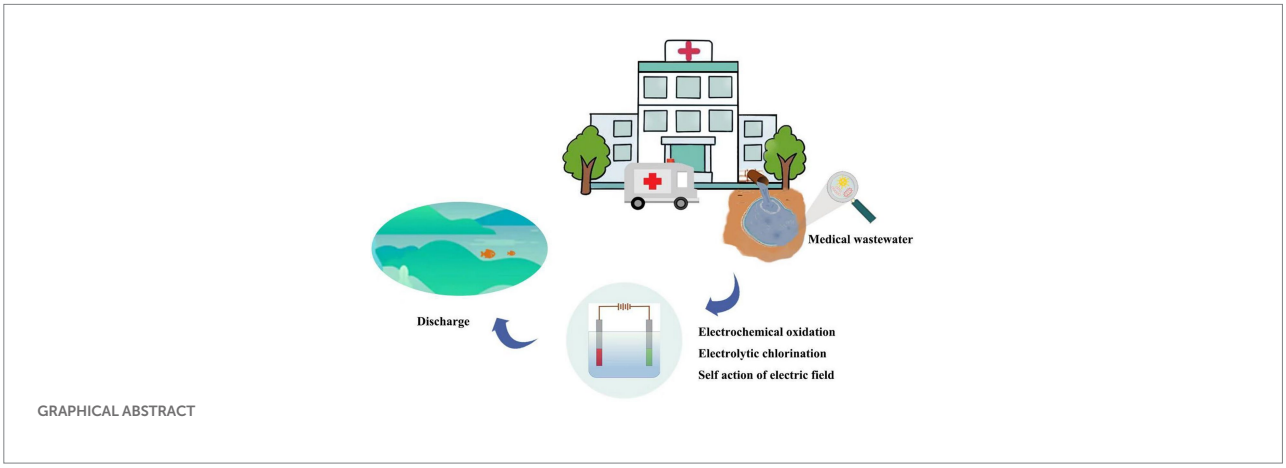


GRAPHICAL ABSTRACT

## 1. Introduction

Medical wastewater treatment is an important part of epidemic prevention and control and urban management, and also an important link between ecological environment protection and public health defense. Medical wastewater, whose source and composition are very complex, contains a large number of pathogenic microorganisms, including bacteria, viruses, insect eggs, etc. With the large-scale outbreak and mutation of COVID-19, the safe treatment of medical wastewater is critical to social security and human health. In addition, a large number of antibiotic-resistant bacteria have been detected in medical wastewater due to the misuse of antibiotics (Yu et al., 2021), such as carbapenem-resistant Enterobacteriaceae (Cahill et al., 2019). The direct discharge of medical wastewater will not only cause water and soil pollution, but also cause various diseases that threaten human health (Bibby et al., 2021). Therefore, it is necessary to thoroughly disinfect medical wastewater to prevent the spread of pathogenic microorganisms, thereby protecting public health and ecological environment safety.

At present, traditional disinfection methods are mainly used in medical wastewater treatment, including ultraviolet disinfection, chloride disinfection, and hydrogen peroxide disinfection (Zhang et al., 2020). Among them, ultraviolet disinfection is ineffective in removing drug-resistant bacteria, and cannot continuously disinfect (Islam et al., 2017). The chlorination method (hypochlorite, liquid chlorine, and chlorine dioxide) has the disadvantages of causing secondary pollution easily and being difficult to store and transport (Wang et al., 2020). Due to the unstable nature of peroxides, it is also not convenient for practical medical wastewater treatment. Notably, drug-resistant microorganisms and viruses in medical wastewater cannot be completely eliminated by traditional disinfection techniques (Majumder et al., 2020). Therefore, it is of great significance to explore green and efficient disinfection methods for medical wastewater.

This review focuses on the application of electrochemical disinfection technology in the field of medical wastewater treatment, including electrochemical oxidation, electrolytic chlorination, and the effect of the electric field. The advantages of electrochemical disinfection technology as wastewater treatment are highlighted, and its sterilization mechanism is discussed, which provides useful insights for the development of electrochemical disinfection technology-based treatment of medical wastewater. Furthermore, an electrochemical three-stage disinfection system is proposed for medical wastewater treatment. In the end, we also look forward to the challenges and future progress of electrochemical technology in medical wastewater treatment.

## 2. Electrochemical oxidation

The mechanism of electrochemical oxidation disinfection is to oxidize the microorganisms through the active groups generated by the redox reaction on the surface of the electrode (Giannakis et al., 2021; Hand and Cusick, 2021). Usually, reactive groups are generated by the electrolysis of water and dissolved oxygen in water, such as hydroxyl radicals, ozone, negative oxygen ions, etc. Due to the existence of sulfate ions, chloride ions, and phosphates, corresponding active groups are also generated, including sulfate radicals, chlorine radicals, and phosphate radicals (Giannakis et al., 2021). Various components in microbial cells are oxidized by strong oxidative active groups, which destroy the permeability of the cell membranes, resulting in irreversible changes, and the death of microorganisms (Wang et al., 2019). As reported, hydroxyl radicals generated during anodization are one of the main substances responsible for the inactivation of *Escherichia coli* in a chlorine-free environment (Jeong et al., 2006).

The performance of electrochemical oxidation treatment of wastewater is closely related to electrode materials, current density, hydraulic conditions, and dissolved oxygen (Hand and Cusick, 2021; Zhang et al., 2021). The effect of disinfection is significantly improved when noble metal oxides (such as platinum, ruthenium, iridium, etc.) are used as anode materials. This might be due to the catalytic effect of noble metal oxides on active

oxygen and active chlorine, which greatly improves the disinfection capability. It has been reported that titanium electrodes coated with metal oxides are currently mature and stable anode materials (Rathinavelu et al., 2022). When Ti/Sb-$SnO_2$/$PbO_2$ is used as an anode and the applied current density is 30 mA·$cm^{-2}$, wastewater disinfection can be achieved within 12 min, and the energy consumption is only 4.978 kwh $m^{-3}$. The sterilization rate increased with the hydraulic holding time increase and remained stable when the current density was constant. In addition, the ratio of electrode area to flow rate is the ratio of anode working area to wastewater volume, and the appropriate ratio is very important for sterilization. In particular, the increase of dissolved oxygen can increase the concentration of reactive oxygen species in wastewater, thereby promoting to kill pathogenic microorganisms (Rathinavelu et al., 2022).

Importantly, electrochemical oxidation technology could achieve complete disinfection of wastewater without adding any chemicals that could alter the physicochemical properties of wastewater. In addition, electrochemical oxidation technology is not a simple process, which is affected by many factors. For example, chloride ions in solution enhance the destruction of bacteria and viruses by promoting the chain reaction of free radicals (Herraiz-Carboné et al., 2020c). Boron-doped diamond electrodes produce reactive oxygen species at a low voltage of 4–10 V, which can completely kill Enterobacteriaceae and pathogens in wastewater, and significantly reduce spores (Schorr et al., 2019). The pilot test results of the boron-doped diamond electrode also showed a good disinfection effect. In general, the traditional disinfection process based on chlorination treatment is expected to be replaced by electrochemical oxidation technology.

In addition, different anode materials lead to differences in sterilization mechanisms during electrochemical oxidation. The boron diamond (BDD) anode promotes the generation of hydroxyl radicals, thereby improving the efficiency of sterilization (Srivastava et al., 2021). Dimensional Stable Anodes enhance the bactericidal effect by increasing the free chlorine generation rate (Feng et al., 2018). *Rhizopus*, *Pseudomonas*, and *Agrobacteria* were effectively killed using mixed metal oxide anodes, which is attributed to the rapid formation of chlorine/hypochlorite (Särkkä et al., 2008). The research shows that the porous $SnO_2$ sb reaction membrane electrode (RME) performs very well in the disinfection of wastewater, generates a large number of hydroxyl radicals under the applied voltage of 3.5 V, and realizes 100% removal of *E. coli* and phage MS2, which has practical application potential (Yang et al., 2022). However, in practical application, the concentration of suspended solids in wastewater is high, which is easy to adhere to the surface of RME, thus reducing the disinfection efficiency. Therefore, it is very necessary to add a preprocessing system to remove suspended solids. In particular, the combination of electrochemical oxidation and other methods also shows a good disinfection effect, such as sequential electrocoagulation and electrooxidation treatment system (Heffron et al., 2019), UV-assisted electrochemical oxidation (Wang et al., 2021), photo-assisted electrochemical advanced oxidation process (Herraiz-Carboné et al., 2021). The mechanism diagram of electrochemical oxidation sterilization is as follows (Figure 1).

## 3. Electrolytic chlorination

Strongly oxidizing hypochlorite (HClO) could be rapidly converted from chloride ions by electrolytic chlorination technology, which is used for disinfection in wastewater treatment processes (Huang et al., 2016; Carter-Timofte et al., 2021). Due to its small molecular weight, neutrality, and strong oxidizing properties, HClO could pass through the cell wall and enter the interior of the bacteria to directly act on the thiol group of bacterial enzymes. Thus, bacterial death is caused by the destruction of the bacterial enzyme system (Neumann and Rosenheck, 1972; Pang et al., 2021). In addition, HClO destroys the virus shell, nucleic acids, proteins, and enzymes in the virus through an oxidation reaction, resulting in the death of the virus (Bastin et al., 2020; Giarratana et al., 2021). In particular, antibiotic-resistant bacteria (ARB) could also be oxidatively decomposed by electrolytic chlorination. Cotillas et al. (2018) study found that diamond anode electric disinfection can effectively remove antibiotic-resistant bacteria in synthetic urine. Organic substances in urine such as urea can react with active chlorine generated by electrolysis to increase the concentration of chloramine, to prevent the formation of harmful by-products chlorate. Hypochlorite and chloramine produced by electrolysis are the main substances for sterilization, which can be used as the pretreatment of wastewater, It can remove antibiotic-resistant bacteria without producing harmful by-products (Herraiz-Carboné et al., 2020b). In addition, the disinfection efficiency could be effectively improved by the combination of electrolysis and ultraviolet disinfection process. As reported, ARB can be completely removed in all current densities and tested anode materials, electrochemical oxidation with BDD and Mixed Metal Oxides anodes at 50 A·$m^{-2}$ can completely remove ARB from urine (Herraiz-Carboné et al., 2020a). Compared with commercial sodium hypochlorite, liquid chlorine, and chlorine

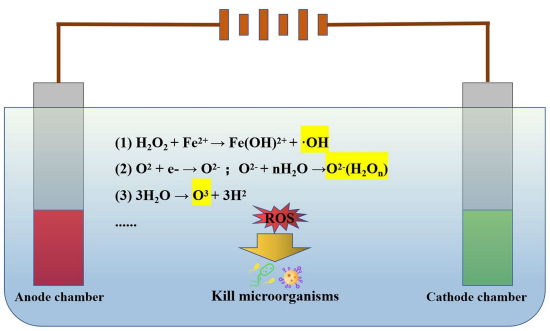


FIGURE 1
Electrochemical oxidation disinfection mechanism. When electrolyzing water, the redox reaction on the electrode surface can produce hydroxyl radicals, ozone, negative oxygen ions, etc., which can inactivate microorganisms in water by destroying their cell membranes.

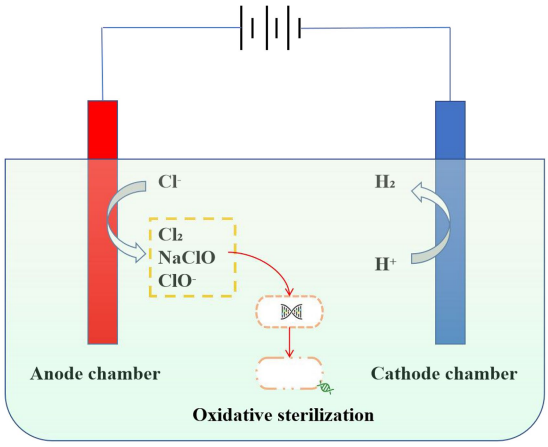


FIGURE.2
Mechanism diagram of electrolytic chlorination disinfection. Hypochlorite (HClO), which can be rapidly converted from chloride ions by electrolytic chlorination techniques, can pass through cell walls into the interior of bacteria and cause microbial death through peroxidation reactions.

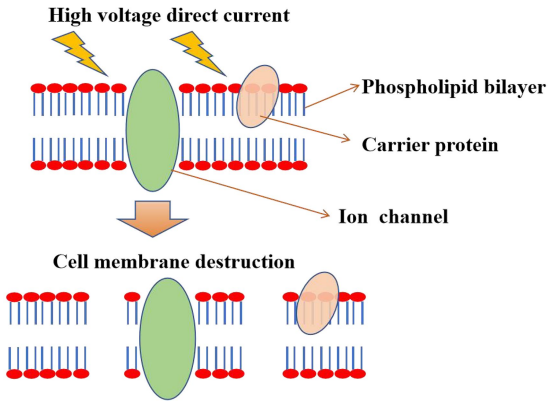


FIGURE 3
Electroporation mechanism. The electric field action causes destabilization of phospholipid bilayers and proteins, causing cell membrane perforation or rupture and cytoplasmic release, which results in microbial death.

dioxide disinfection, electrolytic chlorination has the advantages of safe raw materials, a high degree of automation, and low operating costs (Yan et al., 2021). At present, electrolytic chlorination technology is widely used in wastewater treatment, but there are also some problems, such as high one-time investment and high power consumption (Figure 2).

## 4. Self-action of electric field

The death of microorganisms by electric field self-action (Pulsed Electric Fields, PEF) relies on the breakdown of the cell membrane or electroporation caused by the direct action of the electric field (Elserougi et al., 2016). The thickness of the cell membrane is mechanically compressed under the action of the electric field, disintegrating the cell membrane and the release of the cytoplasm. In addition, cells swell and rupture after the free entry of small molecules into cells, which might be caused by the destabilization of phospholipid bilayers and proteins due to the effect of electric fields (Islam et al., 2017). Under the applied electric field, the radius of the water pores in the cell membrane increased with the pulse duration (Neumann and Rosenheck, 1972). If the radius of induced pores reaches a critical value, the process is irreversible (Weaver and Chizmadzhev, 1996). The cell gradually loses its internal components through this irreversible pore, resulting in cell death (Schoenbach et al., 2000; Heinz et al., 2001). Furthermore, nanowire-assisted electroporation disinfection is an alternative to traditional sterilization methods. Electroporation disinfection cell using three-dimensional copper foam electrodes modified by copper oxide nanowires exhibits the advantages of low operating voltage (1 V), short contact time (7 s), and no chlorine production (Huo et al., 2016). Using triboelectric nanogenerators to drive the copper oxide nanowire electrode array, through the point effect to amplify the electric field, can cause irreversible electroporation to microorganisms. When it is applied to urine polluted by *E. coli*, *Staphylococcus aureus*, *Klebsiella pneumonia*, and *Pseudomonas aeruginosa*, it has high sterilization efficiency (more than 99.9999%), no living chlorine, and simultaneous degradation of organic pollutants, which has great application potential (Zhang et al., 2022).

Usually, most hospital wastewater exhibits great genotoxicity before treatment. PEF treatment shows good disinfection effects without side effects and genotoxicity, indicating that PEF is a sustainable method of sterilization (Gusbeth et al., 2009). In particular, PEF could be used as an independent treatment process at critical control points in wastewater treatment. For example, on-site treatment of wastewater generated from hospitals or other healthcare facilities, or in tandem with other conventional methods to reduce the total bacterial load and clinically relevant ARB concentrations. PEF technology could not only kill *Fusarium oxysporum*, but also kill spores of *Bacillus subtilis* in wastewater (Siemer et al., 2014; Zhong et al., 2019). In particular, PEF is also very effective in inactivating suspended microorganisms in wine, beer, and yellow rice wine (Yang et al., 2016). Currently, high energy consumption is a major obstacle for PEF technology, which can be solved by reducing electrode spacing and applying locally enhanced electric fields (Zhou et al., 2021). The mechanism diagram of sterilization by the electric field itself is shown in Figure 3.

## 5. Expectation

In summary, as a new disinfection technology, electrochemical disinfection plays an important role in medical wastewater treatment and on-site epidemic prevention and control. Electrochemical oxidation sterilization has the advantage of high efficiency, but its electrode material is expensive, and a pretreatment system needs to be added to prevent the suspended solids in wastewater from adhering to the electrode surface, resulting in the

decline of sterilization efficiency. Electrolytic chlorination has a good effect on removing antibiotic-resistant bacteria, but it also has the problems of a high one-time investment and high energy consumption. The self-action sterilization efficiency of the electric field is high, which can kill bacterial spores and degrade organic pollutants. It can be used as an independent process for on-site medical wastewater treatment (such as shelter hospitals), but it has the problem of high power consumption. Compared with electrolytic chlorination and the electric field itself, electrochemical oxidation technology shows obvious advantages in the sterilization process of medical wastewater, such as low energy consumption, simple structure, and convenient combination with other treatment methods. In addition, the actual medical wastewater is very complex, and the damage and impact of medical wastewater on electrode materials and equipment should also be paid attention to.

To better realize electrochemical disinfection of medical wastewater, it is necessary to improve electrode materials, reactors and reduce power consumption, and integrate existing technologies and processes. For example, the three-stage treatment system of "electric field self-action + electrochemical oxidation + electrolytic chlorination" should be explored. The electric field self-action kills most pathogenic microorganisms through electroporation, and the ones which are not killed will be killed by electrochemical oxidation. Finally, a few pathogenic microorganisms that are not treated by electrochemical oxidation are removed by electrolytic chlorine. The traditional treatment method is expected to be replaced by the above three electrochemical technologies in the disinfection of medical wastewater, to improve the health management level of the city. Overall, electrochemical technology has great potential in the disinfection and treatment of medical wastewater.

## Author contributions

JD, JT, HZ, and YW conceived and wrote the first draft of the manuscript. JD, JT, HZ, YW, JC, and JL revised each part of the manuscript in detail. All authors contributed to the article and approved the submitted version.

## Funding

This study was supported by the Hubei Provincial Administration of Traditional Chinese Medicine Research Project of Traditional Chinese Medicine.

## Conflict of interest

The authors declare that the research was conducted in the absence of any commercial or financial relationships that could be construed as a potential conflict of interest.

## Publisher's note



## References

Bastin, G., Loison, P., Vernex-Loset, L., Dupire, F., Challant, J., Majou, D., et al. (2020). Structural organizations of Qβ and MS2 Phages affect capsid protein modifications by oxidants Hypochlorous acid and Peroxynitrite. *Front. Microbiol.* 11:1157. doi: 10.3389/fmicb.2020.01157

Bibby, K., Bivins, A., Wu, Z., and North, D. (2021). Making waves: plausible lead time for wastewater based epidemiology as an early warning system for COVID-19. *Water Res.* 202:117438. doi: 10.1016/j.watres.2021.117438

Cahill, N., O'Connor, L., Mahon, B., Varley, Á., McGrath, E., Ryan, P., et al. (2019). Hospital effluent: a reservoir for carbapenemase-producing Enterobacterales? *Sci. Total Environ.* 672, 618–624. doi: 10.1016/j.scitotenv.2019.03.428

Carter-Timofte, M. E., Arulanandam, R., Kurmasheva, N., Fu, K., Laroche, G., Taha, Z., et al. (2021). Antiviral potential of the antimicrobial drug Atovaquone against SARS-CoV-2 and emerging variants of concern. *ACS Infect Dis.* 7, 3034–3051. doi: 10.1021/acsinfecdis.1c00278

Cotillas, S., Lacasa, E., Saez, C., Canizares, P., and Rodrigo, M. A. (2018). Disinfection of urine by conductive-diamond electrochemical oxidation. *Appl. Catal. B Environ.* 229, 63–70. doi: 10.1016/j.apcatb.2018.02.013

Elserougi, A., Massoud, A., and Ahmed, S. (2016). Conceptual study of a bipolar modular high voltage pulse generator with sequential charging. *IEEE Trans. Dielectr. Electr. Insul.* 23, 3450–3457. doi: 10.1109/TDEI.2016.005803

Feng, W., Ana, D., Wang, Z., Zhang, X., Thomas, G., and Mccarthy, D. T. (2018). Electrochemical oxidation disinfects urban stormwater: major disinfection mechanisms and longevity tests. *Sci. Total Environ.* 646, 1440–1447. doi: 10.1016/j.scitotenv.2018.07.307

Giannakis, S., Lin, K.-Y. A., and Ghanbari, F. (2021). A review of the recent advances on the treatment of industrial wastewaters by Sulfate radical-based advanced oxidation processes (SR-AOPs). *Chem. Eng. J.* 406:127083. doi: 10.1016/j.cej.2020.127083

Giarratana, N., Rajan, B., Kamala, K., Mendenhall, M., and Reiner, G. (2021). A sprayable acid-oxidizing solution containing hypochlorous acid (AOS2020) efficiently and safely inactivates SARS-Cov-2: a new potential solution for upper respiratory tract hygiene. *Eur. Arch. Otorhinolaryngol.* 278, 3099–3103. doi: 10.1007/s00405-021-06644-5

Gusbeth, C., Frey, W., Volkmann, H., Schwartz, T., and Bluhm, H. (2009). Pulsed electric field treatment for bacteria reduction and its impact on hospital wastewater. *Chemosphere* 75, 228–233. doi: 10.1016/j.chemosphere.2008.11.066

Hand, S., and Cusick, R.D., (2021). Electrochemical disinfection in water and wastewater treatment: Identifying impacts of water quality and operating conditions on performance, *Environ. Sci. Technol.*, 55, 3470–3482. doi: 10.1021/acs.est.0c06254

Heffron, J., Ryan, D. R., and Mayer, B. K. (2019). Sequential electrocoagulation-electrooxidation for virus mitigation in drinking water. *Water Res.* 160, 435–444. doi: 10.1016/j.watres.2019.05.078

Heinz, V., Alvarez, I., Angersbach, A., and Knorr, D. (2001). Preservation of liquid foods by high intensity pulsed electric fields-basic concepts for process design. *Trends Food Sci. Technol.* 12, 103–111. doi: 10.1016/S0924-2244(01)00064-4

Herraiz-Carboné, M., Cotillas, S., Lacasa, E., Caizares, P., and Sáez, C. (2020a). Enhancement of UV disinfection of urine matrixes by electrochemical oxidation. *J. Hazard. Mater.* 410:124548. doi: 10.1016/j.jhazmat.2020.124548

Herraiz-Carboné, M., Cotillas, S., Lacasa, E., Cañizares, P., Rodrigo, M. A., and Sáez, C. (2020b). Removal of antibiotic resistant bacteria by electrolysis with diamond anodes: a pretreatment or a tertiary treatment? *J. Water Process Eng.* 38:101557. doi: 10.1016/j.jwpe.2020.101557

Herraiz-Carboné, M., Cotillas, S., Lacasa, E., Sainz de Baranda, C., Riquelme, E., Cañizares, P., et al. (2021). A review on disinfection technologies for controlling the antibiotic resistance spread. *Sci. Total Environ.* 797:149150. doi: 10.1016/j.scitotenv.2021.149150

Herraiz-Carboné, M., Lacasa, E., Cotillas, S., Vasileva, M., Cañizares, P., Rodrigo, M. A., et al. (2020c). The role of chloramines on the electrodisinfection of *Klebsiella pneumoniae* in hospital urines. *Chem. Eng. J.* 409:128253. doi: 10.1016/j.cej.2020.128253

Huang, X., Qu, Y., Cid, C. A., Finke, C., Hoffmann, M. R., Lim, K., et al. (2016). Electrochemical disinfection of toilet wastewater using wastewater electrolysis cell. *Water Res.* 92, 164–172. doi: 10.1016/j.watres.2016.01.040

Huo, Z. Y., Xie, X., Yu, T., Lu, Y., Feng, C., and Hu, H. Y. (2016). Nanowire-modified three-dimensional electrode enabling low-voltage electroporation for water disinfection. *Environ. Sci. Technol.* 50, 7641–7649. doi: 10.1021/acs.est.6b01050

Islam, M. S., Beverung, S., and Steward R Jr, (2017). A review on macroscale and microscale cell Lysis methods. *Micromachines* 8:299. doi: 10.3390/mi8100299

Jeong, J., Kim, J. Y., and Yoon, J. (2006). The role of reactive oxygen species in the electrochemical inactivation of microorganisms. *Environ. Sci. Technol.* 40, 6117–6122. doi: 10.1021/es0604313

Majumder, A., Gupta, A. K., Ghosal, P. S., and Varma, M. (2020). A review on hospital wastewater treatment: a special emphasis on occurrence and removal of pharmaceutically active compounds, resistant microorganisms, and SARS-CoV-2. *J. Environ. Chem. Eng.* 9:104812. doi: 10.1016/j.jece.2020.104812

Neumann, E., and Rosenheck, K. (1972). Permeability changes induced by electric impulses in vesicular membranes. *J. Membr. Biol.* 10, 279–290. doi: 10.1007/BF01867861

Pang, Q., Li, T., Yin, C., Ma, K., and Huo, F. (2021). Comparing the abundance of HClO in cancer/normal cells and visualizing in vivo using a mitochondria-targeted ultra-fast fluorescent probe. *Analyst* 146, 3361–3367. doi: 10.1039/D1AN00375E

Rathinavelu, S., Divyapriya, G., Joseph, A., Nambi, I. M., Muthukrishnan, A. B., and Jayaraman, G. (2022). Inactivation behavior and intracellular changes in *Escherichia coli* during electro-oxidation process using Ti/Sb–$SnO_2$ /$PbO_2$ anode: elucidation of the disinfection mechanism. *Environ. Res.* 210:112749. doi: 10.1016/j.envres.2022.112749

Särkkä, H., Vepsäläinen, M., Pulliainen, M., and Sillanpää, M. (2008). Electrochemical inactivation of paper mill bacteria with mixed metal oxide electrode. *J. Hazard. Mater.* 156, 208–213. doi: 10.1016/j.jhazmat.2007.12.011

Schoenbach, K. H., Joshi, R. P., Stark, R. H., Dobbs, F. C., and Beebe, S. J. (2000). Bacterial decontamination of liquids with pulsed electric fields. *IEEE Trans. Dielectr. Electr. Insul.* 7, 637–645. doi: 10.1109/94.879359

Schorr, B., Ghanem, H., Rosiwal, S., Geißdörfer, W., and Burkovski, A. (2019). Elimination of bacterial contaminations by treatment of water with boron-doped diamond electrodes. *World J. Microbiol. Biotechnol.* 35:48. doi: 10.1007/s11274-019-2624-y

Siemer, C., Toepfl, S., and Heinz, V. (2014). Inactivation of Bacillus subtilis spores by pulsed electric fields (PEF) in combination with thermal energy – I. Influence of process- and product parameters. *Food Control* 39, 163–171. doi: 10.1016/j.foodcont.2013.10.025

Srivastava, V., Suresh Kumar, M., Nidheesh, P. V., and Martínez-Huitle, C. A. (2021). Electro catalytic generation of reactive species at diamond electrodes and applications in microbial inactivation, current opinion. *Electrochemistry* 30:100849. doi: 10.1016/j.coelec.2021.100849

Wang, P., Deng, Y., Hao, L., Zhao, L., Zhang, X., and Deng, C. (2019). Continuous efficient removal and inactivation mechanism of *E. coli* by bismuth-doped $SnO_2$/C electrocatalytic membrane. *Environ. Sci. Poll. Res. Int.* 26, 11399–11409. doi: 10.1007/s11356-019-04576-6

Wang, J., Shen, J., Ye, D., Yan, X., Zhang, Y., Yang, W., et al. (2020). Disinfection technology of hospital wastes and wastewater: suggestions for disinfection strategy during coronavirus disease 2019 (COVID-19) pandemic in China. *Environ. Pollut.* 262:114665. doi: 10.1016/j.envpol.2020.114665

Wang, S., Yang, S., Quispe, E., Yang, H., and Hoffmann, M. R. (2021). Removal of antibiotic resistant bacteria and genes by UV-assisted electrochemical oxidation on degenerative $TiO_2$ nanotube arrays 1, 612–622.

Weaver, J. C., and Chizmadzhev, Y. A. (1996). Theory of electroporation: a review. *Bioelectrochem. Bioenerg.* 41, 135–160. doi: 10.1016/S0302-4598(96)05062-3

Yan, P., Daliri, B. M., and Oh, D. H. (2021). New clinical applications of electrolyzed water: a review. *Microorganisms* 9:136. doi: 10.3390/microorganisms9010136

Yang, N., Kang, H., Lyu, C., and Wang, J. (2016). Pulsed electric field technology in the manufacturing processes of wine, beer, and rice wine: a review. *Food Control* 61, 28–38. doi: 10.1016/j.foodcont.2015.09.022

Yang, C., Wen, L., Li, Y., and Li, X.-Y. (2022). Fabrication of $SnO_2$-Sb reactive membrane electrodes for high-efficiency electrochemical inactivation of bacteria and viruses in water. *Chem. Eng. J.* 446:137327. doi: 10.1016/j.cej.2022.137327

Yu, Z., Rabiee, H., and Guo, J. (2021). Synergistic effect of sulfidated nano zerovalent iron and persulfate on inactivating antibiotic resistant bacteria and antibiotic resistance genes. *Water Res.* 198:117141. doi: 10.1016/j.watres.2021.117141

Zhang, X., Huang, H., Zhang, W., Hu, Z., Li, X., Liu, J., et al. (2022). Self-powered triboelectric nanogenerator driven nanowires electrode array system for the urine sterilization. *Nano Energy* 96:107111. doi: 10.1016/j.nanoen.2022.107111

Zhang, G., Li, W., Chen, S., Zhou, W., and Chen, J. (2020). Problems of conventional disinfection and new sterilization methods for antibiotic resistance control. *Chemosphere* 254:126831. doi: 10.1016/j.chemosphere.2020.126831

Zhang, J., Zhou, Y., Yao, B., Yang, J., and Zhi, D. (2021). Current progress in electrochemical anodic-oxidation of pharmaceuticals: mechanisms, influencing factors, and new technique. *J. Hazard. Mater.* 418:126313. doi: 10.1016/j.jhazmat.2021.126313

Zhong, C., Guan, X., Fan, Z., Song, W., and He, S. (2019). Pulsed electric field disinfection treatment of *Fusarium oxysporum* in nutrient solution. *Water Sci. Technol. Water Supply* 19, 2116–2122. doi: 10.2166/ws.2019.090

Zhou, J., Hung, Y. C., and Xie, X. (2021). Making waves: pathogen inactivation by electric field treatment: from liquid food to drinking water. *Water Res.* 207:117817. doi: 10.1016/j.watres.2021.117817

frontiers | Frontiers in Microbiology

TYPE Original Research
PUBLISHED 17 April 2023
DOI 10.3389/fmicb.2023.1146325



OPEN ACCESS

EDITED BY
Xiaochen Chen,
Fuzhou University, China

REVIEWED BY
Dongru Qiu,
Institute of Hydrobiology (CAS), China
Yan Li,
Fujian University of Technology, China

*CORRESPONDENCE
Yuping Su
✉ ypsu@fjnu.edu.cn

SPECIALTY SECTION
This article was submitted to Microbiotechnology, a section of the journal Frontiers in Microbiology

RECEIVED 17 January 2023
ACCEPTED 27 March 2023
PUBLISHED 17 April 2023

CITATION
Zheng L, Lin H, Balaji-Prasath B, Su Y, Wang Y, Zheng Y and Yu G (2023) A novel algicidal properties of fermentation products from *Pseudomonas* sp. Ps3 strain on the toxic red tide dinoflagellate species. *Front. Microbiol.* 14:1146325. doi: 10.3389/fmicb.2023.1146325



# A novel algicidal properties of fermentation products from *Pseudomonas* sp. Ps3 strain on the toxic red tide dinoflagellate species

Luwei Zheng[1], Hong Lin[1], Barathan Balaji-Prasath[1,2,3], Yuping Su[1,2,3]*, Ying Wang[1], Yi Zheng[4] and Guanglang Yu[1]

[1]College of Environmental and Resource Science, College of Carbon Neutral Modern Industry, Fujian Normal University, Fuzhou, China, [2]Fujian Key Laboratory of Pollution Control and Resource Recycling, Fujian Normal University, Fuzhou, China, [3]Fujian Province Research Centre for River and Lake Health Assessment, Fujian Normal University, Fuzhou, China, [4]Fujian Key Laboratory of Special Marine Bio-resources Sustainable Utilization, Fujian Normal University, Fuzhou, China

The viability of both China's offshore fishing operations and the global marine fishing industry is threatened by the occurrence of red tides caused by *Gymnodinium catenatum* and *Karenia mikimotoi*. Effective control of these dinoflagellate-mediated red tides has become a pressing issue that requires immediate attention. In this study, High-efficiency marine alginolytic bacteria were isolated and underwent molecular biological identification to confirm their algicidal properties. Based on a combination of morphological, physiological, biochemical, and sequencing results, Strain Ps3 was identified as belonging to the species *Pseudomonas* sp. We examine the effects of algicidal bacteria on the red tide species *G. catenatum* and *K. mikimotoi* within an indoor experimental setting. Then gas chromatography– mass spectrometry (GC–MS) was used to analyze the structure of the algolytic active substances. This investigation demonstrated that with exposure to the algae-lysis experiment, the Ps3 strain has the best algae-lysis effect, with *G. catenatum* and *K. mikimotoi* reaching 83.0 and 78.3%. Our results from the sterile fermentation broth experiment showed that the inhibitory effect on the two red tide algae was positively correlated with the concentration of the treatment. At a treatment concentration of 2.0% (v/v), the 48 h lysis rates of *G. catenatum* and *K. mikimotoi* due to exposure to the Ps3 bacterial fermentation broth were 95.2 and 86.7%, respectively. The results of this study suggest that the algaecide may be a rapid and effective method to control dinoflagellate blooms, as evidenced by the observed changes in cellular morphology in all cases. In the ethyl acetate phase of Ps3 fermentation broth, the cyclic (leucine-leucine) dipeptide was the most abundant. The findings of this study contribute to our understanding of red tide prevention and control and provide a theoretical foundation for further research in this field.

KEYWORDS

***Pseudomonas*, dinoflagellate, algicidal bacteria, active substances, red tide**

# 1. Introduction

An expanding body of research has been dedicated to identifying strategies for preventing, managing, and mitigating harmful algal blooms (HABs), which are increasingly spreading and intensifying across different geographical locations (Anderson and Menden-Deuer, 2017; Shi et al., 2018; Baohong et al., 2021; Balaji-Prasath et al., 2022b). A red tide, which is alternatively referred to as a bloom, is a natural ecological phenomenon that occurs when high-density algae cells in seawater cause discoloration. In coastal farming regions, the eruption of red tides leads to the secretion of sticky substances by plankton blooms that attach to the gill tissues of fish, resulting in the death of numerous farmed fish and significant losses to fisheries (Pokrzywinski et al., 2017; Li et al., 2018). In the last decade, scientists have dedicated considerable efforts towards developing various techniques aimed at mitigating the frequency and negative impacts of red tides. These methods entail controlling the growth of harmful species and reducing the concentration of toxic substances (Visciano et al., 2016; Petropoulos et al., 2019; Ko et al., 2022). The factors that contribute to the development of red tide are multifaceted and varied. However, bacteria play a crucial role in the dissipation phase of red tide (Sun et al., 2016; Zohdi and Abbaspour, 2019). It is widely accepted that the bacterial community undergoes quantitative and qualitative changes during an algal bloom and may potentially exert a positive or negative influence on the regulation of algal growth. It is important to highlight that certain organisms, notably algicidal bacteria, have the ability to break down algae by either directly attacking their cells or indirectly through the secretion of compounds such as proteins, polypeptides, biosurfactants, amino acids, and antibiotics with algicidal properties (Zhuang et al., 2018).

The mitigation strategies for HAB species, including microbes such as bacteria, fungi, viruses, and grazers such as copepods, protozoa, and macrophytes have already been investigated and tested by many studies, which are crucial to understand the dynamics and succession of HAB species (Zheng et al., 2013). Several bacterial strains that can inhibit or kill HAB species have been isolated in studies focusing on algal-bacterial interactions. Currently, there is a lack of scientific understanding regarding the mechanism by which these compounds effectively eliminate their target algal species, specifically those associated with red tide, and the ecological function of algicidal bacteria (Meyer et al., 2017). Furthermore, the majority of algicidal bacteria exhibit efficient, algae-specific, and environmentally sound characteristics. These microorganisms employ two mechanisms to target algal cells, which include direct cell-to-cell contact (Li et al., 2016; Van Tussenbroek et al., 2017). Alternatively, these microorganisms may also employ the use of algicidal compounds, such as antibiotics, enzymes from actinomycete, and fungi, to indirectly mediate the interaction between microalgae and other microorganisms (Hussain et al., 2013; Feng et al., 2014; Balaji Prasath et al., 2021). Algicidal bacteria have complex and diverse active substances and show good algicidal activity in controlling harmful red tides. For example, the active substance of *Pseudomonas* to control *Karenia brevis* is saponin, and bacillamide in *Bacillus* showed 50.0% lysis rates in 6 h against *Cochlodinium polykrikoides* (McCoy and Martin, 1977; Jeong et al., 2003). Consequently, algicidal microorganisms and their associated compounds may serve as more effective and environmentally sustainable agents for managing HABs in the aftermath of marine calamities. The identification of multiple dominant species would serve as a valuable reference point for enhancing our comprehension of the incidence, prevention, and management of red tide. As a result, numerous red tide control experts have exerted considerable efforts in identifying efficacious alga-solubilizing bacteria and their potential bioactive compounds for the dissolution of algae. This study delves into the algolytic properties of *Pseudomonas* Ps3, an effective strain with algal lytic and inhibitory capabilities, to enhance its algolytic efficiency. The research provides a valuable technical reference for red tide management and highlights the potential of *Pseudomonas* Ps3 as a promising bacterial agent for controlling algal blooms.

# 2. Materials and methods

## 2.1. Species identification of *Pseudomonas* sp. Ps3

Conducting an examination of bacterial traits and features. This process entails the scrutiny of the physical attributes of bacterial colonies, in addition to utilizing both Gram staining and scanning electron microscopy methodologies to investigate their morphology and structure.

The strain was cultivated in a liquid beef paste medium until it reached the logarithmic phase. Under aseptic conditions, transfer 2.0 ml of the sample to a sterile centrifuge tube, seal it with a sealing film, refrigerate and send it to Beijing Ovison Genetics Co., Ltd. for 16S rDNA identification. The main steps include: (1) PCR amplification, followed by agarose gel electrophoresis of the amplified fragments; (2) purification of the PCR products; (3) BigDye®Terminator v3.1 sequencing reaction and purification; (4) sequencing data collection using the 3,730 xl.

The 16S rDNA sequence obtained from sequencing will be compared to the NCBI GenBank database using BLAST to select bacterial species with a similarity of 99.5% or higher, and to construct a phylogenetic tree to preliminarily confirm the bacterial genus.

## 2.2. Experimental procedure and calculation of algae dissolution rate

The harmful dinoflagellates, *G. catenatum* and *K. mikimotoi*, used in this study were obtained from the State Key Laboratory of Offshore Marine Environmental Science (Xiamen University). The cultures were maintained in a sterile L1 seawater medium at a temperature of 20°C, with a photon flux of 100 μmol photons·$m^{-2}$·$s^{-1}$ and a 14 h:10 h light: dark cycle, as previously described (Shi et al., 2013). The algicidal bacterium, Ps3, was cultured in beef extract peptone medium and amplified on a constant temperature shaker at 30 ± 1°C for 24 h. The bacteria were preserved with 50.0% glycerol at a ratio of 1:1. To prepare the algae sample for observation and counting, 500 μl of the shaken red tide algae culture solution were transferred into a 1.5 ml centrifuge tube, and Lugol's reagent was added gradually to stabilize the algae. Subsequently, 100 μl of the resulting algae solution was carefully dispensed into an algae counting frame and examined under the Jiangnan BM2000 photo microscope. The counting process was repeated three times, and the observed relative error was within 5.0%. The bacterial solution was mixed with *G. catenatum* and *K. mikimotoi*

at a volume ratio of 1.0% (v/v), and a control group was prepared using an equivalent amount of beef extract peptone medium. Samples were collected at predetermined intervals (4, 8, 12, 18, 24, 36, and 48 h), and three replicates were examined for each group to quantify the number of algal cells and the rate of algal dissolution. To ensure the validity of the results, all experimental procedures were conducted in a sterile environment to prevent bacterial contamination.

## 2.3. Determination of growth curve of algolytic bacteria

The plate colony counting method was used to count, and 1.0% of recovered Ps3 bacteria by volume were inoculated into a 100.0 ml medium and cultured in a constant temperature shaker at 30°C and 130 rpm. Samples were taken every 2 h from the same batch of the medium as control and measure the growth absorbance of the bacterial solution at OD600. At the same time, another 100 µl was taken every 4 h and diluted $10^{-6}$, $10^{-7}$, $10^{-8}$, and $10^{-9}$ layers were used for plate coating, three parallel samples. Then placed in a constant temperature incubator at 30 ± 1°C for 24 h after sealing. The bacterial population was quantified for each growth phase, and a growth curve for Ps3 was generated.

## 2.4. Experiment on the action mode of algolytic bacteria

After reaching the logarithmic phase, the Ps3 broth (SBS) was diluted to 1.0% by volume, inoculated into a fresh medium, and subsequently incubated in a constant temperature shaker for 24 h at 30°C and 130 rpm. The OD600 value of the bacterial broth was measured in real-time. After centrifugation at 10,000 rpm for 15 min, the supernatant and precipitated cells were collected separately. The supernatant was filtered three times with a disposable sterile filter tip of 0.22 µm pore size PES membrane to obtain the sterile fermentation broth of *Pseudomonas* Ps3 (S). The precipitated cells were subjected to vortex shaking with an appropriate amount of medium for 1 min, followed by centrifugation at 10,000 rpm to remove the supernatant. This washing process was repeated thrice, and the volume was adjusted to 5.0 ml with sterile water to obtain the bacterial suspension (BS). A fresh medium was used as the control. The prepared SBS, S, and BS were added at a 2.0% volume ratio to 2.0 ml of *G. catenatum* and *K. mikimotoi* during the growth period. Three parallel samples were taken and counted to determine the rate of algal lysis.

## 2.5. Experiment on influencing factors of algal dissolution in a bacterial fermentation broth

### 2.5.1. Experiment on the effect of algae dissolution by the amount of bacterial solution

Ps3 was incubated in beef paste liquid medium at 30°C and 130 rpm for 24 h to prepare the Ps3 fermentation broth. The real-time OD600 value of the bacterial broth was determined. A culture medium was used as the control, and the Ps3 bacterial fermentation broth was inoculated into the algal broth of *G. catenatum* and *K. mikimotoi* at volume ratios of 0.1, 0.5, 1.0, 2.0, and 4.0%.At predetermined intervals, samples were collected and the rate of algae lysis was determined.

### 2.5.2. Experiments on the effect of temperature on algae lysis

Given that the red tide *of G. catenatum* and *K. mikimotoi* in Fujian typically occurs between April and June, with actual water temperatures ranging between 15 and 25°C, we set up three gradient temperatures of 15, 20, and 25°C. Sterile Ps3 fermentation solution was injected separately at a volume ratio of 2.0%, with a light intensity of 3,000 lx and a light–dark ratio of 12 h:12 h. A medium blank control was used to generate three parallel samples, which were then counted under a microscope at regular intervals to calculate the algal lysis rate.

## 2.6. Component separation of fermentation broth

The control consisted of a medium that was prepared in the same batch, and 100.0 ml of cultured bacteria Ps3 was inoculated for 48 h. The OD600 value was measured with three parallel samples, and the Ps3 fermentation broth was obtained using a 0.22 µm acetate fiber filter membrane three times. The solvent was then dried by vacuum distillation at 80°C. Next, 1.0 ml of ethyl acetate was added, and the solution was oscillated in an oscillator at 130 rpm for 10 min. The solution was repeatedly dissolved in the same way 3 times, and finally, the volume was fixed to 10.0 ml, resulting in the ethyl acetate phase solution (A). The remaining phase was dissolved in 1.0 ml water in the oscillator at 130 rpm and oscillated for 10 min, repeated three times, and kept at a constant volume of up to 10.0 ml to obtain the remaining phase (B). Both components A and B were stored in a refrigerator at −4°C for later use.

## 2.7. Experiment of algae solubilization effect of different components

To establish a control, algae of *G. catenatum* and *K. mikimotoi* were subjected to a culture medium. Additionally, ethyl acetate, ethyl acetate phase solution (A), and residual phase (B) were added to the algae at concentrations of 0.1, 0.5, 1.0, 2.0, 4.0, and 5.0% (v/v). The incubation temperature was maintained at 20 ± 1°C, while the light intensity was set at 3000 lx, and the light–dark ratio was set at 12 h:12 h. At predetermined intervals, parallel samples were collected and the number of algal cells was quantified three times at 24 h to assess the impact of algae lysis and calculate the corresponding algae lysis rate.

## 2.8. Qualitative identification of the components of the fermentation broth of the bacteria

A sample of approximately 0.5–1.0 ml of ethyl acetate extract was taken in a sampling bottle, with pure ethyl acetate being used as a control. The composition and structure of the algae-solubilizing substances, as well as the percentage content of the main substances, were analyzed using an Agilent 5977/7890B gas chromatograph-mass spectrometer from Agilent.

TABLE 1 The source and cultivation conditions of the test organisms.

| Species | Source | Temperature | Conditions |
|---|---|---|---|
| *Brachionus plicatilis* | The Institute of Oceanology, Chinese Academy of Sciences | 20 ± 1°C | Mature individual without an ovipositor |
| *Artemia salina* | | | Newly hatched fish (1–2 days old, body length < 1 mm) |
| *Oryzias latipes* | | | Healthy fish with sensitive response, normal appearance, and uniform body weight of 20 ± 2 mg at approximately 60 days old |

## 2.9. Experiment to test the toxicity of aquatic organisms

*Pseudomonas* Ps3 organism acute toxicity experiments organism select common *Brachionus plicatilis*, *Artemia salina*, and *Oryzias latipes*. These three experimental organisms belong to different phyla and trophic levels in marine ecosystems and can comprehensively represent different groups of animals in the ocean. Table 1 outlines the sources and culture requirements of these experimental species. Prior to experimentation, all organisms are subjected to a 24-h period of starvation in seawater. Use a blank group that has not been inoculated with bacterial fermentation solution as a control, with 10 organisms randomly assigned to each experimental group. Parallel samples are established for each group to ensure accuracy and consistency. The Ps3 bacterial solution ($1 \times 10^7$ CFU/ml), in the stationary phase and at a volume ratio of 2.0%, is introduced into three experimental groups. Individual mortality is assessed every 24 h, with the criterion for death being the lack of response to external stimuli. The experiment is conducted under controlled conditions of a light intensity of 2,650 ± 100 lx, a light–dark cycle ratio of 12 h:12 h, and a temperature of 20 ± 1°C.

## 2.10. Data processing

The growth rate of the microalgal culture is calculated according to Balaji Prasath et al. (2021) by the following equation

$$R = \frac{(lnC_2 - lnC_1)}{t_2 - t_1} \quad (1)$$

$C_1$ and $C_2$: represent the initial and current algal cell concentration, cell/ml; $t_1$, $t_2$: initial and current culture time, h; R: specific growth rate, $d^{-1}$.

The formula for calculating the number of bacteria is:

$$C = X \times N \times 10 \quad (2)$$

Where C represents the bacterial concentration of the sample (CFU/ml), X represents the dilution ratio of the sample, and N represents the number of bacterial colonies on the plate.

To determine the calculation of algae dissolution rate in all experimental groups, the following formula was used (Balaji-Prasath et al., 2022a).

$$R = \left(\frac{C_0 - C_1}{C_0}\right) \times 100\% \quad (3)$$

where $C_1$-experimental is the algae density of the treated culture and $C_0$-control is the algae density of the control culture, cell/ml.

# 3. Results

## 3.1. Molecular biology identification results

Ps3 bacterial colony exhibits a round morphology with a slight elevation and a diameter between 1 and 3 mm. The colony surface is smooth, moist, milky-white, and opaque (Supplementary Figure 1). The Gram staining of Ps3, illustrated in Supplementary Figure 2, revealed a blue color, indicating that it is a Gram-negative bacterium. It typically occurs in single rod-shaped or chain-like structures. Based on the Gram staining results and the physiological and biochemical properties of the bacteria, Ps3 was provisionally identified as a straight or slightly curved rod. Subsequently, scanning electron microscopy was employed to further observe the bacterial morphology, as depicted in Supplementary Figure 3. The individual Ps3 bacteria had sizes ranging from 1.5–1.7 μm in length and 1.1–1.3 μm in width, with multiple organisms adhering to each other without flagella. The presence of spores was not detected.

The 16S rDNA gene sequence of the Ps3 strain was amplified, resulting in a base pair count of 1,437 bp according to the identification results. The strain's basic information and gene sequence was uploaded on NCBI[1] with the registration number OK103600.1. The Ps3 gene sequence was compared with BLAST, and it was found that the Ps3 sequence was comparable with that of *Pseudomonas*, a genus with high similarity to Ps3 at 99.5%. In this study, appropriate gene sequences of strains were selected, and a phylogenetic tree was constructed (Supplementary Figure 4). The analysis showed that strains with higher homology to Ps3 were *Pseudomonas* sp. JC5 and *Pseudomonas protegens* CP-M2-5, which were located on the same branch. *Pseudomonas plecoglossicida* strain 2–3 was also found on a larger branch, with both of them in two separate branches.

## 3.2. Growth curve of algolytic bacteria

The growth curve of *Pseudomonas* sp. Ps3 was close to the "S" shape, and the model curve was shown in Supplementary Figure 5, which was well fitted with the actual growth condition of Ps3, with the correlation coefficient $R^2 = 0.992$ ($p < 0.001$), indicating that the curve described the growth condition of *Pseudomonas* sp. Ps3 better. When

1 http://www.ncbi.nlm.nih.gov

combining the two, it was found that *Pseudomonas* Ps3 started to enter exponential growth after 2 h, the maximum rate of bacterial growth reached 1.01 $h^{-1}$ at 5 h, and the bacterial density peaked at 10 h with a maximum number of $5.2 \times 10^8$ CFU/ml then entered the death phase. The average growth rate of Ps3 reached 0.823 $h^{-1}$.

## 3.3. Effects of different growth stages of bacteria on algal dissolution

Bacterial numbers, growth activity, and metabolites vary during different growth stages, leading to notable differences in algal dissolution effects. Consequently, this study examined changes in algae density during the co-culture of Ps3 bacterial solution with two types of algae across various growth stages. The initial densities of *G. catenatum* and *K. mikimotoi* were 210 ± 15 cells/ml. After 48 h, the density of algae in the control group still increased. Compared with the control group, the density of *G. catenatum* and *K. mikimotoi* in logarithmic, stationary and death phases decreased by 17.0, 63.0, 83.0% at 24 h, and 25.0, 85.0, and 92.0% at 48 h (Figure 1). Observations indicate that while the bacterial solution cultured for 5 h can prevent the formation of *G. catenatum*, it is incapable of dissolving the algae. Prior to the 12-h mark, the bacterial solution exhibited a discernible inhibitory effect on the growth of *G. catenatum*, while after 12 h, the solution rapidly began to dissolve the algae. In a certain period of time, the bacteria in the stationary phase or death phase grow more fully, produce more active substances, and have a better effect on algae dissolution. It can be seen from Figure 2 that, by comparing the algae lysis effects of bacteria solution on the two kinds of algae in the death phase at different time points, the algae-dissolving effects of bacteria solution on the two types of algae reached 83.0 and 78.3% at 24 h, basically reaching the algae-dissolving effect. In 48 h, the algae could reach 85.1 and 92.0%, attaining the expected effect of alga dissolution. Based on the results obtained from the three experimental groups, it can be observed that the effect of fermentation broth in controlling *G. catenatum* was slightly more pronounced compared to that of *K. mikimotoi*.

## 3.4. Lytic effects of Ps3 on various red tide species

Samples of supernatant, suspension, and primary bacteria were added to the algae solution at a rate of 2.0%, and their respective algolytic effects on both types of algae were monitored, as depicted in Figure 3. After 48 h in the control group, the density of *G. catenatum* and *K. mikimotoi* were 420 and 460 cells/ml, respectively, indicating a decrease of 4.5 and 14.5% compared to their initial densities. Notably, *G. catenatum* remained stable throughout the experiment, with its density increasing in the control group after 48 h. In contrast, the density of both algae species decreased significantly in the fermentation broth and bacteria liquid groups. Compared to the control group, the density of *G. catenatum* and *K. mikimotoi* decreased by 93.1 and 95.0%, and 90.4 and 93.5%, respectively, after 48 h. There was no significant difference between the two groups. In the 15°C group, the lysis rates at 48 h were 88.4, 97.9, 98.1, and 98.9%. It can be seen from Figure 4. That, after 48 h of inoculation and culture, the algal dissolution rate of bacterial liquid and sterile fermentation liquid reaches more than 95.0%, much higher than the algal dissolution rate of bacterial precipitation.

The observed effects strongly suggest that Ps3 fermentation liquid contains active components that inhibit algal cells, indicating that the algal dissolution mode of Ps3 is indirect. This is supported by the results shown in Figure 4, which demonstrate a significant inhibitory effect on algae by both the bacterial sediment suspension and the bacterial medium. This could be attributed to the growth of bacteria in the algal liquid and the secretion of active algal inhibitory components. As a result, the algal dissolution rates were 32.6 and 48.1% within 48 h.

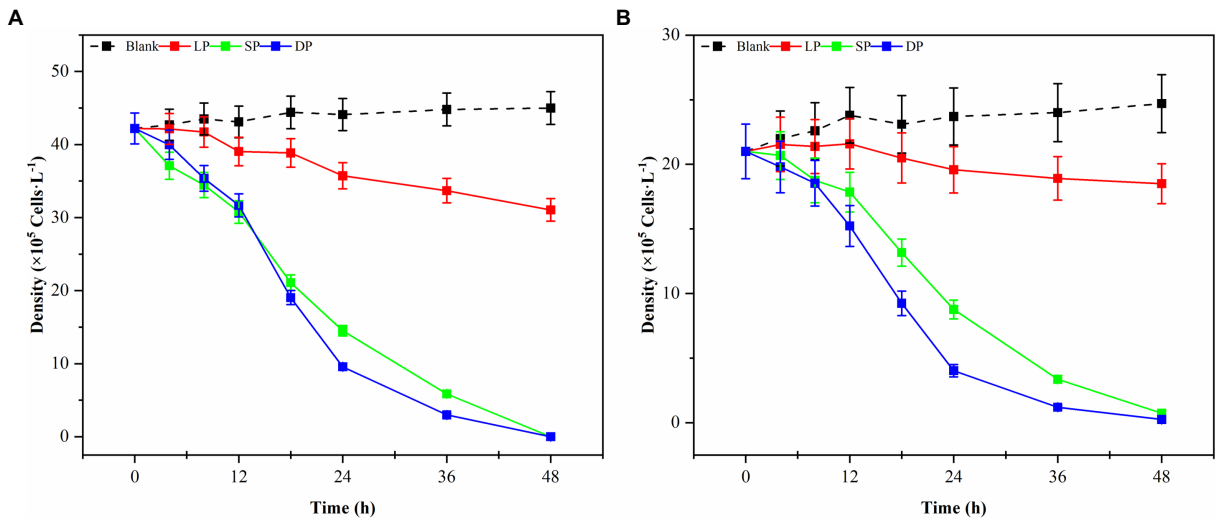


FIGURE 1
Changes in the density of *G. catenatum* **(A)** and *K. mikimotoi* **(B)** with time were observed during the different growth stages of Ps3 bacterial solution (LP-Logarithmic Phase; SP-Stationary Phase; DP-Death Phase).

10.3389/fmicb.2023.1146325

## 3.5. Effects of different dosages of fermentation broth on red tide algae

Local red tides tend to appear and dissipate rapidly, usually within 3–5 days. Therefore, this study aims to enhance the efficiency of algae dissolution and reduce the time required for it by modifying the experimental conditions. Consequently, sterile fermentation broth was supplemented with 0.1, 0.5, 1.0, 2.0, and 4.0% and inoculated into the algae solution of *G. catenatum* and *K. mikimotoi*. The bacterial medium served as the control group to evaluate the impact of the different amounts of supplemented fermentation broth on the effectiveness of algae dissolution, as illustrated in Figure 5. After 48 h, the density of *G.catenatum* and *K. mikimotoi* in the control group was 263 and 480 cells/ml, which decreased by 2.6 and 4.0%, respectively, compared to the initial experiment, and remained constant roughly throughout the investigation. When the fermentation broth was supplemented with 0.1%, there was no significant effect on the algae density. However, at 0.5%, it had a particular inhibitory impact. At 1.0%, the algae dissolution effect was direct. The 2.0 and 4.0% groups had a significant impact on dissolving both types of algae, with a more pronounced effect observed in *K. mikimotoi* than in *G.catenatum*. The 4.0% group significantly reduced the time required to dissolve the algae. The inhibition effect of Ps3 fermentation broth on *G.catenatum* and *K. mikimotoi* was positively correlated with the dosage, with a better inhibition effect observed at higher dosages.

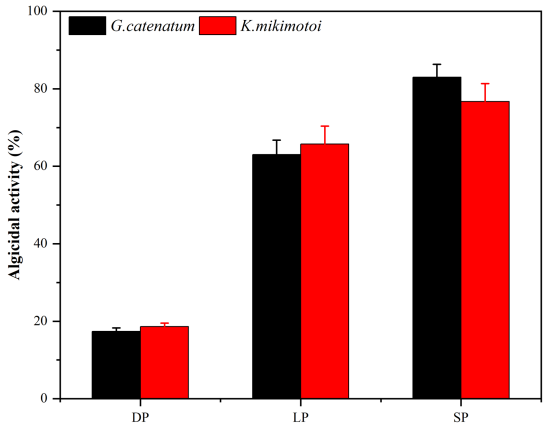


FIGURE 2
Comparison of the 24h-algicidal activity of the growth bacterial solution at different growth phases (LP-Logarithmic Phase; SP-Stationary Phase; DP-Death Phase).

## 3.6. Effect of ambient temperature on the effect of algae lysis in sterile fermentation broth

In this study, three possible temperature gradients (15°C, 20°C, and 25°C) were set up to observe Ps3 algae lysis during the red tide period in simulation. As shown in Figure 6, the algal density of the blank group generally remained unchanged at the end of the experiment for 48 h. Under the influence of 2.0% (v/v) of Ps3 fermentation solution, the density of *G. catenatum* decreased by 93.1 and 95.0% in the 20°C and 25°C groups, and the density of *K. mikimotoi* decreased by 90.4 and 93.5%. The fermentation solution had a good algae lysis effect on both kinds, and there was no significant difference between the 20°C and 25°C groups ($p < 0.05$). As for the 15°C group, the algae lysis rate was 55.3 and 45.0%, and Ps3 has a higher rate of algal lysis for *G. catenatum* than for *K. mikimotoi*.

## 3.7. Morphological changes of algal cells during algal lysis

Dinoflagellates are relatively small in size, with a diameter of 20–40 μm. As depicted in Figure 7A, *G. catenatum* exhibited good cell

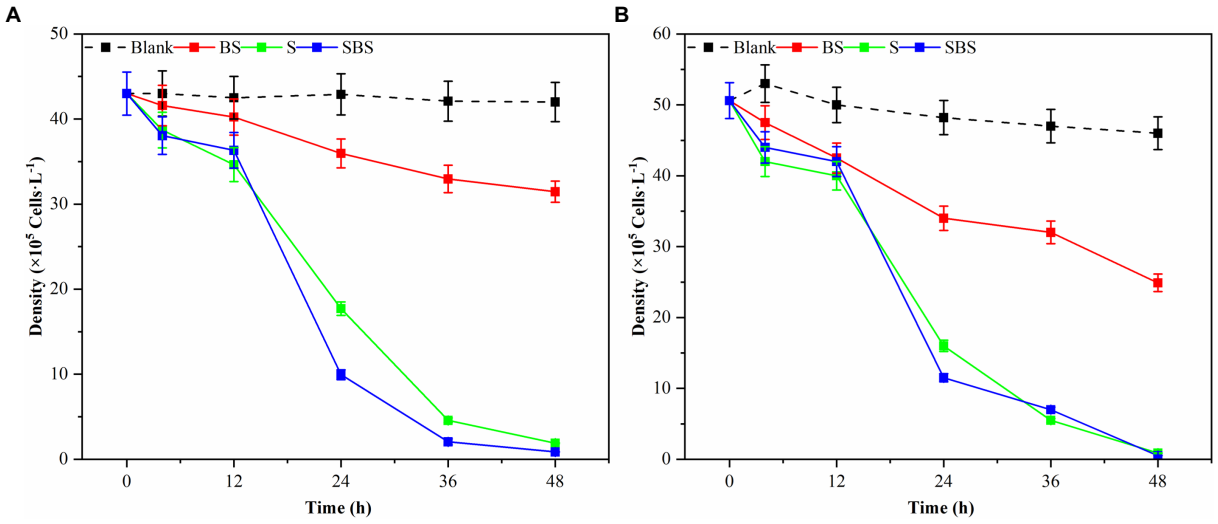


FIGURE 3
Trend of the number of different compositions of Ps3 on *G. catenatum* **(A)** and *K. mikimotoi* **(B)** [Ps3 broth (SBS); bacterial suspension (BS); *Pseudomonas* Ps3 (S)].

10.3389/fmicb.2023.1146325

growth and distinct transverse grooves during the initial stages of bacterial-algal co-culture. Figure 7B illustrates that after 12 h of co-culture, the transverse sulcus of algae cells in the field of vision became unclear, granulation appeared inside, and irregularity emerged at the edge. Following 24 h treatment, the interior of the algae cells became hollow, a small amount of cytoplasm flowed out, and numerous cells died (Figure 7C). In Figure 7D, after 18 h, many algal cells still contained pigments, but their cell membranes were damaged, cytoplasm flowed out, and the cells were considered dead due to their irregularity. Figures 7E,F depict the progressive decomposition of cells and the disappearance of chromophores.

As depicted in Figure 8, due to the small diameter of *K. mikimotoi* (3–6 μm), observing the algae cells at 400 times magnification is challenging. However, cell membrane deformation, blurred broken edges, and impaired integrity are apparent (Figure 8D). The cells then undergo deformation and become granulated (Figure 8E). The chromatophores become dark, and the cell contents diffuse, leading to the fading of chromatophores. Ultimately, the entire cell disintegrates into extremely fine particles, which become blurred and invisible (Figure 8F).

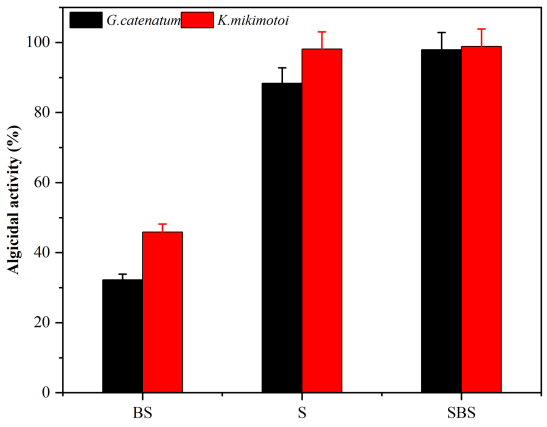


FIGURE 4
Algicidal activity of different composition to *G. catenatum* **(A)** and *K. mikimotoi* **(B)** of bacteria Ps3 at 48h [Ps3 broth (SBS); bacterial suspension (BS); *Pseudomonas* Ps3 (S)].

## 3.8. Algal dissolution of the crude separation liquid of bacterial fermentation liquid

The densities of algal cells in *G. catenatum* and *K. mikimotoi* remained similar and did not exhibit any significant changes during a 48-h period after introducing varying volume ratios of ethyl acetate. As such, the impact of ethyl acetate in the algal lysis experiment can be considered negligible. The experimental results were shown in Figure 9A after different volume ratios of ethyl acetate extracted phase solution and residual phase solution was injected into the *G. catenatum*. The addition of a 4.0% (v/v) extraction phase solution resulted in a significant increase in the algae lysis rate, reaching 98.4%. Conversely, the use of a 4.0% (v/v) residual phase solution led to a low algae lysis rate of only 24.5% after 48 h, suggesting a poor capacity for algae lysis in the residual phase.

*K. mikimotoi* (Figure 9B) exhibited higher algae lysis rates of 15.4 and 54.7% when treated with 0.1 and 0.5% (v/v) ethyl acetate extraction phase solutions, respectively, compared to the *G. catenatum*, indicating a positive effect. The use of a 4.0% (v/v) ethyl acetate extraction phase solution significantly increased the algae lysis rate to 95.9%, exceeding the rates of other groups. Importantly, unlike the *G. catenatum* group, the residual phase solution with a volume fraction of 4.0% also significantly enhanced the algae lysis rate of Karenia mikimotoi to 45.0%, probably due to some differences in the algae species as well as the mechanism of algae lysis. *Pseudomonas* sp. Ps3 is mainly present in the ethyl acetate extraction phase, but the residual material still has a certain effect on algae lysis.

It can be seen that most of the active substances in the fermentation broth of Ps3 bacteria are lipid-soluble substances, which

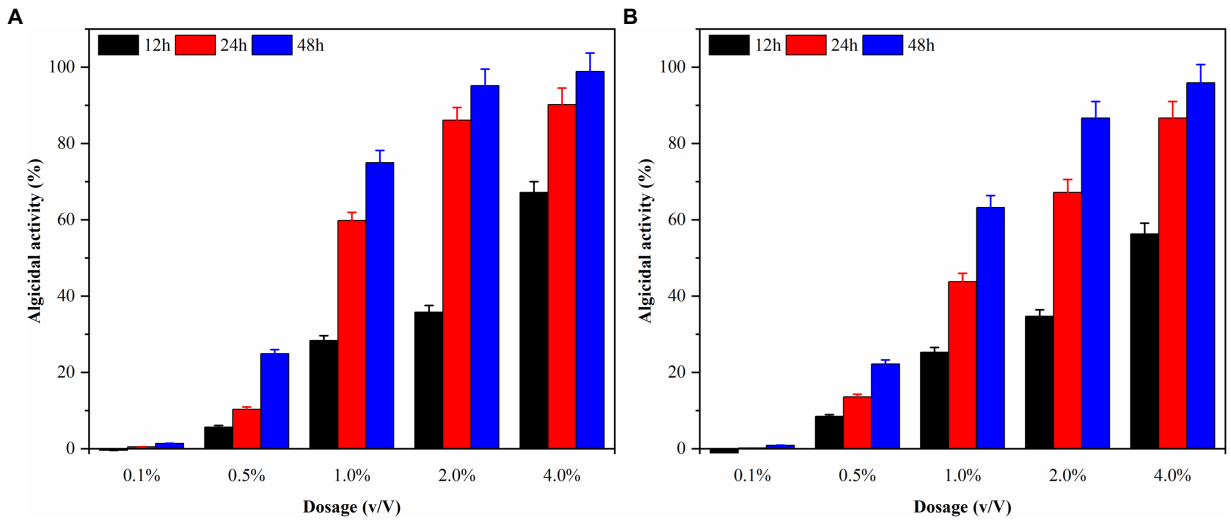


FIGURE 5
The algicidal activity of *G. catenatum* **(A)** and *K. mikimotoi* **(B)** with different dosage of sterile fermentation broth.

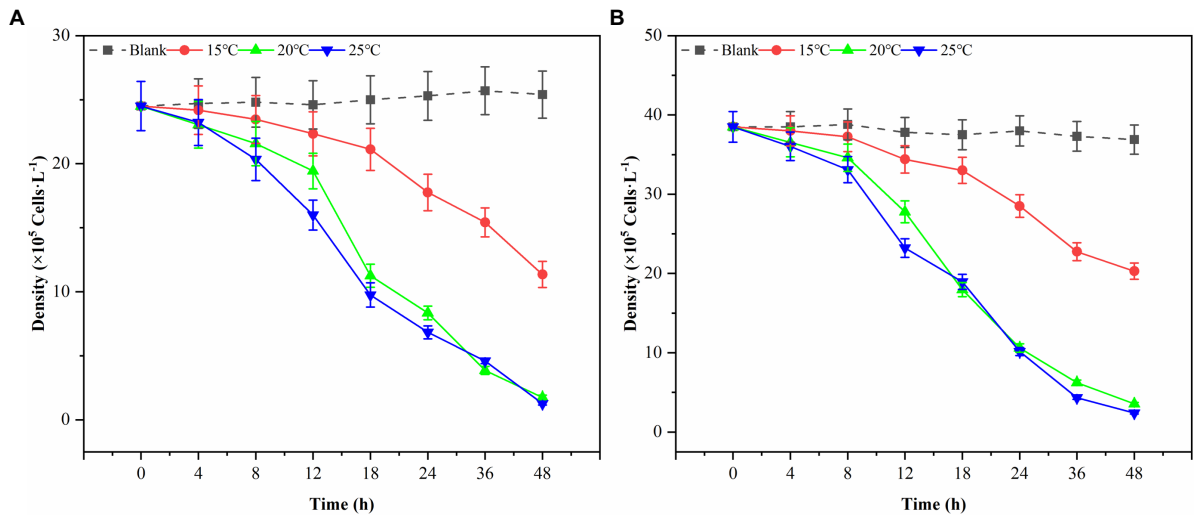


FIGURE 6
The changes of algal density of *G. catenatum* **(A)** and *K. mikimotoi* **(B)** with time were observed by the addition of Ps3 solution at different temperatures.

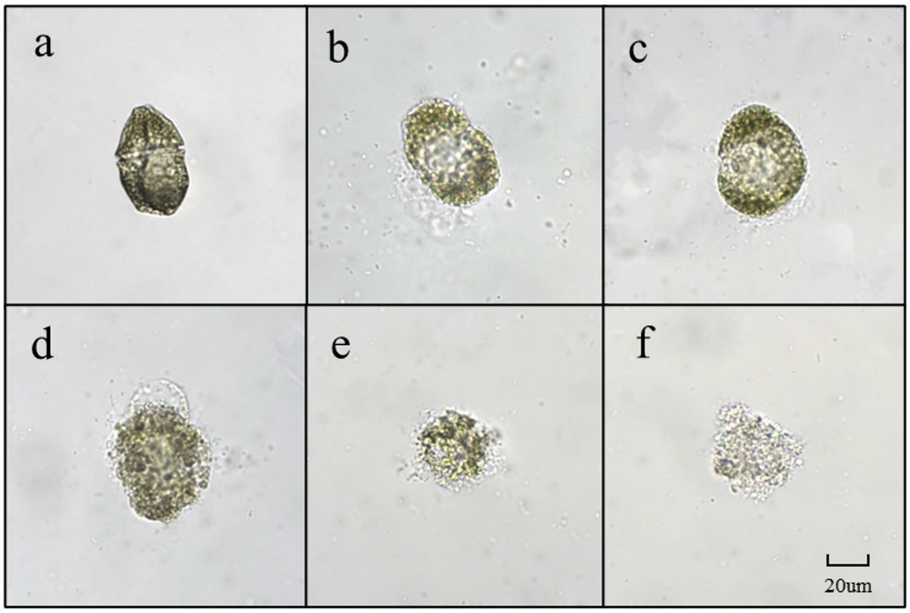


FIGURE 7
The main forms of algae in the algae dissolution process of *G. catenatum* under the influence of *Pseudomonas* sp. Ps3 sterile fermentation broth (**A–F** represent different stages of dissolution process, respectively).

can be extracted by ethyl acetate. Gas chromatography–mass spectrometry (GC–MS) was used to analyze the structure of the algolytic active substances. Chromatograms of volatile components of ethyl acetate extract of Ps3 are shown in Supplementary Figure 6. The peak of the sample was accurately detected by GAS chromatography–mass spectrometry, and the baseline was stable. The volatile components of ethyl acetate extracted phase of Ps3 had more peaks, and the main retention time was between 16 and 26 min. The molecular ion peaks of the higher substances in the content of algal soluble active substances were 20.507, 18.256, 24.285, and 22.349 min. Within the ethyl acetate phase of Ps3 fermentation broth, there were seven absorption peaks observed between 16 and 20 min. Among these peaks, the cyclic (leucine-leucine) dipeptide (20.518 min) was the most prevalent, comprising 34.07% of the total. Several acids and esters exhibit cyclic structures, including the following: cyclic (dipeptides proline-leucine) (with a retention time of 18.266 min and a relative abundance of 25.47%), cyclic (L-leucanyl-L-phenylalanyl) (with a retention time of 24.285 min and a relative abundance of

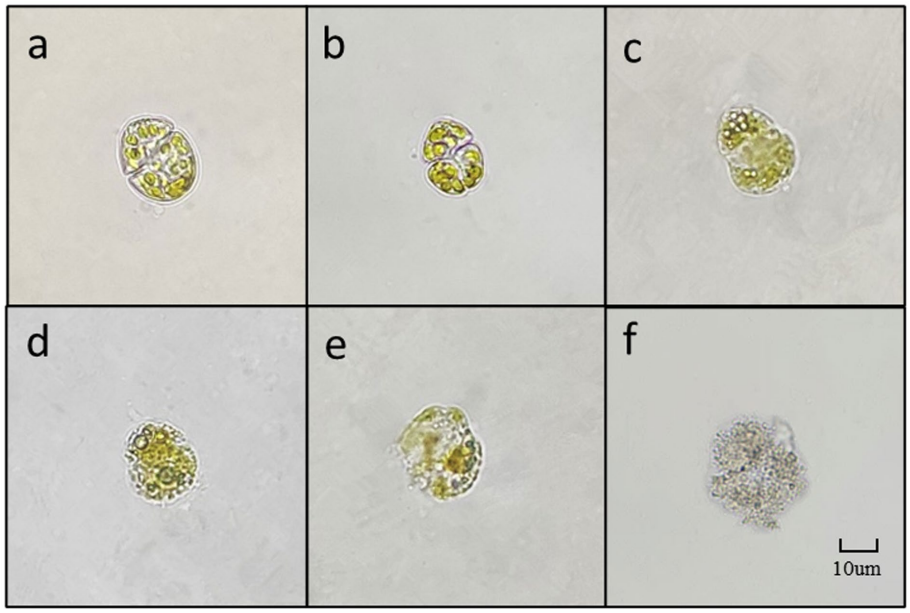


FIGURE 8
The main forms of algae in the algae dissolution process of *K. mikimotoi* under the influence of Ps3 sterile fermentation broth (**A–F** represent different stages of dissolution process, respectively).

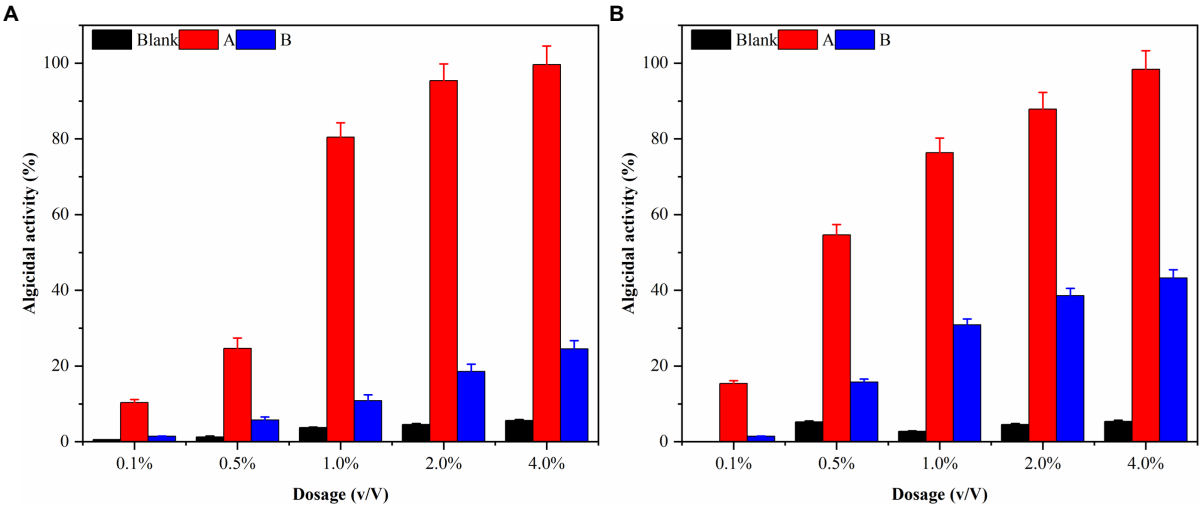


FIGURE 9
The algal lysis of *G. catenatum* **(A)** and *K. mikimotoi* **(B)** by ethyl acetate extraction phase **(A)** and residual phase **(B)** in fermentation broth of *Pseudomonas* sp. Ps3.

10.47%), cyclic (phenylalanine proline) (with a retention time of 22.349 min and a relative abundance of 7.88%), and cyclic (glycylyl prolyl) (with a retention time of 16.425 min and a relative abundance of 4.69%). Additionally, 4-heptanone dihydrazone (with a retention time of 17.351 min and a relative abundance of 2.78%) and DL-alanyl-L-leucine (with a retention time of 16.12 min and a relative abundance of 2.18%) exhibit cyclic structures. The results indicate that the ethyl acetate extract of the fermentation broth of *Pseudomonas* Ps3 mainly contains cyclic dipeptides.

## 3.9. Biotoxicity of the bacterial fermentation broth

The addition of 2.0% (v/v) Ps3 bacterial fermentation solution had little effect on the survival of all experimental organisms, but different organisms had varying sensitivities to toxicity. At 48 h, the survival rates of the control group's *Brachionus plicatilis*, *Artemia salina*, and *Oryzias latipes* were 100, 83.3, and 100%, respectively. The survival rates of the experimental group's *Brachionus plicatilis*, *Artemia salina*

and *Oryzias latipes* were 93.3, 86.7, and 100%, respectively (Figure 10). There was no significant difference in the survival rates of each experimental organism compared to the control group.

## 4. Discussion

In the open ocean, there is a noticeable correlation between the behavior of bacteria and marine dinoflagellates. Specifically, there is a connection between the biomass of dinoflagellates and bacteria that can be observed (Fuhrman and Azam, 1980). Although there has been significant research on microalgae and microbe communities, there has been little focus on examining the interactions between these species at a species-specific level (Bratbak, 1985; Mayali and Azam, 2004; Rooney-Varga et al., 2005). Several studies have also shown that marine bacteria are capable of promoting or inhibiting microalgae growth (Iwata and Barber, 2004; Rooney-Varga et al., 2005).It has been shown that algal blooms associated with coastal ecosystems are mostly dominated by *Alphaproteobacteria*, *Gammaproteobacteria*, and *Bacteroidetes* (Teeling et al., 2012). The death of microalgae in coastal waters, caused by bacteria such as Ps3, can impact the growth rate of the phytoplankton population (Meyer et al., 2017). This phenomenon can potentially contribute to the sudden disappearance of algae blooms in the marine environment. The destruction of microalgae by heterotrophic bacteria is a possible mechanism that could regulate primary productivity in the surface ocean. *Pseudomonas* sp. is an effective biological control agent because it is generally believed to be harmless, non-pathogenic, and poses low risk to the environment, wildlife, and humans (Lee et al., 2011; Chen et al., 2015; Anderson and Kim, 2018).

Non-specific inhibition of diatom growth by *Pseudomonas* sp. has also been observed with *Peridinium bipes*, and *Anabaena cylindrica* (Kang et al., 2007; Jung et al., 2012). A report show supernatants of cultures of *Pseudomonas putida* can kill algae without coming into direct contact with the algae by secreting algicidal substances (Zhang H. et al., 2011). Harmane was isolated in *Pseudomonas* sp. as a kind of algicidal substance. Cultures of K44-1 at a low concentration inhibited *Anabaena* sp. and *Oscillatoria* sp.

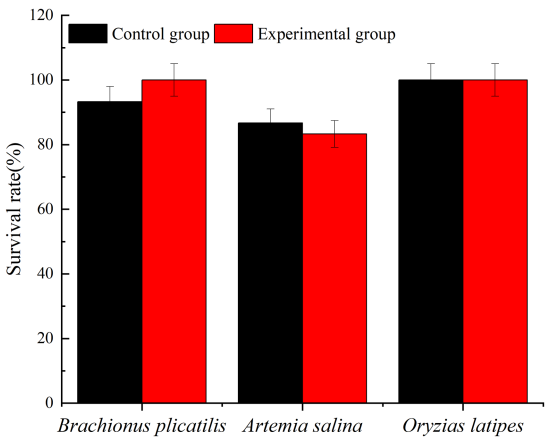


FIGURE 10
The proportion of living organisms.

effectively (Kodani et al., 2002). Additionally, *Pseudomonas* sp. provided a particularly effective inhibitory effect on diatoms. According to the study by Zhang H. et al. (2011), *Stephenodiscus hantzschii* has been identified as a common diatom in winter algae blooms. When $5.0 \times 10^6$ cells/ml were used, the inhibition rate of *Pseudomonas fluorescens* reached 90.0%, explaining the disappearance of diatoms (Kim et al., 2007; Jung et al., 2008). Furthermore, the cellulose fermentation *Pseudomonas fluorescens* displayed better algal control ability when compared with suspended free cells (Kang et al., 2012). The algicidal compounds rupture microalgae cells and lead to the release of more labile organic matter.

In this study, we demonstrate for the first time that Ps3 has high algicidal activity, and therefore, it has high potential as a bio-agent against HABs. The results indicate that Ps3 fermentation solution's soluble algae has a highly significant effect when added at 2.0 and 4.0% quantities, whereas the addition of 0.1 and 0.5% of soluble algae resulted in poor performance. One possible explanation for the low rate of algae lysis is that the inclusion of algal-inhibiting active components is less effective. These findings provide further evidence supporting the notion that Ps3 inhibits algae growth by secreting active substances. In the process of algal dissolution, the change of algal morphology reflects a possible mechanism for algal dissolution. Based on research, the algicidal properties of Ps3 fermentation broth on *G.catenatum* appear to involve damaging the transverse furrow, which subsequently leads to cytoplasm liquefaction and the loss of fundamental cellular functions. Ultimately, the emulsification of the cell membrane and wall occurs, while the chloroplasts undergo decomposition, resulting in discoloration. Studies have shown that the *K. mikimotoi* dissolution process mainly affects the loss of cell membrane integrity, rapid cell rupture, inducing reactive oxygen species (ROS), lipid peroxidation, and photosystem II (PSII) inhibition, and ultimately destroys the subcellular structure, leading to the death of algal (Li et al., 2017). The primary factor that may account for the contrasting effects of Ps3 fermentation broth on *G.catenatum* and *K. mikimotoi* is likely to be their distinct cell size and response mechanisms. In future research, further exploration will be conducted on the relevant mechanisms.

Meanwhile, in the investigation of the impact of environmental temperature on the sterile fermentation solution's ability to lyse algae, it was observed that the Ps3 fermentation solution's efficiency in dissolving algae significantly decreased under lower experimental temperatures. This reduction in efficiency could be attributed to the lowered activity of algae at low temperatures and decreased exchange of substances between the algae and the external environment, which ultimately led to a reduction in the lytic effect of the fermentation solution (Li et al., 2021).

A toxicity testing experiment was conducted on waterborne organisms using Ps3 fermentation solution to evaluate its effectiveness as an algae control method. The results revealed that this approach has minimal toxicity to aquatic organisms as no unusual growth was observed during the experiment. This indicates that it is a relatively safe method for controlling algae. However, further research is necessary to examine any potential toxic effects. The use of algicidal bacteria to control red tides may result in elevated nutrient levels in the surrounding water. This is due to the release of nutrients from various sources, including the deceased red tide algal cells (Tilney et al., 2014). As a result, any remaining

nutrients may promote the regrowth of harmful algal blooms. As such, when utilizing *in situ* methods for controlling red tides, it is important to carefully monitor and manage changes in nutrient levels within the ocean environment. Overall, this method has promising applications for controlling red tides in aquaculture water bodies. The findings suggest that utilizing Ps3 as a bio-controller for reducing or eliminating harmful algae blooms is a cost-effective and sustainable approach with long-term benefits. This *in situ* strategy has greater potential to suppress harmful algal blooms compared to existing methods.

The algal control system successfully eliminated harmful algae from the marine environment using a combination of bacteria, primarily *Pseudomonas* sp. and *Bacillus* sp., which were found to be the most effective in the process of algicidal activity. To achieve optimal results, it was necessary to optimize the fermentation conditions for these bacteria, in order to increase the production of algicidal compounds to the highest level possible (Kim et al., 2015; Hu et al., 2019). Algicidal bacteria face challenges surviving in the complex and unstable marine environment, and may also be inefficient at producing algicidal compounds (Hu et al., 2019; WANG et al., 2021). To mitigate algae blooms using algicidal bacteria, the algicidal compounds were extracted from a fermentation broth that had been optimized for this purpose. Previous studies have reported that several amino acids possess the capability to inhibit algae growth. For instance, a study found that *Streptomyces phaeofaciens* S-9 secretes L-lysine, which can disrupt cyanobacterial cells (Yamamoto and Harayama, 1998). Moreover, the amino acid L-lysine has been observed to exhibit algicidal activity against *Microsystis* cells (Hehmann et al., 2002). We ruled out the possibility of natural amino acids serving as algicidal metabolites from Ps3. This was primarily because Ps3, which was used as a control, exhibited significant algicidal activity despite having the highest concentration of amino acids in the supernatant of its culture. Our experiments suggest that the algicidal activity of Ps3 can be attributed to the presence of natural amino acids within the substance. As a result, it is necessary to perform certain pre-treatments, such as immobilization, to effectively gather the compounds and create a controlled-release formula (Kang et al., 2012; Ni et al., 2015), prior to the dispersion of algicidal compounds. It is important to acknowledge that implementing this HAB-control strategy would also result in an increase in the complexity and cost of biological products. In the fermentation liquid of Ps3, an observable rise in intracellular content was detected within the first 24 h, followed by a stabilization of intercellular content (unpublished data). There seemed to be a dose–response correlation between the fermented liquid and intracellular contents. The rapid escalation in intracellular content is linked to the degree of membrane lipid peroxidation and the intensity of cell membrane lysis (Wang et al., 2011). These findings suggest an immediate strengthening of microalgae antioxidant enzyme activity in response to *P. aeruginosa* damage. Numerous factors, such as toxicant accumulation, can cause a decline in antioxidant enzyme activity, as this toxic substance can harm the cytomembrane system and pigment synthesis of cells (Qian et al., 2008; Zhang F. et al., 2011). To summarize, this report establishes the significant algicidal activity of strain Ps3, which is considered a non-pathogenic bacterium and environmentally safe. Thus, Ps3 has the potential to be an effective bio-controller for harmful algal blooms. Moreover, it was observed that strain Ps3 exhibited greater algicidal activity in all growth stages when grown under fermentation conditions compared to co-culture conditions. This discovery suggests that it may be feasible to manipulate oxygen levels during bacterial growth to improve algicidal activity and achieve greater control over harmful algal blooms. In upcoming studies, the use of clay may also be investigated as a potential complement to algicidal bacteria for red tide control.

## 5. Conclusion

The red tide dinoflagellate exhibited significant impairment when exposed to Ps3 at a fermentation liquid dosage exceeding 5.0% (v/v). High doses of co-culture and fermentation liquid induced abnormal cellular metabolism in the dinoflagellate, including the suppression of its defense system against ROS. Although the intracellular enzyme levels increased in response to the Ps3 fermentation liquid, the red tide cell membrane still underwent decomposition, and there was an excessive accumulation of intracellular contents. Based on these observations, as well as the morphology and structural analysis of the red tide cells, it is suggested that Ps3 primarily exerts its algicidal effects through oxidative damage and membrane destruction. Further investigation is needed to ascertain whether the accumulation of ROS or the impaired antioxidant system is accountable for the algal lysis. This study explored the mechanisms and potential bioactive compounds of *Pseudomonas* Ps3 for algae lysis. In future endeavors, *Pseudomonas* Ps3 could serve as the central element for optimizing the implementation conditions in the field, leading to enhanced efficiency in algal lysis.

## Data availability statement

The datasets presented in this study can be found in online repositories. The names of the repository/repositories and accession number(s) can be found at: https://www.ncbi.nlm.nih.gov/genbank/, OK103600.1.

## Author contributions

LZ wrote the manuscript. HL, YW, and GY performed the data collection and the data collection. YS conceived the idea, supervised the work, and provided bacterial strains. All authors contributed to the article and approved the submitted version.

## Funding

This work was supported by the National Key Research & Development Plan "Strategic International Scientific and Technological Innovation Cooperation" (2016YFE0202100), Marine Red Tide Early Warning and Prevention in Pingtan coastal area (PT2021006), National Natural Science Foundation of China (41573075), and Fujian Provincial Water Conservancy Technology Project (SC-292, DH-1558, 21NB000922, and MSK202202).

## Conflict of interest

The authors declare that the research was conducted in the absence of any commercial or financial relationships that could be construed as a potential conflict of interest.

## Publisher's note

All claims expressed in this article are solely those of the authors and do not necessarily represent those of their affiliated organizations, or those of the publisher, the editors and the reviewers. Any product that may be evaluated in this article, or claim that may be made by its manufacturer, is not guaranteed or endorsed by the publisher.

## Supplementary material

The Supplementary material for this article can be found online at: https://www.frontiersin.org/articles/10.3389/fmicb.2023.1146325/full#supplementary-material

## References


Anderson, A. J., and Kim, Y. C. (2018). Biopesticides produced by plant-probiotic *Pseudomonas chlororaphis* isolates. *Crop Prot.* 105, 62–69. doi: 10.1016/j.cropro.2017.11.009

Anderson, S. R., and Menden-Deuer, S. (2017). Growth, grazing, and starvation survival in three heterotrophic *Dinoflagellate* species. *J. Eukaryot. Microbiol.* 64, 213–225. doi: 10.1111/jeu.12353

Balaji Prasath, B., Wang, Y., Su, Y., Zheng, W., Lin, H., and Yang, H. (2021). Coagulant plus *Bacillus nitratireducens* fermentation broth technique provides a rapid algicidal effect of toxic red tide dinoflagellate. *J. Mar. Sci. Eng.* 9:395. doi: 10.3390/jmse9040395

Balaji-Prasath, B., Wang, Y., Su, Y. P., Chen, M. H., and Zheng, Y. (2022a). Algicidal properties of microbial fermentation products on inhibiting the growth of harmful *Dinoflagellate* species. *Fermentation* 8:8. doi: 10.3390/fermentation8040176

Balaji-Prasath, B., Wang, Y., Su, Y. P., Hamilton, D. P., Lin, H., Zheng, L. W., et al. (2022). Methods to control harmful algal blooms: a review. *Environ. Chem. Lett.* 20, 3133–3152. doi: 10.1007/s10311-022-01457-2

Baohong, C., Kang, W., Xu, D., and Hui, L. (2021). Long-term changes in red tide outbreaks in Xiamen Bay in China from 1986 to 2017. *Estuar. Coast. Shelf Sci.* 249:107095. doi: 10.1016/j.ecss.2020.107095

Bratbak, G. (1985). Bacterial biovolume and biomass estimations. *Appl. Environ. Microbiol.* 49, 1488–1493. doi: 10.1128/aem.49.6.1488-1493.1985

Chen, L., Zou, Y., She, P., and Wu, Y. (2015). Composition, function, and regulation of T6SS in *Pseudomonas aeruginosa*. *Microbiol. Res.* 172, 19–25. doi: 10.1016/j.micres.2015.01.004

Feng, Y., Chi, S., Liu, C., Chen, S., Yu, J., Wang, X., et al. (2014). The discovery of archaea origin phosphomannomutase in algae based on the algal transcriptome. *Acta Oceanol. Sin.* 33, 108–113. doi: 10.1007/s13131-014-0447-0

Fuhrman, J. A., and Azam, F. (1980). Bacterioplankton secondary production estimates for coastal waters of British Columbia, Antarctica, and California. *Appl. Biochem. Microbiol.* 39, 1085–1095. doi: 10.1007/BF00166806

Hehmann, A., Kaya, K., and Watanabe, M. M. (2002). Selective control of Microcystis using an amino acid–a laboratory assay. *J. Appl. Phycol.* 14, 85–89. doi: 10.1023/A:1019546829940

Hu, X.-J., Xu, Y., Su, H.-C., Xu, W.-J., Wang, L.-H., Xu, Y.-N., et al. (2019). Algicidal bacterium CZBC1 inhibits the growth of *Oscillatoria chlorina*, *Oscillatoria tenuis*, and *Oscillatoria planctonica*. *AMB Express* 9, 1–13. doi: 10.1186/s13568-019-0872-8

Hussain, H. S., Fayaz, M., Haneef, M., Hanif, M., Jan, I. U., and Gul, B. (2013). Microfacies and diagenetic-fabric of the Samana Suk formation at Harnoi section, Abbottabad, Khyber Pakhtunkhwa, Pakistan. *J. Himalayan Earth Sci.* 46:79.

Iwata, S., and Barber, J. (2004). Structure of photosystem II and molecular architecture of the oxygen-evolving centre. *Curr. Opin. Struct. Biol.* 14, 447–453. doi: 10.1016/j.sbi.2004.07.002

Jeong, S. Y., Ishida, K., Ito, Y., Okada, S., and Murakami, M. (2003). Bacillamide, a novel algicide from the marine bacterium, *Bacillus* sp. SY-1, against the harmful dinoflagellate, *Cochlodinium polykrikoides*. *Tetrahedron Lett.* 44, 8005–8007. doi: 10.1016/j.tetlet.2003.08.115

Jung, S., Kim, B. H., Katano, T., Kong, D. S., and Han, M. S. (2008). *Pseudomonas fluorescens* HYK0210-SK09 offers species-specific biological control of winter algal blooms caused by freshwater diatom *Stephanodiscus hantzschii*. *J. Appl. Microbiol.* 105, 186–195. doi: 10.1111/j.1365-2672.2008.03733.x

Jung, S. W., Park, J. G., Jeong, D. H., and Lim, D. (2012). Seasonal changes in water masses and phytoplankton communities in the western part of south coastal waters, Korea. *Korean J. Environ. Biol* 30, 328–338. doi: 10.11626/KJEB.2012.30.4.328

Kang, Y.-H., Jung, S. W., Joo, J.-H., and Han, M.-S. (2012). Use of immobilized algicidal bacteria to control natural freshwater diatom blooms. *Hydrobiologia* 683, 151–162. doi: 10.1007/s10750-011-0951-6

Kang, Y. H., Kim, B. R., Choi, H., Seo, J., Kim, B. H., and Han, M. S. (2007). Enhancement of algicidal activity by immobilization of algicidal bacteria antagonistic to *Stephanodiscus hantzschii* (Bacillariophyceae). *J. Appl. Microbiol.* 103, 1983–1994. doi: 10.1111/j.1365-2672.2007.03439.x

Kim, J.-D., Kim, B., and Lee, C.-G. (2007). Alga-lytic activity of *Pseudomonas fluorescens* against the red tide causing marine alga *Heterosigma akashiwo* (Raphidophyceae). *Biol. Control* 41, 296–303. doi: 10.1016/j.biocontrol.2007.02.010

Kim, Y. S., Son, H.-J., and Jeong, S.-Y. (2015). Isolation of an algicide from a marine bacterium and its effects against the toxic dinoflagellate *Alexandrium catenella* and other harmful algal bloom species. *J. Microbiol.* 53, 511–517. doi: 10.1007/s12275-015-5303-1

Ko, S.-R., Jeong, Y., Cho, S.-H., Lee, E., Jeong, B.-S., Baek, S. H., et al. (2022). Functional role of a novel algicidal compound produced by *Pseudoruegeria* sp. M32A2M on the harmful algae *Alexandrium catenella*. *Chemosphere* 300:134535. doi: 10.1016/j.chemosphere.2022.134535

Kodani, S., Imoto, A., Mitsutani, A., and Murakami, M. (2002). Isolation and identification of the antialgal compound, harmane (1-methyl-β-carboline), produced by the algicidal bacterium, *Pseudomonas* sp. K44-1. *J. Appl. Phycol.* 14, 109–114. doi: 10.1023/A:1019533414018

Lee, J. H., Cho, M. H., and Lee, J. (2011). 3-Indolylacetonitrile decreases *Escherichia coli* O157: H7 biofilm formation and *Pseudomonas aeruginosa* virulence. *Environ. Microbiol.* 13, 62–73. doi: 10.1111/j.1462-2920.2010.02308.x

Li, M., Chen, D., Liu, Y., Chuang, C. Y., Kong, F., Harrison, P. J., et al. (2018). Exposure of engineered nanoparticles to *Alexandrium tamarense* (Dinophyceae): healthy impacts of nanoparticles via toxin-producing dinoflagellate. *Sci. Total Environ.* 610-611, 356–366. doi: 10.1016/j.scitotenv.2017.05.170

Li, D., Kang, X., Chu, L., Wang, Y., Song, X., Zhao, X., et al. (2021). Algicidal mechanism of *Raoultella ornithinolytica* against *Microcystis aeruginosa*: antioxidant response, photosynthetic system damage and microcystin degradation. *Environ. Pollut.* 287:117644. doi: 10.1016/j.envpol.2021.117644

Li, Y., Lei, X., Zhu, H., Zhang, H., Guan, C., Chen, Z., et al. (2016). Chitinase producing bacteria with direct algicidal activity on marine diatoms. *Sci. Rep.* 6, 1–13. doi: 10.1038/srep21984

Li, X., Yan, T., Lin, J., Yu, R., and Zhou, M. (2017). Detrimental impacts of the dinoflagellate *Karenia mikimotoi* in Fujian coastal waters on typical marine organisms. *Harmful Algae* 61, 1–12. doi: 10.1016/j.hal.2016.11.011

Mayali, X., and Azam, F. (2004). Algicidal bacteria in the sea and their impact on algal blooms 1. *J. Eukaryot. Microbiol.* 51, 139–144. doi: 10.1111/j.1550-7408.2004.tb00538.x

McCoy, L. F. Jr., and Martin, D. F. (1977). The influence of *Gomphosphaeria aponina* on the growth of *Gymnodinium breve* and the effect of aponin on the ichthyotoxicity of *Gymnodinium breve*. *Chem. Biol. Interact.* 17, 17–24. doi: 10.1016/0009-2797(77)90068-0

Meyer, N., Bigalke, A., Kaulfuß, A., and Pohnert, G. (2017). Strategies and ecological roles of algicidal bacteria. *FEMS Microbiol. Rev.* 41, 880–899. doi: 10.1093/femsre/fux029

Ni, B., Huang, Z., Wu, Y.-F., Fan, Z., Jiang, C.-Y., and Liu, S.-J. (2015). A novel chemoreceptor MCP2983 from *Comamonas testosteroni* specifically binds to cis-aconitate and triggers chemotaxis towards diverse organic compounds. *Appl. Microbiol. Biotechnol.* 99, 2773–2781. doi: 10.1007/s00253-014-6216-3

Petropoulos, K., Bodini, S. F., Fabiani, L., Micheli, L., Porchetta, A., Piermarini, S., et al. (2019). Re-modeling ELISA kits embedded in an automated system suitable for on-line detection of algal toxins in seawater. *Sensors Actuators B Chem.* 283, 865–872. doi: 10.1016/j.snb.2018.12.083

Pokrzywinski, K. L., Tilney, C. L., Modla, S., Caplan, J. L., Ross, J., Warner, M. E., et al. (2017). Effects of the bacterial algicide IRI-160AA on cellular morphology of harmful dinoflagellates. *Harmful Algae* 62, 127–135. doi: 10.1016/j.hal.2016.12.004

Qian, H., Sheng, G. D., Liu, W., Lu, Y., Liu, Z., and Fu, Z. (2008). Inhibitory effects of atrazine on *Chlorella vulgaris* as assessed by real-time polymerase chain reaction. *Environ. Toxicol. Chem.* 27, 182–187. doi: 10.1897/07-163.1

Rooney-Varga, J. N., Giewat, M. W., Savin, M. C., Sood, S., LeGresley, M., and Martin, J. (2005). Links between phytoplankton and bacterial community dynamics in a coastal marine environment. *Microb. Ecol.* 49, 163–175. doi: 10.1007/s00248-003-1057-0

Shi, R. J., Huang, H. H., Qi, Z. H., Hu, W. A., Tian, Z. Y., and Dai, M. (2013). Algicidal activity against *Skeletonema costatum* by marine bacteria isolated from a high frequency harmful algal blooms area in southern Chinese coast. *World J. Microbiol. Biotechnol.* 29, 153–162. doi: 10.1007/s11274-012-1168-1

Shi, X. G., Liu, L. M., Li, Y., Xiao, Y. C., Ding, G. M., Lin, S. J., et al. (2018). Isolation of an algicidal bacterium and its effects against the harmful-algal- bloom dinoflagellate *Prorocentrum donghaiense* (Dinophyceae). *Harmful Algae* 80, 72–79. doi: 10.1016/j.hal.2018.09.003

Sun, Y. Y., Wang, H., Guo, G. L., Pu, Y. F., Yan, B. L., and Wang, C. H. (2016). Isolation, purification, and identification of antialgal substances in green alga Ulva prolifera for antialgal activity against the common harmful red tide microalgae. *Environ. Sci. Pollut. Res.* 23, 1449–1459. doi: 10.1007/s11356-015-5377-7

Teeling, H., Fuchs, B. M., Becher, D., Klockow, C., Gardebrecht, A., Bennke, C. M., et al. (2012). Substrate-controlled succession of marine bacterioplankton populations induced by a phytoplankton bloom. *Science* 336, 608–611. doi: 10.1126/science.1218344

Tilney, C. L., Pokrzywinski, K. L., Coyne, K. J., and Warner, M. E. (2014). Effects of a bacterial algicide, IRI-160AA, on dinoflagellates and the microbial community in microcosm experiments. *Harmful Algae* 39, 210–222. doi: 10.1016/j.hal.2014.08.001

van Tussenbroek, B. I., Hernández Arana, H. A., Rodríguez-Martínez, R. E., Espinoza-Avalos, J., Canizales-Flores, H. M., González-Godoy, C. E., et al. (2017). Severe impacts of brown tides caused by *Sargassum* spp. on near-shore Caribbean seagrass communities. *Mar. Pollut. Bull.* 122, 272–281. doi: 10.1016/j.marpolbul.2017.06.057

Visciano, P., Schirone, M., Berti, M., Milandri, A., Tofalo, R., and Suzzi, G. (2016). Marine biotoxins: occurrence, toxicity, regulatory limits and reference methods. *Front. Microbiol.* 7:1051. doi: 10.3389/fmicb.2016.01051

Wang, J., Sun, P., Bao, Y., Liu, J., and An, L. (2011). Cytotoxicity of single-walled carbon nanotubes on PC12 cells. *Toxicol. in Vitro* 25, 242–250. doi: 10.1016/j.tiv.2010.11.010

Wang, L., Xiang, W.-Z., Wei, H.-N., Lv, J.-T., Wu, H.-L., and Wu, H.-B. (2021). Study on the algicidal characteristics and physiological response of *Microbacterium* sp. CBA01 to *Phaeocystis globosa*. *Biotechnol. Bull.* 37:91. doi: 10.13560/j.cnki.biotech.bull.1985.2021-0161

Yamamoto, S., and Harayama, S. (1998). Phylogenetic relationships of *Pseudomonas putida* strains deduced from the nucleotide sequences of gyrB, rpoD and 16S rRNA genes. *Int. J. Syst. Bacteriol.* 48, 813–819. doi: 10.1099/00207713-48-3-813

Zhang, F., Lau, S. S., and Monks, T. J. (2011). The cytoprotective effect of N-acetyl-L-cysteine against ROS-induced cytotoxicity is independent of its ability to enhance glutathione synthesis. *Toxicol. Sci.* 120, 87–97. doi: 10.1093/toxsci/kfq364

Zhang, H., Yu, Z., Huang, Q., Xiao, X., Wang, X., Zhang, F., et al. (2011). Isolation, identification and characterization of phytoplankton-lytic bacterium CH-22 against *Microcystis aeruginosa*. *Limnologica* 41, 70–77. doi: 10.1016/j.limno.2010.08.001

Zheng, X., Zhang, B., Zhang, J., Huang, L., Lin, J., Li, X., et al. (2013). A marine algicidal actinomycete and its active substance against the harmful algal bloom species *Phaeocystis globosa*. *Appl. Microbiol. Biotechnol.* 97, 9207–9215. doi: 10.1007/s00253-012-4617-8

Zhuang, L., Zhao, L., and Yin, P. (2018). Combined algicidal effect of urocanic acid, N-acetylhistamine and l-histidine to harmful alga *Phaeocystis globosa*. *RSC Adv.* 8, 12760–12766. doi: 10.1039/c8ra00749g

Zohdi, E., and Abbaspour, M. (2019). Harmful algal blooms (red tide): a review of causes, impacts and approaches to monitoring and prediction. *Int. J. Environ. Sci. Technol.* 16, 1789–1806. doi: 10.1007/s13762-018-2108-x

frontiers | Frontiers in Microbiology

TYPE Original Research
PUBLISHED 25 May 2023
DOI 10.3389/fmicb.2023.1196610



OPEN ACCESS

EDITED BY
Xianhua Liu,
Tianjin University, China

REVIEWED BY
Kai Liu,
Guangdong Institute of Eco-environmental Science and Technology, China
Lina Sun,
Shenyang University, China
Xiaojing Li,
Chinese Academy of Agricultural Sciences (CAAS), China

*CORRESPONDENCE
Xuehao Zheng
✉ zhengcwnu2023@163.com

RECEIVED 30 March 2023
ACCEPTED 18 April 2023
PUBLISHED 25 May 2023

CITATION
Zheng X, Oba BT, Shen C, Rong L, Zhang B, Huang L, Feng L, Liu J, Du T and Deng Y (2023) Effect of the bacterial community assembly process on the microbial remediation of petroleum hydrocarbon-contaminated soil. *Front. Microbiol.* 14:1196610. doi: 10.3389/fmicb.2023.1196610



# Effect of the bacterial community assembly process on the microbial remediation of petroleum hydrocarbon-contaminated soil

Xuehao Zheng [1,2,3]*, Belay Tafa Oba [4], Chenbo Shen[5], Luge Rong[6], Bin Zhang[1,2,3], Ling Huang[1], Lujie Feng[1], Jiani Liu[1], Tiantian Du[1] and Yujie Deng[1]

[1]School of Geographical Sciences, China West Normal University, Nanchong, China, [2]Sichuan Provincial Engineering Laboratory of Monitoring and Control for Soil Erosion in Dry Valleys, China West Normal University, Nanchong, China, [3]Liangshan Soil Erosion and Ecological Restoration in Dry Valleys Observation and Research Station, Xide, China, [4]College of Natural Science, Arba Minch University, Arba Minch, Ethiopia, [5]Department of Civil and Environmental Engineering, Carnegie Mellon University, Pittsburgh, PA, United States, [6]School of Biomedical and Chemical Engineering, Liaoning Institute of Science and Technology, Benxi, China

**Introduction:** The accumulation of petroleum hydrocarbons (PHs) in the soil can reduce soil porosity, hinder plant growth, and have a serious negative impact on soil ecology. Previously, we developed PH-degrading bacteria and discovered that the interaction between microorganisms may be more important in the degradation of PHs than the ability of exogenous-degrading bacteria. Nevertheless, the role of microbial ecological processes in the remediation process is frequently overlooked.

**Methods:** This study established six different surfactant-enhanced microbial remediation treatments on PH-contaminated soil using a pot experiment. After 30 days, the PHs removal rate was calculated; the bacterial community assembly process was also determined using the R language program, and the assembly process and the PHs removal rate were correlated.

**Results and discussion:** The rhamnolipid-enhanced *Bacillus methylotrophicus* remediation achieved the highest PHs removal rate, and the bacterial community assembly process was impacted by deterministic factors, whereas the bacterial community assembly process in other treatments with low removal rates was affected by stochastic factors. When compared to the stochastic assembly process and the PHs removal rate, the deterministic assembly process and the PHs removal rate were found to have a significant positive correlation, indicating that the deterministic assembly process of bacterial communities may mediate the efficient removal of PHs. Therefore, this study recommends that when using microorganisms to remediate contaminated soil, care should be taken to avoid strong soil disturbance because directional regulation of bacterial ecological functions can also contribute to efficient removal of pollutants.

KEYWORDS

**petroleum hydrocarbons-contaminated soil, bacterial community assembly process, soil remediation, microbial remediation, surfactant**

# 1. Introduction

Leakage incidents from petroleum production and transportation are inevitable. Petroleum hydrocarbons (PHs) entering the soil can reduce soil porosity and hinder plant growth (Feng et al., 2021). Benzenes and polycyclic aromatic hydrocarbons are typical PHs having strong teratogenic, carcinogenic, and mutagenic effects on soil ecology and human health (Wu et al., 2016; Zheng et al., 2020; Rong et al., 2021).

Exogenous microorganisms can be used to remediate petroleum hydrocarbon-contaminated soil at low cost and with high operability, but their impact on engineering applications is minimal (Feng et al., 2021; Rong et al., 2021; Liu et al., 2022a). Some intensification methods, such as looking for plants to provide root attachment sites for exogenous microorganisms (Zheng et al., 2020), adding nutrients to enable the rapid proliferation of exogenous microorganisms in the soil (Wang et al., 2017), and adding surfactants to increase the bioavailability and microbial activity, can effectively improve the remediation of PHs using microorganisms (Sun et al., 2018; Wang et al., 2018).

Researchers have discovered that the assembly process of microbial communities is influenced by deterministic or stochastic processes as microbial ecology has evolved (Ning et al., 2020). While there is no doubt that microbial assembly processes have a significant impact on organic pollutant bioremediation, studies on the correlation between microbial community assembly and organic degradation are rare. Recent studies have shown that the degradation of TPHs depends more on the interactions among microorganisms than it does on the potential of exogenous-degrading bacteria (Rong et al., 2021), which enriches the traditional understanding of bioremediation of contaminated soil, and also implies that microbial community's assembly may affect pollutant removal. From the points raised above, what are the differences among various treatments in the assembly processes of microbial community structures? and can the process of assembling a microbial community structure result in PHs degradation? In this study, the bacterial assembly process based on bacterial community structure data was calculated, and the correlation between the bacterial assembly and PHs degradation rate was analyzed.

# 2. Methods and materials

## 2.1. Sampling and the remediation process

The contaminated soil was collected from Xinmin petroleum field, Xinmin, Shenyang City, Liaoning Province (123°5′27″, 41°46′33″). The topsoil (0–20 cm) was collected and stored in a dark place for backup after being cleared of debris. The original TPH pollution level was 2,750 mg/kg.

The remediation process which has been described in Rong et al. (2021) is briefly summarized as follows: *Bacillus methylotrophicus* (bacteria N) and *Bacillus subtilis* (bacteria Y) have been carefully chosen as effective soil PH degradation bacteria. According to studies on the toxicity of surfactants to bacteria (Wang et al., 2018; Zheng et al., 2020), a total of six treatments were conducted on 10 kg soil with different exogenous bacteria and surfactants, including (1) CK: no reagent added; (2) N+RL: containing 1 L of N bacterial suspension ($10^8$ CFU per milliliter of bacteria) and a rhamnolipid (RL) solution to achieve a rhamnolipid concentration of 500 mg/kg in the soil; (3) Y+RL: comprising 1 L of Y bacteria suspension and rhamnolipid solution to make the rhamnolipid concentration in the soil reach 500 mg/kg; (4) N+Y+RL: containing 1 L of N bacterial suspension and 1 L of Y bacterial suspension, and rhamnolipid solution to make the concentration of rhamnolipid in the soil reach 500 mg/kg; (5) N+Tween 80: comprised of 1 L of N bacterial suspension and polyethylene glycol sorbitan monooleate (Tween 80) solution to make the rhamnolipid concentration in the soil reach 2,000 mg/kg; (6) Y+SDBS: made of 1 L of Y bacterial suspension and sodium dodecyl benzene sulfonate (SDBS) solution to make the rhamnolipid concentration in the soil reach 3,000 mg/kg. Each treatment was carried out in triplicate.

The pot-based remediation experiment was carried out at Shenyang University. To prevent cross contamination, all flower pots were randomly placed (Figure 1A), with a 20 cm space between each pot. Outdoor weather conditions were reported by Rong et al. (2021). After 30 days, the soil samples in the pot were mixed under sterile conditions, as shown in Figure 1B, for chemical and microbiological testing. The PHs in the soil were measured using an infrared oil meter (Wu et al., 2016). The bacterial community structure in the remediated soil was analyzed using 16S rRNA technology, and the testing process was conducted at Meiji Biotechnology Co., Ltd. The testing process referred to the standard methods issued by the testing company. The sequencing results were uploaded to the SRA database (SUB8645279). After calculating the assembly process of bacterial communities, Pearson's correlation analysis was conducted between the assembly process parameters and the removal rate of PHs.

## 2.2. Calculation of nearest taxon index

MEGA (Version 5.05) was used to build the phylogenetic trees. Using the "ape" and "picante" packages in R (Version 4.1.3) to quantify the mean nearest taxon distance (MNTD) and nearest taxon index (NTI) of microbial communities within a single sample, MNTD calculates the phylogenetic distance between species within a community. MNTD can find the phylogenetic distance between each OTU in the sample and the phylogenetic distance between its closest relatives and then obtain a weighted average of abundance on these phylogenetic distances. NTI is a standardized measure of the phylogenetic distance from each taxon in the sample to the nearest taxon, quantifying the degree of terminal clustering (Zhao et al., 2021). The calculation and analysis procedures were as follows:

(i) Input phylogenetic tree and species abundance table.

(ii) Find the phylogenetic distance between each species in the sample and the phylogenetic distance between their closest relatives. Calculate the weighted average of the phylogenetic distance and relative abundance according to Equation (1) to output $MNTD_{obs}$:

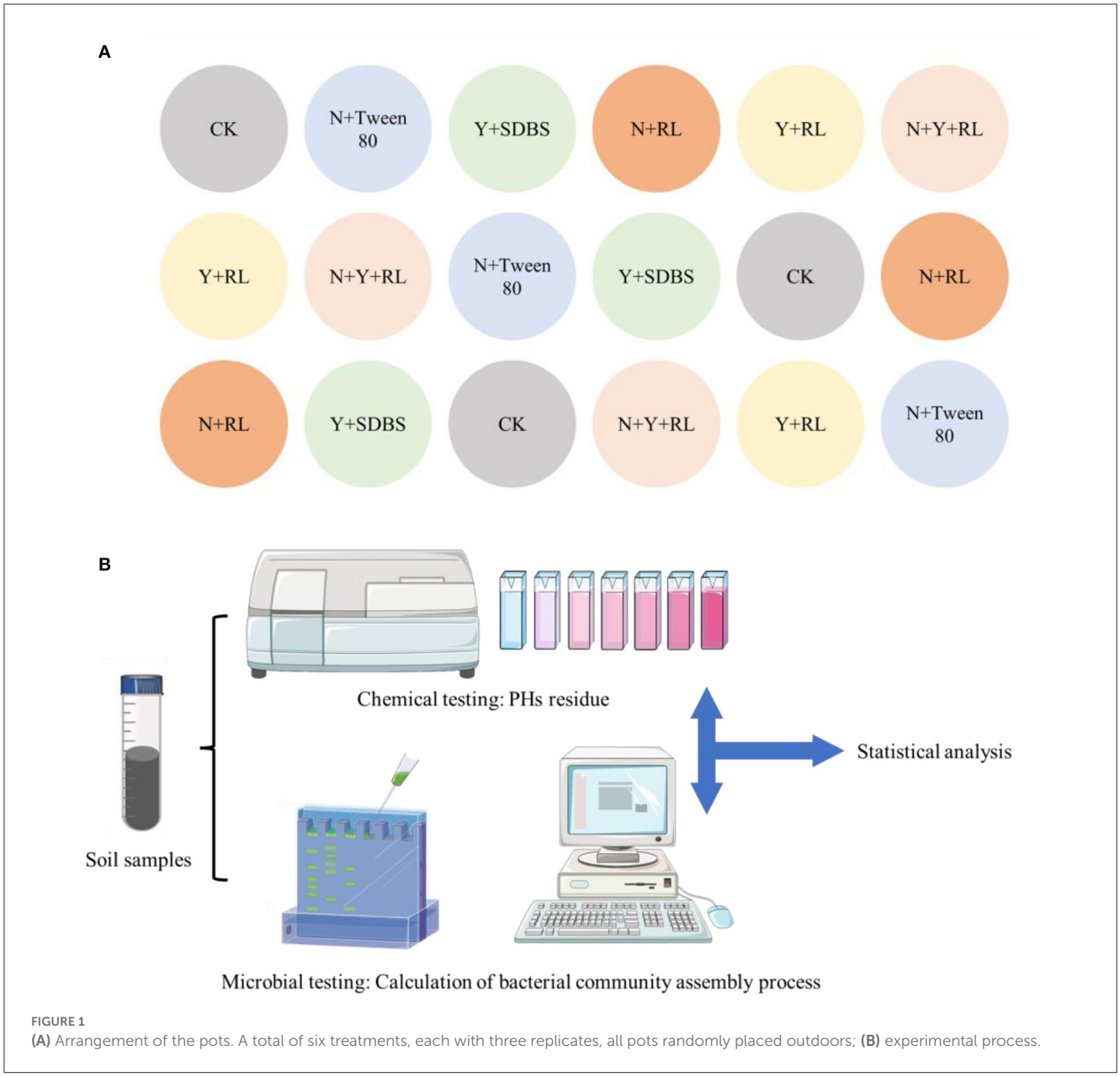


FIGURE 1
**(A)** Arrangement of the pots. A total of six treatments, each with three replicates, all pots randomly placed outdoors; **(B)** experimental process.

$$MNTD_{obs} = \sum_{i_k=1}^{n_k} f_{i_k} min(\triangle_{i_k j_k}) \quad (1)$$

$$NTI = \frac{mean(MNTD_{null}) - MNTD_{obs}}{sd(MNTD_{null})} \quad (2)$$

where $f_{i_k}$ is the relative abundance of species i in the community k, $n_k$ is the number of species in the community k, and $min(_{i_k j_k})$ is the minimum phylogenetic distance between species i and other species j in the community k (Anderson et al., 2011; Stegen et al., 2012).

(iii) After stochastic assigning each species and their relative abundance at each tip of phylogeny for 1,000 times, the MNTD value of the stochastic community is obtained as $MNTD_{null}$. The mean MNTD ($meanMNTD_{null}$) and standard deviation $MNTD_{null}$ ($sdMNTD_{null}$) are calculated, and the NTI was calculated according to the formula Equation (2):

(iv) NTI > 0 indicates that the relationship between coexisting species is closer than expected, and the system undergoes physiological clustering, with a deterministic process dominating structural changes within the community; NTI < 0 indicates that the relationship between coexisting species is farther than expected, and the system is phylogenetic stochastic, with stochastic processes leading to structural changes within the community (Feng et al., 2018). The difference between NTI and 0 represents the degree of clustering or dispersion of the system, that is, the impact of deterministic or stochastic processes on structural changes within a community.

## 2.3. Calculation of beta nearest taxon index

Beta mean nearest taxon distance (βMNTD) and beta nearest taxon index (β-NTI) were used to reflect changes in system development over time or space and were seen as an inter-group analog of MNTD and NTI (Fine and Kembel, 2011).

The calculation formula of $\beta MNTD_{obs}$ was shown in Equation (3):

$$\beta MNTD_{obs} = 0.5\left[\sum_{i_k=1}^{n_k} f_{i_k} min(_{i_k j_m}) + \sum_{i_m=1}^{n_m} f_{i_m} min(\triangle_{i_m j_k})\right] \quad (3)$$

where $\Delta_{i_k j_m}$ is the minimum phylogenetic distance between species i in community k and species j in community m. The other variables are the same as those in Equation (1).

When β-NTI > 2 or β-NTI < −2, it indicates that the actual phylogenetic turnover between two communities is higher or lower than the expected phylogenetic turnover, i.e., the deterministic process dominates the structural changes; when −2 < β-NTI < 2, it indicates that the actual phylogenetic turnover between the two communities is similar to the expected phylogenetic turnover, i.e., the stochastic process dominates the structural changes (Anderson et al., 2011; Zheng et al., 2022). The difference between |β-NTI| and 0 represents the degree of clustering or dispersion of the system, that is, the impact of deterministic or stochastic processes on structural changes within a community.

## 2.4. Null model analysis

To further quantify the effect of deterministic or stochastic processes on changes in the structure of communities, a null model calculation and analysis were performed using the difference and similarity index between communities calculated based on the Bray–Curtis distance (Liu et al., 2022b). The specific steps followed were as follows:

(i) The Bray–Curtis distance calculated using the 'vegan' package was used as an index to characterize the similarity difference between communities, expressed in $D_{obs}$. The range of $D_{obs}$ is 0–1, and the closer the $D_{obs}$ to 1, the greater the difference between the two communities; the similarity index between communities was expressed as $S_{obs}$, in which $S_{obs} = 1 - D_{obs}$, the closer the $S_{obs}$ to 1, the greater the similarity between the two communities. The calculated average value was $\overline{S_{obs}}$.

(ii) Using the randomize Matrix function in the "picante" package of R, keep the frequency of each species constant, randomly allocate the species abundance in each community, calculate the similarity index $S_{null}$ between randomly distributed communities in the null model, and repeat the process 1,000 times to obtain the average value of the similarity index $\overline{S_{null}}$.

(iii) Permutational multivariate analysis of variance is a multivariate analysis of variance based on distance matrices. It uses Perm ANOVA to perform a significant difference analysis of the similarity matrix between the actual microbial community and the randomly distributed microbial community with a null model. If *P*-value is <0.05, it indicates that there is a significant difference between the actual community and the randomly distributed community in the null model, that is, the deterministic process dominates the community. On the contrary, if the stochastic process dominates the community, there is no significant difference between the actual community and the null model randomly distributed community.

(iv) According to the difference between the similarity index obtained from the null model and the actually observed community, which accounts for the proportion of the actually observed community similarity index, the proportion of the impact of the deterministic process in community construction can be quantified and expressed as the deterministic ratio (DR), $DR = (\overline{S_{obs}} - \overline{S_{null}})/\overline{S_{obs}}$; the impact ratio of stochastic processes in community construction is expressed as the stochastic ratio (SR), $SR = 1 - DR$ (Chase et al., 2011; Zhang et al., 2019).

## 2.5. Statistical analysis

Experimental data were analyzed using Excel (Version 2016). GraphPad Prism (Version 8.3.0) was used in the data graphing. Experimental data were presented as the mean and standard error. The significance of the differences was determined using Student's *t*-test and one-way ANOVA. The statistical analyses were performed using SPSS (Version 27).

# 3. Results

## 3.1. PHs removal rate

After 30 days, the removal rates of PHs by different treatments are shown in Figure 2. Data on the residual amount of PHs were published by Rong et al. (2021). The natural degradation rate of PHs in the soil was very low, only below 5%. The effect of N+RL treatment was found to be the best, with a removal rate of 80.24% for TPHs, and 82.03, 81.75, and 75.18% for alkanes ($CH_3$), olefins ($CH_2$), and aromatics (CH), respectively. There was no statistically significant difference in the TPH removal rates among Y + RL, N + Y + RL, N + Tween 80, and Y + SDBS ($P > 0.05$). The effects of various treatments on CH removal vary greatly. The ring-opening process involved in CH degradation required a large amount of energy. It was difficult to determine the main influencing factors related to pollutant removal from the analysis of bacterial species and surfactant species.

## 3.2. Assemble process analysis

This study chose the species with relative abundance >0.2% (RA > 0.2%) and RA > 0.5% in each sample for calculation and analysis because a total of 6,028 species were checked out in the sequencing results, the sequence file was too large to run when creating an evolutionary tree using MEGA (Version 5.05), and the majority of the species were rare species with relative abundance <0.01%. The two microbial groups account for 85 and 75% of total abundance, respectively, and may well-represent the core species that play a significant role in community formation.

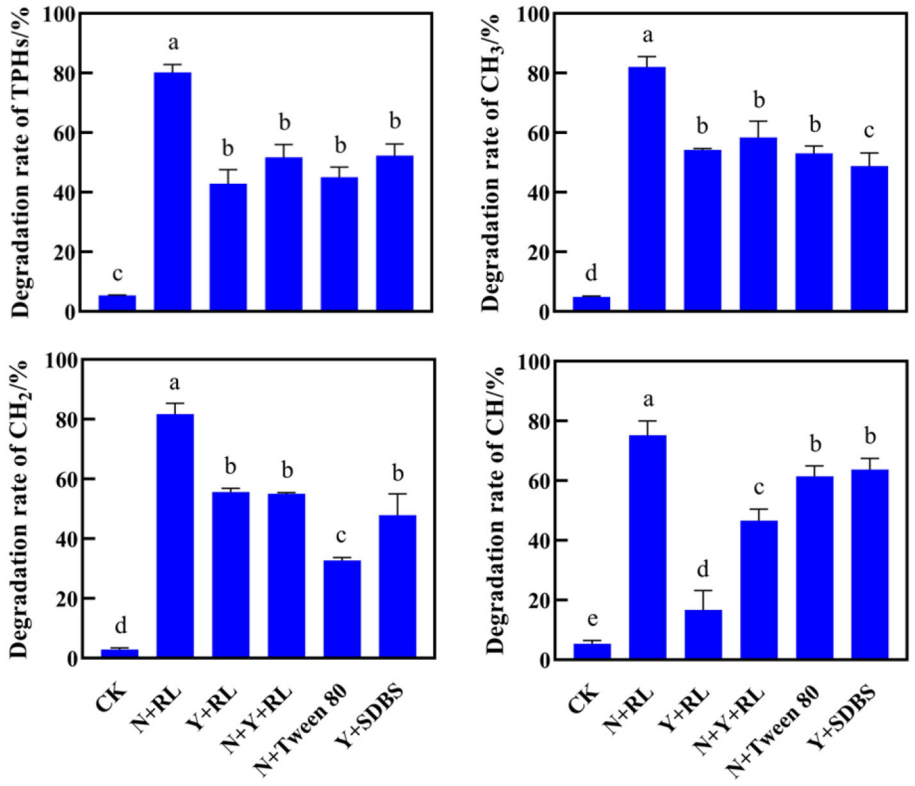


FIGURE 2
Degradation rates of total petroleum hydrocarbons (TPHs), alkanes ($CH_3$), olefins ($CH_2$), and aromatics (CH) by different treatments. The letters on the error bar (mean ± sd) indicate the results of the difference analysis (one-way ANOVA).

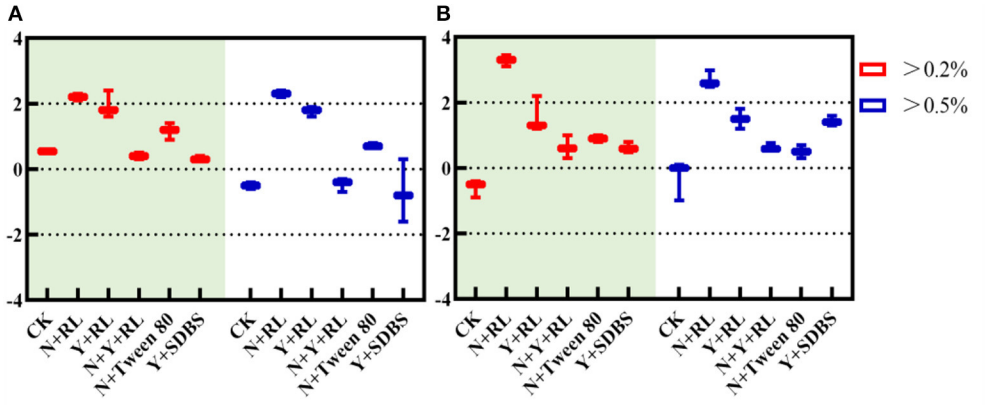


FIGURE 3
**(A)** Nearest taxon index (NTI) and **(B)** β nearest taxon index (β-NTI) in different abundance ranges.

As can be seen in Figure 3A, species with RA > 0.2% in all treatments have an $\overline{NTI} > 0$, indicating that clustering occurred in all systems, and deterministic processes dominated community assembly; when RA > 0.5%, the $\overline{NTI} > 0$ in N + RL, Y + RL, and N + Tween 80 indicates that clustering occurs in the system, and deterministic processes dominate community formation.

As can be seen in Figure 3B, when RA > 0.2%, the N + RL with β-NTI > 2 indicates that the phylogenetic turnover between communities was greater than the expected phylogenetic turnover. The deterministic process dominates the structural changes when the CK, Y + RL, N + Y + RL, N + Tween, and Y + SDBS have a mean β-NTI between −2 and 2, indicating that the phylogenetic turnover between communities was similar to the expected one, and the stochastic process dominates the structural changes.

Combined with NTI and β-NTI, for core communities with high relative abundance, the community of N + RL is assembled

10.3389/fmicb.2023.1196610

TABLE 1 Null model calculation results based on Bray–Curtis distance.

| Treatment | $\overline{S_{obs}}$ | $\overline{S_{null}}$ | *P*-value | DR | SR |
|---|---|---|---|---|---|
| CK | 0.4201 | 0.3438 | 0.2428 | 18.17% | 81.83% |
| N + RL | 0.7363 | 0.2459 | 0.0010 | 66.60% | 33.40% |
| Y + RL | 0.4533 | 0.2352 | 0.0439 | 54.86% | 45.14% |
| N + Y + RL | 0.5848 | 0.3657 | 0.0629 | 37.46% | 62.54% |
| N + Tween 80 | 0.5019 | 0.3660 | 0.1518 | 27.09% | 72.91% |
| Y + SDBS | 0.5303 | 0.2562 | 0.0160 | 51.69% | 48.31% |

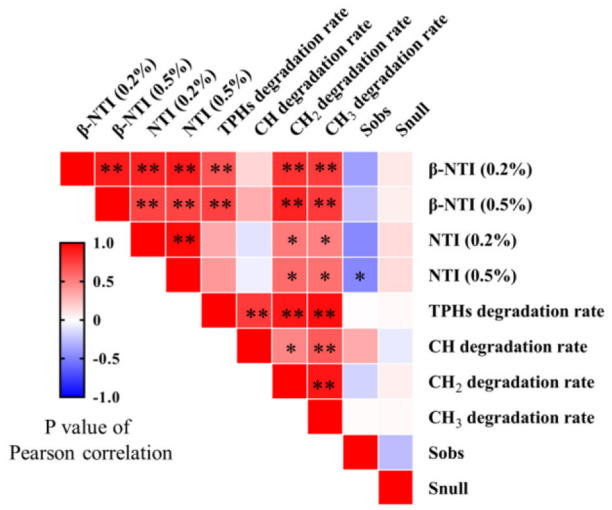


FIGURE 4
Pearson's correlation analysis between microbial community assembly process parameters and PHs' removal rate. The *P*-value and asterisk number were used to show significant differences where $P > 0.05$, ns; $P < 0.05$, *; and $P < 0.01$, **.

with a deterministic process, while the CK, Y + RL, N + Y + RL, N + Tween, and Y + SDBS are assembled with a stochastic process.

## 3.3. Null model fitting

The null model fitting results are shown in Table 1. There was no significant difference between the $\overline{S_{obs}}$ and $\overline{S_{null}}$ in CK, N + Y + RL, and N + Tween 80 ($P > 0.05$), indicating that the impact of the stochastic process on the community structure assembly of the three treatments was greater than that of deterministic processes. There was a significant difference between $\overline{S_{obs}}$ and $\overline{S_{null}}$ in the N + RL, Y + RL, and Y + SDBS, indicating that the deterministic assembly process was dominant ($P < 0.05$).

After quantifying the impact of deterministic processes on community assembly processes using DR, the results showed that the DR of CK, N + Tween, and N+Y+RL was <50%, indicating that stochastic assembly processes lead the structural change. The DR of N + RL, Y + RL, and Y + SDBS was >50%, indicating that the structural change was caused by the deterministic assembly process.

## 3.4. Effect of bacterial community assembly process on the rate of PHs removal

The statistical correlation between microbial community assembly process parameters and PHs removal rate is shown in Figure 4. There was a significant positive correlation between NTI and $CH_2$ and $CH_3$ ($P < 0.05$). There was a significant positive correlation between β-NTI and TPHs, $CH_2$, and $CH_3$ removal rates ($P < 0.01$). The correlation between $\overline{S_{obs}}$ and $\overline{S_{null}}$ and the removal rate was poor, and the statistical correlation was not significant ($P > 0.05$).

# 4. Discussion

The community formation mechanism is critical for maintaining species distribution and diversity, and the theoretical study of community formation is one of the core topics in the field of environmental ecology (Ning et al., 2019). Although the fundamental laws of microbial diversity change are now well-understood, the factors influencing these laws remain unknown. As a result, environmental ecologists are focusing more on the formation of microbial communities and the process of community formation, which is a process of generating microbial diversity and community functions (Ning et al., 2020). In the field of microbial ecology, microbial community formation mechanisms are drawn from many macroeconomic theories and are divided into two major categories: deterministic processes and stochastic processes. Deterministic processes mainly consist of environmental factors, biological interactions, specialization, and priority effects, while stochastic processes include dispersal, birth, stochastic death, differentiation, specialization, and extrapolation (Zhou et al., 2013a,b). Regardless of which of these two processes dominates, community formations will determine the existence and abundance of species, thereby changing the diversity and composition of microorganisms, and have an impact on the function of the system (Feng et al., 2018).

The increase inaccumulation of PHs in the soil has caused changes of in the soil microecological environment, affecting the metabolism of microbial communities and changes in community composition and structure (Chen et al., 2022). When petroleum pollutants enter the soil, they not only have a toxic effect on the majority of soil microorganisms, but they also significantly reduce the number of active microorganisms in the soil, change the community structure, and cause uneven population distribution, resulting in a decrease in the function of microorganisms in the upper soil environment, which is manifested in a decrease in the activity of soil microorganisms (Zheng et al., 2020, 2023). Analyzing the structure–activity relationship between microbial communities and PHs removal efficiency is important for developing efficient microbial remediation techniques for PH-contaminated soil.

From the results of this study, it was discovered that the removal of PHs does not directly depend on the addition of exogenous microorganisms or surfactants (Figure 2); previous research also pointed out that the changes in the structure of indigenous microbial communities in the soil still have a significant impact on the removal of pollutants (Rong et al., 2021). The correlation among NTI, β-NTI, and PHs removal rate was

significant and positive (Figure 4). Therefore, it is possible to conclude that the increase in microbial diversity caused by the deterministic assembly process can mediate the removal rate of PHs. Consequently, the study of microbial communities in the soil is critical for soil remediation research. The remediation of petroleum hydrocarbon-contaminated soil should not only focus on the removal of the pollutants but also on the impact of the remediation process on the diversity and function of the soil microbial community. At the same time, the study of the community formation process should further explore the mechanism of community diversity changes. There are many studies on remediation technology but very few on microbial communities after treatment. Only evaluating the removal rate of a remediation agent while ignoring its collateral effects on microbial communities in the soil cannot provide a comprehensive picture of the remediation process. Although some studies have shown that stochastic assembly can increase microbial diversity, which helps to generate more beneficial species and thus improve the functional diversity of microbial communities (Zhang et al., 2019), this is not consistent with the findings of this study. The deterministic assembly-induced microbial diversity is beneficial to improving the specific functions of microbial communities. This is likely due to increased stochastic, which leads to an increase in microbial species that do not have specific functions, competition with microbial species that do have specific functions, or changes in soil physical and chemical properties caused by their metabolites, which leads to a decline in the abundance of microbial species with specific functions. Therefore, the addition of remediation agents can effectively degrade PHs by regulating the deterministic assembly process of microbial communities in the soil, thereby stimulating microbial diversity.

## 5. Conclusion

This study calculated the assembly process of bacterial community structure under different treatments during microbial remediation of TPHs and analyzed the correlation with NTI, β-NTI, $\overline{S_{obs}}$ and $\overline{S_{null}}$, and the removal rate; it was discovered that the deterministic assembly process of bacterial communities may mediate the more efficient removal of TPHs. Based on the findings of this study, researchers should focus more on the targeted regulation of microbial ecological functions while treating contaminated soils using microbial-based remediation processes, rather than just the rough removal of pollutants through strong soil disturbance.

## Data availability statement

The original contributions presented in the study are included in the article/supplementary material, further inquiries can be directed to the corresponding author.

## Author contributions

XZ: methodology, writing—original draft, and funding acquisition. BO, LH, LF, JL, TD, and YD: writing—reviewing and editing. CS: writing—original draft and data curation. LR: data curation. BZ: validation. All authors contributed to the article and approved the submitted version.

## Acknowledgments

The authors are thankful for the comments and suggestions provided by the editor and the reviewers.

## Conflict of interest

The authors declare that the research was conducted in the absence of any commercial or financial relationships that could be construed as a potential conflict of interest.

## Publisher's note

All claims expressed in this article are solely those of the authors and do not necessarily represent those of their affiliated organizations, or those of the publisher, the editors and the reviewers. Any product that may be evaluated in this article, or claim that may be made by its manufacturer, is not guaranteed or endorsed by the publisher.

## References

Anderson, M. J., Crist, T. O., Chase, J. M., Vellend, M., Inouye, B. D., Freestone, A. L., et al. (2011). Navigating the multiple meanings of β diversity: a roadmap for the practicing ecologist. *Ecol. Lett.* 14, 19–28. doi: 10.1111/j.1461-0248.2010.01552.x

Chase, J. M., Kraft, N., Smith, K. G., Vellend, M., and Inouye, B. D. (2011). Using null models to disentangle variation in community dissimilarity from variation in α-diversity. *Ecosphere* 2, 1–11. doi: 10.1890/ES10-00117.1

Chen, K., He, R., Wang, L., Liu, L., Huang, X., Ping, J., et al. (2022). The dominant microbial metabolic pathway of the petroleum hydrocarbons in the soil of shale gas field: carbon fixation instead of CO2 emissions. *Sci. Total Environ.* 807, 151074. doi: 10.1016/j.scitotenv.2021.151074

Feng, L., Jiang, X., Huang, Y., Wen, D., Fu, T., and Fu, R. (2021). Petroleum hydrocarbon-contaminated soil bioremediation assisted by isolated bacterial consortium and sophorolipid. *Environ. Pollut.* 273, 116476. doi: 10.1016/j.envpol.2021.116476

Feng, M., Adams, J. M., Fan, K., Shi, Y., Sun, R., Wang, D., et al. (2018). Long-term fertilization influences community assembly processes of soil diazotrophs. *Soil Biol. Biochem.* 126, 151–158. doi: 10.1016/j.soilbio.2018.08.021

Fine, P., and Kembel, S. W. (2011). Phylogenetic community structure and phylogenetic turnover across space and edaphic gradients in western Amazonian tree communities. *Ecography* 34, 552–565. doi: 10.1111/j.1600-0587.2010.06548.x

Liu, K., Fang, L., Li, F., Hou, D., Liu, C., Song, Y., et al. (2022a). Sustainability assessment and carbon budget of chemical stabilization based multi-objective remediation of Cd contaminated paddy field. *Sci. Total Environ.* 819, 152022. doi: 10.1016/j.scitotenv.2021.152022

Liu, K., Ran, Q., Li, F., Shaheen, S. M., Wang, H. L., Rinklebe, J., et al. (2022b). Carbon-based strategy enables sustainable remediation of paddy soils in harmony with carbon neutrality. *Carbon Res.* 1, 12. doi: 10.1007/s44246-022-00012-6

Ning, D., Deng, Y., Tiedje, J. M., and Zhou, J. (2019). A general framework for quantitatively assessing ecological stochasticity. *PNAS* 116, 16892–16898. doi: 10.1073/pnas.1904623116

Ning, D., Yuan, M., Wu, L., Zhang, Y., Guo, X., Zhou, X., et al. (2020). A quantitative framework reveals ecological drivers of grassland microbial community assembly in response to warming. *Nat. Commun.* 11, 4717. doi: 10.1038/s41467-020-18560-z

Rong, L., Zheng, X. H., Oba, B. T., Shen, C., Wang, X., Wang, H., et al. (2021). Activating soil microbial community using bacillus and rhamnolipid to remediate TPH contaminated soil. *Chemosphere* 275, 130062. doi: 10.1016/j.chemosphere.2021.130062

Stegen, J. C., Lin, X., Konopka, A., and Fredrickson, J. K. (2012). Stochastic and deterministic assembly processes in subsurface microbial communities. *J. ISME* 6, 1653–1664. doi: 10.1038/ismej.2012.22

Sun, M., Ye, M., Jiao, W., Feng, Y., Yu, P., Liu, M., et al. (2018). Changes in tetracycline partitioning and bacteria/phage-comediated ARGs in microplastic-contaminated greenhouse soil facilitated by sophorolipid. *J. Hazard. Mater.* 345, 131–139. doi: 10.1016/j.jhazmat.2017.11.036

Wang, H., Wang, X., Liu, C., Wang, Y. G., Rong, L. G., and Sun, L. (2017). *In-situ* bioremediation of DDTs and PAH contaminated aging farmland soil using blood meal. *Soil. Sed. Contam.* 26, 623–635. doi: 10.1080/15320383.2017.1385593

Wang, X., Sun, L., Wang, H., Wu, H., Chen, S., and Zheng, X. (2018). Surfactant-enhanced bioremediation of DDTs and PAHs in contaminated farmland soil. *Environ. Technol.* 39, 1733–1744. doi: 10.1080/09593330.2017.1337235

Wu, H., Sun, L. N., Wang, H., and Wang, X. X. (2016). Persulfate oxidation for the remediation of petroleum hydrocarbon-contaminated soils. *Pol. J. Environ. Stud.* 25, 851–857. doi: 10.15244/pjoes/60857

Zhang, Z., Deng, Y., Feng, K., Cai, W., Li, S., Yin, H., et al. (2019). Deterministic assembly and diversity gradient altered the biofilm community performances of bioreactors. *Environ. Sci. Technol.* 53, 1315–1324. doi: 10.1021/acs.est.8b06044

Zhao, W., Wang, X. B., Shi, L. Y., Zhu, W., Ma, L., Wang, J., et al. (2021). Calculation method for stochastic and deterministic assembly processes of prokaryotic communities. *Bioprotocol* 101, e2003400. doi: 10.21769/BioProtoc.2003400

Zheng, X., Aborisade, M. A., Wang, H., He, P., Lu, S., Cui, N., et al. (2020). Effect of lignin and plant growth-promoting bacteria (*Staphylococcus pasteuri*) on microbe-plant co-remediation: A PAHs-DDTs co-contaminated agricultural greenhouse study. *Chemosphere* 256, 127079. doi: 10.1016/j.chemosphere.2020.127079

Zheng, X., Oba, B. T., Wang, H., Shen, C., Zhao, R., Zhao, D., et al. (2022). Organo-mineral complexes alter bacterial composition and induce carbon and nitrogen cycling in the rhizosphere. *Sci. Total Environ.* 836, 155671. doi: 10.1016/j.scitotenv.2022.155671

Zheng, X., Oba, B. T., Wang, H., Zhang, B., Shu, C., Song, Y., et al. (2023). Revealing the potential of organo-mineral complexes in agricultural application using bibliometrics. *J. Clean. Prod.* 401, 136728. doi: 10.1016/j.jclepro.2023.136728

Zhou, J., Deng, Y., Zhang, P., and Arkin, A. P. (2013a). Stochasticity, succession, and environmental perturbations in a fluidic ecosystem. *PNAS* 111, 836–845. doi: 10.1073/pnas.1324044111

Zhou, J., Liu, W., Deng, Y., Jiang, Y. H., Xue, K., He, Z. L., et al. (2013b). Stochastic assembly leads to alternative communities with distinct functions in a bioreactor microbial community. *MBio.* 4, e00584-12. doi: 10.1128/mBio.00584-12

frontiers | Frontiers in Microbiology

TYPE Original Research
PUBLISHED 25 July 2023
DOI 10.3389/fmicb.2023.1211761



OPEN ACCESS

EDITED BY
Hongbo Li,
Nanjing University, China

REVIEWED BY
Shrameeta Shinde,
Miami University, United States
Devendra Dusane,
Nationwide Children's Hospital, United States

*CORRESPONDENCE
Jihyang Kweon
✉ jhkweon@konkuk.ac.kr

RECEIVED 25 April 2023
ACCEPTED 11 July 2023
PUBLISHED 25 July 2023

CITATION
Song W, Ryu J, Jung J, Yu Y, Choi S and Kweon J (2023) Dispersive biofilm from membrane bioreactor strains: effects of diffusible signal factor addition and characterization by dispersion index. *Front. Microbiol.* 14:1211761. doi: 10.3389/fmicb.2023.1211761



# Dispersive biofilm from membrane bioreactor strains: effects of diffusible signal factor addition and characterization by dispersion index

Wonjung Song[1], Junhee Ryu[2], Jaehyun Jung[3], Youngjae Yu[4], Suyoung Choi[1] and Jihyang Kweon[5]*

[1]The Academy of Applied Science and Technology, Konkuk University, Seoul, Republic of Korea, [2]Department of Civil and Environmental Engineering, Konkuk University, Seoul, Republic of Korea, [3]HANSU Technical Service Ltd, Sungnam-si, Gyeonggi-do, Republic of Korea, [4]Department of Chemical and Environmental Engineering, University of Arizona, Tucson, AZ, United States, [5]Department of Environmental Engineering Konkuk University, Seoul, Republic of Korea

**Introduction:** Biofilm occurs ubiquitously in water system. Excessive biofilm formation deteriorates severely system performance in several water and wastewater treatment processes. Quorum sensing systems were controlled in this study with a signal compound *cis*-2-Decenoic acid (CDA) to regulate various functions of microbial communities, including motility, enzyme production, and extracellular polymeric substance (EPS) production in biofilm.

**Methods:** The addition of CDA to six strains extracted from membrane bioreactor sludge and the *Pseudomonas aeruginosa* PAO1 strain was examined for modulating biofilm development by regulating DSF expression.

**Results and discussion:** As the CDA doses increased, optical density of the biofilm dispersion assay increased, and the decrease in EPS of the biofilm was obvious on membrane surfaces. The three-dimensional visual images and quantitative analyses of biofilm formation with CDA proved thinner, less massive, and more dispersive than those without; to evaluate its dispersive intensity, a dispersion index was proposed. This could compare the dispersive effects of CDA dosing to other biofilms or efficiencies of biofouling control practices such as backwashing or new cleaning methods.

KEYWORDS

**membrane bioreactor, *cis*-2-Decenoic acid, diffusible signal factor (DSF), quorum sensing, biofilm, extracellular polymeric substances (EPS)**

## 1. Introduction

Membrane separation processes including membrane bioreactors (MBRs) are widely applied in wastewater treatment, water reuse, and reclamation. The biggest weakness of the membrane process is that, as the filtration process proceeds, fouling gradually arises on the membrane surfaces. Biofouling has been recognized as the most problematic fouling to control and occurs when microorganisms accumulate and cultivate on the membrane surface (Nguyen et al., 2012; Gkotsis et al., 2014; Tijing et al., 2015). Biofilm formation causes severe performance loss to the membrane system because it yields a shutdown of the process and membrane replacement when the output water quality cannot be sustained through costly cleaning and extensive maintenance

(Flemming, 2011; Nguyen et al., 2012; Siebdrath et al., 2019; Maletskyi, 2020; Obotey Ezugbe and Rathilal, 2020). These problems occur more frequently in the MBR process for treating wastewater which contained hazardous substances. Hazardous substances reduce the process performance by weakening microbial activity, and promote biofouling by accelerating or increasing biofilm formation on membrane surfaces. EPS can be increased by humic acid present in the bulk (Ryu et al., 2021), and the increased hazardous substances load in influent develop a denser and thicker biofilm on the membrane surface and have a significant effect on the increase in mean thickness and the viability of the biofilm (Zheng et al., 2022).

Many methods have been developed to control biofilms on membrane surfaces. Extensive pretreatment has been applied to reduce biofouling, mainly by decreasing particulate and organic matter concentrations in the system (Nguyen et al., 2012). Enhancement of the backwashing and *in-situ* cleaning processes was also sought to detach or remove foulants from membrane surfaces. However, technologies to regulate microbial behaviors such as adhesion to the surface, secretion of extracellular polymeric substances, and built-up biofilm structures, for improving biofouling reduction, are still in their early stages. Recently, studies have reported the use of intermicrobial signaling materials as biofouling control strategies (Shahid et al., 2020; Wan et al., 2022; Song et al., 2023). The quorum sensing (QS) system is a communication system involved in the generation of *in vitro* metabolites of microbial cells and communities. Diffusible signal factors (DSF) are a signaling family used in QS systems (Papenfort and Bassler, 2016; Dow, 2017). The DSF family of signal substances are fatty acid-assisted compounds, such as *cis*-2-Decenoic acids (CDA), and regulate various functions of microbial communities, such as motility, enzyme production, EPS production, stress response, and antibacterial resistance (Marques et al., 2015). The regulation of DSF expression can be therefore used to control behavioral patterns of biofilm formation by microbial cells.

A second-messenger molecule, cyclic dimeric guanosine monophosphate (c-di-GMP), is the key factor in the transition from a motile planktonic lifestyle to fixed biofilm formation. Increasing intracellular c-di-GMP levels accelerates exopolysaccharide synthesis, which enhances the induction of biofilm formation and surface aggregation. Binding of DSF to the signal conversion component stimulates the c-di-GMP phosphodiesterase activity of the protein, and biofilm dispersion is induced because the intercellular c-di-GMP level is consequently lowered (Schmid et al., 2012; Suppiger et al., 2016). Biofilm dispersion occurs at the final stage of biofilm development, and microbial cells are released into the bulk liquid. The induction of dispersion is an important control measure for persistent biofilms in wastewater treatment, because dispersion is a mechanism by which bacteria escape overcrowding or unfavorable conditions, allowing fixed cells to migrate to bulk liquids (Davies and Marques, 2009).

Biofilms are composed of a matrix of microorganisms attached to a solid surface and EPS around the outer surface of the organisms (Costa et al., 2018; Karygianni et al., 2020). The EPS produced by microorganisms, regardless of the growth environment, performs several functions, such as stabilizing the biofilm structure and forming a protective barrier against stressed environments (Laspidou and Rittmann, 2002; Joo and Aggarwal, 2018). Loosely and tightly bound EPS produce a substantial filtration resistance, which is an important reason for membrane fouling in MBRs (Teng et al., 2020). The major constituents of EPS are polysaccharides and proteins. Polysaccharides determine the physical properties of biofilms because they contribute to their adhesion, cohesion, scaffolding, stability, intercellular bonding, and antimicrobial protection (Karygianni et al., 2014; Turnbull et al., 2016; Ogran et al., 2019; Reichhardt and Parsek, 2019). Proteins are another important component of the matrix and contribute to the structural stability of biofilms by promoting cell adhesion and aggregation between bacterial cells, leading to the development of designed cell clusters, that is, microcolonies (Drescher et al., 2016; Bowen et al., 2018; Duanis-Assaf et al., 2018). DSF, such as CDA, are responsible for inducing dispersion in microbial biofilms; therefore, increasing CDA concentration in the bulk yield variations in EPS compositions and structures of microbial biofilms (Marques et al., 2014; Sepehr et al., 2014).

The degree of dispersion was examined by measuring the optical density of released cells, microscopic observation of disaggregation of microcolonies, and quantification of dye colorization in a microtiter dish assay (Sepehr et al., 2014; Rahmani-Badi et al., 2015). In addition, three-dimensional image analysis using confocal laser scanning microscopy has been utilized in numerous studies as it provides a visualization of the structure of biofilm and quantitative values of biofilm structure factors such as total biomass, surface-to-biovolume ratio (SBR), mean thickness, and roughness using a specific software of the CLSM image analysis program. However, the degree of dispersion varies greatly with the experimental conditions, making it difficult to evaluate the effects of control technologies for biofouling reduction and determination of operational conditions in water processes.

The integrated index approach has been used in several applications, including risk assessment for drought and climate change, because this approach needs to integrate a wide range of relevant features, especially owing to complicated factors such as physical, social, and environmental elements (Sullivan et al., 2006; Chang et al., 2016). The climate vulnerability index (CVI) was developed using six potential variables: resource, access, capacity, use, environment, and geospatial components. One of the component, for instance, environment included livestock and human population density, loss of habitats, and flood frequency; which provided insights into the vulnerability situation in many different cases. This integrated index approach seemed proper to assess the degree of biofilm dispersion (that is dispersion index, DI) since various factors such as roughness, water channel structure and biomass were related to determine dispersive properties of biofilm.

In this study, the control of microbial dispersion by DSF was examined to determine the possibility of biofouling inhibition technology in the MBR operation of wastewater treatment processes. Previous studies have examined the dispersion induction of strains in dental plaque and biofilms from a variety of single strains, such as *P. aeruginosa* and *P. mirabilis*, by CDA addition (Davies and Marques, 2009; Rahmani-Badi et al., 2015). However, few attempts have been made to apply the DSF system to control biofilms in membrane bioreactors for wastewater treatment, where

Abbreviations: BSA, Bovine serum albumin; CDA, *cis*-2-Decenoic acid; CDC biofilm reactor, Center for Disease Control biofilm reactor; c-di-GMP, cyclic dimeric guanosine monophosphate; CLSM, Confocal laser scanning microscope; CVI, Climate vulnerability index; DI, Dispersion index; DSF, Diffusible signal factors; EPS, Extracellular polymeric substance; MBR, Membrane bioreactor; OD, Optical density; PVDF, Polyvinylidene fluoride; QS, Quorum sensing; SBR, Surface-to-biovolume ratio.

heterogeneous strains work together to degrade organic matter in water. This study aimed to develop a biofouling abatement technology by interfering with the expression of the QS system by adding CDA, which controls the c-di-GMP level in the DSF system. The effects of CDA addition on strains extracted from MBR sludge, in addition to *Pseudomonas aeruginosa* PAO1, were investigated, focusing on the variation in EPS composition. The degree of dispersion was examined using the optical density of released cells, three-dimensional image CLSM, and changes in polysaccharides and proteins of EPS. In addition, the DI was introduced as a useful tool for comparing numerous inhibitory technologies for dispersion effects.

# 2. Materials and methods

## 2.1. Bacterial strains and growth conditions

*Pseudomonas aeruginosa* PAO1 was selected as the single pure culture for biofilm formation. A mixed culture of six strains was used to extend the understanding of the effects of CDA addition to heterogeneous microbial cultures. Six strains were extracted from the MBR sludge: *Pseudomonas aeruginosa* PAO1, *Pseudomonas aeruginosa* PA14, *Pseudomonas aeruginosa* 15422, *Aeromonas hydrophila* 11163, *Escherichia coli*, and *Streptococcus* sp. Some strains were also identified in a previous study from this laboratory. Lade et al. (2014) reported that 12 isolates, including *Aeromonas, Enterobacter*, *Serratia, Leclercia*, *Pseudomonas*, *Klebsiella*, *Raoultella*, and *Citrobacter*, were recognized by a nucleotide BLAST analysis of the 16SrRNA gene sequence from QS signal-producing bacterial isolates in a domestic wastewater treatment plant. The isolated strains were stored below −65°C. Before the experiment, each strain was inoculated into 2.5% LB broth (Difco BD, Franklin Lakes, NJ, United States) and used after 24 h incubation at 28–30°C.

## 2.2. Antibacterial activity of CDA

The minimum inhibitory concentration test was conducted to investigate the effect of CDA on microbial growth. The CDA (≥95.0% HPLC grade) was purchased from Sigma-Aldrich (St. Louis, MO, USA). CDA doses ranged from 0 to 1,000 nM. The maximum dose was chosen based on the results of a study by Jennings et al. (2012), in which a concentration higher than one μM exhibited microbial growth. In addition, the fact that the CDA concentration found in the supernatant of the inoculated PAO1 culture was at nanomolar concentrations was considered (Davies and Marques, 2009). The MIC test procedure is briefly explained as follows: A growth culture of *P. aeruginosa* (incubated for 24 h at 37°C) was prepared in LB broth. Ethanol (10%) was used as a carrier for CDA samples. A CDA solution of 1 mg/mL was diluted to different concentrations of 10, 50, 100, 200, 500, and 1,000 nM in Mueller-Hinton broth. Each solution (1800 μL) was placed in a 24-well culture plate, and 200 μL of the bacterial suspension was injected. After 24 h of incubation at 37°C, bacterial growth was evaluated by adding 200 μL of the colorimetric indicator of 2, 3, 5-triphenyltetrazolium chloride (TTC; Sigma-Aldrich, St. Louis, MO, USA) at a concentration of 5 mg/mL in each well. Thereafter, the plates were incubated again for 1 h at 37°C, and the intensity of coloration was observed.

## 2.3. Biofilm dispersion assay

The biofilm was grown on a petri dish and the optical density (OD) of the suspension in the petri dish was measured to evaluate biofilm dispersion, since dispersed cells were released into the bulk liquid. The biofilm was grown on a Petri dish by changing the medium every 24 h, which is a semi-batch culture method. After overnight incubation, the culture was diluted with 15 mL of the growth medium, inoculated into a sterile Petri dish, and incubated at 30°C on a shaker at a mixing speed of 30 rpm. The medium was changed every 24 h for three days. On the third day after the last change in the medium, the cells were incubated for approximately 1 h and then replaced with fresh medium containing CDA. Microbial cells were incubated for an additional hour and the medium containing the dispersed cells was separated by sonication for 30 s. CDA concentrations of 100, 200, and 300 nM were used. The cell density in the suspension was determined by measuring OD600 using a UV/VIS spectrophotometer (DR6000, Hach Co., United States). The biofilm dispersion assay was repeated three times for each concentration. The carrier control containing medium plus 10% ethanol was also evaluated in parallel.

## 2.4. Operation of Center for Disease Control (CDC) biofilm reactor

The effect of CDA concentration on biofilm formation was investigated using a Center for Disease Control (CDC) biofilm reactor (BioSurface Technologies Corp., Bozeman, MT, United States). The CDC reactors, a reservoir for medium, polypropylene coupon holders, magnetic bars, and tubes were autoclaved at 121°C for 20 min prior to conducting the experiments for biofilm formation. A commercial microfiltration flat membrane (Merck Millipore, Darmstadt, Germany) composed of polyvinylidene fluoride (PVDF) was purchased. The membrane with a pore size of 0.22 μm was cut into 1.5 cm x 1.5 cm pieces and sterilized using 40% ethanol, followed by UV light exposure for 1 h. The membrane specimen was then fixed on one side of the coupon holder using a double-sided cellophane tape. Two specimens were attached to a coupon rod, and eight rods were attached to the CDC reactor. The CDC reactor was operated at 150 rpm for 24 h. All processes were conducted on a clean bench.

Microbial strains were prepared as follows. The PAO1 culture or the multi-strains were incubated in 2.5% LB broth and filled in the CDC reactors at a concentration of $10^6$–$10^7$ CFU/mL. Then, the CDA concentration was determined as 100 nM, 200 nM, and 300 nM by adding 6.8 μL, 13.6 μL, and 20.4 μL of l mg/mL CDA solution (w/10% ethanol), respectively. The total volume of the mixture was 400 mL. A CDC reactor, as a blank control, was also operated under the same conditions without adding CDA. After 24 h of operation, the membranes were removed for EPS and optical imaging analyses.

## 2.5. Extraction and measurement of extracellular polymeric substance (EPS)

EPS formed on the membrane surface was extracted using a thermal method. The membrane was carefully removed from the CDC rod and the residue was washed with 20 mL of 0.9% NaCl solution. After washing, the membrane was transferred to a conical

tube containing 15 mL of 0.9% NaCl solution, vortexed for 5 min, and sonicated for 60 min (B5510; Branson Ultrasonics, United States). The membrane was then removed from the solution and centrifuged (5,000 × g, 20 min, 4°C) to extract the biofilm. After centrifugation, the supernatant was removed to obtain the biofilm fraction. After adding the same liquid amount of 0.9% NaCl solution, it was heated in a drying oven at 100°C for 60 min and then cooled to room temperature. After centrifugation (5,000 × g, 20 min, 4°C), the supernatant was removed and filtered with a 0.45 μm syringe filter, and the filtrate was collected. EPS is defined as the sum of proteins and polysaccharides.

The proteins were quantified using the Bradford method. Briefly, a standard curve was obtained using several concentrations of bovine serum albumin (BSA). Standard solutions were prepared by diluting a stock solution with 2 mg/mL BSA in the range 0–10 μg/mL, and the absorbance was analyzed for protein quantification. Each sample and 1 mL of protein dye were placed in a microcuvette and allowed to stand for 10 min. The absorbance was measured at 595 nm. The protein contents of the samples were calculated from the absorbance data of the standard solutions. The protein contents of the samples were calculated from the absorbance data of the standard solutions. The regression curve was obtained as $y = 0.0602x + 0.0031$, $r^2 = 0.9971$. A Protein Assay Kit (BR500, Bio-Rad, United States) was used to analyze the BSA solutions and dye. A Genesys 10 UV/vis spectrophotometer (Thermo Scientific, USA) was used for absorbance measurements. The amount of polysaccharides was measured using a TOC analyzer (SIEVERS 5310C, GE, Australia). The amount of EPS was then divided by the area of the membrane specimens.

## 2.6. Bacterial strains and growth conditions

Confocal laser scanning microscopy (CLSM) analysis was performed to observe biofilms on membrane surfaces. The experimental methods have been described by Lade et al. (2017). Briefly, the detached membranes were dyed for 30 min with 200 μL SYTO 9 (Molecular Probes, Eugene, OR, USA) and wrapped in aluminum foil to block light. Excess stain was carefully washed with deionized sterile water, and the membranes were mounted on glass slides (covered with a coverslip). Microscopic observation and image acquisition were performed on stained membranes using confocal laser scanning microscopy (LSM 710, ZEISS, Germany). The membrane surface was observed at 20 × magnification using CLSM. The observed area was 1,024 × 1,024 μm$^2$, with a resolution of 1,024 × 1,024 pixels. The biofilm structure was quantified from the confocal stack using COMSTAT image analysis software. In this study, the biofilm differences generated under each condition were determined using the four COMSTAT parameters. These parameters were the total biomass, surface-to-biovolume ratio (SBR), mean thickness, and roughness coefficient.

The roughness coefficient ($R_a$) indicates variability in the measured biofilm thickness (Murga et al., 1995). The formula for calculating is as follows:

$$R_a^* = \frac{1}{N}\sum_{i=1}^{N}\frac{\left|L_{fi} - \overline{L_f}\right|}{\overline{L_f}}$$

where $L_{fi}$ is the i-th measured individual thickness, $L_f$ is the average thickness, and N is the number of thickness measurements.

## 2.7. Determination of dispersion index (DI)

An integrated index approach has been adapted to assess the degree of biofilm dispersion in this study. The integrated index was developed to describe a wide range of relevant features on establishment of dispersive biofilm. The experimental factors, including cell density, EPS, total biomass, SBR, thickness, and roughness, were examined to represent biofilm dispersion, and the relevant factors were used to calculate the DI of the biofilm.

The correlation of several factors, such as structural properties, was considered for selecting appropriate variables for inclusion in the DI framework. The variables for DI included OD values and two biofilm structural factors from COMSTAT analyses, that is, SBR and roughness. The value of DI was calculated as a weighted average of all components, as shown below, for which the equation in Sullivan et al. (2006) was followed.

$$DI = \frac{ro * O.D + rs * SBR + rr * Roughness}{ro + rs + rr}$$

where the weight given for each component is determined by a factor r representing the relevance of the component. Factor r (i.e., ro, rs and rr) was obtained by fitting the DI and EPS concentrations to obtain the greatest R-squared value, which represents the strength of the correlation between the independent and dependent variables. The R-squared value was 0.9326, which indicated that DI was well correlated with the EPS concentration.

## 2.8. Statistical analysis

Biofilm dispersion was statistically analyzed using Microsoft Excel software (Microsoft, Redmond, WA, United States). The data shown represents the mean values obtained from three independent experiments, with error bars indicating the corresponding standard deviations. Biofilm dispersion induced by the addition of CDA was evaluated in terms of the Statistical significance. $p$ value <0.05 is considered statistically significant.

# 3. Results and discussion

## 3.1. Effects of CDA addition on dispersal and EPS concentrations in biofilm

The dispersion was evaluated by measuring OD at 600 nm; the results are shown in Figure 1. The OD values ($n = 3$) of the blank experiment with the PAO1 strain and without the addition were 0.357 ± 0.017, as shown in Figure 1A. Compared with the control experiment, the OD values increased with CDA addition. An OD value of 0.490 ± 0.016 was observed at a CDA concentration of 300 nM. The results indicate the occurrence of an increase in planktonic cell populations, probably owing to the release of microbial cells from the biofilm to the bulk liquid when CDA was added to the

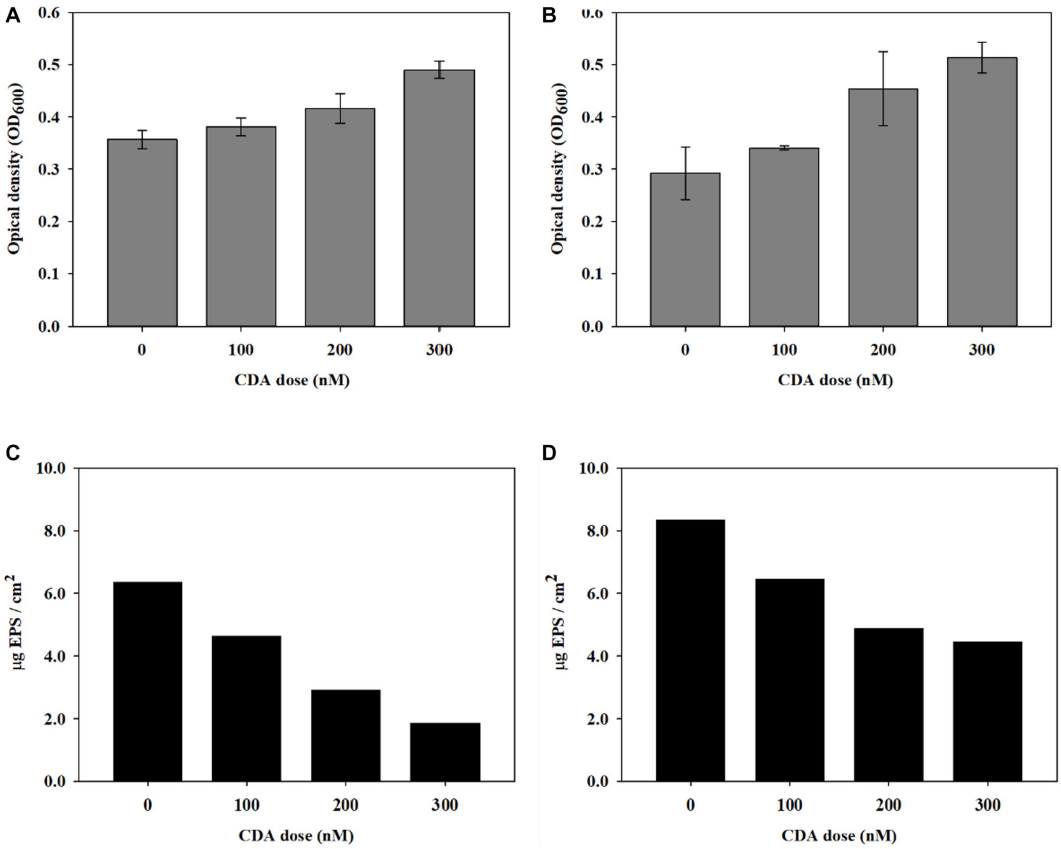


FIGURE 1
Induction of biofilm dispersal by CDA addition on **(A)** PAO1 and **(B)** multi-strains ($n = 3$) and variations in EPS concentration on biofilms by **(C)** PAO1 and **(D)** multi-strains.

PAO1 strain. The OD values of the multi-strain experiments are shown in Figure 1B. Also, OD values ($n = 3$) increased with increasing CDA concentrations. The OD value was $0.292 \pm 0.050$ in the experiment without CDA, $0.381 \pm 0.017$ with 100 nM CDA, $0.416 \pm 0.028$ with 200 nM CDA, and $0.490 \pm 0.017$ with 300 nM CDA. The variation in the OD values with increasing CDA was relatively large in the multi-strain experiments. The statistical analysis between the application and non-application of CDA revealed significant differences in both the PAO1 and multi-strain experiments, with $p$-values of 0.042 and 0.011, respectively. Davies and Marques (2009) showed the effects of dispersion of different bacterial biofilms, including PAO1, by CDA using a microtiter plate dispersion bioassay with a 4-day cultivation. The results indicated an increase in released cells (evaluated with OD570) with 10 nM CDA dose for the experimented bacteria such that the dispersion efficacy reached 24.6%. The authors suggested further studies on biofilms with multiple species and the impacts of the degradation of extracellular polymers produced by neighboring microorganisms of other species. In contrast to passive detachment, dispersion is an active process, involving a coordinated response to changes in the surrounding environment and requiring the contribution of cell-to-cell signals (Light, 2017). The higher OD values were detected from PAO1 strain. The high OD was due to numerous factors including debris materials and interference of biomolecules. The changes in OD values with CDA doses were greater in the multiple strains, which may indicate that effective dispersion was achieved by CDA addition, in part, because a variety of microbial cells were involved, demonstrating that induction of dispersion might be a useful technology for biofouling reduction in systems with numerous bacterial consortia, such as an MBR for wastewater treatment.

To understand whether the QS compound affected the biofilm composition in addition to dispersal behavior, the EPS concentration of the biofilm was evaluated with CDA addition. CDC reactors were operated to obtain sufficient biofilms for EPS analysis. The variation in EPS concentrations with different CDA concentrations of 100, 200, and 300 nM are presented for PAO1 in Figures 1C,D for multi-strains. The EPS content of the PAO1 biofilm without CDA was 6.37 μg EPS/cm$^2$. The EPS of the PAO1 biofilm decreased to 4.64, 2.93, and 1.87 μg EPS/cm$^2$ by adding 100 nM, 200 nM, and 300 nM of CDA, respectively. The variations in EPS concentrations of the biofilm formed by multi-stain showed a trend similar to that of PAO1. The total EPS of the biofilm without CDA was 8.34 μg EPS/cm$^2$ and decreased to 6.46, 4.90, and 4.47 μg EPS/cm$^2$ by adding 100 nM, 200 nM, and 300 nM of CDA, respectively. The EPS declined by 46% at a CDA dose of 300 nM.

Several studies have shown that fatty acid signaling molecules, including CDA, are responsible for inducing biofilm dispersion in a range of gram-negative and gram-positive bacteria (Davies and Marques, 2009; Sepehr et al., 2014; Kumar et al., 2020). They discussed that a variety of saturated and unsaturated fatty acids act as inhibitors

TABLE 1 Polysaccharide and protein concentrations in the biofilm formed by PAO1 and multi-strains.

| CDA doses (nmol/L) | | 0 | 100 | 200 | 300 |
|---|---|---|---|---|---|
| PAO1 | Polysaccharide (μg C/cm$^2$) | 3.61 | 2.61 | 2.18 | 1.42 |
| | Protein (μg BSA/cm$^2$) | 2.75 | 2.03 | 0.75 | 0.46 |
| Multi-strains | Polysaccharide (μg C/cm$^2$) | 4.90 | 4.62 | 4.05 | 3.81 |
| | Protein (μg BSA/cm$^2$) | 3.44 | 1.83 | 0.85 | 0.65 |

of bacterial colonization and biofilm development by affecting the adhering surface, changing cell membrane fluidity, reducing EPS, and modulating QS systems (Kumar et al., 2020). However, the exact mechanisms and important factors that determine the dispersive effects during biofilm development, including the amount and characteristics of EPS, have been poorly established. The measured EPS concentrations of biofilms from PAO1 and multiple strains shown in Figures 1C,D quantitatively revealed that the injection of CDA lowered the amount of EPS in biofilms. Polymeric substances adhere to the membrane surface, block pores in the membrane, and affect cake layer properties, resulting in severe membrane fouling (Teng et al., 2020). Changes in biofilm composition modulate the characteristics of biofilms, such as persistence to shear force and resistance to antibacterial chemicals, which enhance efficiencies in backwash and other cleaning procedures for MBR operation.

The EPS concentration in the biofilm formed by the multi-strain mixture showed relatively high values compared with that of the PAO1 single strain, regardless of the CDA doses, indicating that coordinated patterns of behavior inside biofilms by polymicrobial cells increased interactions and synergic effects between microorganisms; this was related to improvement in tolerance, persistence, and EPS production of the biofilm (DeLeon et al., 2014; Song et al., 2018). The extent of EPS decrease by CDA addition was also lower in the biofilm with multiple strains than that in the PAO1 strain. The formation of biofilms provided a protective barrier against stressed environments; thus, the high concentrations of EPS in the biofilms with multiple strains probably hindered the effects of CDA addition, including dispersion, and vice versa. Understanding the EPS characteristics is necessary for evaluating the effects of CDA addition on biofilm modulation.

## 3.2. Variation in protein and polysaccharide of EPS by CDA addition

EPS is known to be a medium that allows the aggregation of microorganisms and stable proximity of bacteria, thus producing biofilms (Laspidou and Rittmann, 2002; Joo and Aggarwal, 2018). The major components of EPS are polysaccharides and proteins. In general, proteins participate in stabilizing the aggregate structures of biofilms and in the digestion of macromolecules and particular compounds in the surrounding microbial cells (Ryu et al., 2021). Proteins contain high amounts of negatively charged amino acids, and are thus involved in electrostatic bonds with multivalent cations. Laspidou and Rittmann (2002) also indicated that extracellular proteins act as enzymes for the digestion of macromolecules and particulate materials in the microenvironment surrounding biofilms.

The variations in the relative compositions of proteins and polysaccharides in the EPS are summarized in Table 1 and Figure 2. The polysaccharide content in the PAO1 biofilm decreased as the concentration of CDA increased, corresponding to a decrease in the total EPS. The polysaccharide amount of the PAO1 biofilm without CDA was 3.61 μg C/cm$^2$ and decreased to 2.61, 2.18, and 1.42 μg C/cm$^2$ by adding 100 nM, 200 nM and 300 nM of CDA, respectively. Protein levels also showed a decreasing pattern with increasing CDA concentrations in the PAO1 biofilm. At a dose of 300 nM, protein was detected at 0.46 μg BSA/ cm$^2$ in the PAO1 biofilm and 2.75 μg BSA/ cm$^2$ in the control sample. As in the PAO1 biofilm, polysaccharide concentrations in the multi-strain biofilm decreased with increasing CDA doses. However, the extent of polysaccharide reduction was rather dampened; as such, the reduction rate of multi-strain biofilm was only 22%, while that of PAO1 biofilm was approximately 61% at a CDA dose of 300 nM. Compared with the polysaccharide, changes in protein content in the multi-strain biofilm were remarkable, as over 80% of reduction was observed at the CDA dose of 300 nM. In PAO1 biofilm, the protein content in the total EPS was 43% at 0 nM CDA dose and declined to 24% at 300 nM. The protein content of the multi-strain biofilm without CDA was 3.44 μg BSA/cm$^2$ and decreased to 1.83, 0.85, and 0.65 μg C/cm$^2$ when 100 nM, 200 nM and 300 nM of CDA were added, respectively. In multi-strain biofilm, the relative content of protein in the total EPS was 41% at CDA dose of 0 nM and decreased to 15% at 300 nM. Compared with the PAO1 biofilm, the reduction in protein in the multi-strain biofilm was considerably more extraordinary.

Dispersion involves an active and organized response of microorganisms to changes in the surrounding environment, requiring cell-to-cell communication. To escape the protective EPS matrix in biofilms, cells secrete degrading enzymes such as proteases, lipases, and lyases (Light, 2017). Enzymatic degradation may be a major factor when the strong gel types of adhesive, which anchor microbial cells in the biofilm, are dissolved, leading to a rapid loss of biofilm integrity (Laspidou and Rittmann, 2002). Dispersed cells are distinct in terms of protein production from biofilms and planktonic cells (Sauer et al., 2002). The study divided proteins into four general classes (Class I, II, III, IV, and V), depending on differential regulation during the course of biofilm development. Proteins encoded metabolic processes for adhesion and involved in various bio-synthesis reactions and molecular transport for bacterial extracellular solute-binding proteins, adaptation, and protection. However, the protein types differed significantly at each stage of biofilm development. In the final stage of biofilm development, the dispersion stage allows microbial cells to move back into the bulk liquid to gain better access to nutrients and to leave behind a shell-like structure. Ren et al. (2016) investigated the ratio of proteins and polysaccharides in EPS in a moving-bed biofilm reactor. Depending on the operational temperature, the protein ratio was between 40–60%. Ryu et al. (2021) examined EPS concentrations of mixed liquor in an MBR and demonstrated that, regardless of substrate biodegradability, the fraction of polysaccharide in the bulk

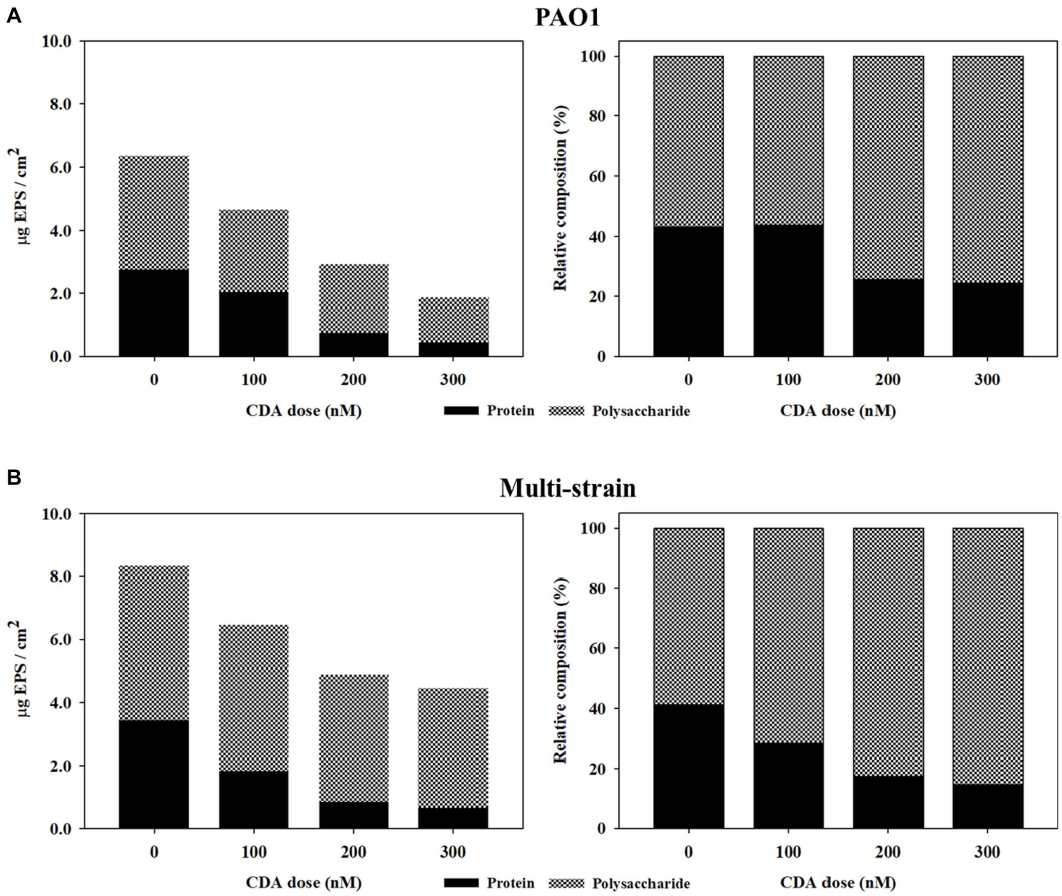


FIGURE 2
Effects of CDA addition regarding variations in relative compositions of protein and polysaccharide in EPS of biofilms formed by **(A)** PAO1 and **(B)** multi-strains.

was greater than 84%. Sauer et al. (2002) also mentioned that the protein properties in the dispersion stage biofilms were closer to the properties of planktonic bacteria than those of biofilms in the maturation stage, in which a single strain, such as PAO1 or *Pseudomonas putida*, was used to build biofilms. Biofilm dispersion can be influenced not only by the degradation of polysaccharide matrix but also by changes in the protein composition within the biofilm structure (Guilhen et al., 2017). The results of our study indicated that the addition of CDA in the MBR process has the potential to regulate the cell-to-cell signals of multi-strains, resulting in changes in the concentrations and characteristics of proteins within the biofilm. This leads to a significant decrease in the protein fraction, potentially increasing biofilm dispersion.

## 3.3. Variations in biofilm structures by CDA addition

Numerous studies have visualized clustering patterns or particular shapes of biofilm structures in specific biofilm development stages using CLSM images (Karygianni et al., 2014; Hartmann et al., 2021). CLSM analyses were also conducted in this study to observe the biofilm structures of PAO1 and multiple strains by adding CDA, as shown in Figure 3. Several physical properties, such as roughness and thickness, were obtained from the quantification analysis of the CLSM images, as presented in Table 2.

The left-hand side images are from the PAO1 biofilm (Figure 3A), and the right-hand side images are from the multi-strain biofilm (Figure 3B). The image from PAO1 without CDA addition displayed a large amount of green color on the membrane surface, which covered the entire surface of the membrane after 24 h of incubation. Substantial amounts of PAO1 biofilm were clearly visible with a significant green fluorescence intensity in the CLSM image of the membrane. As shown in Figure 3A, the intensity of the green fluorescence of the PAO1 biofilm decreased gradually with increasing CDA concentration. The decrease in green color intensity with CDA doses indicate that extensive amounts of cells fled from the biofilm to the bulk liquid. Previous studies have also shown that shell-like structures with hollow centers and walls of chunks of bacteria were displayed during the dispersion stage because bacteria actively moved away from the interior portions of the cell cluster (Sauer et al., 2002; Marques et al., 2015).

The CLSM images for multi-strain biofilms showed a pattern similar to that of the PAO1 biofilm, such that the greatest intensity was observed in the biofilm without CDA dose and diminished with increasing CDA doses (Figure 3B). In addition, the multi-strain biofilm showed a relatively stronger intensity than the PAO1 biofilm at the same CDA dose, indicating that the multi-strain biofilm was more robust to CDA addition.

10.3389/fmicb.2023.1211761

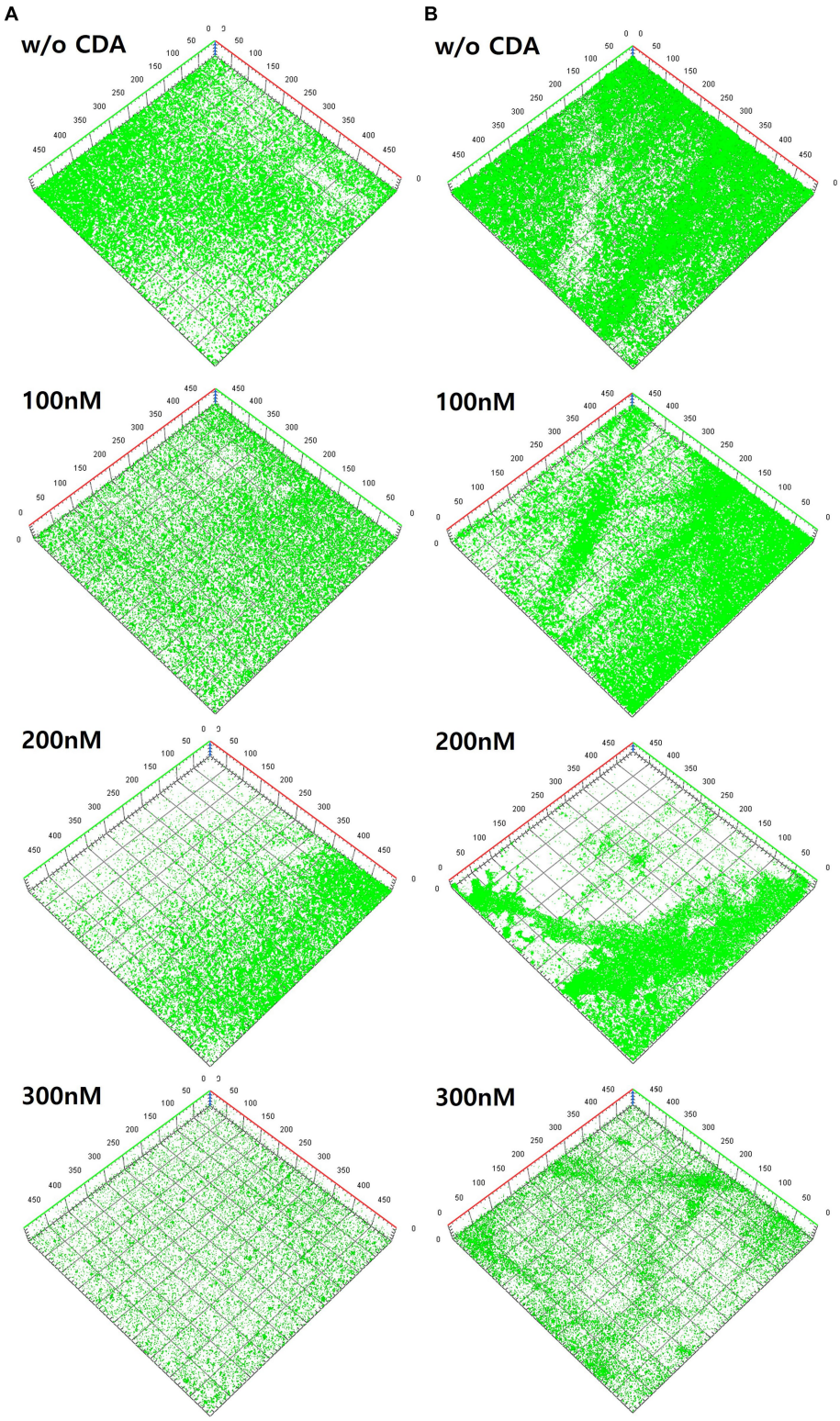


FIGURE 3
Variations of three-dimensional structures of biofilms by different CDA concentrations on **(A)** PAO1 biofilm and **(B)** multi-strains biofilm.

CLSM images were used to quantify factors such as total biomass, SBR, mean thickness, and roughness through the image quantitative analysis program, i.e., COMSTAT (An and Parsek, 2007; Reichhardt and Parsek, 2019). The total biomass ($\mu m^3/\mu m^2$) was obtained by multiplying the number of biomass pixels in all images by the unit volume of the pixel and dividing by the substratum area. The SBR reflects the fraction of the biofilm that is exposed to nutrient flow. For instance, the ratio supposedly

TABLE 2 Biofilm properties from COMSTAT analyses: effects of CDA on PAO1 and multi strain biofilms.

| PAO1 | Total biomass ($\mu m^3\ \mu m^{-2}$) | Surface to biovolume ratio ($\mu m^2\ \mu m^{-3}$) | Mean thickness ($\mu m$) | Roughness coefficient |
|---|---|---|---|---|
| 0 nM | 12.897 ± 3.661 | 5.476 ± 0.803 | 38.989 ± 1.877 | 0.005 ± 0.005 |
| 100 nM | 5.435 ± 4.319 | 8.701 ± 3.134 | 8.474 ± 6.020 | 0.374 ± 0.357 |
| 200 nM | 0.109 ± 0.010 | 18.174 ± 0.108 | 1.170 ± 0.063 | 1.967 ± 0.026 |
| 300 nM | 0.044 ± 0.021 | 19.300 ± 0.397 | 1.003 ± 0.045 | 1.993 ± 0.007 |
| Multi-strains | Total biomass ($\mu m^3\ \mu m^{-2}$) | Surface to biovolume ratio ($\mu m^2\ \mu m^{-3}$) | Mean thickness ($\mu m$) | Roughness coefficient |
| 0 nM | 26.071 ± 2.980 | 4.237 ± 0.283 | 43.914 ± 0.679 | 0.002 ± 0.004 |
| 100 nM | 17.933 ± 0.961 | 5.507 ± 0.489 | 27.977 ± 2.390 | 0.034 ± 0.048 |
| 200 nM | 7.619 ± 1.876 | 6.397 ± 1.163 | 12.077 ± 1.073 | 0.051 ± 0.037 |
| 300 nM | 0.441 ± 0.500 | 16.373 ± 2.929 | 11.433 ± 5.535 | 0.066 ± 0.032 |

increases with a low nutrient concentration to optimize access to nutrient supply (Heydorn et al., 2000). The values calculated from the COMSTAT program were useful for quantitatively examining the biofilm matrix as well as the amount of adherent biomass (Reichhardt and Parsek, 2019). The biofilm properties obtained from COMSTAT analyses in this study are presented in Table 2. As the CDA doses were increased, total biomass and mean thickness decreased while SBR and roughness coefficient increased for both PAO1 and multi-strain biofilms. The extent of variation at different CDA doses was greater in the PAO1 biofilm than the polymicrobial biofilm from the six strains extracted from the MBR sludge.

In the operating condition without CDA, the total biomass of PAO1 was 12.897 $\mu m^3/\mu m^2$, but when CDA was dosed at 300 nM, it decreased considerably to 0.044 $\mu m^3/\mu m^2$. The reduction of total biomass by CDA dosing corresponded increasing SBR. A CDA dose of 300 nM on the PAO1 biofilm increased the SBR by approximately 3.5 times (i.e., 19.300 $\mu m^2/\mu m^3$) from the SBR without CDA addition (i.e., 5.476 $\mu m^2/\mu m^3$). The mean thickness also decreased from 38.989 μm without CDA to 1.003 μm with 300 nM CDA in PAO1 biofilm. The roughness coefficient increased with increasing CDA dose. The addition of CDA to the PAO1 biofilm yielded not only a lower total biomass and thinner biofilm but also more pathways for nutrient flow and greater roughness in biofilm structures compared with those without CDA. The greater values of SBR and roughness with increasing CDA doses might indicate that biofilm development transferred to the dispersion stage; thus, nutrient flow relatively prevailed in the biofilm.

The decreasing or increasing trends of COMSTAT factors in the multi-strain biofilms with increasing CDA doses were the same as those in the PAO1 biofilm. Interestingly, percentage variations in the total biomass, SBR, and roughness of PAO1 biofilm were comparable to those in the multi-strain biofilms, such that the reduction in total biomass at the CDA dose of 300 nM was 99% for PAO1 biofilm and 98% for multi-strain biofilm. The greatest difference was shown with the thickness values: 97.4% in the PAO1 biofilm and 73.9% in the multi-strain biofilm at a dose of 300 nM. The diversity of the mixture of species probably increased the complex patterns of behavior inside the biofilm. The characteristics of polymicrobial biofilms demonstrate that the interactions and synergy of multiple microorganisms affect growth, persistence of biofilm, production of EPS, and biofilm structures (Mastropaolo et al., 2005; Burmølle et al., 2006; DeLeon et al., 2014).

The addition of CDA to PAO1 and multiple strains evidently lowered the green color intensities in biofilms and affected the structural properties of biofilms, indicating an increase in the dispersive characteristics of the biofilm, such as SBR and roughness. Quantifying the degree of biofilm dispersion is necessary for developing strategies for enhancing biofilm dispersion by adding CDA.

## 3.4. Correlation of biofilm dispersion using an integrated index approach

The application of CDA induced biofilm dispersion (measured by OD values in this study), which resulted in an EPS reduction on the membrane surface (Figure 1). Each factor was correlated with EPS, as shown in Figure 4. Cell dispersal was inversely correlated with EPS concentrations, since dispersive biofilm showed a low concentration of EPS, which was similar to that of bulk liquid. The SBR and roughness also followed the same inverse trend as cell dispersal, whereas total biomass and thickness showed positive correlations with EPS, which was opposite to the trend of OD values.

The degree of biofilm dispersion was proposed to be assessed with the integrated index approach, which was designated as DI for the biofilm. The DI with CDA doses for PAO1 and multi-strain biofilms is shown in Figure 5. The DI increased proportionally with increasing CDA dose, corresponding to the experimental results from the dispersal assay. The DI values also revealed that the PAO1 biofilm was more dispersive than the multi-strain biofilm, which is also consistent with the complexity of the polymicrobial biofilm characteristics. The measurement of EPS, dispersal assays, and COMSTAT analyses are common analytical tools for biofilm studies, and these results were conveniently applied for calculating DI, which provided a quantitative number of biofilm dispersions.

The R-squared ($R^2$) of DI values were 0.959 with PAO1 strain and 0.978 with multi-strains. The biofilm formation affected by various factors including a composition of microbial species like single or multiple strains and the surrounding environment like presences of chemicals or signaling compounds. The resulting properties such as roughness and surface to biovolume were also varied significantly corresponding to the complexity of biofilm. The $R^2$ was used to evaluate representatives of dispersion index values on effects of CDA addition on the PAO1 and multiple strain biofilms. The correlation could be clearly evaluated by multiple CDA dosage.

The integrated index approach adapted to assess the degree of biofilm dispersion was effective to evaluate the effects of CDA

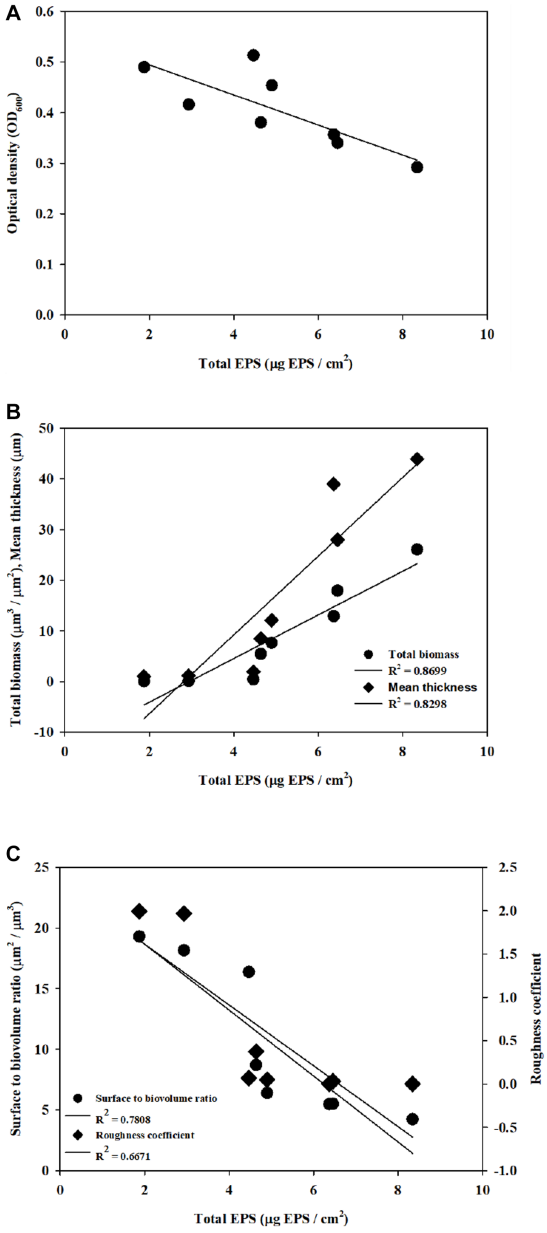


FIGURE 4
Correlation of structural properties and dispersal with EPS was obtained with **(A)** cell density, **(B)** total biomass and thickness, and **(C)** SBR and roughness.

on controlling biofilm structures. The proposed DI would be useful for assessing the degree of dispersion of biofilms; thus, the effects of CDA doses on other biofilms could be compared with DI values, or the effects of biofouling control practices, such as backwashing, could be evaluated with DI values for better cleaning methods.

## 4. Conclusion

The results of this study demonstrated that compared with the polysaccharide fraction, the protein fraction of the total EPS decreased noticeably with increasing CDA doses, implying that adding CDA possibly modified characteristics such as structural stability, cell adhesion, and cell aggregation for dispersive biofilm. The CDA addition yielded biofilms with less total biomass, thinner depth, more pathways for nutrient flow, and rougher structures, compared with those without CDA. Biofilm dispersion was quantified using the DI, and it was useful for comparing biofouling control methods such as backwashing with CDA to determine the most effective cleaning methods. To effectively apply CDA as an advanced biofouling control technology, further research is necessary to evaluate its economic feasibility for practical implementation, explore various application approaches, and conduct ongoing assessments through long-term operation to ensure sustained effectiveness.

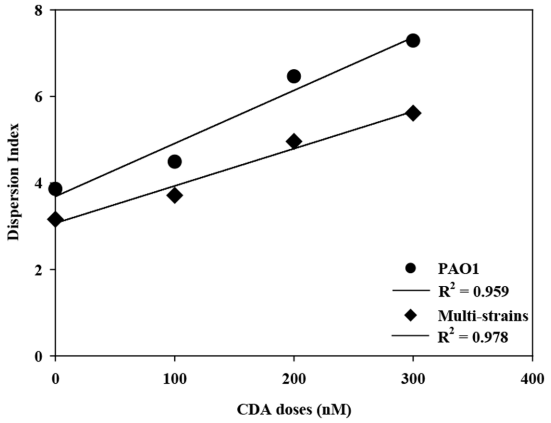


FIGURE 5
Correlation of DI with increasing CDA doses for PAO1 and multi-strain biofilms.

## Data availability statement

The original contributions presented in the study are included in the article/supplementary material, further inquiries can be directed to the corresponding author.

## Author contributions

WS: conceptualization, writing – original draft preparation, investigation, and validation. JR and JJ: validation. YY and SC: investigation. JK: conceptualization, writing – review and editing, project administration. All authors contributed to the article and approved the submitted version.

## Funding

This work was supported by a National Research Foundation of Korea (NRF) grant, funded by the Korean government (MSIT) (no. NRF-2021R1A2C2014255).

## Conflict of interest

JJ was employed by HANSU Technical Service Ltd., Republic of Korea.

The remaining authors declare that the research was conducted in the absence of any commercial or financial relationships that could be construed as a potential conflict of interest.

## Publisher's note



## References

An, D., and Parsek, M. R. (2007). The promise and peril of transcriptional profiling in biofilm communities. *Curr. Opin. Microbiol.* 10, 292–296. doi: 10.1016/j.mib.2007.05.011

Bowen, W. H., Burne, R. A., Wu, H., and Koo, H. (2018). Oral biofilms: pathogens, matrix, and polymicrobial interactions in microenvironments. *Trends Microbiol.* 26, 229–242. doi: 10.1016/j.tim.2017.09.008

Burmølle, M., Webb, J. S., Rao, D., Hansen, L. H., Sørensen, S. J., and Kjelleberg, S. (2006). Enhanced biofilm formation and increased resistance to antimicrobial agents and bacterial invasion are caused by synergistic interactions in multispecies biofilms. *Appl. Environ. Microbiol.* 72, 3916–3923. doi: 10.1128/AEM.03022-05

Chang, J., Li, Y., Wang, Y., and Yuan, M. (2016). Copula-based drought risk assessment combined with an integrated index in the Wei River basin. *China. J. Hydrol.* 540, 824–834. doi: 10.1016/j.jhydrol.2016.06.064

Costa, O. Y., Raaijmakers, J. M., and Kuramae, E. E. (2018). Microbial extracellular polymeric substances: ecological function and impact on soil aggregation. *Front. Microbiol.* 9:1636. doi: 10.3389/fmicb.2018.01636

Davies, D. G., and Marques, C. N. (2009). A fatty acid messenger is responsible for inducing dispersion in microbial biofilms. *J. Bacteriol.* 191, 1393–1403. doi: 10.1128/JB.01214-08

DeLeon, S., Clinton, A., Fowler, H., Everett, J., Horswill, A. R., and Rumbaugh, K. P. (2014). Synergistic interactions of Pseudomonas aeruginosa and *Staphylococcus aureus* in an in vitro wound model. *Infect. Immun.* 82, 4718–4728. doi: 10.1128/IAI.02198-14

Dow, J. M. (2017). Diffusible signal factor-dependent quorum sensing in pathogenic bacteria and its exploitation for disease control. *J. Appl. Microbiol.* 122, 2–11. doi: 10.1111/jam.13307

Drescher, K., Dunkel, J., Nadell, C. D., Van Teeffelen, S., Grnja, I., Wingreen, N. S., et al. (2016). Architectural transitions in *Vibrio cholerae* biofilms at single-cell resolution. *Proc. Natl. Acad. Sci. U. S. A.* 113, E2066–E2072. doi: 10.1073/pnas.1601702113

Duanis-Assaf, D., Duanis-Assaf, T., Zeng, G., Meyer, R. L., Reches, M., Steinberg, D., et al. (2018). Cell wall associated protein TasA provides an initial binding component to extracellular polysaccharides in dual-species biofilm. *Sci. Rep.* 8, 1–10. doi: 10.1038/s41598-018-27548-1

Flemming, H. C. (2011). "Microbial biofouling: unsolved problems, insufficient approaches, and possible solutions" in *Biofilm highlights*, eds. F. Hans-Curt, W. Jost and S. Ulrich (Berlin, Heidelberg: Springer), 81–109. doi: 10.1007/978-3-642-19940-0_5

Gkotsis, P. K., Banti, D. C., Peleka, E. N., Zouboulis, A. I., and Samaras, P. E. (2014). Fouling issues in membrane bioreactors (MBRs) for wastewater treatment: major mechanisms, prevention and control strategies. *PRO* 2, 795–866. doi: 10.3390/pr2040795

Guilhen, C., Forestier, C., and Balestrino, D. (2017). Biofilm dispersal: multiple elaborate strategies for dissemination of bacteria with unique properties. *Mol. Microbiol.* 105, 188–210. doi: 10.1111/mmi.13698

Hartmann, R., Jeckel, H., Jelli, E., Singh, P. K., Vaidya, S., Bayer, M., et al. (2021). Quantitative image analysis of microbial communities with biofilm. *Nat. Microbiol.* 6, 151–156. doi: 10.1038/s41564-020-00817-4

Heydorn, A., Nielsen, A. T., Hentzer, M., Sternberg, C., Givskov, M., Ersbøll, B. K., et al. (2000). Quantification of biofilm structures by the novel computer program COMSTAT. *Microbiology* 146, 2395–2407. doi: 10.1099/00221287-146-10-2395

Jennings, J. A., Courtney, H. S., and Haggard, W. O. (2012). Cis-2-decenoic acid inhibits *S. aureus* growth and biofilm in vitro: a pilot study. *Clin. Orthop. Rel. Res.* 470, 2663–2670. doi: 10.1007/s11999-012-2388-2

Joo, S. H., and Aggarwal, S. (2018). Factors impacting the interactions of engineered nanoparticles with bacterial cells and biofilms: mechanistic insights and state of knowledge. *J. Environ. Manag.* 225, 62–74. doi: 10.1016/j.jenvman.2018.07.084

Karygianni, L., Ren, Z., Koo, H., and Thurnheer, T. (2020). Biofilm matrixome: Extracellular components in structured microbial communities. *Trends Microbiol.* 28, 668–681. doi: 10.1016/j.tim.2020.03.016

Karygianni, L., Ruf, S., Follo, M., Hellwig, E., Bucher, M., Anderson, A. C., et al. (2014). Novel broad-spectrum antimicrobial photoinactivation of in situ oral biofilms by visible light plus water-filtered infrared a. *Appl. Environ. Microbiol.* 80, 7324–7336. doi: 10.1128/AEM.02490-14

Kumar, P., Lee, J. H., Beyenal, H., and Lee, J. (2020). Fatty acids as antibiofilm and antivirulence agents. *Trends Microbiol.* 28, 753–768. doi: 10.1016/j.tim.2020.03.014

Lade, H., Paul, D., and Kweon, J. H. (2014). Isolation and molecular characterization of biofouling bacteria and profiling of quorum sensing signal molecules from membrane bioreactor activated sludge. *Int. J. Mol. Sci.* 15, 2255–2273. doi: 10.3390/ijms15022255

Lade, H., Song, W. J., Yu, Y. J., Ryu, J. H., Arthanareeswaran, G., and Kweon, J. H. (2017). Exploring the potential of curcumin for control of N-acyl homoserine lactone-mediated biofouling in membrane bioreactors for wastewater treatment. *RSC Adv.* 7, 16392–16400. doi: 10.1039/C6RA28032C

Laspidou, C. S., and Rittmann, B. E. (2002). A unified theory for extracellular polymeric substances, soluble microbial products, and active and inert biomass. *Water Res.* 36, 2711–2720. doi: 10.1016/S0043-1354(01)00413-4

Light, C. J. (2017) *Cis-2-Decenoic acid Signaling and dispersion in Pseudomonas aeruginosa: The role of dispersed cells in virulence and pathogenesis* State University of New York. Binghamton

Maletskyi, Z. (2020). Advances in membrane materials and processes for water and wastewater treatment. *In Multidisciplinary Advances in Efficient Separation Processes. American Chemical Society.* 3–35. doi: 10.1021/bk-2020-1348.ch001

Marques, C. N., Davies, D. G., and Sauer, K. (2015). Control of biofilms with the fatty acid signaling molecule cis-2-decenoic acid. *Pharmaceuticals* 8, 816–835. doi: 10.3390/ph8040816

Marques, C. N., Morozov, A., Planzos, P., and Zelaya, H. M. (2014). The fatty acid signaling molecule cis-2-decenoic acid increases metabolic activity and reverts persister cells to an antimicrobial-susceptible state. *Appl. Environ. Microbiol.* 80, 6976–6991. doi: 10.1128/AEM.01576-14

Mastropaolo, M. D., Evans, N. P., Byrnes, M. K., Stevens, A. M., Robertson, J. L., and Melville, S. B. (2005). Synergy in polymicrobial infections in a mouse model of type 2 diabetes. *Infect. Immun.* 73, 6055–6063. doi: 10.1128/IAI.73.9.6055-6063.2005

Murga, R., Stewart, P. S., and Daly, D. (1995). Quantitative analysis of biofilm thickness variability. *Biotechnol. Bioeng.* 45, 503–510. doi: 10.1002/bit.260450607

Nguyen, T., Roddick, F. A., and Fan, L. (2012). Biofouling of water treatment membranes: a review of the underlying causes, monitoring techniques and control measures. *Membranes* 2, 804–840. doi: 10.3390/membranes2040804

Obotey Ezugbe, E., and Rathilal, S. (2020). Membrane technologies in wastewater treatment: a review. *Membranes* 10:89. doi: 10.3390/membranes10050089

Ogran, A., Yardeni, E. H., Keren-Paz, A., Bucher, T., Jain, R., Gilhar, O., et al. (2019). The plant host induces antibiotic production to select the most-beneficial colonizers. *Appl. Environ. Microbiol.* 85, e00512–e00519. doi: 10.1128/AEM.00512-19

Papenfort, K., and Bassler, B. L. (2016). Quorum sensing signal–response systems in gram-negative bacteria. *Nat. Rev. Microbiol.* 14:576. doi: 10.1038/nrmicro.2016.89

Rahmani-Badi, A., Sepehr, S., Fallahi, H., and Heidari-Keshel, S. (2015). Dissection of the cis-2-decenoic acid signaling network in *Pseudomonas aeruginosa* using microarray technique. *Front. Microbiol.* 6:383. doi: 10.3389/fmicb.2015.00383

Reichhardt, C., and Parsek, M. R. (2019). Confocal laser scanning microscopy for analysis of *Pseudomonas aeruginosa* biofilm architecture and matrix localization. *Front. Microbiol.* 10:677. doi: 10.3389/fmicb.2019.00677

Ren, B., Young, B., Variola, F., and Delatolla, R. (2016). Protein to polysaccharide ratio in EPS as an indicator of non-optimized operation of tertiary nitrifying MBBR. *Water Qual. Res. J. Canada.* 51, 297–306. doi: 10.2166/wqrjc.2016.040

Ryu, J., Jung, J., Park, K., Song, W., Choi, B., and Kweon, J. (2021). Humic acid removal and microbial community function in membrane bioreactor. *J. Hazard. Mater.* 417:126088. doi: 10.1016/j.jhazmat.2021.126088

Sauer, K., Camper, A. K., Ehrlich, G. D., Costerton, J. W., and Davies, D. G. (2002). *Pseudomonas aeruginosa* displays multiple phenotypes during development as a biofilm. *J. Bacteriol.* 184, 1140–1154. doi: 10.1128/jb.184.4.1140-1154.2002

Schmid, N., Pessi, G., Deng, Y., Aguilar, C., Carlier, A. L., Grunau, A., et al. (2012). The AHL-and BDSF-dependent quorum sensing systems control specific and overlapping sets of genes in *Burkholderia cenocepacia* H111. *Plo S one* 7:e49966. doi: 10.1371/journal.pone.0049966

Sepehr, S., Rahmani-Badi, A., Babaie-Naiej, H., and Soudi, M. R. (2014). Unsaturated fatty acid, cis-2-decenoic acid, in combination with disinfectants or antibiotics removes pre-established biofilms formed by food-related bacteria. *PLoS One* 9:e101677. doi: 10.1371/journal.pone.0101677

Shahid, M. K., Kashif, A., Rout, P. R., Aslam, M., Fuwad, A., Choi, Y., et al. (2020). A brief review of anaerobic membrane bioreactors emphasizing recent advancements, fouling issues and future perspectives. *J. Environ. Manag.* 270:110909. doi: 10.1016/j.jenvman.2020.110909

Siebdrath, N., Farhat, N., Ding, W., Kruithof, J., and Vrouwenvelder, J. S. (2019). Impact of membrane biofouling in the sequential development of performance indicators: feed channel pressure drop, permeability, and salt rejection. *J. Membr. Sci.* 585, 199–207. doi: 10.1016/j.memsci.2019.05.043

Song, W., Kim, C., Han, J., Lee, J., Jiang, Z., and Kweon, J. (2023). Application of acyl-homoserine lactones for regulating biofilm characteristics on PAO1 and multi-strains in membrane bioreactor. *Membr. Water Treat.* 14, 35–45. doi: 10.12989/mwt.2023.14.1.035

Song, W., Lade, H., Yu, Y., and Kweon, J. (2018). Effects of N-acetylcysteine on biofilm formation by MBR sludge. *Membr. Water Treat.* 9, 195–203. doi: 10.12989/mwt.2018.9.3.195

Sullivan, C., Meigh, J., and Lawrence, P. (2006). Application of the water poverty index at different scales: a cautionary tale: in memory of Jeremy Meigh who gave his life's work to the improvement of peoples lives. *Water Int.* 31, 412–426. doi: 10.1080/02508060608691942

Suppiger, A., Eshwar, A. K., Stephan, R., Kaever, V., Eberl, L., and Lehner, A. (2016). The DSF type quorum sensing signalling system RpfF/R regulates diverse phenotypes in the opportunistic pathogen Cronobacter. *Sci. Rep.* 6, 1–8. doi: 10.1038/srep18753

Teng, J., Wu, M., Chen, J., Lin, H., and He, Y. (2020). Different fouling propensities of loosely and tightly bound extracellular polymeric substances (EPSs) and the related fouling mechanisms in a membrane bioreactor. *Chemosphere* 255:126953. doi: 10.1016/j.chemosphere.2020.126953

Tijing, L. D., Woo, Y. C., Choi, J. S., Lee, S., Kim, S. H., and Shon, H. K. (2015). Fouling and its control in membrane distillation—a review. *J. Membr. Sci.* 475, 215–244. doi: 10.1016/j.memsci.2014.09.042

Turnbull, L., Toyofuku, M., Hynen, A. L., Kurosawa, M., Pessi, G., Petty, N. K., et al. (2016). Explosive cell lysis as a mechanism for the biogenesis of bacterial membrane vesicles and biofilms. *Nat. Commun.* 7, 1–13. doi: 10.1038/ncomms11220

Wan, C., Fu, L., Li, Z., Liu, X., Lin, L., and Wu, C. (2022). Formation, application, and storage-reactivation of aerobic granular sludge: a review. *J. Environ. Manag.* 323:116302. doi: 10.1016/j.jenvman.2022.116302

Zheng, P., Li, Y., Chi, Q., Cheng, Y., Jiang, X., Chen, D., et al. (2022). Structural characteristics and microbial function of biofilm in membrane-aerated biofilm reactor for the biodegradation of volatile pyridine. *J. Hazard. Mater.* 437:129370. doi: 10.1016/j.jhazmat.2022.129370

frontiers | Frontiers in Microbiology

TYPE Methods
PUBLISHED 27 July 2023
DOI 10.3389/fmicb.2023.1218933



OPEN ACCESS

EDITED BY
Hongbo Li,
Nanjing University, China

REVIEWED BY
C. French,
University of Edinburgh, United Kingdom
Xuehua Wan,
Nankai University, China
Gonzalo Durante-Rodriguez,
Spanish National Research Council (CSIC), Spain

*CORRESPONDENCE
Nai-xing Zhang
✉ zhanghealth@126.com
Hao Luo
✉ lh426@gdmu.edu.cn
Chang-ye Hui
✉ hcy_sypu@hotmail.com

†These authors have contributed equally to this work

RECEIVED 08 May 2023
ACCEPTED 10 July 2023
PUBLISHED 27 July 2023

CITATION
Zhu D-l, Guo Y, Ma B-c, Lin Y-q, Wang H-j, Gao C-x, Liu M-q, Zhang N-x, Luo H and Hui C-y (2023) Pb(II)-inducible proviolacein biosynthesis enables a dual-color biosensor toward environmental lead.
*Front. Microbiol.* 14:1218933.
doi: 10.3389/fmicb.2023.1218933



# Pb(II)-inducible proviolacein biosynthesis enables a dual-color biosensor toward environmental lead

De-long Zhu[1†], Yan Guo[2†], Bing-chan Ma[3], Yong-qin Lin[2], Hai-jun Wang[2], Chao-xian Gao[2], Ming-qi Liu[1], Nai-xing Zhang[2*], Hao Luo[1*] and Chang-ye Hui[1,2*]

[1]School of Public Health, Guangdong Medical University, Dongguan, China, [2]Shenzhen Prevention and Treatment Center for Occupational Diseases, Shenzhen, China, [3]School of Public Health, Tongji Medical College, Huazhong University of Science and Technology, Wuhan, China

With the rapid development of synthetic biology, various whole-cell biosensors have been designed as valuable biological devices for the selective and sensitive detection of toxic heavy metals in environmental water. However, most proposed biosensors are based on fluorescent and bioluminescent signals invisible to the naked eye. The development of visible pigment-based biosensors can address this issue. The *pbr* operon from *Klebsiella pneumoniae* is selectively induced by bioavailable Pb(II). In the present study, the proviolacein biosynthetic gene cluster was transcriptionally fused to the *pbr* Pb(II) responsive element and introduced into *Escherichia coli*. The resultant biosensor responded to Pb(II) in a time- and dose-dependent manner. After a 5-h incubation with Pb(II), the brown pigment was produced, which could be extracted into n-butanol. Extra hydrogen peroxide treatment during n-butanol extract resulted in the generation of a stable green pigment. An increased brown signal was observed upon exposure to lead concentrations above 2.93 nM, and a linear regression was fitted from 2.93 to 3,000 nM. Extra oxidation significantly decreased the difference between parallel groups. The green signal responded to as low as 0.183 nM Pb(II), and a non-linear regression was fitted in a wide concentration range from 0.183 to 3,000 nM. The specific response toward Pb(II) was not interfered with by various metals except for Cd(II) and Hg(II). The PV-based biosensor was validated in monitoring bioaccessible Pb(II) spiked into environmental water. The complex matrices did not influence the regression relationship between spiked Pb(II) and the dual-color signals. Direct reading with the naked eye and colorimetric quantification enable the PV-based biosensor to be a dual-color and low-cost bioindicator for pollutant heavy metal.

KEYWORDS

**whole-cell biosensors, proviolacein biosynthesis, lead pollution, bioavailability, ecotoxicity**

## Introduction

Heavy metal pollution has become a global environmental problem that seriously endangers human health and ecological safety (Adimalla, 2020; Zhu et al., 2022). Some heavy metals, including lead (Pb), mercury (Hg), arsenic (As), chromium (Cr), and cadmium (Cd), can cause significant damage to multiple organs such as the liver, kidneys, and brain by disrupting the

body's metabolic functions, and lead to different types of cancer, neurological disorders, and other endocrine abnormalities (Bridges and Zalups, 2017; Klotz and Goen, 2017; Rehman et al., 2018). As one of the critical heavy metal pollutants, Pb can quietly threaten human life through various hidden pathways (Mulhern et al., 2022). Due to its high toxicity and non-biodegradability (Yuvaraja et al., 2019), Pb can accumulate in living organisms through the food chain and threaten their bioactivities (Naikoo et al., 2019). Pb is toxic to almost all human organs (Charkiewicz and Backstrand, 2020; Hemmaphan and Bordeerat, 2022). Thus, the biological exposure limit of blood lead is constantly being lowered from 60 μg/dL in 1960 to 3.5 μg/dL in 2016 (Rocha and Trujillo, 2019).

Implementation of rational control policies and continuous environmental monitoring are prerequisites for avoiding increased Pb pollution (Pohl et al., 2017). Accurate detection of bioavailable Pb in soil and water is necessary to predict its ecological risk (Roux and Marra, 2007; Kumar et al., 2020). From available studies, most methods for detecting Pb rely on expensive instruments that are not portable and limited to specific analytical systems (Klotz and Goen, 2017; Tudosie et al., 2021; Manousi et al., 2022). Although the mainstream instrumental methods are sensitive and accurate, the analytical results mainly reflect the total amount of elemental Pb. The bioavailable Pb that is genuinely hazardous to organisms was not exactly reflected using traditional instruments, including atomic absorption spectroscopy and inductively coupled plasma-mass spectrometry. The specification analysis of toxic Pb largely depends on complex pre-treatment (Manousi et al., 2022). As an alternative to instrumental assays, the novel microbial cell-based approach showed potential in the practical determination of bioavailable heavy metals (Cui et al., 2018; Hui et al., 2020). These biological methods also have the advantage of solid operability, low cost, and ease of use (Kannappan and Ramisetty, 2022). Despite the lack of rigorous selectivity and background noise, microbial cell-based biosensors can be continuously improved by evolving genetic techniques to meet on-site testing requirements (Wang and Buck, 2012).

Bioaccessible Pb(II) is critical to the transcription initiation of Pb resistance genes, mediated by the metalloregulator PbrR (Borremans et al., 2001). The Pb(II)-resistant *pbr* operon, a member of the *mer*-like operons, was commonly engineered to develop several microbial cell-based biosensors toward Pb (Fang and Zhang, 2022). With the rapid advances in synthetic biology, it is now possible to artificially reconstruct heavy metal-resistant operons, including optimization of the sensory modules (Levin-Karp et al., 2013; Jia et al., 2020) and development of novel reporter modules (Jiang et al., 2008). When bioavailable metals enter the biosensing cell, the transcription and translation of downstream reporter genes will be induced, and the resultant biosensing signals can be emitted. Various biosensing reporters are employed to develop genetic devices responsive to heavy metal pollutants. Versatile engineered microbial cells became bioluminescent biosensors (Viviani et al., 2022), fluorescent biosensors (Guo et al., 2021b; Hui et al., 2021b), and colorimetric biosensors (Hui et al., 2021a) toward toxic metals.

Bioluminescent and fluorescent reporters as primary actuators depend highly on expensive instruments to determine biosensing signals (Hui et al., 2021b; Viviani et al., 2022). These instruments, such as photometers, multi-wavelength microplate readers, and fluorescence spectrometers, are not conducive to rapidly detecting Pb contamination in the field. Recently, several natural pigments as easy-to-read biosensing reporters were successfully designed to develop whole-cell biosensors for the detection of environmental Hg(II) (Hui et al., 2021a), Cd(II) (Hui et al., 2022a) and Pb(II) (Hui et al., 2022b). These novel pigment-based biosensors have great potential in developing rapid colorimetric methods for *in situ* detection of contaminant metals, with low-cost, mini-equipment, and high-throughput advantages.

Pigments with striking colors could be used to develop visual bacterial biosensors toward pollutants. Several studies have clarified that the branched violacein biosynthetic pathway can produce four-color metabolites, including violacein (V), deoxyviolacein (DV), proviolacein (PV), and prodeoxyviolacein (PDV) (Yang et al., 2021). Differential colored signals contribute to the design of multiple functional biosensors. Whole-cell biosensors based on navy V (Hui et al., 2020) and purple DV (Hui et al., 2022b) showing differential responsive properties have been successfully developed. The PV-based colored signal responsive to Pb(II) was previously obtained by employing a *vioABDE* gene cluster as a reporter module fused downstream of the Pb(II) sensory element. Due to the high reducibility of the chromogenic compounds, the color rendering of PV is unstable. Thus its feasibility as a biosensing reporter has yet to be verified in previous studies. In the current study, The PV biosynthesis was demonstrated to be selectively activated by soluble Pb(II) in a time- and dose–response manner. Due to the extreme reducibility of PV, green and brown PV derivatives were generated under oxidizing and non-oxidizing conditions, and the dual-color signals could be quantified by visible light colorimetry. A high-throughput colorimetric method based on a 96-well plate was developed to detect environmental Pb pollutants. It has the potential to become a complementary tool to instrumental means.

## Materials and methods

### Biosensing construct, bacterial strains, and reagents

The biosensing construct pPb-vioABDE with a *vioABDE* gene cluster located downstream of the Pb(II) sensory element was previously constructed (Hui et al., 2022b). In brief, the Pb(II) sensing element contains a reverse transcriptional *pbrR* gene and divergent *pbr* promoter originating from *Klebsiella. pneumoniae* CG43 (NCBI Accession AY378100) was artificially synthesized (Sangon Biotech, Shanghai, China). The proviolacein biosynthetic genes originating from *Chromobacterium violaceum* were designed according to the preference codon of *E. coli* and synthesized (Sangon Biotech). An overlap PCR assembled two genetic modules and inserted them into the *Bgl*II and *Sac*I sites of pET-21a to generate the vector pPb-vioAEDE. *E. coli* TOP10 was used as the bacterial host and transformed with pPb-vioABDE to assemble bacterial biosensor TOP10/pPb-vioABDE. Chemically inert violacein and deoxyviolacein have been validated as becoming potential reporters in our previous studies (Hui et al., 2020, 2022b). The biosensing performance of unstable proviolacein was investigated in the current study. More colored pigment choices are beneficial for developing versatile biosensors for detecting toxic metals of different concentrations or even types. Engineered strains were grown in Luria-Bertani (LB) broth (10 g/L tryptone, 5 g/L yeast extract, 10 g/L NaCl, and 50 μg/mL

ampicillin) in a 15 mL bio-reaction tube with a vent cap (Jet Bio-Filtration, Guangzhou, China) at 37°C with shaking at 250 rpm under aerobic conditions. Inorganic metal compounds, including $HgCl_2$, $CaCl_2$, $MgCl_2$, $FeSO_4$, $MnSO_4$, $NiSO_4$, $CuSO_4$, $ZnSO_4$, $CdCl_2$, and $Pb(NO_3)_2$ were analytical grade reagents and obtained from Sigma Aldrich (St. Louis, MO, United States). Various metal stock solutions were freshly prepared using purified water at 1 mM. Other chemical reagents were purchased from Sangon Biotech (Shanghai, China).

## Chromogenic stability of two colored PV derivatives

Overnight cultures of TOP10/pPb-vioABDE were inoculated into 10 mL fresh LB medium at a 1:100 dilution and induced with 1 μM Pb(II) at 37°C for 5 h. Intracellular accumulated PV aggregates were extracted with n-butanol. After vortex extraction using 4 mL n-butanol, the n-butanol phase was separated after centrifugation and divided into the average non-oxidation and oxidation treatment groups. The difference was that 30% $H_2O_2$ in a ratio of 1:9 was supplemented into the oxidation group during n-butanol extraction. Both n-butanol extracts were placed at 25°C and sampled at 1-h intervals. The visible absorption spectra of the samples were scanned in a microplate reader (BioTek Epoch, USA) ranging from 400 to 700 nm at 1-nm intervals.

## The time-dose–response pattern of PV-based biosensors toward Pb(II)

Overnight cultures of TOP10/pPb-vioABDE were inoculated into 2 mL LB medium at a ratio of 1:100 in 15 mL tubes, then exposed to Pb(II) at final concentrations of 0, 0.15, and 1.5 μM. The induced cultures were incubated at 37°C with shaking at 250 rpm for 8 h and sampled at 1-h intervals. All samples were divided into oxidation and non-oxidation treatment groups on average and stored at 4°C until detection. Aliquots of 100 μL culture were first determined at 600 nm for the bacterial density ($OD_{600}$). The residual 900 μL culture was directly extracted with 360 μL n-butanol in non-oxidation treatment groups; the residual 900 μL culture was extracted with 360 μL n-butanol mixed with 100 μL 30% $H_2O_2$ in oxidation treatment groups. After being vigorously vortexed for 2 min, the upper n-butanol phase was separated by centrifugation at 12000 × g for 1 min and placed at room temperature to ensure the sufficient derivation of PV. Then, aliquots of 100 μL organic phase were transferred into a 96-well microplate and read at 652 nm to determine the dual-color signals using a microplate reader.

## Dose–response curves for Pb(II)-induced PV-based biosensors

Overnight cultures of TOP10/pPb-vioABDE were diluted at 1:100 in fresh LB medium. A 2-fold dilution method (Hui et al., 2021c) was used to obtain 12,000, 6,000, 3,000, 1,500, 750, 375, 187.5, 93.8, 46.9, 23.4, 11.7, 5.86, 2.93, 1.46, 0.732, 0.366, 0.183, 0.0915 and 0 nM Pb(II) exposure group. After incubation at 37°C for 5 h, an aliquot containing 100 μL cultures was measured for bacterial density at 600 nm. Intracellular PV aggregates were extracted with n-butanol after oxidation and non-oxidation treatment, as described above. An aliquot containing 100 μL organic phase was measured at 652 nm to determine the dual-color signals.

## Response selectivity of PV-based biosensors

To investigate the response selectivity, the overnight cultures of TOP10/pPb-vioABDE were diluted at 1:100 in fresh LB medium and exposed to 1.5 μM various metal ions, including Pb(II), Cr(III), Hg(II), Zn(II), Mg(II), Ni(II), Mn(II), Ca(II), Fe(II), Cd(II), and Cu(II). To assess the influence of various metal ions on the response of TOP10/pPb-vioABDE toward Pb(II), target Pb(II) was mixed with various interference metal ions at 1.5 μM and exposed to biosensor cells. After incubation at 37°C for 5 h, the bacterial cell density and dual-color signals were measured at 600 nm and 652 nm, respectively.

## Detection of bioavailable Pb(II) in environmental samples

Lead salt was spiked into four environmental water samples: pure water, tap water, lake water, and soil extracts. The response of PV-based biosensors toward bioaccessible Pb(II) in the environmental matrices was investigated. Environmental surface water and surface (0–20 cm) lateritic soil samples were collected from a local park (Luohu District, Shenzhen, China). Air-dried soil samples (10 g) were fully suspended using 200 mL of pure water and vortexed for 1 h. After being placed at 26°C for 5 h, the supernatant was filtered through a 0.22 μM filter. The LB medium was freshly prepared by mixing 90% v/v filtered purified water, tap water from our laboratory, ambient surface water, and soil extract with 10% v/v 10 × LB broths. Overnight cultures of TOP10/pPb-vioABDE were diluted at 1:100 in four media. A double dilution method was used to obtain 3,000, 1,500, 750, 375, 187.5, 93.8, 46.9, 23.4, 11.7, 5.86, 2.93, and 0 nM Pb(II) exposure groups for non-oxidation treatment, and 6,000, 3,000, 1,500, 750, 375, 187.5, 93.8, 46.9, 23.4, 11.7, 5.86, 2.93, 1.46, 0.732, 0.366, 0.183, 0.0915 and 0 nM Pb(II) exposure groups for oxidation treatment. After incubation at 37°C for 5 h, bacterial density and dual-color signals were determined at 600 nm and 652 nm, respectively.

# Results

## Pb(II)-initiated proviolacein synthesis resulting in the accumulation of chromogenic substances

Pb(II) sensory element originating from the natural lead-resistant bacterium *Klebsiella. pneumoniae* CG43 was transcriptionally fused with the PV biosynthesis genes cluster to generate a biosensing construct of the plasmid pPb-vioABDE. The molecular mechanism of Pb(II) inducible PV biosynthesis is shown in Figure 1A. Bacterial cells usually acquire metal ions through the ATP-binding cassette transporters, which lack transport selectivity and transport various

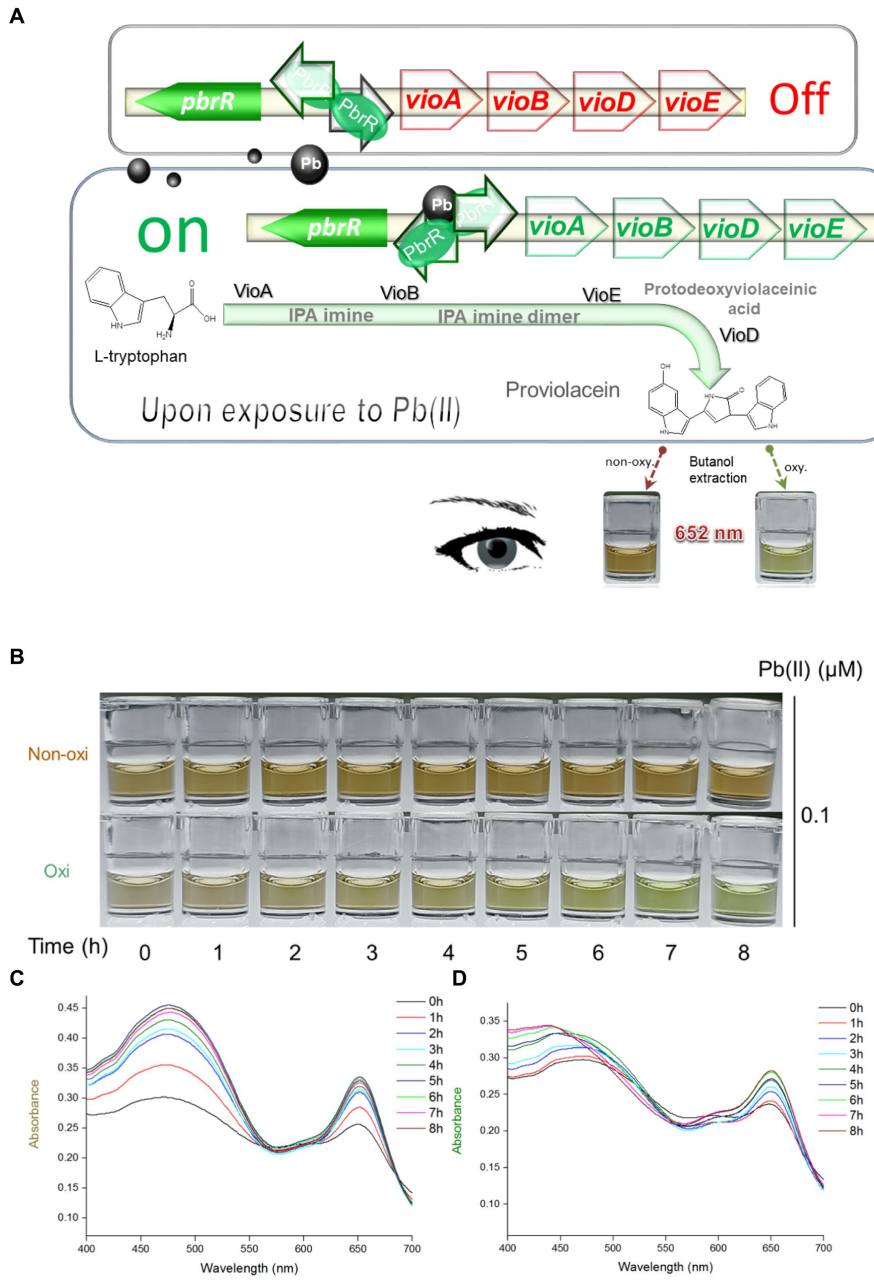


FIGURE 1
Pb(II) triggers the biosynthesis of proviolacein, which can be converted into two colored substances under non-oxidizing and oxidizing conditions. **(A)** Design of PV-based whole-cell biosensor toward Pb(II). The PV biosynthetic module is artificially synthesized and genetically fused downstream of the Pb(II) sensory module. A tetracistronic unit is transcribed upon exposure to intracellular bioavailable Pb(II). PV biosynthesis is based on the branched violacein biosynthetic pathway catalyzed by VioA, VioB, VioE, and VioD. After n-butanol extraction accompanied by oxidation and non-oxidation treatments, PV in the organic phase was converted into two colored substances. PbrR, Pb(II) responsive metalloregulator; IPA, indole-3-pyruvate acid imine; oxy, oxidizing condition; non-oxy, non-oxidizing condition. **(B)** After non-oxidation and oxidation treatment, the n-butanol phase containing PV was placed at 25°C for 8 h. Representative photos from three independent experiments are shown. Visible absorption spectra of PV derivatives after non-oxidation **(C)** and oxidation **(D)** treatment were scanned at 1-h intervals. The wavelength range is from 400 to 700 nm in 1 nm intervals. Representative results from three independent assays are shown.

metal ions, including Pb(II) inside a bacterial cell (Locher, 2016). Intracellular Pb(II) can transform dimeric PbrR from a repressor into an activator. Then the *vioABDE* gene cluster is transcribed and translated in a Pb(II) concentration-dependent manner, resulting in the activated metabolic flux toward proviolacein forms in the cytoplasm.

As an intermediate of the branched violacein biosynthetic pathway, the unstable PV in the organic phase was rapidly converted into a grayish-brown substance upon exposure to air (Figure 1B), and brown gradually darkened under autoxidation conditions (non-oxidation treatment group). However, the PV in the organic phase was gradually converted into a green substance within 8 h under the oxidation of

intense oxidant hydrogen peroxide (oxidation treatment group). The visible absorption spectra in the 400–700 nm wavelength showed that the absorption values of two colored derivatives increased with the prolonged incubation time. The rising trend of the non-oxidation group (Figure 1C) was significantly more evident than that of the oxidation group (Figure 1D). Importantly, the absorbance of two colored PV derivatives became invariant after 6-h incubation. Both colored PV derivatives showed two prominent absorption peaks. A 400 to 550 nm peak was flat, but another sharp peak was located at about 652 nm. According to the above results, unchanging absorbance of 652 nm could be determined after the n-butanol phases containing PV derivatives were placed for 6 h. In the subsequent experiments, stable brown and green signals were determined after 6 h following n-butanol extraction under non-oxidizing and oxidizing conditions.

## PV-based biosensors responsive to Pb(II) in a time-dependent manner

Engineered TOP10/pPb-vioABDE was exposed to Pb(II) at concentrations of 0, 0.15, and 1.5 μM, bacterial density increased within 7 h, and the $A_{652}$ of the n-butanol phases containing PV derivatives showed an apparent time-dose–response relationship in both non-oxidation treatment groups (Figure 2A), and oxidation treatment groups (Figure 2B). The induction coefficient ($A_{652}$ of Pb(II) exposure group / $A_{652}$ of no Pb(II) exposure group) in the non-oxidation treatment group and oxidation treatment group is shown in Supplementary Tables S1, S2, respectively. The induction coefficient continuously increased with 7 h Pb(II) induction in a non-oxidation group (Supplementary Table S1). However, the oxidation group's induction coefficient reached the maximum at 5 h Pb(II) induction (Supplementary Table S2). The green signal was also stable after 5 h Pb(II) induction (Figure 2B). Interestingly, the standard deviations of the non-oxidation treatment group were more extensive than that of the oxidation treatment group upon exposure to 0 and 0.15 μM Pb(II). The n-butanol phase containing PV derivatives changed from colorless to light brown. The brown continued to deepen until 6 h induction in the non-oxidation treatment group (Figure 2C). By comparison, the n-butanol phase containing PV derivatives darkened to a stable brown-green after 5 h Pb(II) induction in the oxidation treatment group (Figure 2D). Finally, five h Pb(II) induction was chosen before the determination of dual-color signals in the subsequent experiments.

## PV-based biosensors responsive to Pb(II) in a dose-dependent manner

Engineered TOP10/pPb-vioABDE was exposed to increased concentrations of Pb(II). Pb(II) concentrations below 12,000 nM did not adversely affect bacterial growth (Supplementary Figure S2). The brown signal was unstable in the non-oxidation treatment group with a significant relative standard deviation. Thus, a significantly increased brown signal was observed upon exposure to 2.93 nM Pb(II) (Figure 3A). However, the green signal was stable with a slight relative standard deviation, so the limit of detection (LOD) was decreased to 0.183 nM after oxidation treatment (Figure 3B). The biosynthesis of PV was Pb(II) dose-dependently induced. The dose–response curves were similar between the non-oxidation (Figure 3C) and oxidation (Figure 3D) treatment groups. The brown signal was not increased above 1,024 nM Pb(II) induction, and the green signal was not above 2048 nM Pb(II) induction. The brown signal and Pb(II) exposure concentration tended to be fitted to a linear regression ranging from 2.93 to 3,000 nM (Figure 3E). After oxidation treatment, the green signal and Pb(II) exposure concentration tended to be fitted to a non-linear regression with a wide concentration range from 0.183 to 3,000 nM (Figure 3F). As shown in Figure 3G, the background (no Pb exposure) of the oxidation treatment group was almost colorless to the naked eye, but slight brown was observed in the background of non-oxidation treatment group. Both colors were visually deepened with the increased Pb(II) exposure.

## PV-based biosensors selectively respond to toxic Pb(II)

Engineered TOP10/pPb-vioABDE was exposed to Pb(II) and ten other metal ions at 1.5 μM. Supplement of various metal ions at 1.5 μM exerted no apparent cytotoxicity on bacterial cells (Supplementary Figures S3A,B). PV-based biosensors selectively responded to Pb(II). Notably, the non-oxidation treatment (Figure 4A) and oxidation treatment (Figure 4B) did not influence the output of biosensors' selectivity. Upon exposure to Cd(II), a decreased background response compared to other non-target metal ions was observed. The effect of coexisting metals exerted slight cytotoxicity on biosensor cells (Supplementary Figures S3C,D). Various metal ions' interaction with an accumulation of colorant was further investigated. In both non-oxidation (Figure 4C) and oxidation (Figure 4D) treatment groups, coexisting Hg(II) and Cd(II) impaired the response of TOP10/pPb-vioABDE toward Pb(II). All used metals together weakened the biosensing response to Pb(II), possibly due to the existence of Hg(II) and Cd(II). The production of PV responsive to Pb(II) was restored exactly when Hg(II) and Cd(II) were eliminated from all used metals. Notably, the brown and green color in n-butanol phases visible to the naked eye were still observed in all exposure groups containing Pb(II).

## Bioavailable Pb(II) in environmental water matrices is detected using PV-based biosensors

In order to validate the capability of engineered biosensors in monitoring bioavailable Pb(II) in different matrices, environmental water samples artificially contaminated with Pb(II) were mixed into the culture systems. The overall procedure for the Pb(II) field testing is shown in Figure 5A. Bacterial density was stable with 0–6,000 nM Pb(II) exposure (Supplementary Figure S4). Considering soluble Pb(II) cytotoxicity, bacterial viability was calculated by spreading serial ten-fold dilution cultures on the LB plates containing 50 μg/mL ampicillin. Compared with the control group (no Pb exposure), the number of colony-forming units (CFU) slightly decreased in high concentrations of Pb(II) induced bacterial culture (Supplementary Figure S5). The concentration range of Pb(II) used in the study has no significant lethal effect on bacteria.

Brown signal fluctuations caused by environmental matrix effects (Figure 5B) were significantly higher than green signal fluctuations

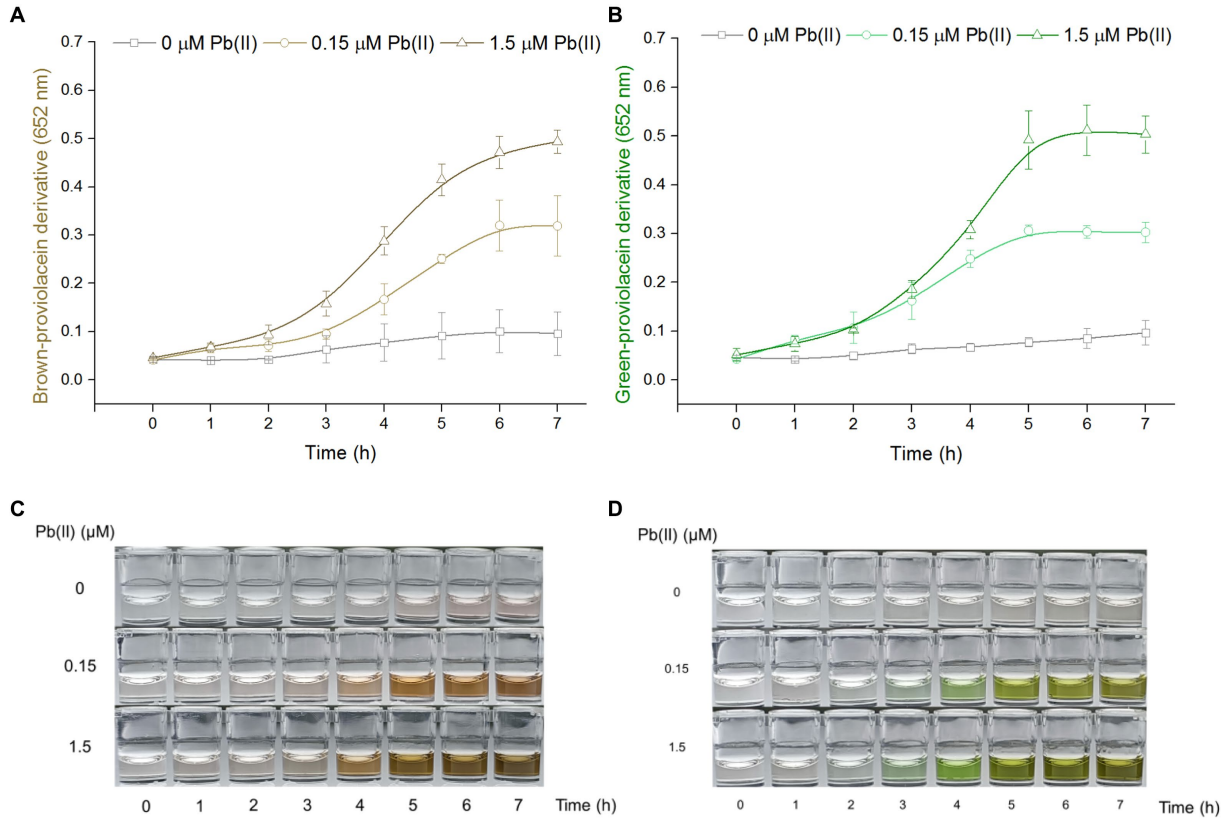


FIGURE 2
The time-dose–response relationship of PV-based biosensors exposed to Pb(II). Cultures of TOP10/pPb-vioABDE were induced with three concentrations of Pb(II) at 37°C and sampled at 1-h intervals. The n-butanol extracts were separated and transferred into a 96-well plate. The time-dose–response curves using $A_{652}$ of 100 μL n-butanol phase after non-oxidation **(A)** and oxidation **(B)** treatment were made. The result was the mean ± standard deviation of three independent determinations. Representative photos of two colored n-butanol phases from non-oxidation treatment **(C)** and oxidation treatment **(D)** groups are shown.

(Figure 5C). Compared with the green signal, an significantly increased brown signal was observed with higher concentrations of Pb(II) exposure. The overall dose–response curves were highly similar at low concentrations of Pb(II) exposure (Figures 5D,E). Similar to the regression analysis under experimental conditions, a linear regression relationship was found in the non-oxidation treatment group with Pb(II) concentration ranging from 46.9 to 750 nM (Figure 5F). A non-linear regression was demonstrated in the oxidation treatment group with Pb(II) concentration ranging from 0.732 to 750 nM (Figure 5G). Furthermore, the relative standard deviations were significantly decreased in the oxidation treatment group (Supplementary Tables S3, S4). A high background was found in the non-oxidation treatment group (Figure 5H). In contrast, a more pronounced gradient of green color was observed in the oxidation group (Figure 5I).

## Discussion

Microorganisms are inexpensive weapons for defending against heavy metal pollution, as they can adapt to high concentrations of heavy metal exposure through metal ions sequestration, transport, and export (Dave et al., 2020). The primary heavy metal pollutants in environmental water include Pb(II), Hg(II), Cd(II), As(III), and Cr(III) (Kiran Marella et al., 2020). Recently, biological assays have been extensively investigated to detect residual heavy metals in surface water or soil using genetically modified bacteria. Compared with non-cellular devices such as protein-based biosensors, DNA-based biosensors, and electrochemical sensors, whole-cell biosensors can potentially monitor cytotoxic, bioavailable, and bioaccessible metals in a low-cost, mini-equipment, and high-throughput manner. Various whole-cell biosensors have been successfully developed with fluorescent (Hui et al., 2021b; Kolosova et al., 2022), and colorimetric (Hui et al., 2021a) signal outputs.

Recent studies showed that natural pigment biosynthesis based on metabolic engineering made designed bacteria become colorimetric biosensors toward pollutants (Watstein and Styczynski, 2017; Hui et al., 2020, 2021a, 2022c; Guo et al., 2021a). Redesign of the metabolic pathway facilitated the biosynthesis of interested colorants (Hui et al., 2022b). The colored PV could be selectively accumulated by interrupting the branched violacein biosynthetic pathway (Tong et al., 2021; Hui et al., 2022b). The PV biosynthetic gene cluster was employed as a pigment-based reporter and transcriptionally fused to the well-characterized Pb(II) sensing element. The resultant engineered bacterium was expected to become a PV-based Pb(II) biosensor. As an intermediate of the violacein biosynthetic pathway, PV is chemically active (Zhao et al., 2019). Its extreme reducibility was first demonstrated in the present study.

10.3389/fmicb.2023.1218933

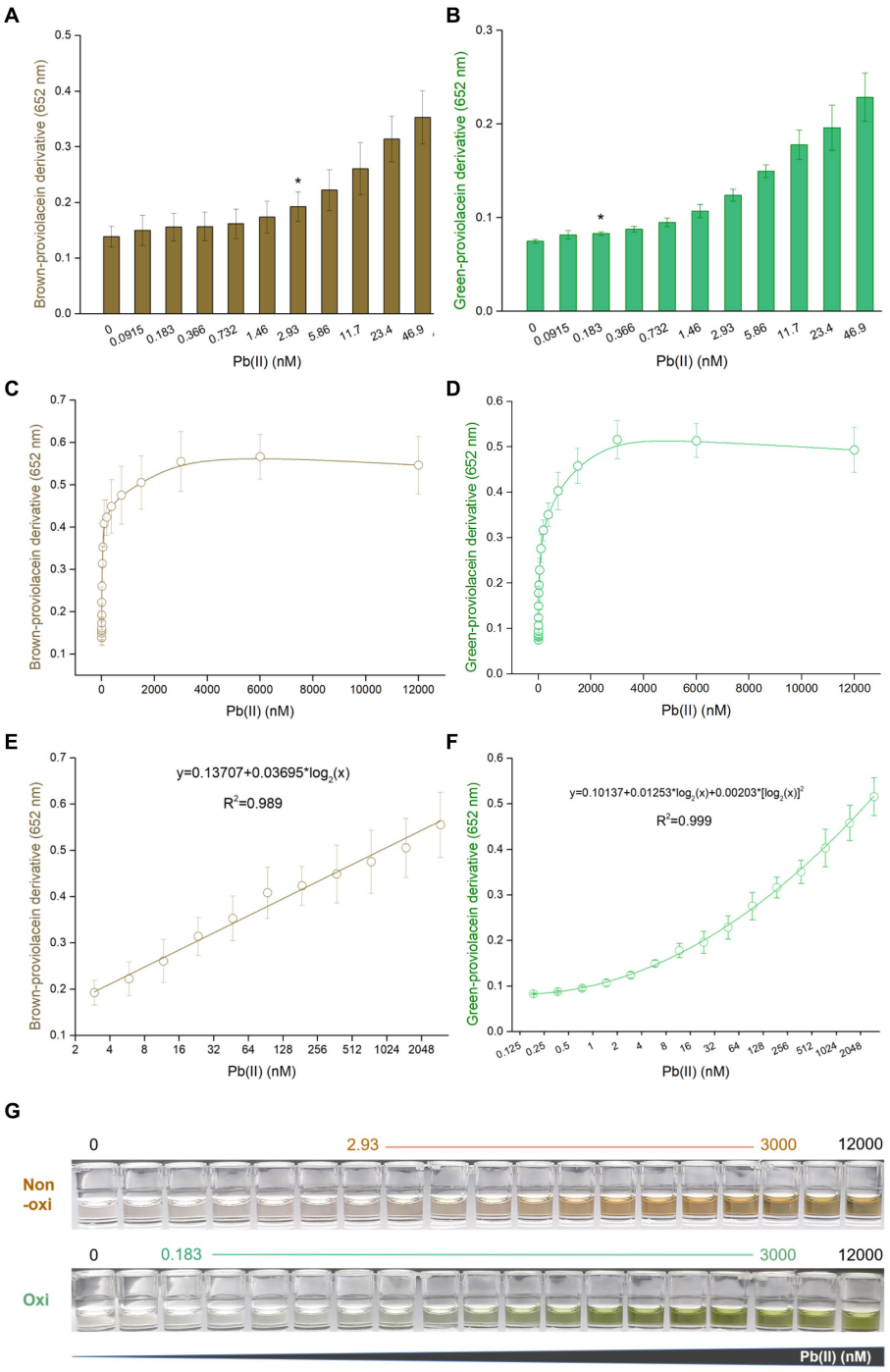


FIGURE 3
Dose–response performance of PV-based biosensor toward Pb(II) under laboratory conditions. Comparison of response sensitivity of TOP10/pPb-vioABDE toward Pb(II) between the non-oxidation treatment group **(A)** and oxidation treatment group **(B)**. The asterisk indicates LOD (the absorbance at 2.93 or 0.183 nM Pb(II) exposure group was checked against the background by t-Student analysis, and the difference was statistically significant ($P < 0.05$)) representing the lowest Pb(II) concentration inducing significantly increased pigment biosynthesis. Dose–response curves are based on the brown signal, captured after non-oxidation treatment **(C)**, and the green signal, captured after oxidation treatment **(D)**. **(E)** Linear regression analysis of the brown signal and Pb(II) relationship ranging from 2.93 to 3,000 nM ($R^2 = 0.989$). **(F)** Non-linear regression analysis of the relationship between the green signal and Pb(II) ranging from 0.183 to 3,000 nM ($R^2 = 0.999$). The *x*-axis shows the Pb(II) concentration on the $\log_2$ scale. The result was the mean ± standard deviation of three independent assays. **(G)** Representative photos of two colored n-butanol phases are shown, and the Pb(II) concentration ranges of regression analysis are marked.

Bimodal PV derivatives with two peaks at about 480 nm and 652 nm were gradually generated, and stable dual-color signals could be captured at about 6 h after extraction into butanol (Figures 1C,D). Our findings shew that natural oxidation led to the accumulation of brown-colored PV derivatives in the n-butanol phase. Unexpectedly, more stable green-colored PV derivatives were predominantly

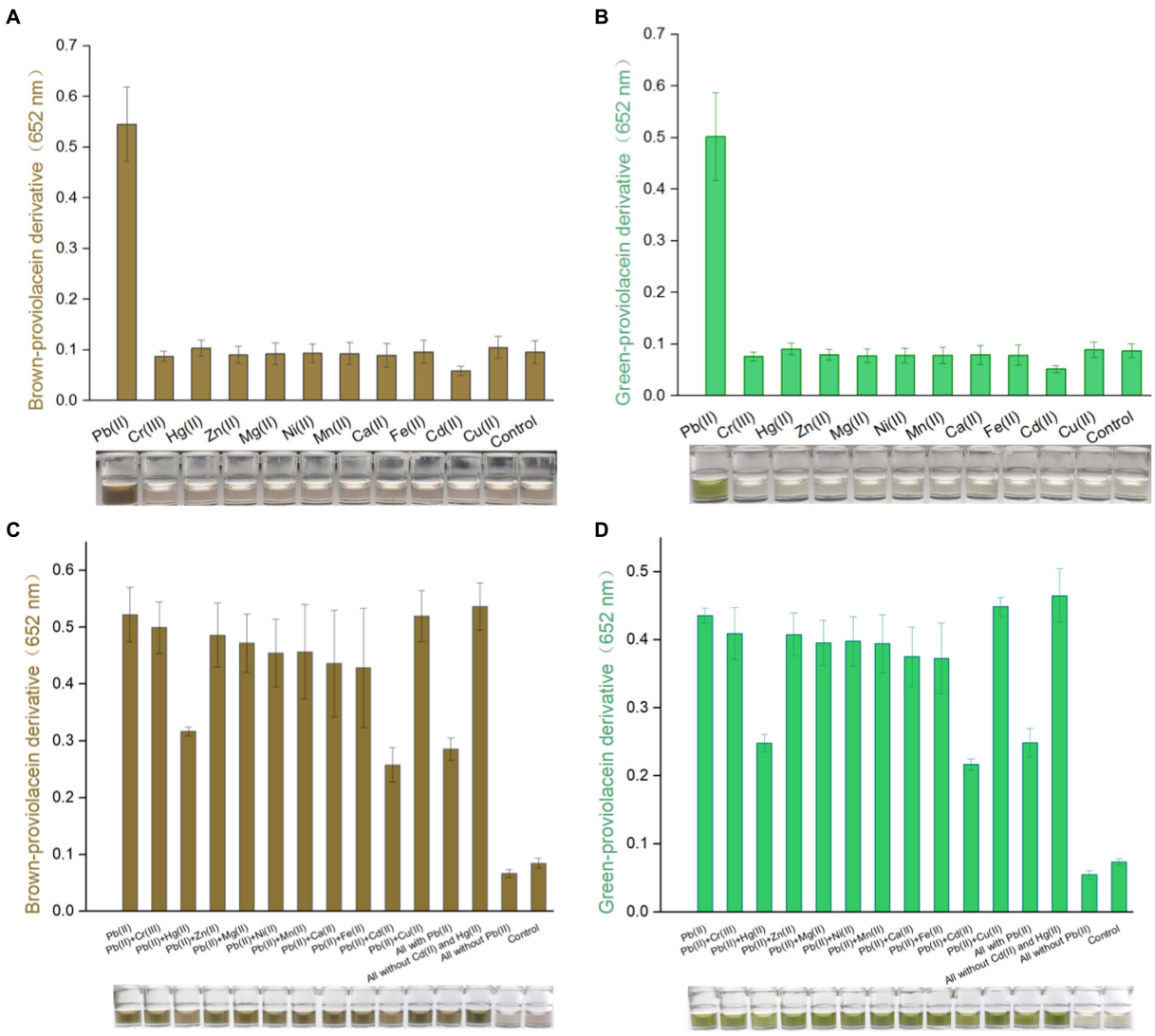


FIGURE 4
Differential responses of PV-based biosensors in response to various metal ions. Various metal ions induced TOP10/pPb-vioABDE at a concentration of 1.5 μM. The brown signal **(A)** and the green signal **(B)** were read at 652 nm following non-oxidation and oxidation treatment. Various metal mixtures induced TOP10/pPb-vioABDE at a concentration of 1.5 μM. The brown signal **(C)** and the green signal **(D)** were determined following non-oxidation and oxidation treatment. The control group was set without metal exposure. The result was the mean ± standard deviation of three independent assays. Representative photos of the n-butanol phase are shown below the bar chart.

generated due to the rapid and intense oxidation mediated by hydrogen peroxide. Although background signal noise is difficult to eliminate in whole-cell biosensors employing natural metalloregulators as sensory elements (Bereza-Malcolm et al., 2016; Hui et al., 2021a), the results showed that the intense oxidant treatments facilitated stabling and decreasing the background in the control group and reducing signal fluctuations in parallel groups (Figure 2).

Due to the stable green signal, the PV-based biosensor had a low LOD of 0.183 nM after an extra oxidation treatment (Figure 3B). However, the LOD was increased to 2.93 nM when PV suffered from natural oxidation (Figure 3A), which was consistent with previously developed V- and DV-based bacterial biosensors toward Pb(II) (Hui et al., 2022b). Considering the antibacterial activity of V, the signal intensities of both non-cytotoxic PV and DV were significantly more robust than that of V under the same concentration of lead exposure (Hui et al., 2022b). As expected, the LOD of the PV-based biosensor is significantly lower than that of fluorescent biosensors resulting from the amplification effect of continuous pigment biosynthesis. Furthermore, no linear relationship was observed between the fluorescent signal and Pb(II) concentration (Wei et al., 2014). A good regression relationship was found in this study. The quantifiable Pb(II) concentration reached 3,000 nM, which was similar to the DV-based lead biosensor but significantly more comprehensive than previously developed cytotoxic V-based biosensors (Hui et al., 2022b), non-cellular biosensors (Zhang et al., 2019; Yu et al., 2022) and cellular fluorescent biosensors (Bereza-Malcolm et al., 2016). In contrast to fluorescent or bioluminescent biosensors, the naked eye could directly distinguish gradient changes of dual-color signals (Figure 3G). The accumulation of visible colorants helps direct the

10.3389/fmicb.2023.1218933

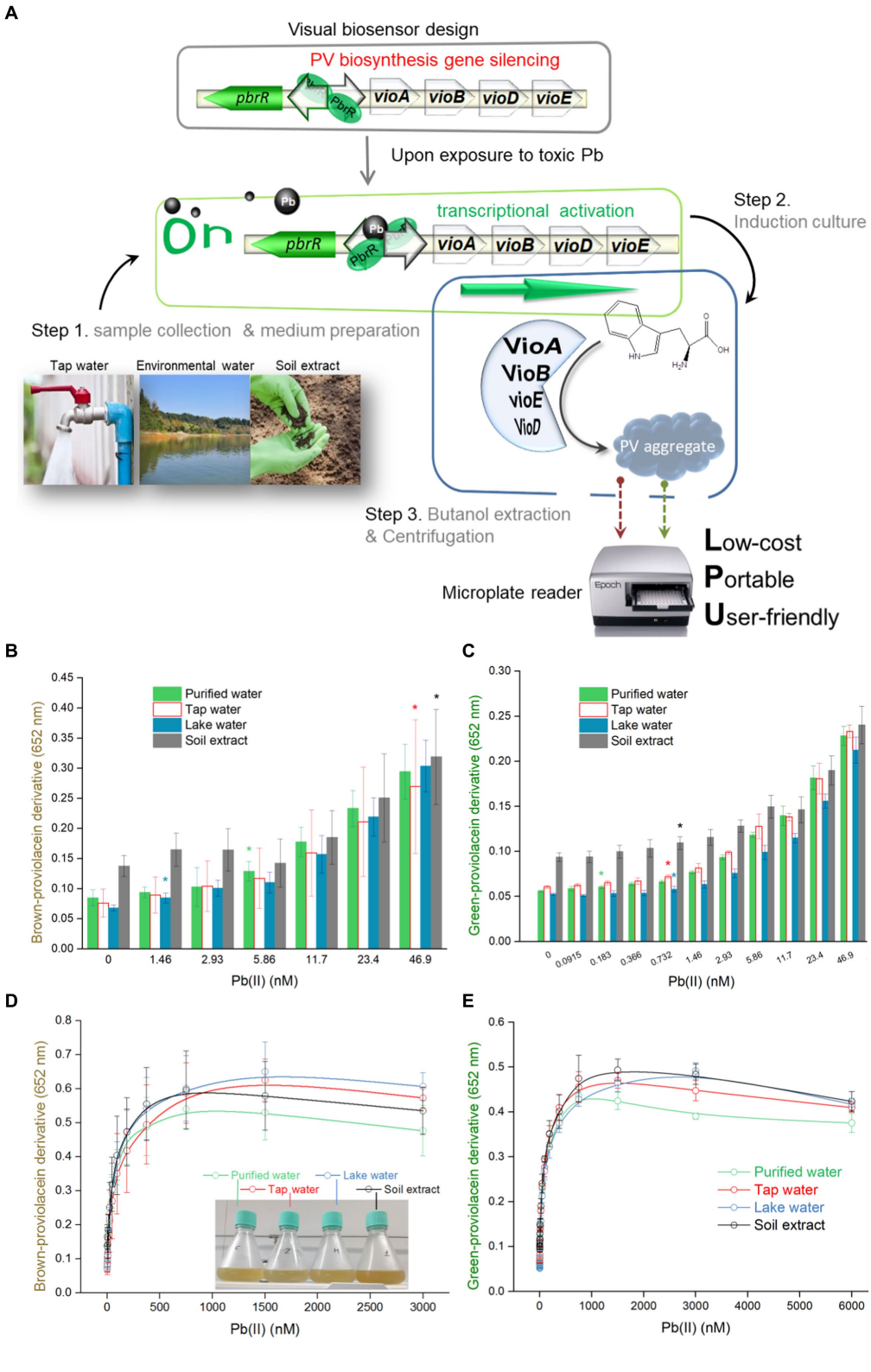


(*Continued*)

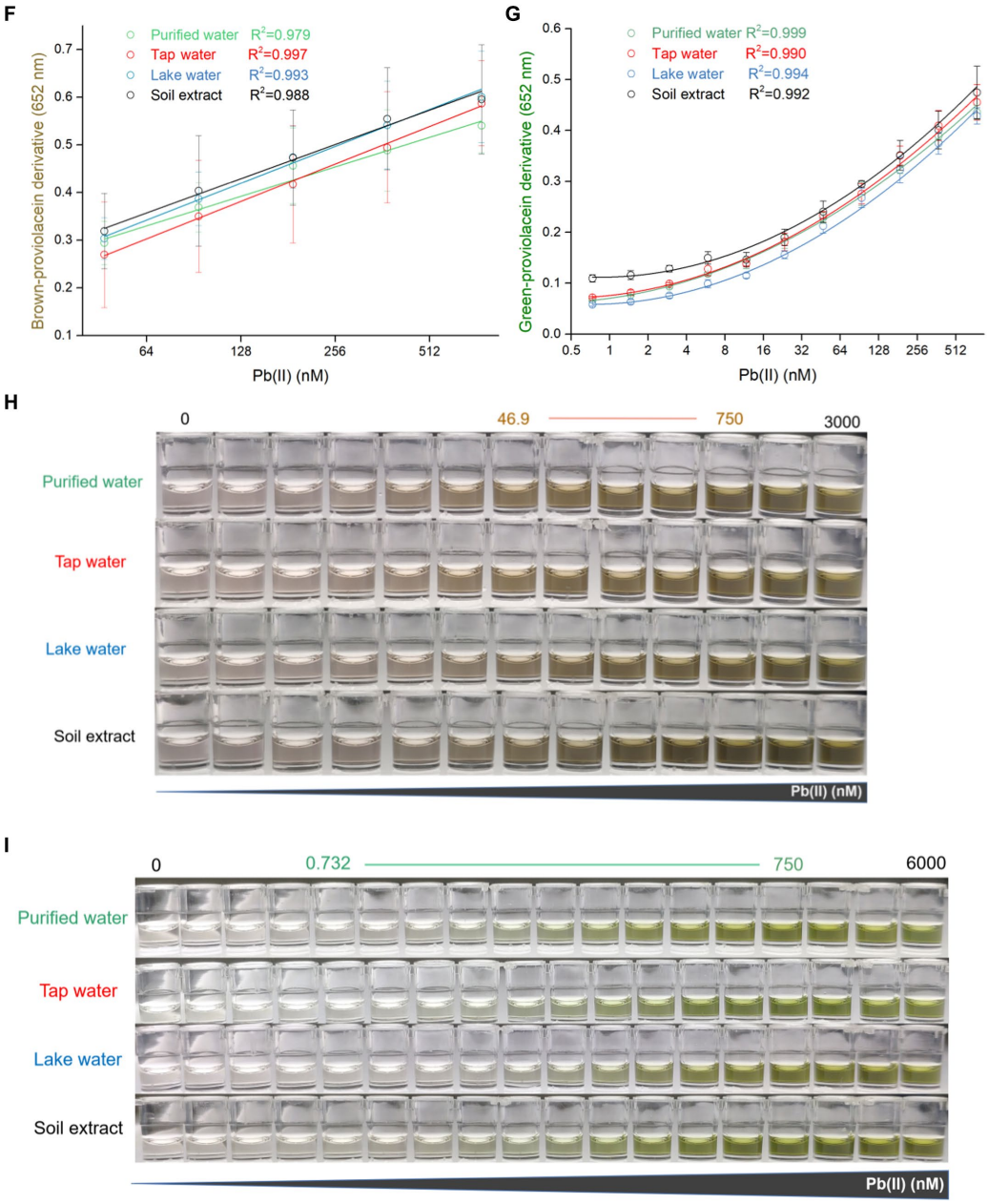


FIGURE 5
Dose–response performance of PV-based biosensor in detecting Pb(II) in environmental samples. **(A)** A detailed protocol for environmental Pb(II) bioindication using PV-based biosensors. Engineered TOP10/pPb-vioABDE was cultured in LB medium prepared using four different water samples, including purified water, tap water, lake water, and soil extract. Comparison of response sensitivity of TOP10/pPb-vioABDE toward Pb(II) between the non-oxidation treatment group **(B)** and oxidation treatment group **(C)** in the four culture substrates. The different colored asterisk indicates LOD (the absorbance was checked against the background by t-Student analysis, and the difference was statistically significant ($P<0.05$)), representing the lowest Pb(II) concentration inducing significantly increased pigment biosynthesis in four cultures. The dose–response curves based on the resultant brown signal **(D)** and the resultant green signal **(E)** were drawn after non-oxidation and oxidation treatment. **(F)**Linear regression analysis of the relationship between the brown signal and Pb(II) concentrations ranging from 46.9 to 750nM. **(G)** Non-linear regression analysis of the relationship between the green signal and Pb(II) concentrations ranging from 0.732 to 750nM. The inset shows the $R^2$ values of the regression equations. The *x*-axis shows the Pb(II) concentration on the $\log_2$ scale. The result was the mean±standard deviation of three independent assays. Representative photos of the n-butanol phases containing PV derivatives after non-oxidation **(H)** and oxidation **(I)** treatment are shown, and the Pb(II) concentration ranges of regression analysis are marked.

reading of high Pb(II) exposure with the naked eye and the development of visible light colorimetric methods.

The biosensing selectivity largely depends on the metal sensory element. Previous studies showed that group 12 metals exerted some influence on the response of biosensors employing metalloregulator PbrR as a Pb(II) sensory component (Hui et al., 2022b). The developed biosensor comprised a PbrR-based sensory element and a *vioABDE* reporter gene cluster. As expected, excellent biosensing selectivity was demonstrated when PV-based biosensors were exposed to metal ions alone (Figures 4A,B). Only Cd(II) and

Hg(II) exerted some adverse effects on the Pb(II) induced signal output (Figures 4C,D). The electrochemical property is similar among Pb, Cd, and Hg (Chen et al., 2005). The Cd(II) and Hg(II) may compete with Pb(II) to occupy the metal binding domains of dimeric PbrR. However, the association with non-target metal cannot efficiently trigger the downstream reporter gene's transcription (Hui et al., 2022b). The molecular evolution of metalloregulator was always thought to be a promising solution to improve the metal selectivity of biosensors (Jia et al., 2020; Cai et al., 2022).

Soluble inorganic and organic components in natural aquatic systems can change metal morphology, resulting in its differential bioavailability and ecotoxicity (Ryan et al., 2009). It is necessary to validate a novel biosensor in monitoring environmental pollutant metals (Gavrilas et al., 2022). This study developed a simple and three-step detection process to detect residual Pb(II) in the environmental water (Figure 5A). Artificially contaminated environmental water samples were prepared and mixed into the biosensing culture system. Engineered biosensor cells were simulated to be exposed to increased Pb(II) concentrations in four water samples. Although the whole dose–response curves of environmental water are similar to that under experimental conditions, environmental water matrices exerted a specific influence on the generation of pigment signals, particularly on the heterogeneous brown biosensing signal toward Pb(II), which might lead to a differential LOD (Figure 5B) and a narrow quantifiable concentration range (Figure 5F) in detecting various environmental samples. The naked eye quickly identified the gradient changes in color deepening (Figures 5H,I).

Interestingly, a significantly decreased relative standard deviation was observed in the oxidation treatment group compared to the non-oxidation treatment group (Supplementary Tables S3, S4). It can be well explained that PV may be oxidized into homogeneous derivatives under extreme oxidizing conditions. However, the autoxidation of PV in the n-butanol tends to produce more ambiguous products. The above findings suggest that PV-based biosensors, especially employing green signals after oxidation treatment, become a semi-quantitative device powerful in warning high dose Pb(II) pollution through direct reading with the naked eye.

Novel visible pigment-based bacterial biosensors share the same advantages over luminescent and fluorescent bacterial biosensors (Liao et al., 2006; Hui et al., 2021b). It differs from widely used enzyme-based biosensors because no extra substrate is necessary. The pigment-based colorimetric method is also superior to traditional colorimetric methods. The critical devices involved in these biosensors are a cheap incubator, a low-speed centrifuge, and a microplate reader with a visible detection range. Regarding the initial investment in equipment, its cost is far lower than traditional sensors. The biosensing plasmid and host cells are stably stored at low temperatures. Fresh biosensor cells may be transformed regularly to avoid genetic variation. However, the costs associated with bacterial culture, plasmid preservation, and transformation can be ignored. All these properties make metabolically engineered bacteria potentially become low-cost and mini-equipment biosensors (Naik and Dubey, 2013; Guo et al., 2021a).

In conclusion, this study transformed an intermediate of the branched violacein biosynthetic pathway into a dual-color biosensing reporter. The PV-derived dual-color signals had excellent biosensing properties and showed great potential in developing whole-cell biosensors toward pollutants such as toxic Pb(II). Colored signals read directly by the naked eye enabled a PV-based biosensor, a potential on-site detection method. The sensitivity and selectivity of bacterial biosensors are expected to be improved by optimization of genetic circuits and molecular evolution of metalloregulator PbrR in future studies.

## Data availability statement

The original contributions presented in the study are included in the article/Supplementary material, further inquiries can be directed to the corresponding authors.

## Author contributions

C-yH, N-xZ, and HL designed the experimental protocol. D-lZ and C-yH drafted the manuscript. D-lZ, YG, B-cM, M-qL, C-xG, Y-qL, and H-jW carried out most of the study. D-lZ, YG, and B-cM analyzed the data. All authors contributed to the article and approved the submitted version.

## Funding

This work was supported by the National Natural Science Foundation of China (82073517), the Natural Science Foundation of Guangdong Province (2021A1515012472 and 2023A1515011184), the Science and Technology Program of Shenzhen (KCXFZ20201221173602007), Shenzhen Key Medical Discipline Construction Fund (SZXK068), and Shenzhen Fund for Guangdong Provincial High-level Clinical Key Specialties (SZGSP015).

## Conflict of interest

The authors declare that the research was conducted in the absence of any commercial or financial relationships that could be construed as a potential conflict of interest.

## Publisher's note



## Supplementary material

The Supplementary material for this article can be found online at: https://www.frontiersin.org/articles/10.3389/fmicb.2023.1218933/full#supplementary-material

# References


Adimalla, N. (2020). Heavy metals pollution assessment and its associated human health risk evaluation of urban soils from Indian cities: a review. *Environ. Geochem. Health* 42, 173–190. doi: 10.1007/s10653-019-00324-4

Bereza-Malcolm, L., Aracic, S., and Franks, A. E. (2016). Development and application of a synthetically-derived Lead biosensor construct for use in gram-negative Bacteria. *Sensors (Basel)* 16:16. doi: 10.3390/s16122174

Borremans, B., Hobman, J. L., Provoost, A., Brown, N. L., and Van Der Lelie, D. (2001). Cloning and functional analysis of the pbr lead resistance determinant of *Ralstonia metallidurans* CH34. *J. Bacteriol.* 183, 5651–5658. doi: 10.1128/JB.183.19.5651-5658.2001

Bridges, C. C., and Zalups, R. K. (2017). Mechanisms involved in the transport of mercuric ions in target tissues. *Arch. Toxicol.* 91, 63–81. doi: 10.1007/s00204-016-1803-y

Cai, Y., Zhu, K., Shen, L., Ma, J., Bao, L., Chen, D., et al. (2022). Evolved biosensor with high sensitivity and specificity for measuring cadmium in actual environmental samples. *Environ. Sci. Technol.* 56, 10062–10071. doi: 10.1021/acs.est.2c00627

Charkiewicz, A. E., and Backstrand, J. R. (2020). Lead toxicity and pollution in Poland. *Int. J. Environ. Res. Public Health* 17:4385. doi: 10.3390/ijerph17124385

Chen, P., Greenberg, B., Taghavi, S., Romano, C., Van Der Lelie, D., and He, C. (2005). An exceptionally selective lead(II)-regulatory protein from *Ralstonia metallidurans*: development of a fluorescent lead(II) probe. *Angew. Chem. Int. Ed. Engl.* 44, 2715–2719. doi: 10.1002/anie.200462443

Cui, Z., Luan, X., Jiang, H., Li, Q., Xu, G., Sun, C., et al. (2018). Application of a bacterial whole cell biosensor for the rapid detection of cytotoxicity in heavy metal contaminated seawater. *Chemosphere* 200, 322–329. doi: 10.1016/j.chemosphere.2018.02.097

Dave, D., Sarma, S., Parmar, P., Shukla, A., Goswami, D., Shukla, A., et al. (2020). Microbes as a boon for the bane of heavy metals. *Environ. Sustain* 3, 233–255. doi: 10.1007/s42398-020-00112-2

Fang, C., and Zhang, Y. (2022). Bacterial MerR family transcription regulators: activationby distortion. *Acta Biochim. Biophys. Sin. Shanghai* 54, 25–36. doi: 10.3724/abbs.2021003

Gavrilas, S., Ursachi, C. S., Perta-Crisan, S., and Munteanu, F. D. (2022). Recent trends in biosensors for environmental quality monitoring. *Sensors (Basel)* 22:1513. doi: 10.3390/s22041513

Guo, Y., Hui, C. Y., Liu, L., Chen, M. P., and Huang, H. Y. (2021a). Development of a bioavailable hg(II) sensing system based on MerR-regulated visual pigment biosynthesis. *Sci. Rep.* 11:13516. doi: 10.1038/s41598-021-92878-6

Guo, Y., Hui, C. Y., Zhang, N. X., Liu, L., Li, H., and Zheng, H. J. (2021b). Development of cadmium multiple-signal biosensing and bioadsorption systems based on artificial cad operons. *Front. Bioeng. Biotechnol.* 9:585617. doi: 10.3389/fbioe.2021.585617

Hemmaphan, S., and Bordeerat, N. K. (2022). Genotoxic effects of lead and their impact on the expression of DNA repair genes. *Int. J. Environ. Res. Public Health* 19:4307. doi: 10.3390/ijerph19074307

Hui, C. Y., Guo, Y., Li, H., Gao, C. X., and Yi, J. (2022a). Detection of environmental pollutant cadmium in water using a visual bacterial biosensor. *Sci. Rep.* 12:6898. doi: 10.1038/s41598-022-11051-9

Hui, C. Y., Guo, Y., Li, L. M., Liu, L., Chen, Y. T., Yi, J., et al. (2021a). Indigoidine biosynthesis triggered by the heavy metal-responsive transcription regulator: a visual whole-cell biosensor. *Appl. Microbiol. Biotechnol.* 105, 6087–6102. doi: 10.1007/s00253-021-11441-5

Hui, C. Y., Guo, Y., Liu, L., and Yi, J. (2021c). Recent advances in bacterial biosensing and bioremediation of cadmium pollution: a mini-review. *World J. Microbiol. Biotechnol.* 38:9. doi: 10.1007/s11274-021-03198-w

Hui, C. Y., Guo, Y., Liu, L., Zhang, N. X., Gao, C. X., Yang, X. Q., et al. (2020). Genetic control of violacein biosynthesis to enable a pigment-based whole-cell lead biosensor. *RSC Adv.* 10, 28106–28113. doi: 10.1039/D0RA04815A

Hui, C. Y., Guo, Y., Wu, J., Liu, L., Yang, X. Q., Guo, X., et al. (2021b). Detection of bioavailable cadmium by double-color fluorescence based on a dual-sensing bioreporter system. *Front. Microbiol.* 12:696195. doi: 10.3389/fmicb.2021.696195

Hui, C. Y., Guo, Y., Zhu, D. L., Li, L. M., Yi, J., and Zhang, N. X. (2022b). Metabolic engineering of the violacein biosynthetic pathway toward a low-cost, minimal-equipment lead biosensor. *Biosens. Bioelectron.* 214:114531. doi: 10.1016/j.bios.2022.114531

Hui, C. Y., Hu, S. Y., Li, L. M., Yun, J. P., Zhang, Y. F., Yi, J., et al. (2022c). Metabolic engineering of the carotenoid biosynthetic pathway toward a specific and sensitive inorganic mercury biosensor. *RSC Adv.* 12, 36142–36148. doi: 10.1039/D2RA06764A

Jia, X., Ma, Y., Bu, R., Zhao, T., and Wu, K. (2020). Directed evolution of a transcription factor PbrR to improve lead selectivity and reduce zinc interference through dual selection. *AMB Express* 10:67. doi: 10.1186/s13568-020-01004-8

Jiang, T., Xing, B., and Rao, J. (2008). Recent developments of biological reporter technology for detecting gene expression. *Biotechnol. Genet. Eng. Rev.* 25, 41–76. doi: 10.5661/bger-25-41

Kannappan, S., and Ramisetty, B. C. M. (2022). Engineered whole-cell-based biosensors: sensing environmental heavy metal pollutants in water-a review. *Appl. Biochem. Biotechnol.* 194, 1814–1840. doi: 10.1007/s12010-021-03734-2

Kiran Marella, T., Saxena, A., and Tiwari, A. (2020). Diatom mediated heavy metal remediation: a review. *Bioresour. Technol.* 305:123068. doi: 10.1016/j.biortech.2020.123068

Klotz, K., and Goen, T. (2017). Human biomonitoring of Lead exposure. *Met. ions Life Sci.* 17:6. doi: 10.1515/9783110434330-006

Kolosova, E. M., Sutormin, O. S., Shpedt, A. A., Stepanova, L. V., and Kratasyuk, V. A. (2022). Bioluminescent-inhibition-based biosensor for full-profile soil contamination assessment. *Biosensors (Basel)* 12:12. doi: 10.3390/bios12050353

Kumar, D., Malik, D. S., Kumar, N., Gupta, N., and Gupta, V. (2020). Spatial changes in water and heavy metal contamination in water and sediment of river ganga in the river belt Haridwar to Kanpur. *Environ. Geochem. Health* 42, 2059–2079. doi: 10.1007/s10653-019-00471-8

Levin-Karp, A., Barenholz, U., Bareia, T., Dayagi, M., Zelcbuch, L., Antonovsky, N., et al. (2013). Quantifying translational coupling in *E. coli* synthetic operons using RBS modulation and fluorescent reporters. *ACS Synth. Biol.* 2, 327–336. doi: 10.1021/sb400002n

Liao, V. H., Chien, M. T., Tseng, Y. Y., and Ou, K. L. (2006). Assessment of heavy metal bioavailability in contaminated sediments and soils using green fluorescent protein-based bacterial biosensors. *Environ. Pollut.* 142, 17–23. doi: 10.1016/j.envpol.2005.09.021

Locher, K. P. (2016). Mechanistic diversity in ATP-binding cassette (ABC) transporters. *Nat. Struct. Mol. Biol.* 23, 487–493. doi: 10.1038/nsmb.3216

Manousi, N., Kabir, A., Furton, K. G., Stathogiannopoulou, M., Drosaki, E., and Anthemidis, A. (2022). An automatic on-line sol-gel pyridylethylthiopropyl functionalized silica-based sorbent extraction system coupled to flame atomic absorption spectrometry for lead and copper determination in beer samples. *Food Chem.* 394:133548. doi: 10.1016/j.foodchem.2022.133548

Mulhern, R., Roostaei, J., Schwetschenau, S., Pruthi, T., Campbell, C., and Macdonald Gibson, J. (2022). A new approach to a legacy concern: evaluating machine-learned Bayesian networks to predict childhood lead exposure risk from community water systems. *Environ. Res.* 204:112146. doi: 10.1016/j.envres.2021.112146

Naik, M. M., and Dubey, S. K. (2013). Lead resistant bacteria: lead resistance mechanisms, their applications in lead bioremediation and biomonitoring. *Ecotoxicol. Environ. Saf.* 98, 1–7. doi: 10.1016/j.ecoenv.2013.09.039

Naikoo, M. I., Dar, M. I., Khan, F. A., Raghib, F., and Rajakaruna, N. (2019). Trophic transfer and bioaccumulation of lead along soil-plant-aphid-ladybird food chain. *Environ. Sci. Pollut. Res. Int.* 26, 23460–23470. doi: 10.1007/s11356-019-05624-x

Pohl, H. R., Ingber, S. Z., and Abadin, H. G. (2017). Historical view on lead: guidelines and regulations. *Met. Ions Life Sci.* 17:13. doi: 10.1515/9783110434330-013

Rehman, K., Fatima, F., Waheed, I., and Akash, M. S. H. (2018). Prevalence of exposure of heavy metals and their impact on health consequences. *J. Cell. Biochem.* 119, 157–184. doi: 10.1002/jcb.26234

Rocha, A., and Trujillo, K. A. (2019). Neurotoxicity of low-level lead exposure: history, mechanisms of action, and behavioral effects in humans and preclinical models. *Neurotoxicology* 73, 58–80. doi: 10.1016/j.neuro.2019.02.021

Roux, K. E., and Marra, P. P. (2007). The presence and impact of environmental lead in passerine birds along an urban to rural land use gradient. *Arch. Environ. Contam. Toxicol.* 53, 261–268. doi: 10.1007/s00244-006-0174-4

Ryan, A. C., Tomasso, J. R., and Klaine, S. J. (2009). Influence of pH, hardness, dissolved organic carbon concentration, and dissolved organic matter source on the acute toxicity of copper to *Daphnia magna* in soft waters: implications for the biotic ligand model. *Environ. Toxicol. Chem.* 28, 1663–1670. doi: 10.1897/08-361.1

Tong, Y., Zhou, J., Zhang, L., and Xu, P. (2021). A golden-gate based cloning toolkit to build violacein pathway libraries in yarrowia lipolytica. *ACS Synth. Biol.* 10, 115–124. doi: 10.1021/acssynbio.0c00469

Tudosie, M. S., Caragea, G., Popescu, D. M., Avram, O., Serban, D., Smarandache, C. G., et al. (2021). Optimization of a GF-AAS method for lead testing in blood and urine: a useful tool in acute abdominal pain management in emergency. *Exp. Ther. Med.* 22:985. doi: 10.3892/etm.2021.10417

Viviani, V. R., Pelentir, G. F., and Bevilaqua, V. R. (2022). Bioluminescence color-tuning firefly luciferases: engineering and prospects for real-time intracellular pH imaging and heavy metal biosensing. *Biosensors (Basel)* 12:400. doi: 10.3390/bios12060400

Wang, B., and Buck, M. (2012). Customizing cell signaling using engineered genetic logic circuits. *Trends Microbiol.* 20, 376–384. doi: 10.1016/j.tim.2012.05.001

Watstein, D. M., and Styczynski, M. P. (2017). Development of a pigment-based whole-cell zinc biosensor for human serum. *ACS Synth. Biol.* 7, 267–275. doi: 10.1021/acssynbio.7b00292

Wei, W., Liu, X., Sun, P., Wang, X., Zhu, H., Hong, M., et al. (2014). Simple whole-cell biodetection and bioremediation of heavy metals based on an engineered lead-specific operon. *Environ. Sci. Technol.* 48, 3363–3371. doi: 10.1021/es4046567

Yang, D., Park, S. Y., and Lee, S. Y. (2021). Production of rainbow colorants by metabolically engineered *Escherichia coli*. *Adv. Sci. (Weinh)* 8:e2100743. doi: 10.1002/advs.202100743

Yu, Q., Fu, Y., Xiao, K., Zhang, X., Du, C., and Chen, J. (2022). A label-free photoelectrochemical biosensor with ultra-low-background noise for lead ion assay based on the cu(2)O-CuO-TiO(2) heterojunction. *Anal. Chim. Acta* 1195:339456. doi: 10.1016/j.aca.2022.339456

Yuvaraja, G., Pang, Y., Chen, D. Y., Kong, L. J., Mehmood, S., Subbaiah, M. V., et al. (2019). Modification of chitosan macromolecule and its mechanism for the removal of Pb(II) ions from aqueous environment. *Int. J. Biol. Macromol.* 136, 177–188. doi: 10.1016/j.ijbiomac.2019.06.016

Zhang, L., Deng, H., Yuan, R., and Yuan, Y. (2019). Electrochemical lead(II) biosensor by using an ion-dependent split DNAzyme and a template-free DNA extension reaction for signal amplification. *Mikrochim. Acta* 186:709. doi: 10.1007/s00604-019-3857-z

Zhao, E. M., Suek, N., Wilson, M. Z., Dine, E., Pannucci, N. L., Gitai, Z., et al. (2019). Light-based control of metabolic flux through assembly of synthetic organelles. *Nat. Chem. Biol.* 15, 589–597. doi: 10.1038/s41589-019-0284-8

Zhu, S., Khan, M. A., Kameda, T., Xu, H., Wang, F., Xia, M., et al. (2022). New insights into the capture performance and mechanism of hazardous metals Cr(3+) and cd(2+) onto an effective layered double hydroxide based material. *J. Hazard. Mater.* 426:128062. doi: 10.1016/j.jhazmat.2021.128062

# Frontiers in Microbiology

**Explores the habitable world and the potential of microbial life**

The largest and most cited microbiology journal which advances our understanding of the role microbes play in addressing global challenges such as healthcare, food security, and climate change.

---

## Discover the latest Research Topics

See more →


**Frontiers**

Avenue du Tribunal-Fédéral 34
1005 Lausanne, Switzerland
frontiersin.org

**Contact us**

+41 (0)21 510 17 00
frontiersin.org/about/contact